DYNAMICS OF SINGLE AND MULTIPHOTON IONIZATION PROCESSES IN MOLECULES

Thesis by

Diane Lynn Lynch

In Partial Fulfillment of the Requirements
for the Degree of
Doctor of Philosophy

1987

California Institute of Technology
Pasadena, California

(Submitted July 23, 1986)

To Tom, my mom, and

in memory of my father

ACKNOWLEDGEMENTS

I would like to express my appreciation to my research advisor, Professor Vincent McKoy, for his patience, encouragement, and advice throughout the course of this work. I have also had the privilege of working with and learning from several outstanding scientists and would like to thank Dr. Sham Dixit and Dr. Tom Gibson for both their guidance and friendship during my graduate studies at Caltech. I am also grateful to Marco Lima, Maile Smith, Richard Dubs, and Henrik Rudolph for their instructive and helpful discussions, as well as for providing a lighter side to graduate school. Finally, I wish to express my gratitude to Tom. Without his support, particularly over the last two years, I would not have been able to finish this work.

ABSTRACT

Single-photon and resonant multiphoton ionization studies, which can now be carried out using synchrotron radiation and lasers, respectively, are providing important dynamical information on molecular photoionization. We have studied the underlying dynamical features of these ionization processes using Hartree-Fock continuum orbitals generated using the Iterative Schwinger Variational method for solving the photoelectron collisional equations. Our single-photon studies examine the important role that shape and autoionizing resonances play in molecular photoionization, while the multiphoton studies investigate the ionization dynamics of excited electronic states.

We have demonstrated the subtle nature of shape resonances in polyatomic systems such as C_2H_2 and C_2N_2, where the possibility of multiple resonances in a single channel is observed. In addition, these resonant states induce the breakdown of the Franck-Condon approximation as well as the frozen core approximation in K-shell ionization, as illustrated in our vibrationally resolved studies of CO and the K-Shell studies of N_2 and CO_2, respectively. Critical comparisons with other theoretical results and available experimental data have been made for these systems.

Molecular autoionizing resonances are known to dominate regions of the photoionization spectra. We have

adapted and applied a generalization of the Fano treatment for autoionization to molecular systems. Results for H_2 and C_2H_2 autoionizing resonances are presented and discussed.

Resonant enhanced multiphoton ionization (REMPI) is currently being used to study the dynamics of state-selected photoionization processes by laser excitation to specific vibrational and rotational levels. As first applications of a quantitative analysis for molecular REMPI we have studied several ionization schemes in H_2, such as (3+1) REMPI via the $C^1\Pi_u$ state, (2+1) REMPI via the $B^1\Sigma_u^+$ state, and (2+1) REMPI via the double-well $E,F^1\Sigma_g^+$ state. These <u>ab initio</u> studies are very useful in understanding the underlying dynamics of molecular REMPI, e.g., the observed non-Franck-Condon behavior of the vibrational branching ratios in the $C^1\Pi_u$ and $E,F^1\Sigma_g^+$ states can be primarily attributed to the internuclear distance dependence of the electronic transition moments. We compare and discuss our theoretical results with the available experimental data.

TABLE OF CONTENTS

CHAPTER I

INTRODUCTION

Recent progress in experimental methods for studying molecular photoionization has led to detailed characterization of the underlying dynamics for this process. As discussed by Dehmer et al.,[1] synchrotron radiation provides the tunable source of photons necessary to study the continuous variation of molecular single photon ionization cross sections with energy. Such experiments have shown that electronic resonance phenomena play a very important role in molecular photoionization. These resonces can be classified as either single-particle (shape) or two-electron (autoionizing) in nature. In addition to the strong influence of these resonances on the cross sections and angular distributions, they also lead to dynamical features in the photoelectron spectra such as non-Franck-Condon vibrational state distributions and vibrational-state dependent photoelectron asymmetry parameters. These single photon studies are thus sensitive probes of the molecular continuum. Furthermore, the technique of resonant multiphoton ionization using pulsed dye lasers combined with photoelectron kinetic energy analysis is now used to probe aspects of the dynamics of molecular photoionization which are complimentary to those usually studied with synchrotron radiation.[2-6] A remarkable feature of photoelectron

spectroscopy based on such multiphoton ionization is that the resonant state can be selected with respect to both vibrational and rotational levels by specific laser excitation. With this technique the spectroscopy and dynamics of the excited resonant state can be studied with very high resolution; also vibrational intensities and photoelectron angular distributions can now be measured for rotationally and vibrationally state-selected molecules. Experimental studies to date in this area have already shown interesting features, including non-Franck-Condon distributions of vibrational states of the ion, Rydberg-valence mixing, rotational and vibrational state dependence of the photoelectron angular distributions, and vibrational and rotational autoionization. These and other properties make resonant multiphoton ionization a versatile state-specific probe of molecules.

It is clearly important to develop a theoretical framework that would not only enable us to understand and predict the underlying dynamical content of these molecular photoionization processes but would also be useful in the analysis of experimental data, which is becoming increasingly available in this field. At the heart of any theoretical treatment of molecular photoionization is the determination of the final electronic continuum state. The solution of the equations for these continuum states is complicated due to the

non-local and highly anisotropic molecular-ion core potential. For these reasons, accurate theoretical treatments for molecular photoionization are less developed than those used in the determination of bound molecular electronic states and in related studies of atomic photoionization.

In this thesis we discuss our theoretical studies of these single and multiphoton processes. Our approach to molecular photoionization assumes the Born-Oppenheimer approximation and hence we work in the body-frame with the nuclear motion taken into account in an adiabatic fashion. This reduces the problem to solving the Schrödinger equation for the electronic motion with the nuclear geometry fixed and considered parametrically. The N-electron final state wavefunctions are composed of (N-1) bound electrons representing the ionic core and the continuum photoelectron. In general, we use the frozen-core Hartree-Fock approximation with the N-electron wavefunction represented as a single configuration and the (N-1) bound orbitals constrained to be identical with those of the neutral molecule. The continuum orbital is then determined in this realistic potential by the direct solution of the electron-molecular ion collisional equations using the iterative Schwinger variational method of Lucchese et al.[7] Final state correlation effects are included by the method of configuration interaction in the continuum,

originally proposed by Fano.[8] In the expansion for the final-state wavefunction we use the single-particle Hartree-Fock continuum orbitals as a zeroth order basis.

SHAPE RESONANCES

Chapter II of this thesis discusses the application of the iterative Schwinger variational method to the study of shape resonance phenomena. These quasi-bound states are formed by the trapping of the photoelectron by the centrifugal barrier of the molecular force field. Being one-electron in nature, these resonances should be adequately described in the static-exchange approximation with Hartree-Fock continuum orbitals. This has been previously demonstrated in N_2, CO_2 and NO.[7] Applications of this method are extended to larger polyatomic systems, e.g., C_2H_2 and C_2N_2, which display more subtle shape resonant structure. These features are discussed in Sections A and B. In addition, non-Franck-Condon behavior is investigated in valence photoionization of CO, where excellent data for vibrational branching ratios and vibrationally resolved asymmetry parameters are available.[9,10] This behavior is induced by the presence of a shape resonance, which causes a rapid variation of the electronic wavefunction with internuclear distance. We report and compare our calculated results with the experimental data and other theoretical approaches.[11] In

contrast to earlier interpretations, our results indicate that the observed structure probably results from autoionization with the shape resonance induced non-Franck-Condon behavior occurring outside the measured photon energy range. Finally, shape resonances have been investigated in K-Shell photoionization. The use of the frozen core approximation can become inadequate for low kinetic energy shape resonances since the trapped photoelectron experiences the relaxation of the molecular-ion core. Approximate methods for incorporating relaxation effects are discussed and implemented for K-Shell ionization of N_2 and CO_2.

FINAL STATE CORRELATION EFFECTS

In Chapter III we discuss the development and application of our ab initio treatment of autoionization in molecular photoionization. The autoionizing state is a discrete level embedded in an underlying continuum, and it is the inclusion of correlation effects, instantaneous electron-electron repulsion, which couples these zeroth order states. We have tested our method with a study of the known autoionizing Rydberg $^1\Sigma_u^+$ $(1\sigma_u 2\sigma_g)$ state of H_2 and compared our results to previous treatments.[12] Of greater current interest is the role that autoionizing states play in the pronounced double-bump structure seen in the 12-17 eV region for

ionization of the $1\pi_u$ level of C_2H_2. Presently, there is no definitive quantitative understanding of the observed resonant structure. We have assessed the influence of the autoionizing $^1\Pi_u$ ($2\sigma_u \rightarrow 1\pi_g$) valence state on the photoionization cross sections and asymmetry parameters. These results are discussed and compared to the experimental data[13-16] and previous semi-empirical treatments.[17] To our knowledge this is the first non-empirical study of autoionization in such polyatomic systems.

RESONANT ENHANCED MULTIPHOTON IONIZATION (REMPI)

Chapter IV details our initial investigations of multiphoton processes in molecules. The purpose of this work is to understand the dynamical features observed in the photoionization spectra and photoelectron angular distributions. Our approach consists of viewing the (n+m) REMPI process as a two-step event. The resonant intermediate state is reached by n-photon excitation from an isotopic initial state. The orientation of the resonant state is nonisotropic and is characteristic of the n-photon absorption. This oriented state is subsequently ionized by absorption of m additional photons. If m is greater than one, accidental resonances may occur in the ionization step which can influence the resulting ion/electron signal. Therefore (n+1) REMPI processes are attractive, both experimentally and

theoretically, as the probe of the resonant state is "clean."

In our first set of REMPI studies we have analyzed the vibrational branching ratios and photoelectron angular distributions via the Rydberg $C^1\Pi_u^-$, the Rydberg-valence $E,F^1\Sigma_g^+$ state, and the $B^1\Sigma_u^+$ state of H_2. In addition to final vibrational state resolution the $B^1\Sigma_u^+$ state calculations were rotationally resolved. These studies were motivated by the recent REMPI experiments by Pratt et al.[4,5] and Anderson et al.[6] Pratt et al.[4] reported the photoelectron energy spectra resulting from (3+1) ionization through the $C^1\Pi_u^-$ state. This experiment illustrates the remarkable selectivity achievable in resonant multiphoton ionization since, although the ν'=0-4 levels of the $C^1\Pi_u^+$ state are perturbed by various levels of the $B^1\Sigma_u^+$ state, the $C^1\Pi_u^-$ component is unaffected. In this experiment these perturbations were avoided by tuning the laser in resonance with the Q(1) line, which accesses only the Π^- component. The measured branching ratios displayed highly non-Franck-Condon behavior. Non-Franck-Condon behavior was also observed by Anderson et al.[6] in the photoelectron spectra and angular distributions for (2+1) REMPI via the double-well $E,F^1\Sigma_g^+$ state. Here, significant non-Franck-Condon behavior is expected because of the sensitivity of the electronic wavefunction of this Rydberg-valence state to the internuclear distance (R). This study also demonstrates that

REMPI processes can be used to probe complicated neutral excited states. In another experiment Pratt et al.[5] reported partially resolved rotational photoelectron spectra in the (3+1) REMPI via the $B^1\Sigma_u^+$ state of H_2. They observed several interesting features such as photoelectron spectra, which depend on the rotational levels of the intermediate state and the suppression of transitions that involve the transfer of three units of angular momentum.

Our theoretical studies addressed the influence of the energy and internuclear distance dependence of the electronic transition moments on these branching ratios and photoelectron angular distributions. Critical comparisons with the existing experimental data are made and reasonable agreement is found. These calculations indicate the usefulness of a quantitative theoretical treatment for a detailed understanding of REMPI processes in small molecules.

REFERENCES

1. J. L. Dehmer, D. Dill, and A. C. Parr, in Photophysics and Photochemistry in the Vacuum Ultraviolet, edited by S. McGlynn, G. Findley, and R. Huebner (D. Reidel, Dordrecht, Holland, 1984), pp. 341-408.
2. See, for example: K. Kimura, Adv. Chem. Phys. (1985).
3. P. M. Dehmer, S. T. Pratt, and J. L. Dehmer, Second Topical Meeting on Laser Techniques in the Extreme Ultraviolet , March 5-7, 1984, Boulder, CO.
4. S. T. Pratt, P. M. Dehmer, and J. L. Dehmer, Chem. Phys. Lett. 105, 28 (1984).
5. S. T. Pratt, E. D. Poliakoff, P. M. Dehmer, and J. L. Dehmer, J. Chem. Phys. 78, 65 (1983).
6. S. L. Anderson, G. D. Kubiak and R. N. Zare, Chem. Phys. Lett. 105, 22 (1984).
7. Robert R. Lucchese, Kazuo Takatsuka, and Vincent McKoy, Phys. Rept. 131, 147 (1986).
8. U. Fano, Phys. Rev. 124, 1866 (1961).
9. R. Stockbauer, B. E. Cole, D. L. Ederer, J. B. West, A. C. Parr, and J. L. Dehmer, Phys. Rev. Lett. 43, 757 (1979).
10. B. E. Cole, D. L. Ederer, R. Stockbauer, K. Codling, A. C. Parr, J. B. West, E. D. Poliakoff, and J. L. Dehmer, J. Chem. Phys. 72, 6308 (1980).

11. J. A. Stephens, D. Dill, and J. L. Dehmer, J. Phys. B **14**, 3911 (1981).

12. G. Raseev, J. Phys. B **18**, 423 (1985).

13. R. Unwin, I. Khan, N. Y. Richardson, A. M. Bradshaw, L. Cederbaum, and W. Domke, Chem. Phys. Lett. **77**, 242 (1981).

14. A. C. Parr, D. L. Ederer, J. B. West, D. M. P. Holland, and J. L. Dehmer, J. Chem. Phys. **76**, 4349 (1982).

15. P. R. Keller, D. Mehaffy, J. W. Taylor, F. A. Grimm, and T. A. Carlson, J. Electron Spectrosc. **27**, 223 (1982).

16. J. Kreile, A. Schweig, and W. Thiel, Chem. Phys. Lett. **79**, 549 (1981).

17. Z. H. Levine and P. Soven, Phys. Rev. Lett. **50**, 2074 (1983).

CHAPTER II

SHAPE RESONANCES

SECTION A

STUDIES OF THE PHOTOIONIZATION CROSS SECTIONS OF ACETYLENE

I. INTRODUCTION

Recent experimental[1-6] and theoretical[7-9] studies have shown that shape resonances play a major role in molecular photoionization. Shape resonances lead to important effects in the photoionization cross sections and photoelectron angular distributions. For example, such resonances can induce large deviations of the vibrational branching ratios from those based on Franck-Condon factors. To date, studies have shown that the Hartree-Fock approximation can provide a very useful quantitative description of these shape resonant effects in molecular photoionization cross sections.[8-14]

In this paper we present the results of our studies of the photoionization cross sections of acetylene and, in particular, of the role of shape resonances in these cross sections. The cross sections are obtained from the direct solution of the electron-molecular ion collisional equations in the frozen-core Hartree-Fock (FCHF) approximation at the ground state equilibrium geometry of acetylene. The continuum Hartree-Fock equations were solved by the iterative Schwinger method[15] which we have used in our earlier studies of the photoionization of N_2,[16] CO_2,[17] NO,[18] and CO.[19]

We have obtained the photoionization cross sections and photoelectron asymmetry parameters for the valence molecular orbitals ($1\pi_u$, $3\sigma_g$, $2\sigma_u$, and $2\sigma_g$) and for the K-shell orbitals ($1\sigma_g$ and $1\sigma_u$) of acetylene. These results are compared with available experimental data[6,20-23] and with results obtained using the Stieltjes-Tchebycheff moment theory (STMT) approach[24]

and the continuum multiple scattering model.[21,22] Of particular interest in C_2H_2 is the double bump structure around 14eV in the $^2\Pi_u$ photoionization spectrum. Several recent experimental[6,20-22,25,26] and theoretical[20,21,26,27] studies have addressed the question of the nature of the underlying resonances in this region, e.g., to what extent is this structure due to shape or autoionizing resonances or to some combination of such resonances. Although no firm understanding of this resonant excitation mechanism has yet emerged, it seems certain that the autoionizing $^1\Pi_u(2\sigma_u \rightarrow 1\pi_g)$ valence state contributes to the structure in this region.[6,20] The present results show that, while the $1\pi_u \rightarrow k\sigma_g$ and $k\delta_g$ one-electron continua are nonresonant in this region, the cross section could be significantly enhanced by a shape resonance in the $1\pi_u \rightarrow k\pi_g$ continuum around 13eV. This interpretation depends very critically on the question of the location of the $^1\Sigma_u^+(1\pi_u \rightarrow 1\pi_g)$ state in acetylene. Electronic structure calculations indicate that this transition lies just above the $1\pi_u$ ionization threshold and, in fact, causes the shape resonance in the $1\pi_u \rightarrow k\pi_g$ continuum. This is quite different from the analogous situation in N_2 where the $^1\Sigma_u^+(1\pi_u \rightarrow 1\pi_g)$ state is known to lie well into the discrete region of the spectrum and hence the $k\pi_g$ continuum function can be constructed orthogonal to the $1\pi_g$ orbital.[16,28] Final-state correlation effects must play an important role in any quantitative interpretation of the resonant structure in this region.

As expected, the σ_u photoionization continuum of acetylene

is shape-resonance enhanced. The cross sections and eigenphase sums for this continuum show some interesting features. For example, the eigenphase sums indicate that there are two shape resonances in this channel. Around a photoelectron kinetic energy of 2eVs the first shape resonance has a pronounced effect on the cross section and asymmetry parameter for ionization out of the $3\sigma_g$ level. This shift in shape resonant activity from a photoelectron kinetic energy of about 15eV in N_2 to 2eV in C_2H_2 is consistent with the changes in nuclear separations and confirms the trends previously seen in the measured cross sections[20] and in the STMT calculations.[24] The second shape resonance feature is much broader, lies at higher energy, and is not noticeable in the vibrationally unresolved cross sections and angular distributions for the $3\sigma_g$ level. However, the effects of both this resonance and the lower energy one are very evident in the $2\sigma_g$ photoionization cross sections. The effects of these shape resonances on the valence shell and K-shell cross sections are discussed in some detail.

II. METHOD

The rotationally unresolved, fixed-nuclei photoionization cross section is given by

$$\sigma(R) = \frac{4\pi^2\omega}{3c} \left| < \Psi_i(\underset{\sim}{r},R) | \vec{\mu} | \Psi_f(\underset{\sim}{r},R) > \right|^2 \qquad (1)$$

where $\vec{\mu}$ is the dipole moment operator and ω the photon frequency. In Eq.(1) $\Psi_i(\underset{\sim}{r},R)$ is the initial state of the molecule

and $\Psi_f(\underset{\sim}{r},R)$ the final ionized state. In these studies the final state wave function is obtained using the frozen-core Hartree-Fock (FCHF) approximation. In this approximation the final state is described by a single electronic configuration in which the ionic core orbitals are constrained to be identical to the HF orbitals of the neutral molecule and the continuum orbital hence satisfies the one-electron Schrödinger equation

$$(-\frac{1}{2}\nabla^2 + V_{N-1}(\underset{\sim}{r},R) - \frac{k^2}{2})\,\phi_{\underset{\sim}{k}}(\underset{\sim}{r},R) = 0 \qquad (2)$$

where $\frac{k^2}{2}$ is the photoelectron kinetic energy and $\phi_{\underset{\sim}{k}}$ satisfies the appropriate boundary conditions. The key step in the study of molecular photoionization cross sections at any level of approximation is the determination of these Hartree-Fock continuum functions, $\phi_{\underset{\sim}{k}}$.

To obtain the continuum orbital $\phi_{\underset{\sim}{k}}$ it is convenient to work with the integral form of Eq.(2). The partial wave components of $\phi_{\underset{\sim}{k}}$, which are defined by the expansion

$$\phi_k^{(-)}(\vec{r}) = (\tfrac{2}{\pi})^{\frac{1}{2}} \sum_{\ell=0}^{\ell_p} \sum_{m=-\ell}^{\ell} i^{\ell}\, \psi_{k\ell m}^{(-)}(\vec{r})\, Y_{\ell m}^{*}(\Omega_{\hat{k}}), \qquad (3)$$

then satisfy the Lippmann-Schwinger equation

$$\psi_{k\ell m}^{(-)} = S_{k\ell m} + G_c^{(-)}\, U\, \psi_{k\ell m}^{(-)} \qquad (4)$$

where $G_c^{(-)}$ is the Coulomb Green's function with incoming-wave boundary conditions, U = 2V where V is the molecular ion potential , V_{N-1}, with the Coulomb component removed, and $S_{k\ell m}$ is the appropriate partial wave Coulomb function. In Eq.(3) an infinite sum over ℓ has been truncated at $\ell = \ell_p$. We have recently developed an iterative approach to the solution of Eq.(4) which is based on the Schwinger variational principle.[15,29] Applications[16-19] have shown that the method is an effective approach to the determination of these continuum solutions for molecular ion potentials. Details have been discussed elsewhere[15] and here we will discuss only a few essential features of the method. In this approach we first solve the Lippmann-Schwinger equation by assuming an approximate separable form for the scattering potential, U

$$U(\underset{\sim}{r},\underset{\sim}{r}') \cong U^S(\underset{\sim}{r},\underset{\sim}{r}') = \sum_{\alpha_i,\alpha_j} \langle \underset{\sim}{r} | U | \alpha_i \rangle (U^{-1})_{ij} \times \langle \alpha_j | U | \underset{\sim}{r}' \rangle \qquad (5)$$

where the matrix $(U^{-1})_{ij}$ is the inverse of the matrix with elements $U_{ij} = \langle \alpha_i | U | \alpha_j \rangle$. With this approximate potential, U^S, the solutions of Eq.(4) are simply

$$\psi^{(0)}_{k\ell m}(\underset{\sim}{r}) = S_{k\ell m}(\underset{\sim}{r}) + \sum_{\alpha_i,\alpha_j} \langle \underset{\sim}{r} | G_c^{(-)} U | \alpha_i \rangle (D^{-1})_{ij} \langle \alpha_j | U | S_{k\ell m} \rangle \qquad (6)$$

where

$$D_{ij} = \langle \alpha_i | U - U G_c^{(-)} U | \alpha_j \rangle . \qquad (7)$$

The use of a separable potential of the form of Eq.(5) in the solution of the Lippmann-Schwinger equation for $\psi_{k\ell m}^{(0)}$ can be shown to be equivalent to using the functions, $\alpha_i(\underset{\sim}{r})$, in the Schwinger variational principle for collisions.[30] At this stage these functions can be chosen to be entirely discrete basis functions such as Cartesian or spherical Gaussian functions which are known to be very effective in representing the multicenter nature of molecular electronic eigenfunctions.[31]

With suitable basis sets, the solutions $\psi_{k\ell m}^{(0)}$ can already provide quantitatively reliable photoionization cross sections which, moreover, can be shown to be variationally stable at the Hartree-Fock level.[19] We have, however, also developed an iterative procedure for obtaining the converged solutions of Eq.(2). The details of this approach are discussed elsewhere.[29] The results presented in this paper were generally calculated with continuum functions obtained after two steps in the iterative procedure.

For the initial state Ψ_i of Eq.(1), we generally use the SCF wave function but, in certain cases, we will include some effects due to electron correlation by using a configuration interaction wave function. In addition to the dipole length form given in Eq.(1) we also obtain cross sections and asymmetry parameters in the dipole velocity form. The difference between these two forms of the cross section can generally be viewed as a measure of electron correlation effects.[32]

III. RESULTS

The ground state electronic configuration of acetylene is $1\sigma_g^2\ 1\sigma_u^2\ 2\sigma_g^2\ 2\sigma_u^2\ 3\sigma_g^2\ 1\pi_u^4$. The SCF wave function for the neutral C_2H_2 molecule was constructed from a [3s2p|2s] Cartesian Gaussian basis set contracted from a primitive (9s5p|4s) basis[31] augmented with a set of d and p polarization functions on the C and H centers respectively. The exponent for the d function was 0.75 and 1.0 for the p function. The calculations were done at the equilibrium geometry with C-C and C-H bond lengths of 2.2734 a.u. and 2.003 a.u. respectively. The SCF energy with this basis and geometry is -76.831406 a.u.

To obtain the final state one-electron continuum functions used in these studies, the various matrix elements associated with Eq.(6) must be evaluated. All matrix elements were computed by a single-center expansion technique with radial integrals obtained using a Simpson's rule quadrature. Detailed discussions of the numerical methods used have been given elsewhere.[16,17] The various partial wave expansion parameters were chosen as follows:

(1) maximum partial wave included in the expansion of the scattering solution = ℓ_p = 10(σ_g,π_g), 11(σ_u,π_u), and 8(δ_g);

(2) maximum partial wave retained in the expansion of the occupied orbitals in the direct potential = ℓ_i^{dir} = 30;

(3) maximum partial wave retained in the expansion of the occupied orbitals in the exchange terms = ℓ_i^{ex} = 20($1\sigma_g$), 12($2\sigma_g$), 12($3\sigma_g$), 19($1\sigma_u$), 11($2\sigma_u$), and 11($1\pi_u$);

(4) maximum partial wave retained in the expansion of $1/r_{12}$ in the direct potential = $\lambda_m^{dir} = 60$;

(5) maximum partial wave retained in the expansion of $1/r_{12}$ in the exchange terms = $\lambda_m^{ex} = 30$.

All other partial wave expansions were truncated at $\ell = 30$. For the radial integrations, the grid contained 1000 points and extended to 79 a.u. with the smallest step size being 0.01a.u. and the largest step size 0.16 a.u.

Table I lists the initial basis sets used in Eq.(6) for each symmetry. The basis set contained spherical Gaussian functions, defined by

$$\alpha(\vec{r}) = N_{\gamma,\ell,m} \, |\vec{r} - \vec{A}|^{\ell} \, e^{-\gamma|\vec{r} - \vec{A}|^2} \, Y_{\ell m}(\Omega_{\vec{r}-\vec{A}}) \, . \qquad (8)$$

A. The $X\,^2\Pi_u$ state

In photoionization leading to the $X\,^2\Pi_u$ state of $C_2H_2^+$, an electron is ejected from the $1\pi_u$ orbital into a continuum orbital of σ_g, π_g, or δ_g symmetry. We take the ionization potential for this channel to be 11.4eV.[33] Figure 1 shows the $k\sigma_g$, $k\pi_g$, and $k\delta_g$ components of this cross section obtained using continuum functions which are solutions of the appropriate static-exchange potential for the singlet-coupled final states, e.g., $^1\Sigma_u^+(1\pi_u^3 k\pi_g)$. Results using continuum solutions obtained after one iteration and a Hartree-Fock initial wave function are shown. In Fig. 2 we compare

the calculated total cross sections with the synchrotron radiation measurements of Unwin and Bradshaw.[20] This data has been normalized to our calculated dipole length cross sections at a photon energy of 24eV.

A comparison of the cross sections in Fig. 2 shows clearly that the double bump structure around 14eV is due to autoionizing resonances, the effects of which are not included in the present calculations. This structure has been interpreted previously in terms of autoionization[6,20] but our results indicate that the prominent peaks around 13eV and 15eV are due to one, or possibly two, autoionizing resonances interacting with a shape-resonance enhanced background continuum. This is essentially the interpretation of these features recently given by Parr et al.[6] in which the autoionizing transitions were identified as $3\sigma_g \rightarrow n\sigma_u$ and $2\sigma_u \rightarrow 1\pi_g$ at around 13.3eV and 15.5eV respectively. We note that the $3\sigma_g \rightarrow n\sigma_u$ ($^1\Sigma_u^+$) and $2\sigma_u \rightarrow 1\pi_g(^1\Pi_u)$ transitions will be coupled to the $1\pi_u \rightarrow k\pi_g(^1\Sigma_u^+)$ and $1\pi_u \rightarrow k\sigma_g$, $k\delta_g(^1\Pi_u)$ continua respectively. Recently, Levine and Soven,[34] using a time-dependent local-density approximation to the RPA, accounted for the 15.5eV peak and about half of the peak at around 13eV assuming a single $2\sigma_u \rightarrow 1\pi_g$ autoionizing resonance. In this model substantial intensity is shifted from below the ionization threshold in the continuum due to electron correlation. This view differs from our present suggestion that the $1\pi_g \rightarrow n\pi_g$ state already lies in the continuum at the Hartree-Fock level of approximation.

The cross sections of Fig. 1 show the shape-resonance enhancement of the π_g continuum. This enhancement is due to the "$1\pi_u \rightarrow 1\pi_g$" transition which lies in the continuum, at least in the Hartree-Fock approximation. No definitive assignment of an intravalence $^1\Sigma_u^+(1\pi_u \rightarrow 1\pi_g)$ transition has yet been made in the discrete spectrum of acetylene. If such a transition does lie well below the $^2\Pi_u$ ionization threshold, then the enhancement of the $1\pi_u \rightarrow k\pi_g$ cross sections in Fig. 2 could be an artifact of our Hartree-Fock description of the final state

wave function in which electron correlation effects are neglected. This is exactly what happens in the $1\pi_u \rightarrow k\pi_g$ continuum of N_2 where the $^1\Sigma_u^+(1\pi_u \rightarrow 1\pi_g)$ intravalence state is clearly spuriously pushed into the continuum in the Hartree-Fock approximation.[28] In Ref. 16 and 28 this deficiency of the Hartree-Fock potential was removed by constructing the $k\pi_g$ continuum to be orthogonal to the valence-like $1\pi_g$ orbital of the $^3\Sigma_u^+(1\pi_u \rightarrow 1\pi_g)$ state. As expected, the resulting cross section was substantially reduced and, in fact, was essentially equivalent to those obtained using the $k\pi_g$ continuum of the static-exchange potential of the $^3\Sigma_u^+(1\pi_u \rightarrow 1\pi_g)$ state, i.e.,the triplet potential. Figure 3 compares the cross sections for the $^2\Pi_u$ state in which the $k\pi_g$ contribution was obtained with continuum solutions of the singlet and triplet potentials. With the use of the triplet potential all evidence of the shape resonance has disappeared and the corresponding cross section has been reduced to a very small value. The use of the triplet $k\pi_g$ continuum is extreme since we have seen that it is virtually equivalent to orthogonalization to a very valence-like π_g orbital of the $^3\Sigma_u^+(1\pi_u^3\, 1\pi_g)$ state which lies at around 5.2eV.[35] The $^1\Sigma_u^+(1\pi_u^3 1\pi_g)$ state lies at higher energy and its π_g orbital can be substantially different from that of the triplet state. In fact, extensive RPA calculations give a valence-like $^1\Sigma_u^+$ state at 12.95eV with an oscillator strength of about 0.5.[36] This result indicates that the valence-like $^1\Sigma_u^+$ state may actually be in the $^2\Pi_u$ continuum or, if not, at least close to its threshold. The probable role of final-state correlation effects on this shape

resonance along with the autoionizing features in this same spectral region will make studies of these cross sections both challenging and fruitful. Absolute measurements of these cross sections would be useful.

A comparison of the results of Fig. 1 and 2 obtained with the dipole length and velocity forms of the oscillator strength again shows that electron correlation effects are important in these photoionization cross sections. Such effects are expected to be more pronounced in the $k\pi_g$ subchannel than in the $k\sigma_g$ and $k\delta_g$. The difference between these two forms of the cross sections is substantial even out at a photon energy of 24eV where the experimental results of Ref. 20 were normalized to the length form of the calculated cross sections in Fig. 2. With this choice of normalization, the autoionizing feature around 15eV has a cross section close to 60 Mb while Fig. 4 shows that a similar normalization to the velocity cross sections at 24eV gives the same feature a cross section of about 30 Mb. Although the synchrotron radiation measurements of Unwin and Bradshaw[20] are relative, the absolute cross sections in this spectral region have been studied with conventional light sources.[25,37,38] The measurements of Walker and Weissler[37] and of Schoen[38] both give a value of about 60 Mb for the cross section for the autoionizing feature at 15eV whereas Metzger and Cook[25] report a value of about 37 Mb. The discrepancy between these two measurements is large enough that one cannot unambiguously decide, on this basis, which normalization of Unwin et al.'s data, e.g., to the calculated length cross sections of Figs. 2 or 3, leads to the correct cross sections. This is unfortunate since such a comparison would tell

whether the $1\pi_u \rightarrow k\pi_g$ shape resonance feature in the cross sections of Fig. 2 is spurious or not. However, a comparison of the relative data of Unwin et al.[20] with the measurements of Refs. 25, 37 and 38 does suggest that the normalized cross sections of Fig. 1 are probably closer to the correct ones. Such a conclusion would indicate that the $k\pi_g$ continuum is shape resonant.

In Fig. 5 we compare our calculated photoionization cross sections with those of the continuum multiple scattering model.[21] There are clearly substantial differences between these two sets of cross sections which arise primarily from the $k\pi_g$ and $k\delta_g$ continua. In the π_g continuum this difference must be due to the sensitivity of the cross section on the implied location of the "$1\pi_u \rightarrow 1\pi_g$" transition relative to threshold. Differences in the $1\pi_u \rightarrow k\delta_g$ component result more directly from the approximate potentials assumed in the multiple scattering model.

Figure 6 compares the $1\pi_u^{-1}$ cross sections obtained by the Stieltjes moment theory method[24] with our calculated cross sections of Fig. 3. In these moment theory calculations the $1\pi_u \rightarrow k\pi_g$ contribution was obtained with the triplet-coupled potential, a procedure we have shown to be essentially equivalent to orthogonalizing the singlet π_g continuum functions to the valence-like $1\pi_g$ orbital.[16,28] Moreover, the $1\pi_u \rightarrow k\delta_g$ partial channel cross section was also calculated with the triplet potential since the singlet potential appropriate to the $1\pi_u^3 k\delta_g$ configuration is not expressible in terms of the usual Coulomb and exchange operators when real valued molecular orbitals are used.

The moment theory calculations[24] were performed using standard bound state computer codes which require that all potentials be expressible in terms of the usual J and K operators. In our cross sections of Fig. 3 the π_g contribution is obtained with the triplet potential but for the δ_g component we used the correct singlet-coupled potential. The significant difference at low energy between the present cross sections and those of the moment theory occurs in the δ_g component. In fact, the use of the triplet potential in this channel has led to a broad peak in the cross section around 12 to 13eV which is not present if the correct singlet potential is used and which fortuitously coincides with the first peak of the double bump structure observed around 13eV.

In Fig. 7 we compare our calculated asymmetry parameters for the $1\pi_u$ orbital with the measured values of Parr et al.[6] for the $\nu_2 = 0$ vibrational band and with the multiple scattering results of Ref. 22. For clarity, we do not show the complete set of data actually reported in Ref. 6. We also choose to compare our fixed-nuclei results with the measured values of the $\nu_2 = 0$ band since this is the dominant vibrational transition. The calculated asymmetry parameters clearly do not show the strong dip around 14eV seen in the measured data and which is clearly due to an autoionizing resonance. Characteristically of photoionization of a π orbital the calculated parameters rise rapidly from a low value near threhold to a value of about unity at higher energy. The calculated parameters are obtained with the singlet-coupled potential. The parameters obtained with the triplet potential are similar in shape to those of

Fig. 7 but notably smaller in magnitude between threshold and 20eV.

B. The $A^2\Sigma_g^+$ state

In the one-electron picture used here the $A^2\Sigma_g^+$ channel corresponds to photoionization from the $3\sigma_g$ orbital into the σ_u or π_u continuum. Figure 8 shows the calculated photoionization cross sections using continuum solutions obtained after one iteration and a Hartree-Fock initial state wave function. The use of à correlated initial state wave function changed these cross sections only slightly and hence, for this and the remaining channels, we will discuss only the results obtained with a Hartree-Fock initial state. In Fig. 8 we also show the synchrotron radiation measurements of Unwin and Bradshaw[20] normalized to the calculated dipole length cross sections at a photon energy of 20eV. Our photon energy scale assumes the experimental ionization potential of 16.4eV.[33]

The sharp feature in these cross sections just above threshold is caused by the shape resonance in the σ_u continuum. This behavior is clearly analogous to that of the $3\sigma_g \rightarrow k\sigma_u$ channel in N_2 and, moreover, the shift in the shape resonant activity from a photoelectron kinetic energy of 15eV in N_2 to about 2eV in C_2H_2 is consistent with the changes in nuclear separations of these two molecules. With the experimental data arbitrarily normalized to the calculated values at 24eV, our peak cross sections near threshold are obviously too low. The difference between the calculated and observed cross sections in this important region clearly depends on where this

normalization is carried out. Absolute measurements of these cross sections would be useful. Our cross sections and those of the Stieltjes moment theory method[24] show the same overall behavior.

The calculated asymmetry parameters of Fig. 9 show the expected dip near threshold and agree quite well with the measurements of Keller[22] which unfortunately do not extend to low enough energy to show the rapid change in β predicted near threshold. Extension of these measurements to lower energies would be desirable. The β values based on the multiple scattering model[22] do not agree very well with either our calculated values or with the experimental data.[22]

In Fig. 10 we show the calculated eigenphase sum for the σ_u continuum of this $A^2\Sigma_g^+$ ion. The rapid increase in this eigenphase sum between threshold and around 21eV is obviously due to the shape resonance responsible for the pronounced features in both the fixed-nuclei cross section and asymmetry parameters of Figs. 8 and 9 respectively. However, the behavior of the eigenphase sum above 35eV indicates the presence of a broad resonance which does not have any noticeable effect on the calculated vibrationally unresolved cross section or asymmetry parameters. The effect of this broad shape resonance may be more evident in vibrationally resolved cross sections or in photoionization out of lower lying levels.

C. The $B^2\Sigma_u^+$ state

In the $B^2\Sigma_u^+$ channel photoionization occurs out of the $2\sigma_u$ level into the σ_g and π_g continua. Figure 11 shows the $2\sigma_u \rightarrow k\sigma_g$ and $k\pi_g$ components of this cross section along with their sum, the synchrotron radiation measurements of Unwin and Bradshaw,[20] and the cross sections obtained by the Stieltjes moment theory method.[24] The experimental data has been normalized to our calculated cross sections at a photon energy of 28eV. The photon energy scale assumes an ionization potential of 18.7eV.[33]

From the results of Fig. 11 we see that the calculated cross sections rise too rapidly below 25eV and are considerably larger than the measured values near threshold. Although this behavior is more pronounced in the σ_g continuum, it is also evident in the π_g cross sections. In contrast the experimental cross sections are quite flat over the range of photon energies in Fig. 11. As suggested previously,[24] this behavior in the $2\sigma_u \rightarrow k\sigma_g$ photoionization cross sections is caused by a discrete valence-like $2\sigma_u \rightarrow n\sigma_g$ transition about 1eV below ionization which leads to this threshold value. We believe that the similar behavior of the π_g cross sections is probably due to the influence of the intense discrete $2\sigma_u \rightarrow n\pi_g$ transition.[24] We note that in N_2, the calculated $2\sigma_u$ photoionization cross sections did not show these large threshold values in either the σ_g or π_g continuum and, in fact, were quite flat and in good agreement with the measured values.[16] For N_2 the calculated spectrum of excitation frequencies and oscillator strengths[39] does not show any analogous

strong $2\sigma_u \rightarrow n\sigma_g$ discrete transition and the relevant intense $2\sigma_u \rightarrow n\pi_g$ transition occurs near 5eV below threshold, about 2eV lower than in the case of C_2H_2. Finally, our calculated cross sections are quite similar to those of the Stieltjes moment theory method.[24]

Figure 12 shows the calculated asymmetry parameters for the $2\sigma_u$ level. The behavior of these β values near threshold is again probably influenced by the strong $2\sigma_u \rightarrow n\sigma_g$ transition just below threshold. The single experimental result shown is the value reported for vertical ionization at the HeI line.[40]

D. The $2\sigma_g$ level

For ionization out of this inner-valence region in C_2H_2 and other hydrocarbons, the intensities of satellite bands can be substantial and hence the association of one spectral line with photoionization out of a particular molecular orbital becomes less valid.[41] Of the two bands at 23.5 and 27.5eV that can be associated with ionization from the $2\sigma_g$ level, the $2\sigma_g$ ionization potential is assigned to the dominant peak at 23.5eV.[41] For the present purposes, we will present cross sections assuming that ionization occurs exclusively from the $2\sigma_g$ level. These cross sections display the important characteristics of the electronic continua and can, moreover, be used in conjunction with amplitudes and poles of the one-body Green's function to obtain the correct intensities.[41]

Figure 13 shows the calculated photoionization cross sections for this level along with the results obtained by the STMT method.[24] These cross sections show the enhancement due to the shape resonant behavior of the σ_u continuum around 26eV and again around 45eV. From these cross sections, as well as from the associated σ_u eigenphase sums in Fig. 14, we see that the resonance at higher energy is considerably broader than the resonance near threshold. The σ_u eigenphase sum for this channel is quite similar to that of the $3\sigma_g^{-1}$ channel but, whereas the enhancement of the cross section due to the higher energy shape resonance is quite evident for ionization out of this inner-valence $2\sigma_g$ level, no such enhancement is seen in the vibrationally unresolved cross sections for the valence $3\sigma_g$ level. By comparison, the cross sections of the STMT method indicate that this approach has smoothed away the broad double-hump structure in our cross sections caused by these two shape resonances.

Figure 15 shows the β parameters for this level calculated in the dipole length approximation. The effect of the near-threshold shape resonance on these β parameters is very evident whereas there is essentially no effect due to the higher energy resonance. Vibrationally resolved studies of these angular distribution parameters would be useful.

E. The K-shell

Figure 16 shows the four partial cross sections for photoionization from the $1\sigma_g$ and $1\sigma_u$ K-shell levels. The photon

energy scale in this figure assumes an ionization potential of 291.1eV.[23] The $1\sigma_g$ cross section is dominated by the σ_u shape resonance which has a peak position at about 311eV. The low energy resonance feature in this continuum seen in the $2\sigma_g$ and $3\sigma_g$ cross sections is no longer present suggesting that the resonance state has moved below threshold. For comparison we also show the values for this $1\sigma_g \rightarrow k\sigma_u$ cross section obtained by the STMT method.[24] The STMT results show a slightly broader resonance feature with a peak value and position shifted to lower values. The $1\sigma_u \rightarrow k\sigma_g$ partial cross section is again relatively large near threshold reflecting the influence of the valence-like $1\sigma_u \rightarrow n\sigma_g$ transition.

The four components of the $1\sigma_g$ and $1\sigma_u$ cross sections of Fig. 16 are combined in Fig. 17 and compared with the measured (e,2e) intensities for K-shell photoionization[23] and with the results of the STMT method.[24] Both sets of calculated intensities were obtained from the corresponding photoionization cross sections.[42] The present results have been normalized to the experimental intensities at 320eV. Normalization was carried out at 320eV in order to avoid the threshold region where shake-up effects are evident. Moreover, both sets of calculated cross sections agreed at this energy. A comparison of these cross sections shows that the resonance feature around 310eV is more pronounced in our results than in both the experimental or STMT intensities. This difference between the calculated intensities comes primarily from the behavior in the $1\sigma_g \rightarrow k\sigma_u$

channel. These differences can be due to the use of too few spectral points in the region of the shape resonance in the STMT studies.[17] Vibrational averaging of these resonant cross sections could broaden these calculated intensities and remove some of the differences between our results and the experimental data in this region. The calculated K-shell asymmetry parameters are shown in Fig. 18. The effects of the shape resonance around 310eV is clearly evident. No measured values of these parameters have been reported.

IV. CONCLUSION

Accurate fixed-nuclei frozen-core Hartree-Fock photoionization cross sections have been obtained for the valence, inner-valence, and K-shell orbitals of C_2H_2. We have compared these cross sections with available experimental data and with the results of calculations by the STMT method and the multiple scattering approach. These comparisons illustrate the need to obtain photoionization cross sections at the Hartree-Fock continuum level as an initial step in the understanding of molecular photoionization spectra. For example, the present results show that a shape-resonance enhanced π_g continuum may play an important role in the $^2\Pi_u(1\pi_u^{-1})$ photoionization cross sections in the same 11-16eV region where features due to autoionizing resonances are now well established.[6,20] Further clarification of the underlying resonant structure in this spectral region will require studies of these cross sections which include final state correlation effects for both

the shape and autoionizing resonances. Absolute measurements of the vibrationally resolved cross sections in this region are needed. Another important conclusion of these studies concerns the behavior of the σ_u continuum where two shape resonances are seen. For ionization out of the $3\sigma_g$ level the lower energy resonance is very pronounced in both the cross sections and asymmetry parameters whereas the higher energy resonance is not at all evident in these fixed-nuclei results. Vibrationally resolved studies in the region of this higher energy shape resonance would be useful. On the other hand the effects of both shape resonances are obvious in photoionization out of the inner-valence $2\sigma_g$ level.

ACKNOWLEDGMENTS

One of the authors (VMcK) thanks Wolfgang Domcke for several helpful discussions concerning these results. We also thank Jeffrey Nichols and Danny Yeager for providing us with the results of their calculations on the excitation spectrum of C_2H_2. This material is based upon work supported by the National Science Foundation under Grant No. CHE-8218166. The authors acknowledge computing support from the National Center for Atmospheric Research (NCAR) which is sponsored by the National Science Foundation. The research reported in this paper made use of the Dreyfus-NSF Theoretical Chemistry Computer which was funded through grants from the Camille & Henry Dreyfus Foundation, the National Science Foundation (Grant No. CHE78-20235), and the Sloan Fund of the California Institute of Technology.

REFERENCES

[1]J. B. West, A. C. Parr, B. E. Cole, D. L. Ederer, R. Stockbauer, and J. L. Dehmer, J. Phys. B 13, L105 (1980).

[2]R. Stockbauer, B. E. Cole, D. L. Ederer, J. B. West, A. C. Parr, and J. L. Dehmer, Phys. Rev. Lett. 43, 757 (1979).

[3]B. E. Cole, D. L. Ederer, R. Stockbauer, K. Codling, A. C. Parr, J. B. West, E. D. Poliakoff, and J. L. Dehmer, J. Chem. Phys. 72, 6308 (1980).

[4]T. A. Carlson, M. O. Krause, D. Mehaffy, J. W. Taylor, F. A. Grimm, and J. D. Allen, J. Chem. Phys. 73, 6056 (1980).

[5]E. W. Plummer, T. Gustafsson, W. Gudat, and D. E. Eastmann, Phys. Rev. A 15, 2339 (1977).

[6]A. C. Parr, D. L. Ederer, J. B. West, D. M. P. Holland, J. L. Dehmer, J. Chem. Phys. 76, 4349 (1982).

[7]J. L. Dehmer, D. Dill, and S. Wallace, Phys. Rev. Lett. 43, 1005 (1979).

[8]N. Padial, G. Csanak, B. V. McKoy, and P. W. Langhoff, J. Chem. Phys. 69, 2992 (1978).

[9]R. R. Lucchese and V. McKoy, J. Phys. B. 14, L629 (1981).

[10]R. R. Lucchese and V. McKoy, J. Phys. Chem. 85, 2166 (1981).

[11]G. Raseev, H. Le Rouzo, and H. Lefebvre-Brion, J. Chem. Phys. 72, 5701 (1980).

[12]N. Padial, G. Csanak, B. V. McKoy, and P. W. Langhoff, Phys. Rev. A 23, 218 (1981).

[13]A. Gerwer, C. Asaro, B. V. McKoy, and P. W. Langhoff, J. Chem. Phys. 72, 713 (1980).

[14]A. E. Orel, T. N. Rescigno, B. V. McKoy, and P. W. Langhoff, J. Chem. Phys. 72, 1265 (1980).

[15]R. R. Lucchese, D. K. Watson, and V. McKoy, Phys. Rev. A 22, 421 (1980).

[16]R. R. Lucchese, G. Raseev, and V. McKoy, Phys. Rev. A 25, 2572 (1982).

[17]R. R. Lucchese and V. McKoy, Phys. Rev. A 26, 1406 (1982).

[18]M. E. Smith, R. R. Lucchese, and V. McKoy, J. Chem. Phys. (accepted for publication).

[19]R. R. Lucchese and V. McKoy, Phys. Rev. A (accepted for publication).

[20]P. W. Langhoff, B. V. McKoy, R. Unwin, and A. Bradshaw, Chem. Phys. Lett. 83, 270 (1981).

[21]J. Kreile, A. Schweig, and W. Thiel, Chem. Phys. Lett. 79, 547 (1981).

[22]P. R. Keller, D. Mehaffy, J. W. Taylor, F. A. Grimm, and T. A. Carlson, J. Electron Spectrosc. 27, 223 (1982).

[23]A. P. Hitchcock and C. E. Brion, J. Electron Spectrosc. 10, 317 (1977); 22, 283 (1981).

[24]L. E. Machado, E. P. Leal, G. Csanak, B. V. McKoy, and P. W. Langhoff, J. Electron Spectrosc. 25, 1 (1982).

[25]P. H. Metzger and G. R. Cook, J. Chem. Phys. 41, 642 (1964).

[26]R. Unwin, I. Khan, N. V. Richardson, A. M. Bradshaw, L. Cederbaum, and W. Domcke, Chem. Phys. Lett. 77, 242 (1981).

[27]R. R. Lucchese and V. McKoy, XII International Conference on the Physics of Electronic and Atomic Collisions, Book of Abstracts, July 15-21, 1981, Gatlinburg, Tennessee, p. 80.

[28]T. N. Rescigno, A. Gerwer, B. V. McKoy, and P. W. Langhoff, Chem. Phys. Lett. 66, 116 (1979).

[29]R. R. Lucchese and V. McKoy, Phys. Rev. A 24, 770 (1981).

[30]See, for example, W. H. Miller, J. Chem. Phys. 50, 407 (1969).

[31]T. H. Dunning and P. J. Hay, in Modern Theoretical Chemistry 3, ed. H. F. Schaefer III (Plenum, New York, 1977) p. 1.

[32]J. R. Swanson and J. L. Armstrong, Jr., Phys. Rev. A 15, 661 (1977).

[33]D. W. Turner, C. Baker, A. D. Baker, and C. B. Brundle, Molecular Photoelectron Spectroscopy (Wiley, New York, 1970).

[34]Z. H. Levine and P. Soven, Phys. Rev. Lett. 50, 2074 (1983).

[35]S. Trajmar, J. K. Rice, P. S. P. Wei, and A. Kuppermann, Chem. Phys. Lett. 1, 703 (1968).

[36]J. Nichols and D. L. Yeager (private communication).

[37]W. C. Walker and G. L. Weissler, J. Chem. Phys. 23, 1547 (1955).

[38]R. I. Schoen, J. Chem. Phys. 37, 2032 (1962).

[39]T. N. Rescigno, C. F. Bender, B. V. McKoy, P. W. Langhoff, J. Chem. Phys. 68, 970 (1978).

[40]J. Kreile and A. Schweig, Chem. Phys. Lett. 69, 71 (1980).

[41]A. M. Bradshaw, W. Eberhardt, H. J. Levinson, W. Domcke, and L. S. Cederbaum, Chem. Phys. Lett. 70, 36 (1980).

[42] M. Inokuti, Rev. Mod. Phys. 43, 297 (1978).

TABLE I. Starting basis sets for solution of Eq.(6).

Symmetry of continuum solution	Center	ℓ	m	
σ_g	H	0	0	1.0,0.5,0.25
		1	0	1.0,0.5,0.25
	C	0	0	4.0,2.0,1.0,0.5,0.25
		1	0	1.0,0.5,0.25
		2	0	1.0,0.5,0.25
	Origin	0	0	4.0,2.0
		2	0	1.0
		4	0	0.5
		6	0	0.5
σ_u	H	0	0	1.0,0.5,0.25
		1	0	1.0,0.5,0.25
	C	0	0	4.0,2.0,1.0,0.5
		1	0	1.0,0.5
		2	0	1.0,0.5
	Origin	1	0	4.0,2.0
		3	0	1.0
		5	0	0.5
		7	0	0.5
π_u	H	1	1	1.0,0.5,0.25
		2	1	0.5
	C	1	1	1.0,0.5,0.25
		2	1	1.0,0.5,0.25
	Origin	1	1	1.0,0.5
		3	1	1.0,0.5
		5	1	0.5
π_g	H	1	1	1.0,0.5,0.25
		2	1	0.5
	C	1	1	1.0,0.5,0.25
		2	1	1.0,0.5
	Origin	2	1	1.0
		4	1	0.5
		6	1	0.5
δ_g	H	2	2	1.0,0.5,0.25
		3	2	0.5
	C	2	2	1.0,0.5,0.2
		3	2	1.0,0.5,0.25
	Origin	2	2	1.0,0.5
		4	2	1.0,0.5
		6	2	0.5

FIGURE CAPTIONS

Figure 1: The $1\pi_u \rightarrow k\sigma_g$, $k\pi_g$, and $k\delta_g$ partial channel photoionization cross sections for $C_2H_2^+$ (dipole length and dipole velocity forms): ▭▭▭, $1\pi_u \rightarrow k\delta_g$ (length); ⊖⊖, $1\pi_u \rightarrow k\delta_g$ (velocity); ▷–▷, $1\pi_u \rightarrow k\sigma_g$ (length); —+—, $1\pi_u \rightarrow k\sigma_g$ (velocity); ×–×, $1\pi_u \rightarrow k\pi_g$ (length); ◆—◆, $1\pi_u \rightarrow k\pi_g$ (velocity).

Figure 2: Photoionization cross sections for the $X\ ^2\Pi_u$ state of $C_2H_2^+$: ——— , present results using the dipole length form; – – – – , dipole velocity form; ▶ , experimental results (Ref. 20) normalized to the dipole length cross sections at 24eV.

Figure 3: Comparison of the dipole length cross sections for the $X\ ^2\Pi_u$ state of $C_2H_2^+$ using the singlet and triplet potentials to obtain the $1\pi_u \rightarrow k\pi_g$ component: ——— , singlet potential; – – – – triplet potential, experimental results (Ref. 20) normalized to the triplet potential results at 24eV.

Figure 4: Photoionization cross sections for the $X\ ^2\Pi_u$ state of $C_2H_2^+$ (same labels as in Fig. 2 but with the experimental data normalized to the dipole velocity results at 24eV).

Figure 5: Calculated cross sections for the X $^2\Pi_u$ state of $C_2H_2^+$: ——— , present results with the dipole length form and the singlet potential to obtain the $1\pi_u \rightarrow k\pi_g$ component; – – – – , multiple scattering model (Ref. 21).

Figure 6: Calculated cross sections for the X $^2\Pi_u$ state of $C_2H_2^+$: ——— , present results using the triplet potential for the $1\pi_u \rightarrow k\pi_g$ component (dipole length form); – – – –, Stieltjes moment theory results (Ref. 24).

Figure 7: Photoelectron asymmetry parameters for the X $^2\Pi_u$ state of $C_2H_2^+$: — — —, present results using the singlet potential for the $1\pi_u \rightarrow k\pi_g$ component (dipole length form); —— – —— –, multiple scattering results (Ref. 22); □ , experimental results ($\nu_2 = 0$; Ref. 6).

Figure 8: Photoionization cross section for the A $^2\Sigma_g^+$ state of $C_2H_2^+$: ——— , present results (dipole length form); – – – – , present results (dipole velocity form); —— – —— – , Stieltjes moment theory results (Ref. 24); + , experimental results (Ref. 20) normalized to our dipole length cross sections at 20eV.

Figure 9: Photoelectron asymmetry parameters for the A $^2\Sigma_g^+$ state of $C_2H_2^+$: — — —, present results (dipole length form); —— - —— , multiple scattering results (Ref. 22); □ , experimental results (Ref. 22).

Figure 10: Eigenphase sum for the $3\sigma_g \rightarrow k\sigma_u$ component.

Figure 11: Photoionization cross sections for the B $^2\Sigma^+$ state of $C_2H_2^+$: - - - , the $2\sigma_u \rightarrow k\sigma_g$ component; —— - —— - the $2\sigma_u \rightarrow k\pi_g$ component; ——— , $2\sigma_u$ cross section (dipole length form); —— - —— - , Stieltjes moment theory results (Ref. 24); + , experimental results (Ref. 20) normalized to our cross sections at 28eV.

Figure 12: Photoelectron asymmetry parameters for the B $^2\Sigma_u^+$ state of $C_2H_2^+$: ——— , present results (dipole length form); ⬡, experimental result at 21.22eV (Ref.40).

Figure 13: Cross section for the $(2\sigma_g^{-1})$ $^2\Sigma_g^+$ state of $C_2H_2^+$: —⊟— , present results (dipole length form); - - - - , Stieltjes moment theory results (Ref. 24).

Figure 14: Eigenphase sum for the $2\sigma_g \rightarrow k\sigma_u$ component.

Figure 15: Photoelectron asymmetry parameters for the $(2\sigma_g^{-1})$ $^2\Sigma_g^+$ state of $C_2H_2^+$.

Figure 16: Calculated partial channel photoionization cross sections for the K-shell of $C_2H_2^+$ (dipole length form): ——— , $1\sigma_u \rightarrow k\sigma_g$ component; — — — , $1\sigma_u \rightarrow k\pi_g$ component; — – — – , $1\sigma_g \rightarrow k\sigma_u$ component; —— —— , $1\sigma_g \rightarrow k\pi_u$ component; —— – —— – , Stieltjes moment theory results for the $1\sigma_g \rightarrow k\sigma_u$ resonant component (Ref. 24).

Figure 17: K-shell photoionization intensities: ——— , present results normalized to experiment at 320eV; —— – —— –, Stieltjes moment theory results normalized at threshold (Ref. 24); – – – – , experimental results (Ref. 23).

Figure 18: K-shell photoelectron asymmetry parameters (dipole length form).

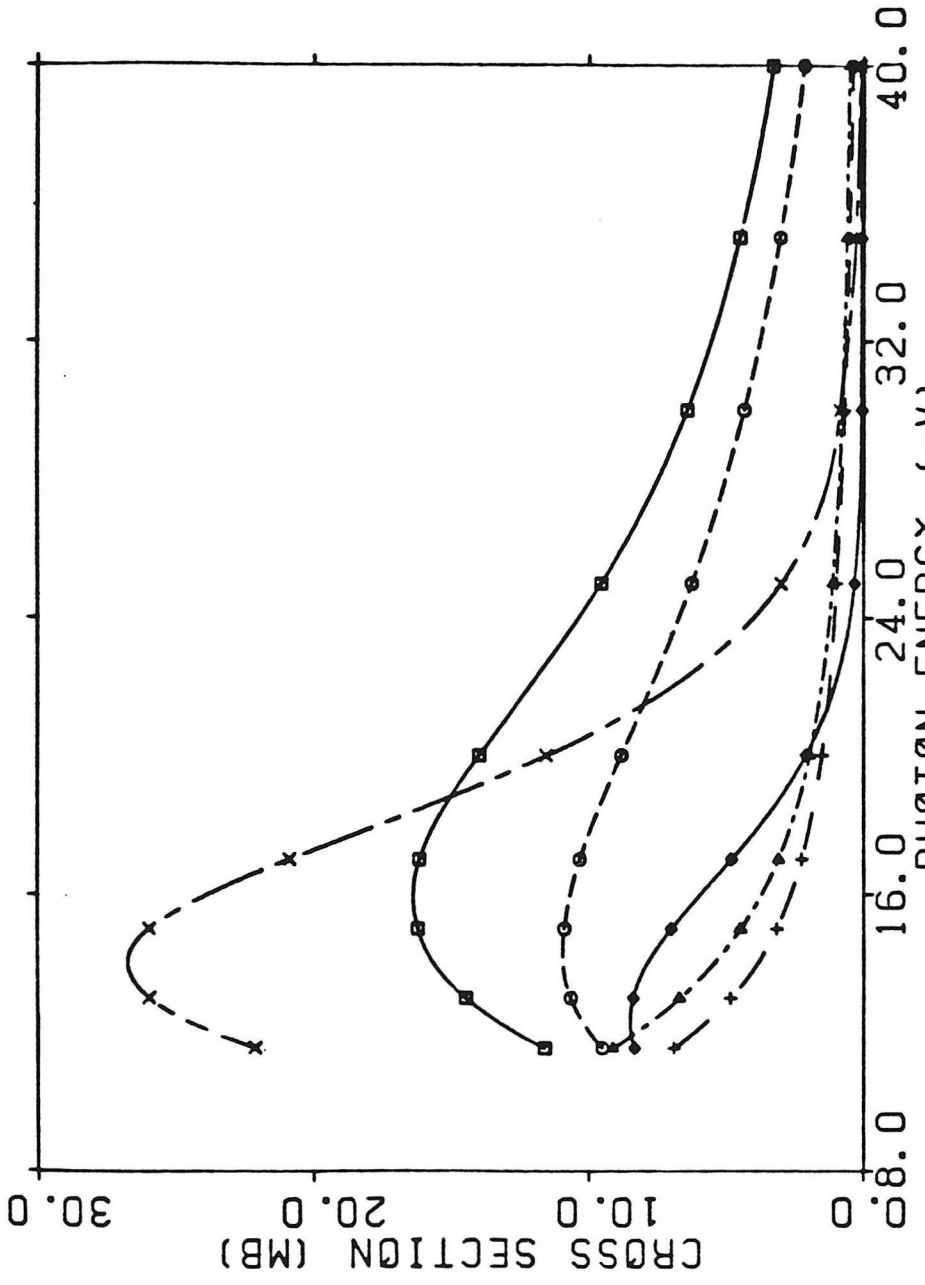
CROSS SECTION (MB)
0.0
10.0
20.0
30.0
8.0
16.0
24.0
32.0
40.0
PHOTON ENERGY (eV)

Figure 1

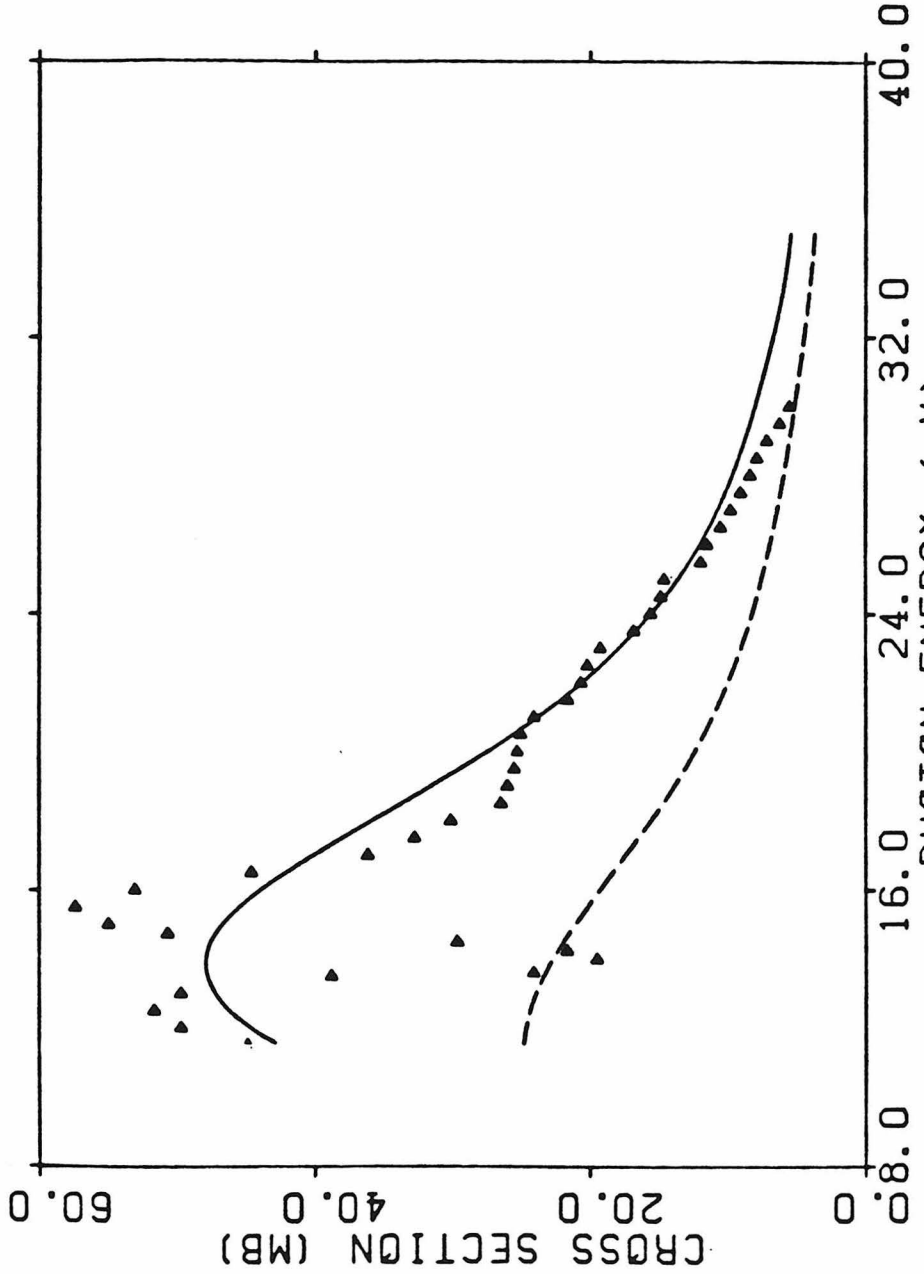
CROSS SECTION (MB)
0.0
20.0
40.0
60.0
8.0
16.0
24.0
32.0
40.0
PHOTON ENERGY (eV)

Figure 2

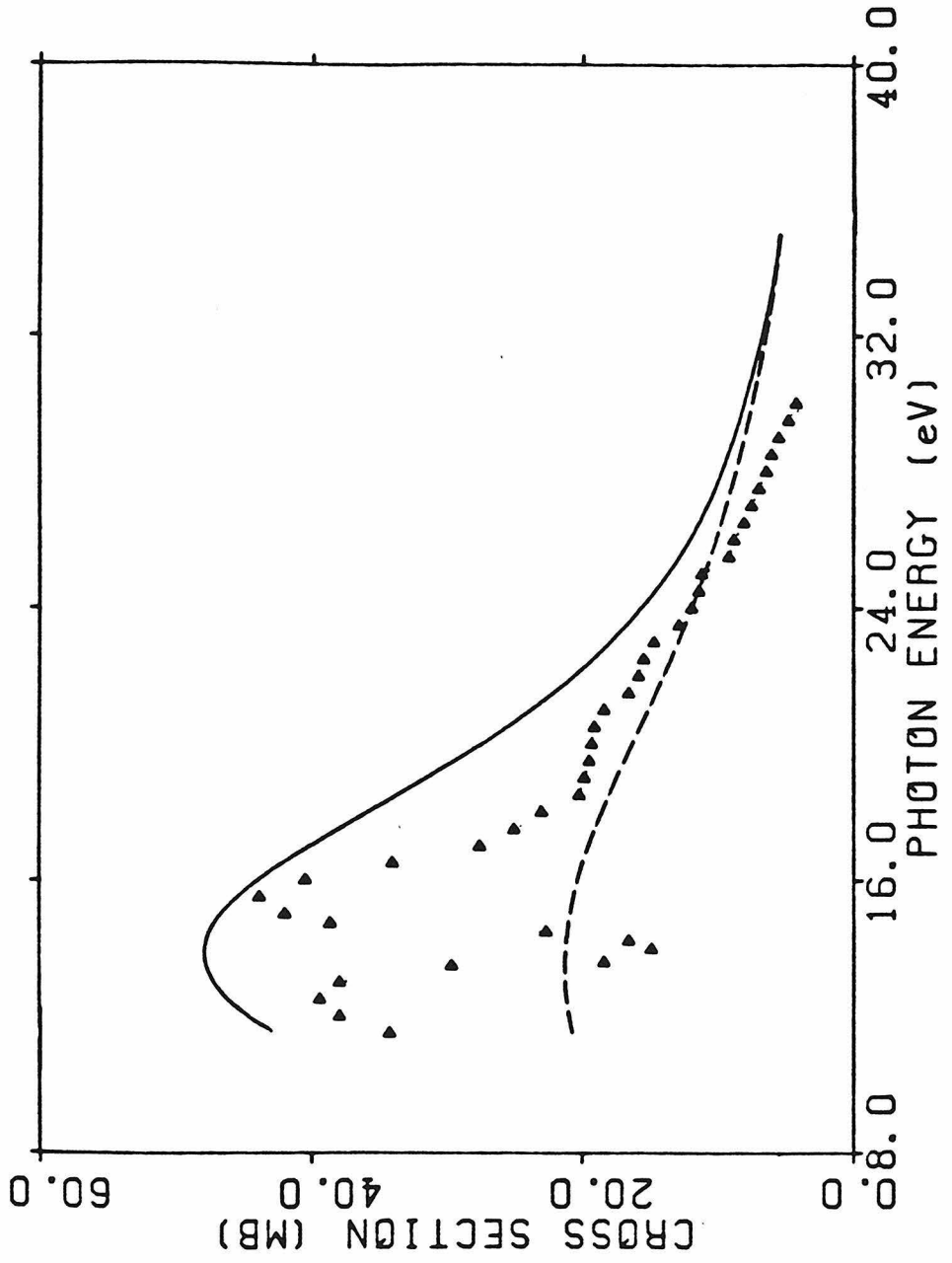
CROSS SECTION (MB)
0.0
20.0
40.0
60.0
8.0
16.0
24.0
32.0
40.0
PHOTON ENERGY (eV)

Figure 3

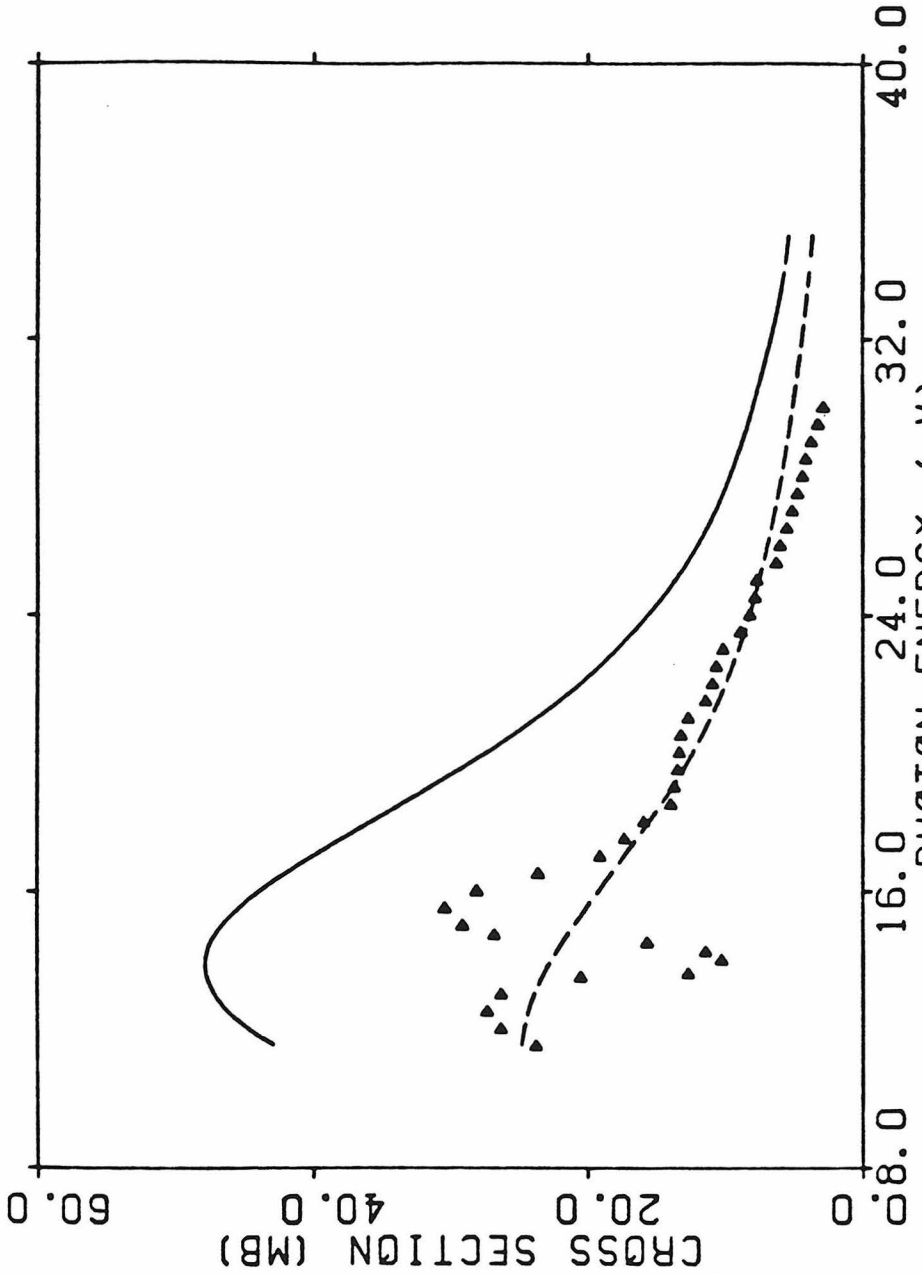
CROSS SECTION (MB)
0.0
20.0
40.0
60.0
8.0
16.0
24.0
32.0
40.0
PHOTON ENERGY (eV)

Figure 4

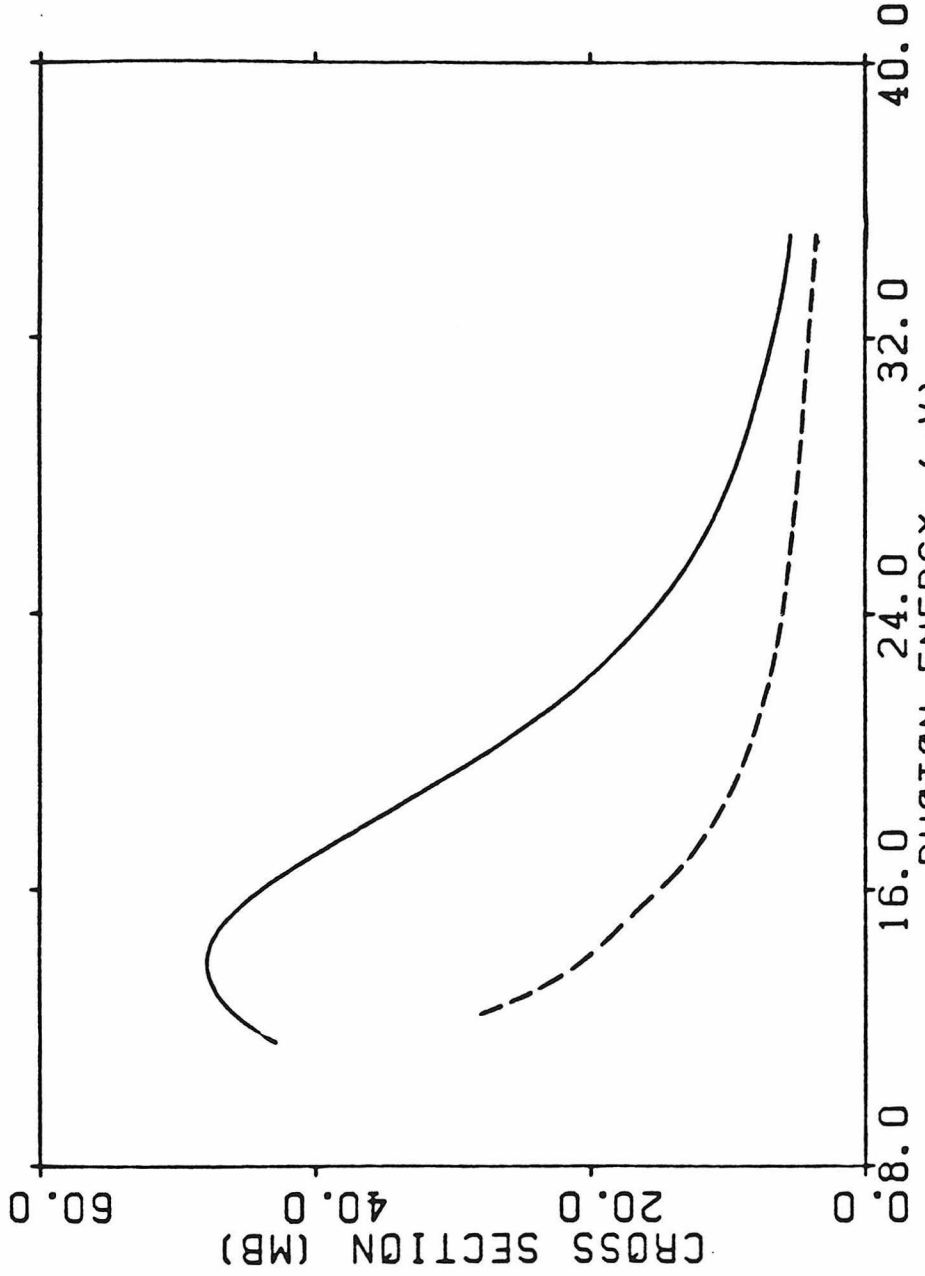
CROSS SECTION (MB)
0.0
20.0
40.0
60.0
8.0
16.0
24.0
32.0
40.0
PHOTON ENERGY (eV)

Figure 5

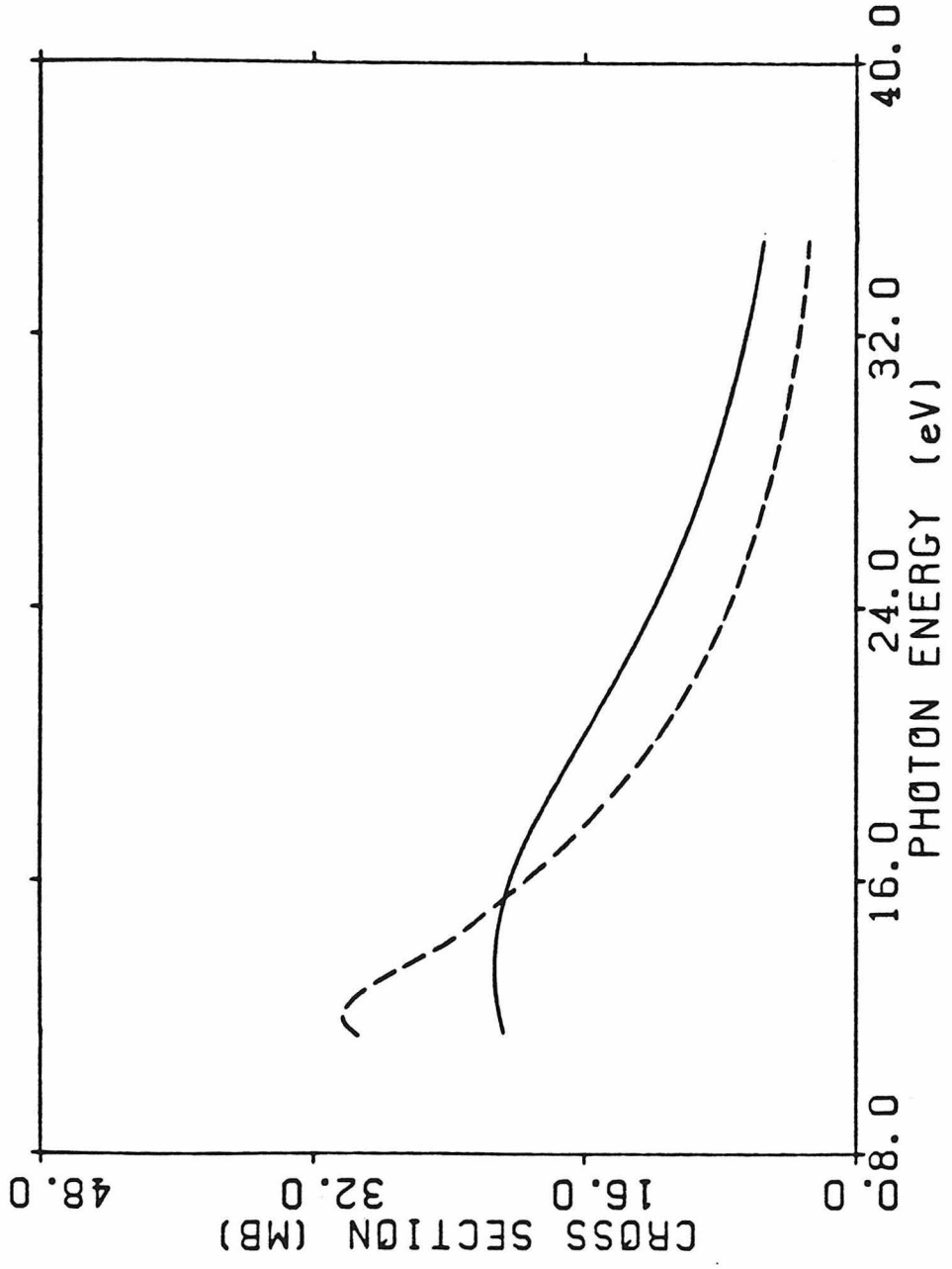
CROSS SECTION (MB)
0.0
16.0
32.0
48.0
8.0
16.0
24.0
32.0
40.0
PHOTON ENERGY (eV)

Figure 6

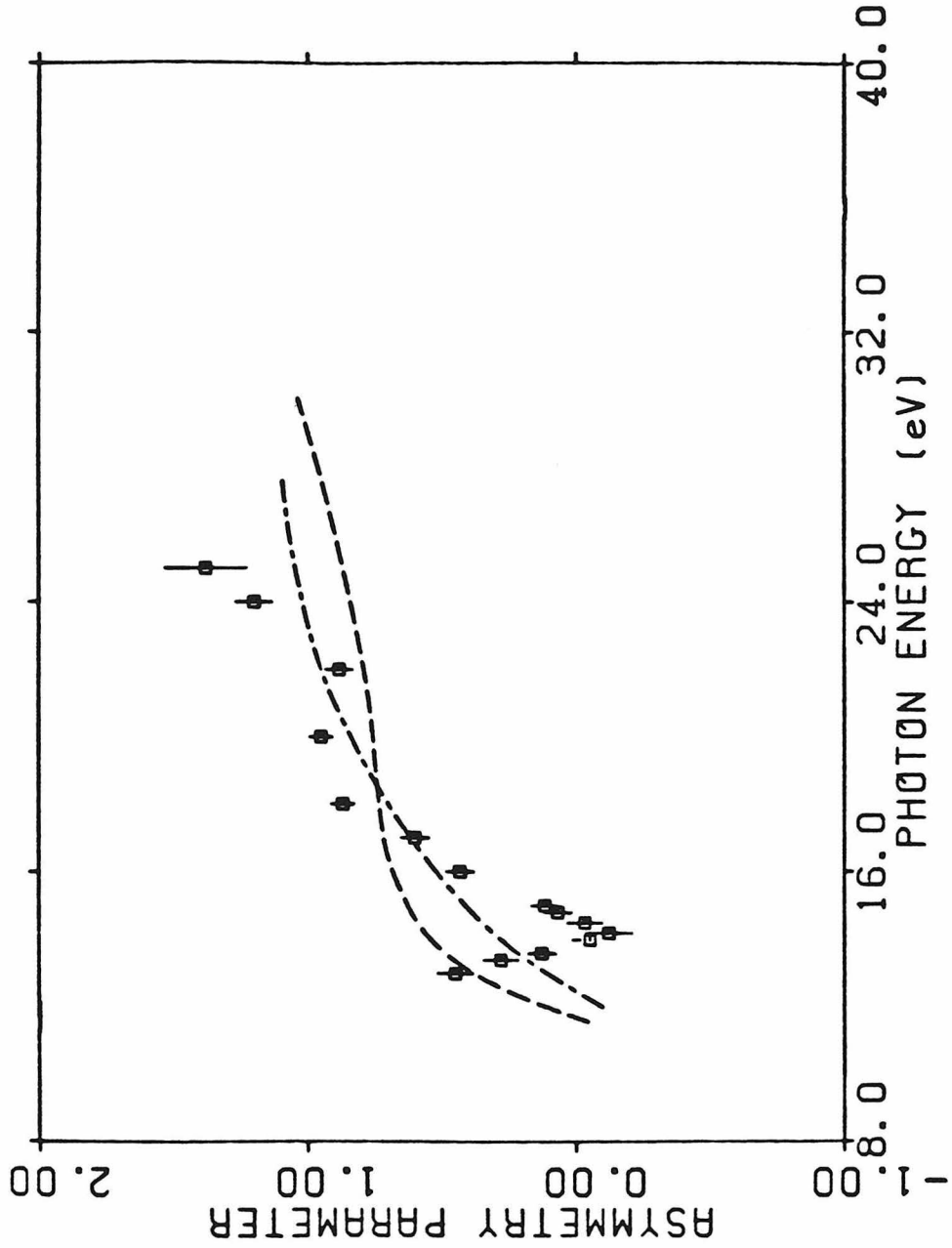
ASYMMETRY PARAMETER
2.00
1.00
0.00
-1.00
8.0
16.0
24.0
32.0
40.0
PHOTON ENERGY (eV)

Figure 7

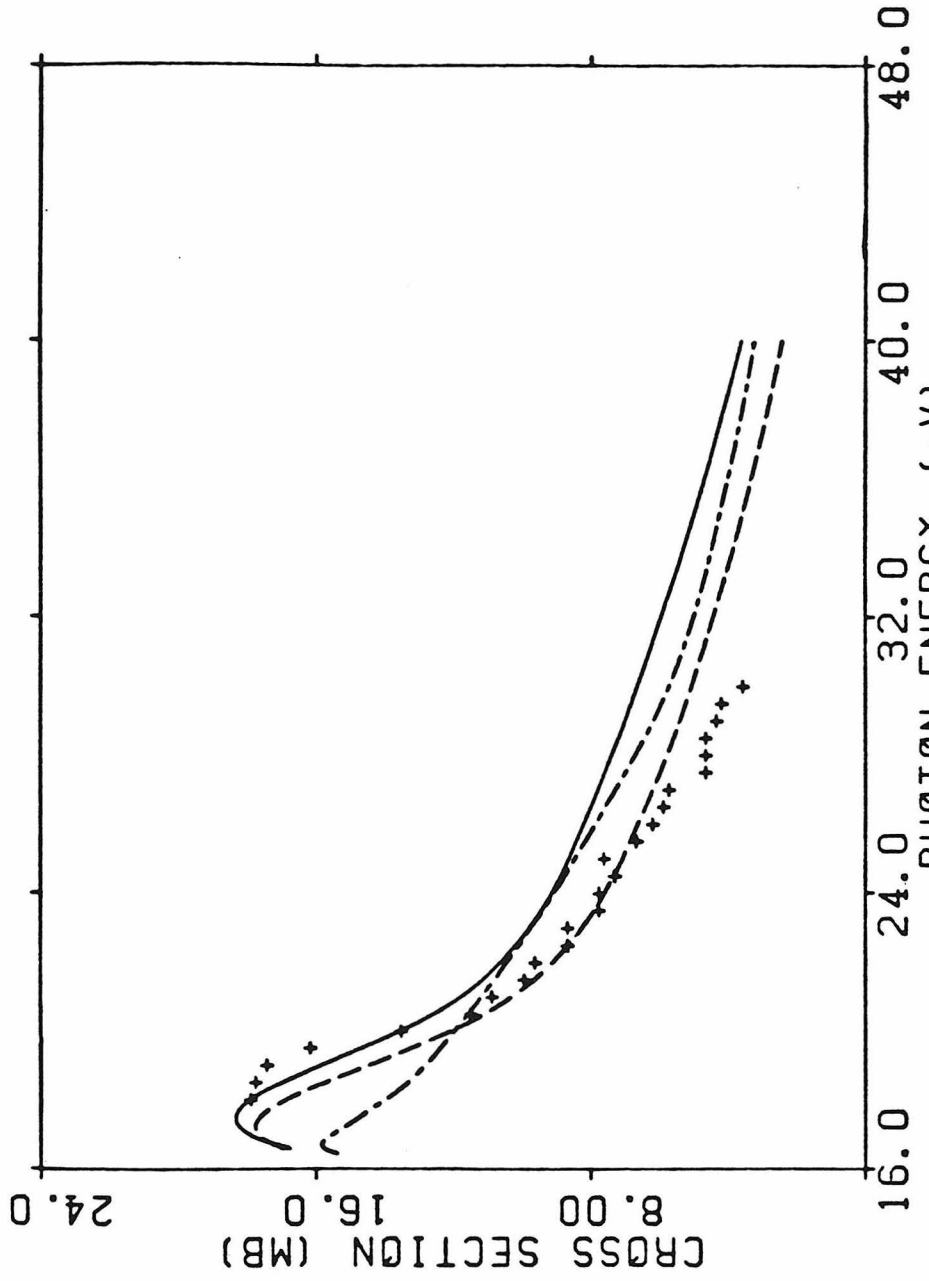
CROSS SECTION (MB)
8.00
16.0
24.0
16.0
24.0
32.0
40.0
48.0
PHOTON ENERGY (eV)

Figure 8

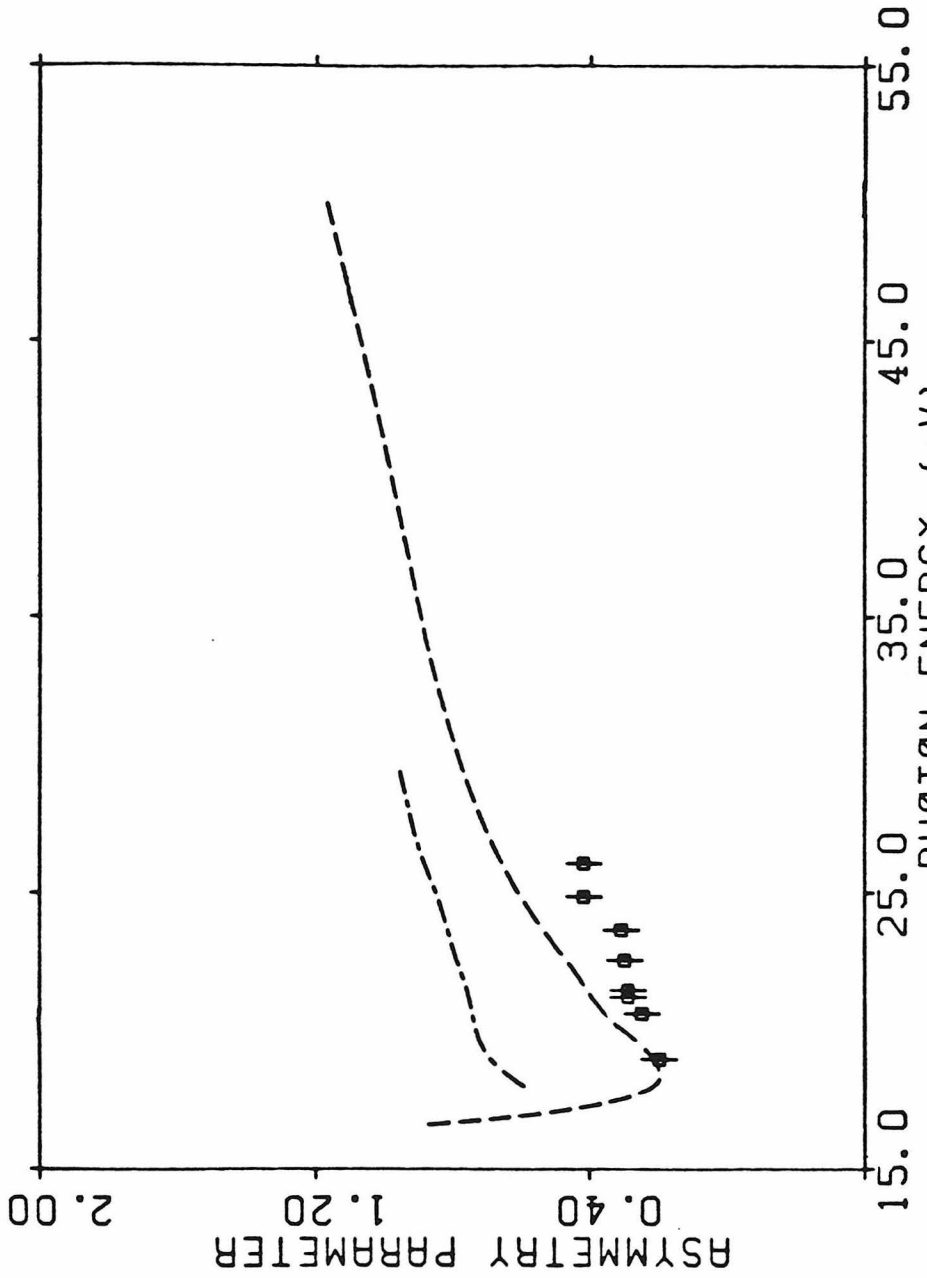
ASYMMETRY PARAMETER
0.40
1.20
2.00
15.0
25.0
35.0
45.0
55.0
PHOTON ENERGY (eV)

Figure 9

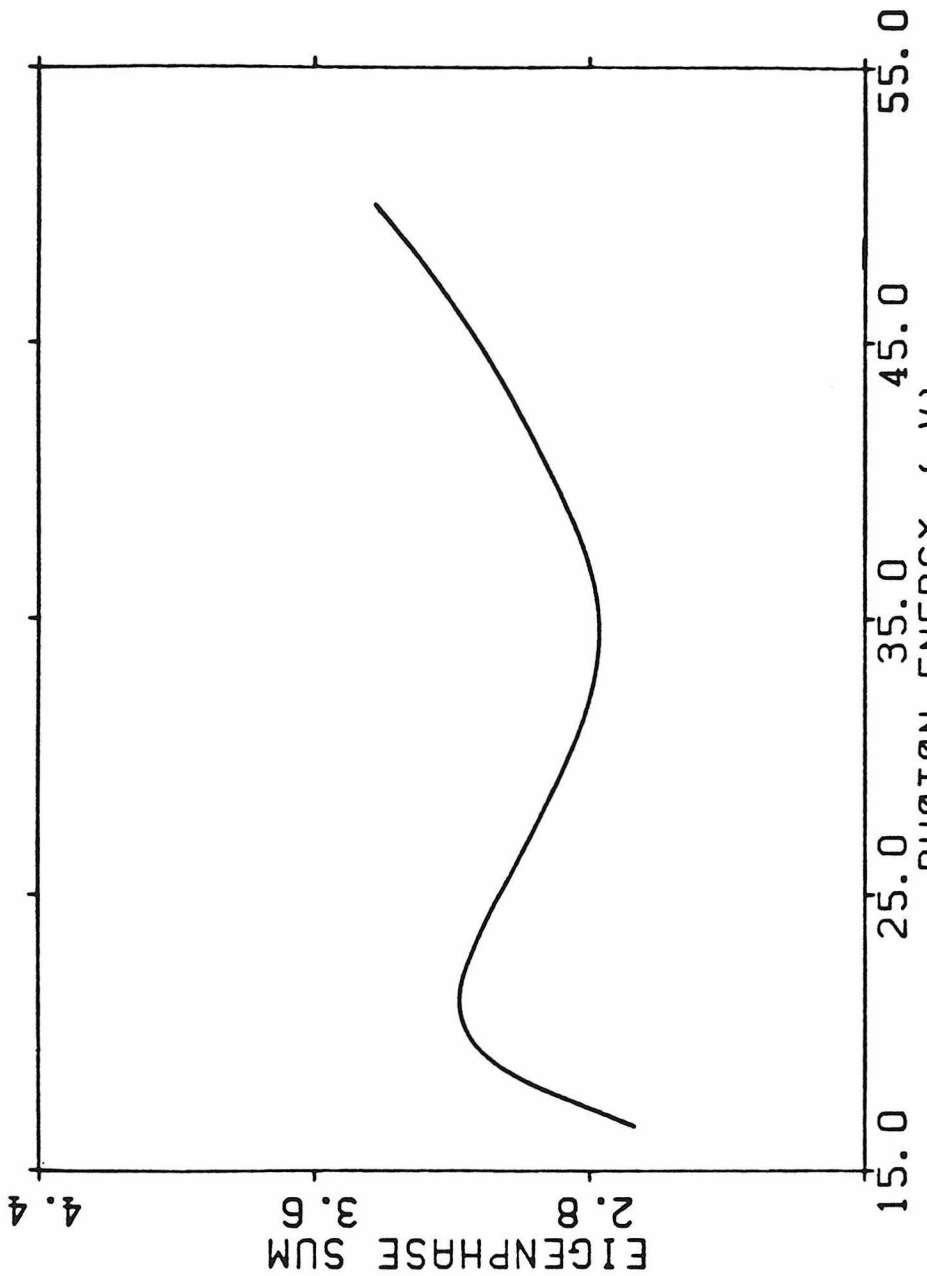

Figure 10

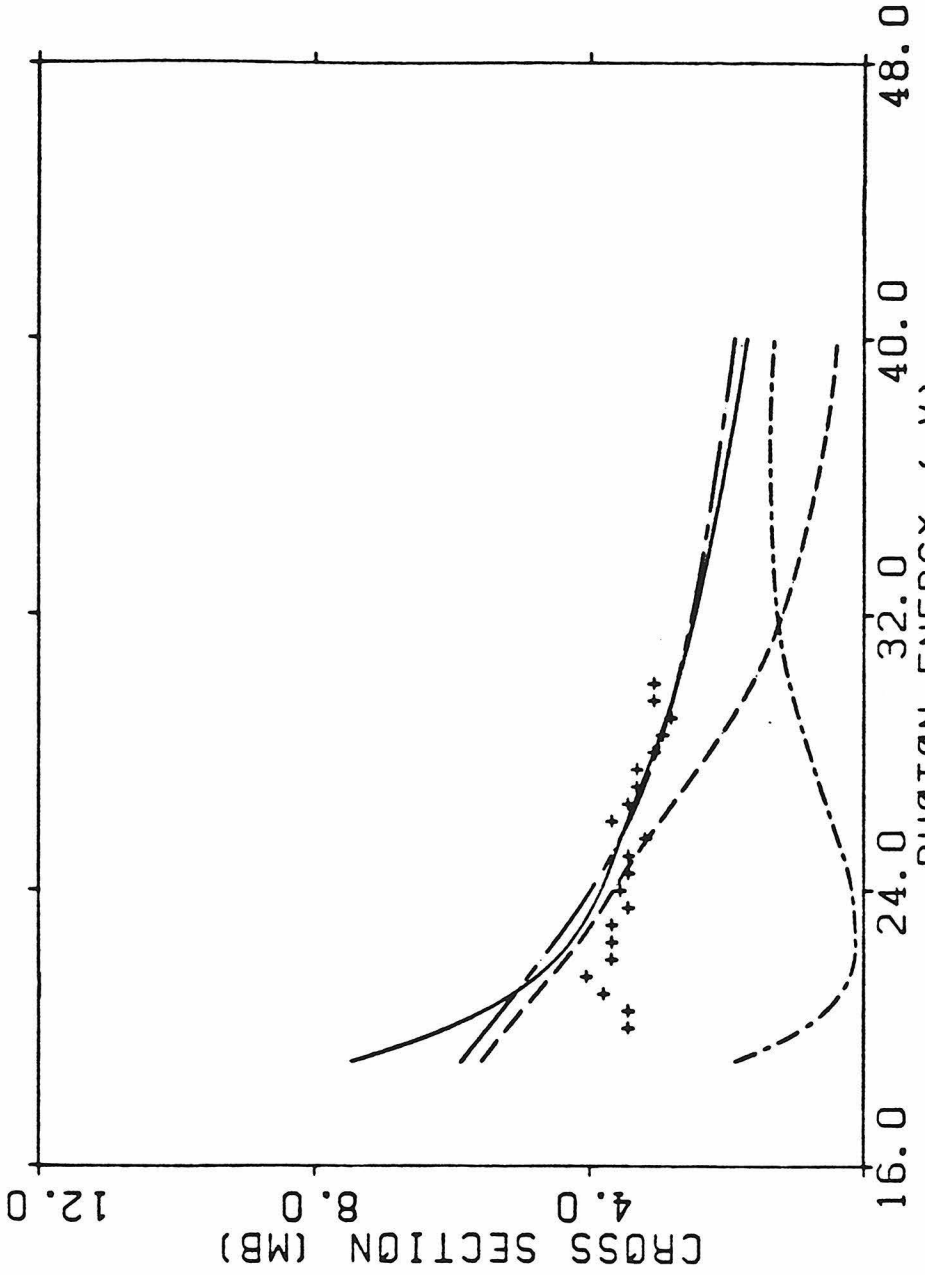
CROSS SECTION (MB)
4.0
8.0
12.0
16.0
24.0
32.0
40.0
48.0
PHOTON ENERGY (eV)

Figure 11

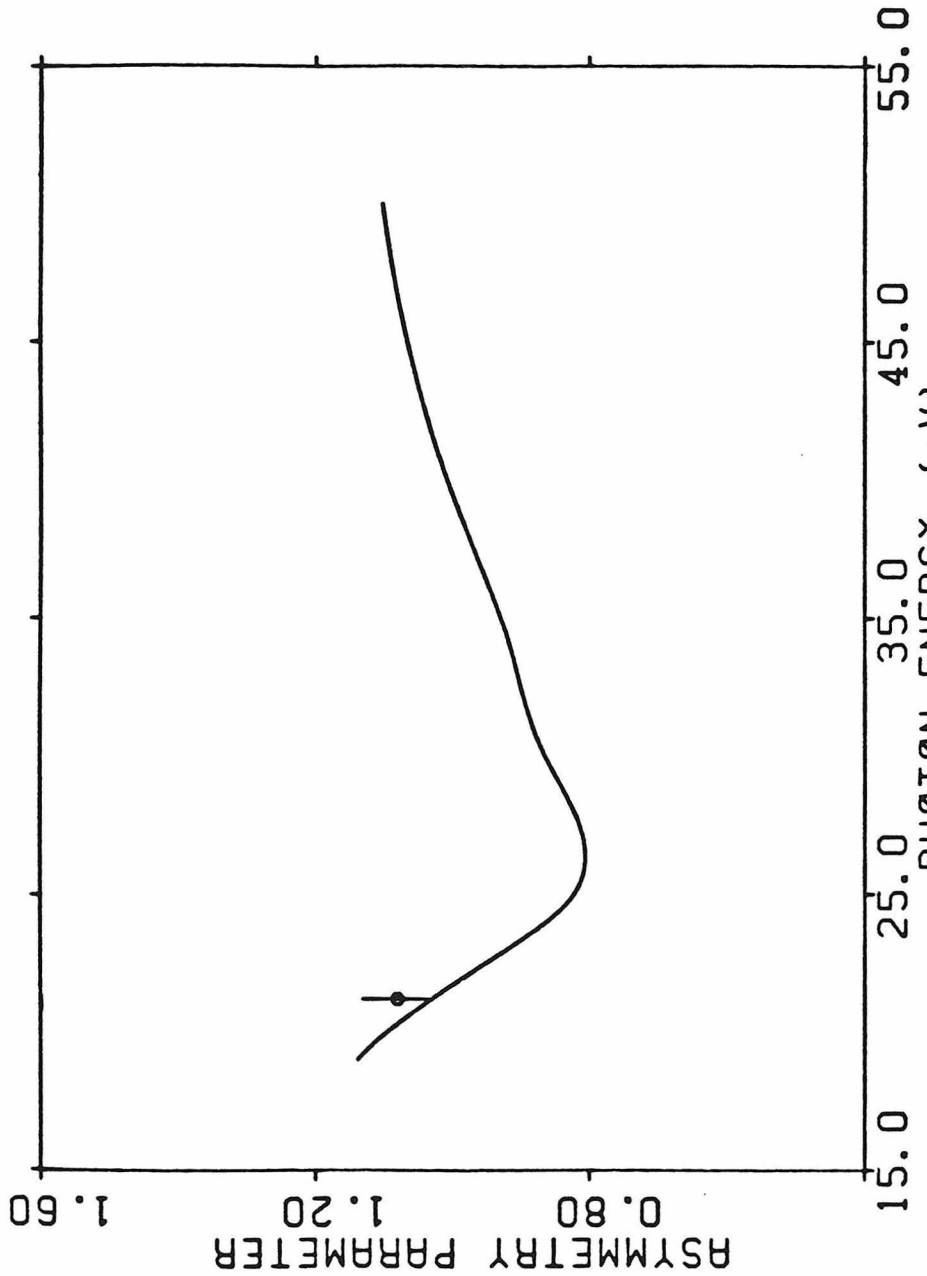
ASYMMETRY PARAMETER
0.80
1.20
1.60
15.0
25.0
35.0
45.0
55.0
PHOTON ENERGY (eV)

Figure 12

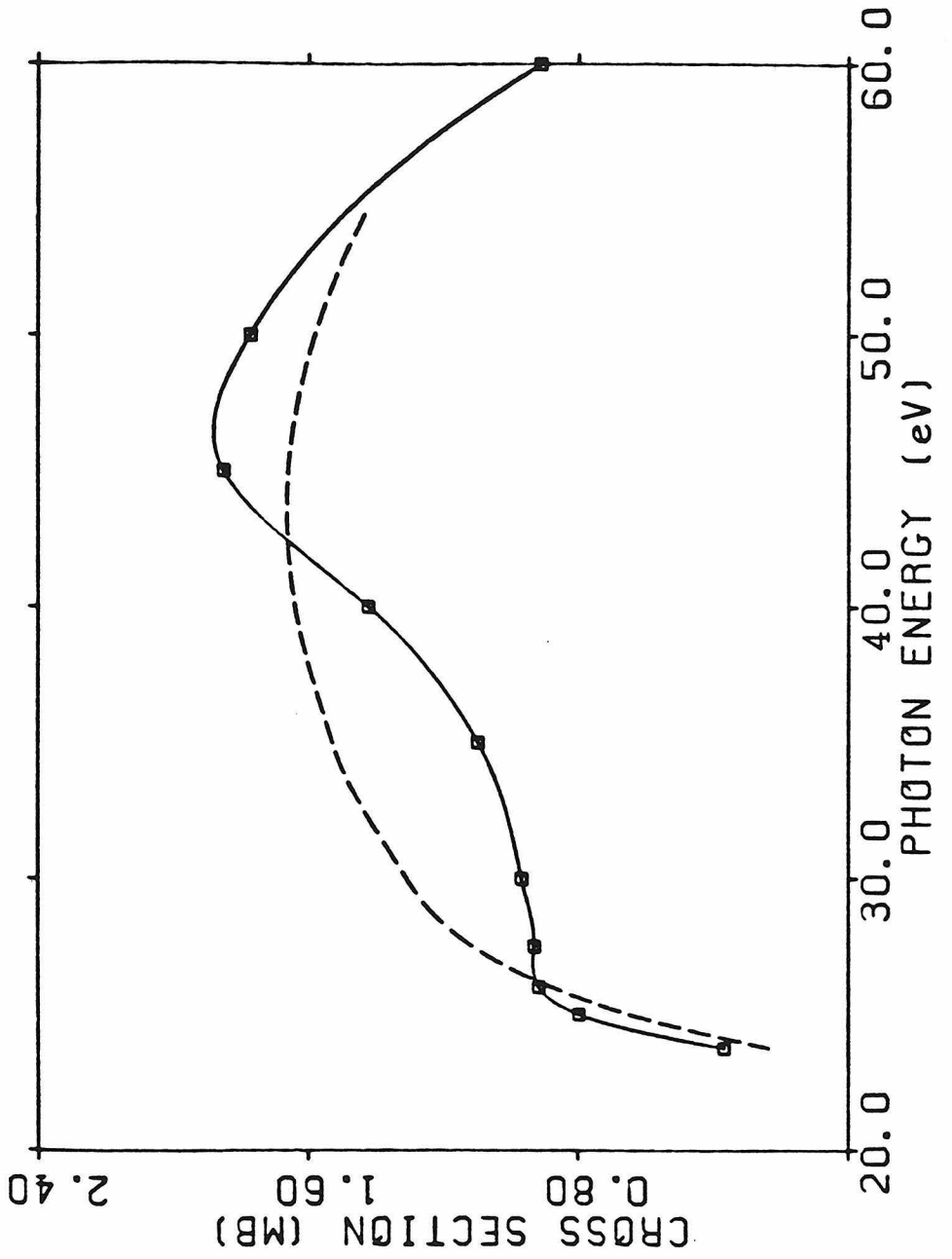
CROSS SECTION (MB)
0.80
1.60
2.40
20.0
30.0
40.0
50.0
60.0
PHOTON ENERGY (eV)

Figure 13

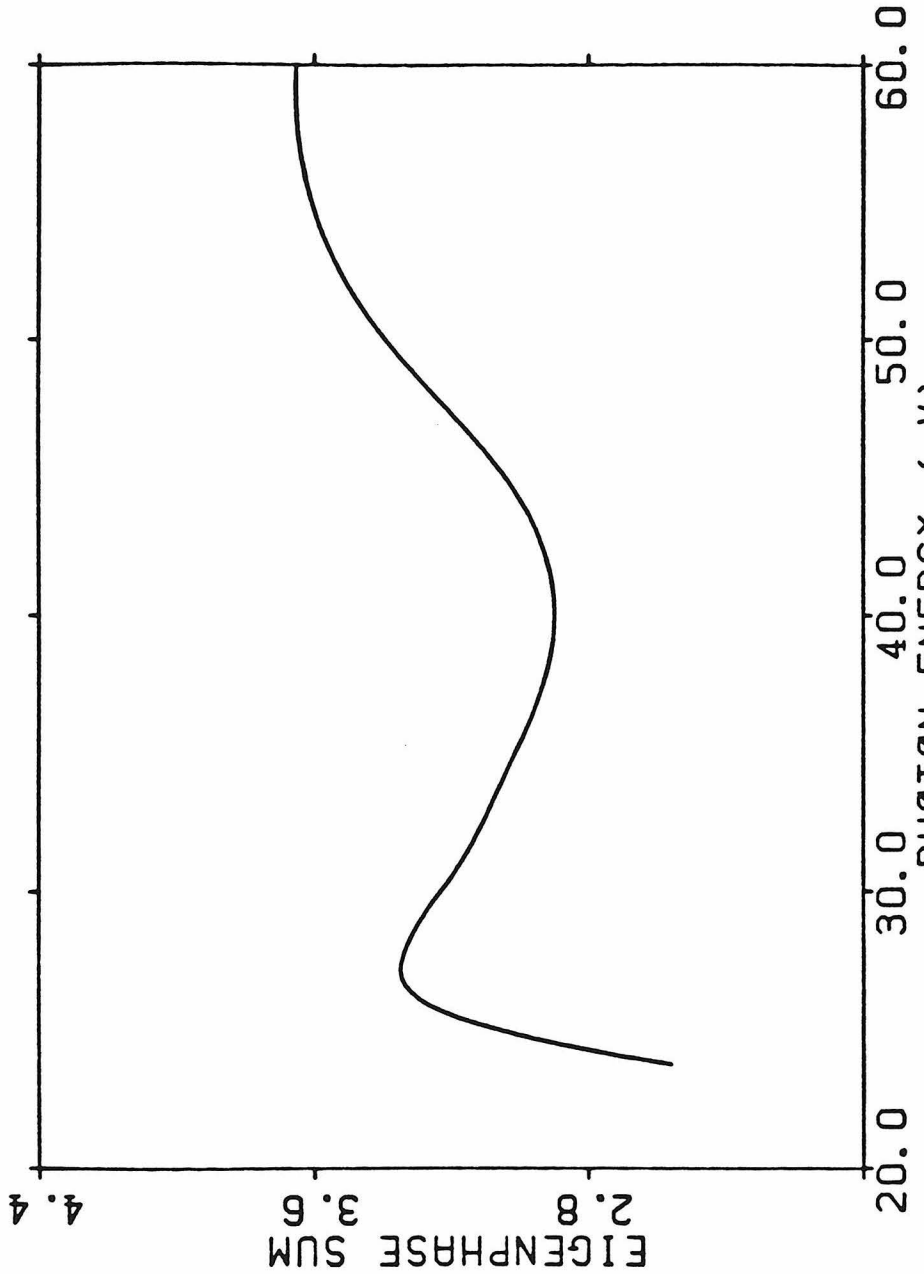

Figure 14

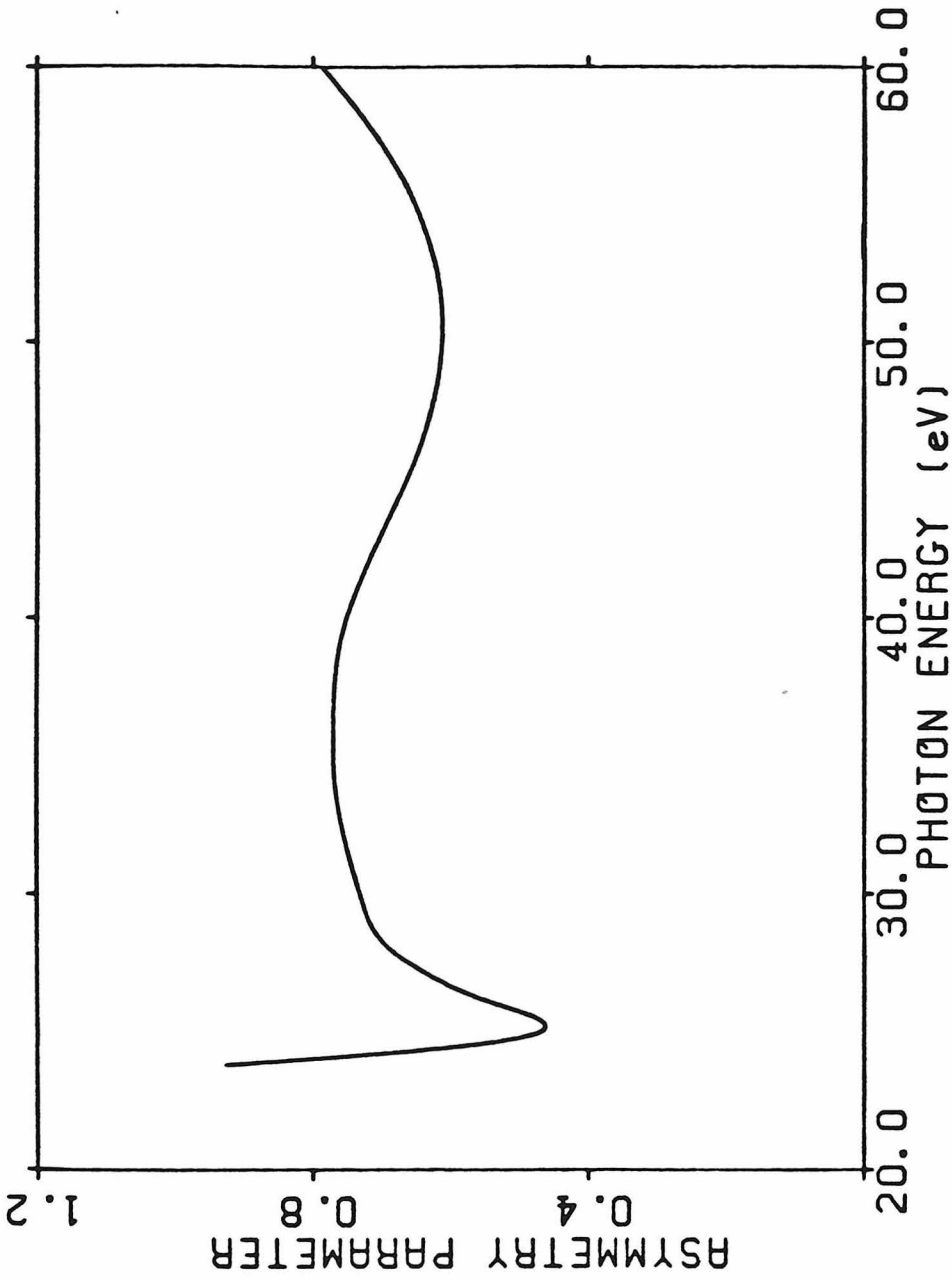
ASYMMETRY PARAMETER
0.4
0.8
1.2
20.0
30.0
40.0
50.0
60.0
PHOTON ENERGY (eV)

Figure 15

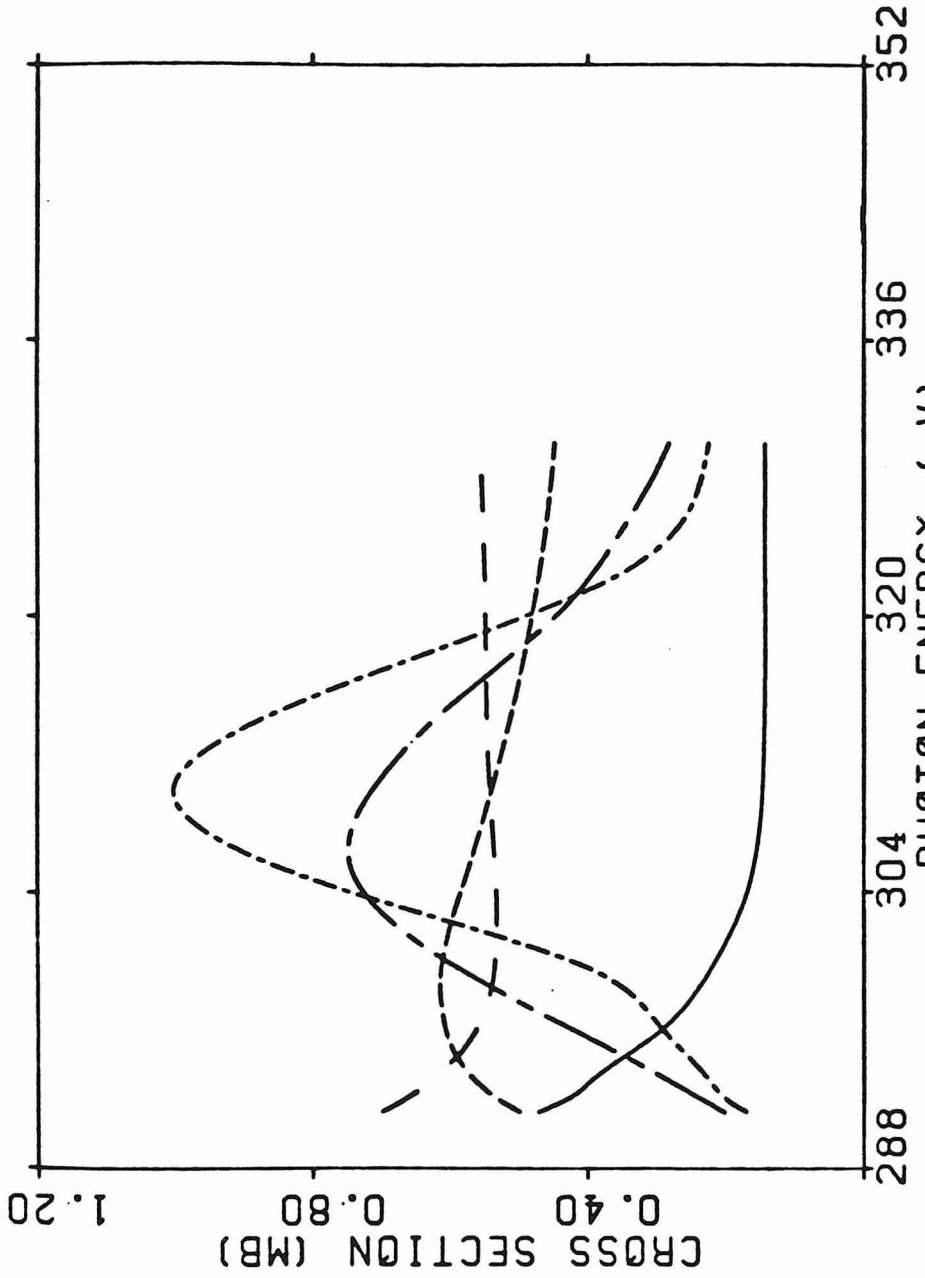
CROSS SECTION (MB)
0.40
0.80
1.20
288
304
320
336
352
PHOTON ENERGY (eV)

Figure 16

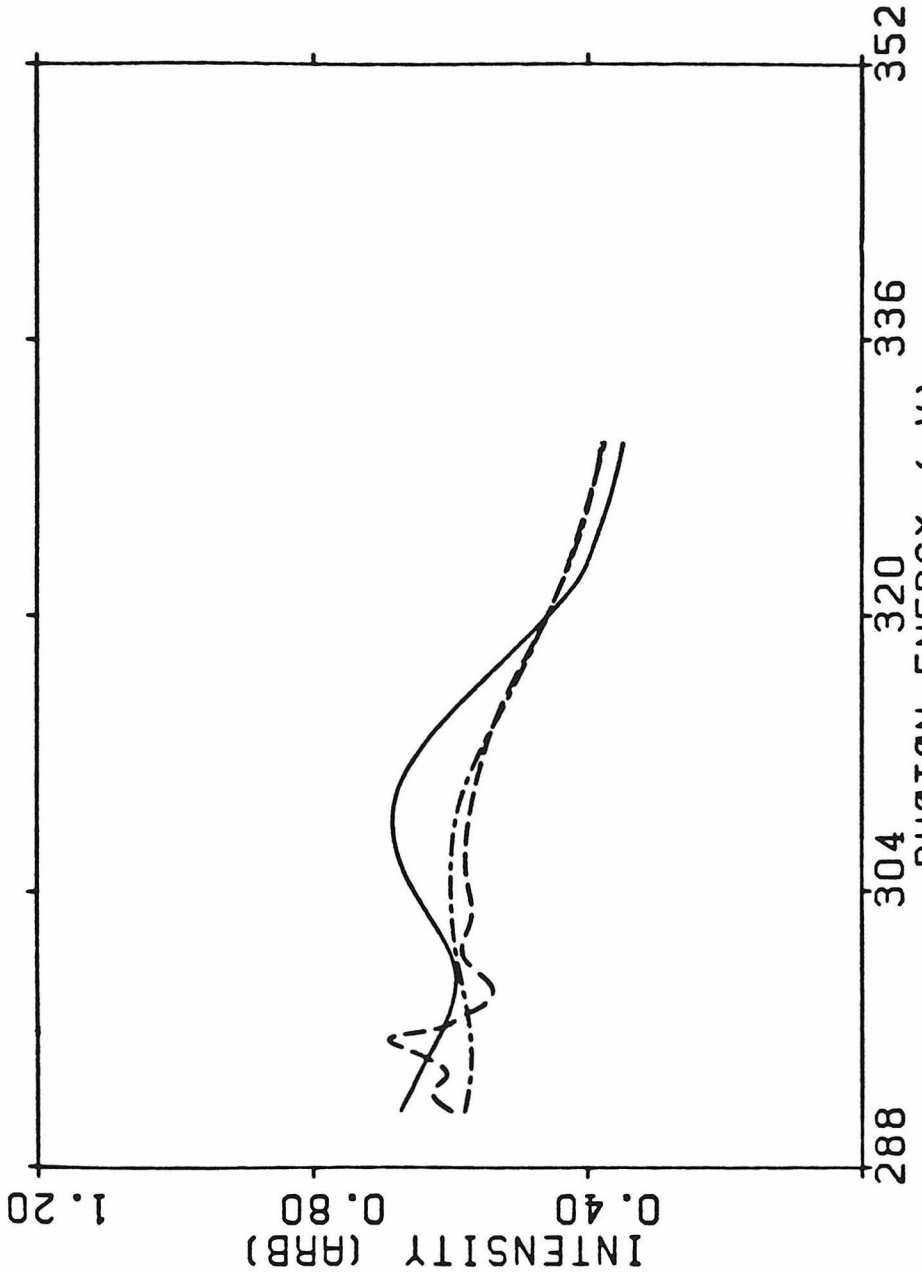
INTENSITY (ARB)
0.40
0.80
1.20
288
304
320
336
352
PHOTON ENERGY (eV)

Figure 17

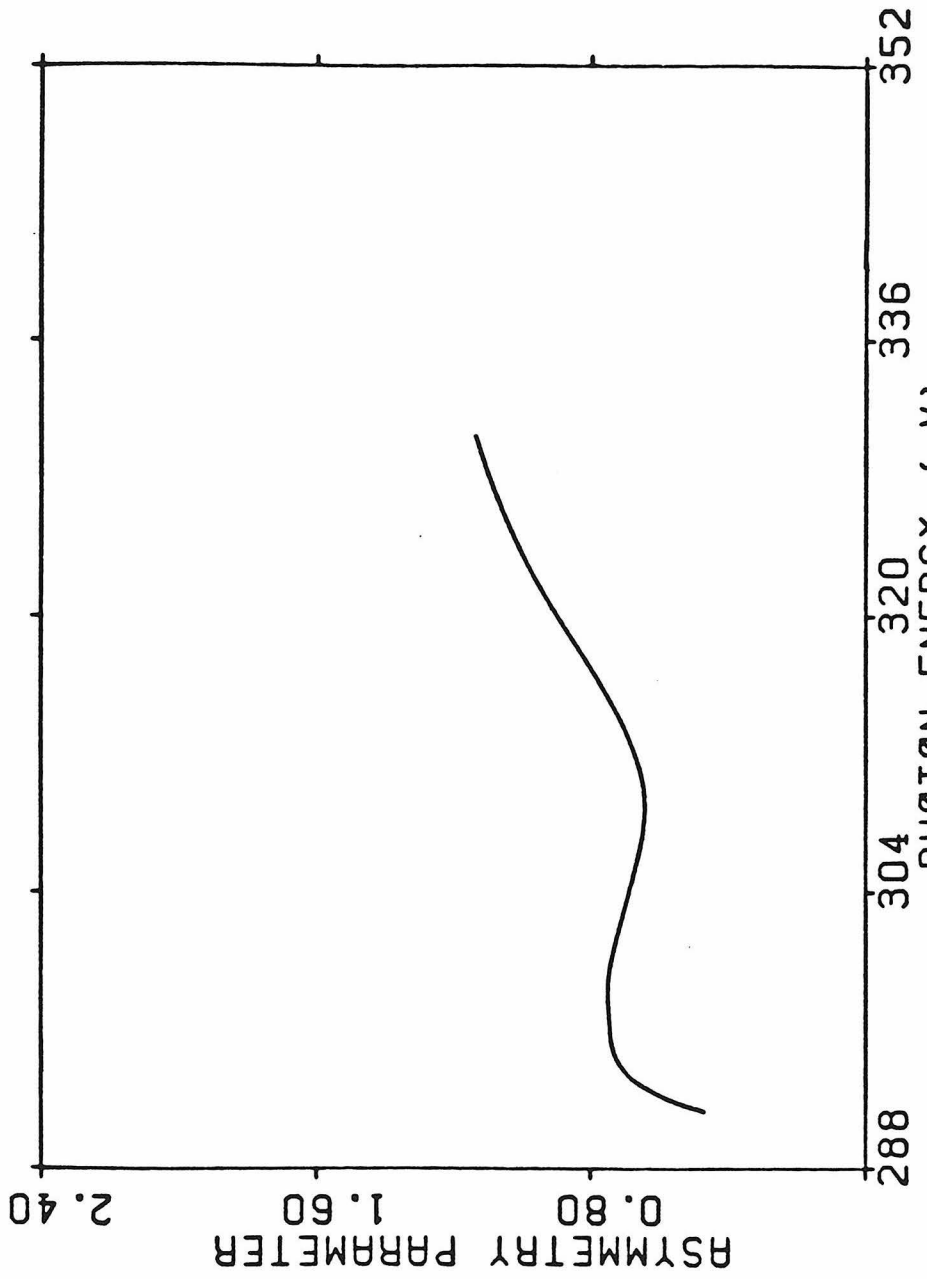
ASYMMETRY PARAMETER
0.80
1.60
2.40
288
304
320
336
352
PHOTON ENERGY (eV)

Figure 18

SECTION B

SHAPE RESONANCES IN THE PHOTOIONIZATION OF CYANOGEN

I. INTRODUCTION

Shape resonances play a central role in studies of the dynamics of molecular photoionization. They give rise to several distinct features in the photoionization of molecules such as an enhancement of the cross sections, a pronounced influence on the angular distributions of photoelectrons, and non-Franck-Condon effects in vibrationally resolved spectra.[1,2] These shape resonances are quasibound states formed by the trapping of the photoelectron by the centrifugal barrier of the molecular force field. A study of these resonant features naturally provides significant physical insight into the underlying photoionization process.

The effects of shape resonances and autoionizing features have been studied in many molecules over a wide range of photon energies using synchrotron radiation. These systems include, among others,[3] N_2,[4] CO,[5] CO_2,[6] CS_2,[7] and C_2H_2.[8] The availability of such experimental data and the difficulties associated with theoretical studies of molecular photoionization have stimulated the development of various approaches to the calculation of these photoionization cross sections. These approaches include the Stieltjes moment theory method which avoids the need for the direct solution of the collision equations by extracting photoionization cross sections from spectral moments of the oscillator strength distribution,[9] the continuum multiple scattering model in which the molecular potential is approximated so that the continuum equations can be readily solved,[10] and several methods for the direct solution of the Hartree-Fock equations for the photoelectron continuum orbitals.[11-15] These experimental and related theoretical studies have served to clarify many important features such as the positions and symmetries of shape resonances in several diatomic molecules including N_2,[4,14,16-I8] CO,[5,16,19-21] O_2,[1,22,23] and NO,[24-26] and in polyatomic molecules, e.g., CO_2[6,27,28] CS_2[7,29] and C_2H_2.[8,30,31] The results for CO_2[6,28] and C_2H_2[8,31] have already shown that resonance features in

the photoionization of polyatomic molecules can behave very differently from what could be expected on the basis of results for simple diatomic molecules. Our understanding of the dynamics of shape and autoionizing resonances would clearly benefit from an extension of current studies to larger molecular systems.

In this paper we report the results of studies of the photoionization cross sections and photoelectron asymmetry parameters for ionization of the $1\pi_g(X^2\Pi_g)$, $5\sigma_g(A^2\Sigma_g^+)$ and $4\sigma_u(B^2\Sigma_u^+)$ levels of cyanogen, C_2N_2. We chose this system primarily for the interesting shape resonant structure which it can be expected to exhibit. Specifically, there is the possibility of shape resonant trapping arising from both the CN components of the molecule and from the C– C bond itself. Moreover, the presence of two CN groups should result in resonances corresponding to the in-phase and out-of-phase combinations of these trapping sites. These resonances, which are derived from the C≡ N analogue of the well-known σ shape resonances in diatomic molecules, should occur in both the σ_g and σ_u continua. We can hence expect two shape resonances in the σ_u continuum, the lower energy one arising from the C– C bond and the higher one arising from the CN groups, and a single shape resonance in the σ_g continuum.

These σ_u and σ_g shape resonant features in the photoionization of the $1\pi_g$, $5\sigma_g$, $4\sigma_u$, and $1\pi_u$ levels of C_2N_2 have been discussed previously by Holland et al.[32] and by Kreile et al.[33] The synchrotron radiation studies[32] extended from threshold to a photon energy of 24 eV and hence, as we will see, did not include the energy region where the σ_u and σ_g CN-related resonances occur. However, our results show that the pronounced dip in the photoelectron asymmetry parameter curve for the $5\sigma_g$ level occurring at a photon energy of 16.5 eV is due to the σ_u C– C shape resonance. On the other hand, the similar behavior of the asymmetry parameters for the $1\pi_g$ level in the same energy region[32] is not due to this shape resonance and is almost certainly an autoionization feature.[32] The

NeI, HeI, and NeII line source measurements of the vibrationally resolved asymmetry parameters also show strong evidence of the C–C σ_u resonance in photoionization of the $5\sigma_g$ orbital.[33] Studies of these photoionization cross sections using the multiple scattering model predict both a high and a low energy shape resonance in the σ_u continuum, a σ_g shape resonance, and a very pronounced shape resonance in the π_g continuum.[33]

A summary of our results for the shape resonant behavior in the electronic continua of $C_2N_2^+$ is as follows. The C–C σ_u shape resonance occurs at a photoelectron kinetic energy of about 2.5 eV while the σ_g and σ_u shape resonances associated with the CN groups are seen at kinetic energies of 18 eV and 27 eV, respectively, or a σ_g-σ_u splitting of about 9 eV. However, we also predict a broad shape resonance in the π_u continuum with an onset just below a photon energy of 26 eV. This shape resonance has not been previously identified. The measured photoelectron asymmetry parameters, β, do show a pronounced vibrational state dependence at a photon energy of 26.91 eV with values of 0.52 and 1.09 for $\nu_1 = 0$ and 1, respectively, in the symmetric C≡N stretching mode.[33] Our calculated fixed-nuclei β value of about 1.1 at this energy is in poor agreement with these measured β's since the photoelectron spectra at this energy and below[32,34] show that the intensity of the ν_1=1 member of this $^2\Sigma_g^+(5\sigma_g^{-1})$ band is much smaller than that of the ν_1=0 member and hence the fixed-nuclei result can be expected to be close to $\beta(\nu_1=0)$. These results will be discussed further in Section IIIB. With this π_u shape resonance and the two resonances in the σ_u continuum, photoionization out of the $5\sigma_g$ orbital shows three resonance features. The actual influence of a shape resonance in a specific continuum on the vibrationally unresolved cross sections is also seen to vary significantly from channel to channel. For example, while the $k\pi_u$ shape resonance is pronounced in the cross

sections for photoionization out of the $5\sigma_g$ level, we see essentially no evidence of this shape resonance in the vibrationally unresolved $1\pi_g$ cross sections. This shape resonance is, however, seen in the eigenphase sums in both channels. Eigenphase sums are clearly very useful in identifying the presence and nature of these shape resonances. In contrast to the results of the continuum multiple scattering model[33] we do not see a shape resonance in the $4\sigma_u \rightarrow k\pi_g$ cross sections. Furthermore, the photoionization cross sections in some channels can be affected substantially by electron correlation. For example, in the Hartree-Fock approximation, a discrete level can be incorrectly forced into the continuum, or too close to threshold, resulting in spurious behavior of the cross sections. For cyanogen, this occurs in photoionization of the $1\pi_g$ level into the $k\pi_u$ and $k\sigma_u$ continua. These results suggest that vibrationally resolved measurements of the photoionization cross sections and asymmetry parameters for cyanogen will provide a rich source of dynamical information on molecular photoionization.

An outline of the paper is as follows. In Section II we give a brief discussion of the method used to obtain the Hartree-Fock electronic continuum orbitals needed in these studies along with several relevant computational details. In Section III we present our calculated photoionization cross sections and photoelectron asymmetry parameters for the $1\pi_g$, $5\sigma_g$, and $4\sigma_u$ levels of C_2N_2 and compare these results with available experimental data and with the results of other calculations.[33]

II. METHOD

The rotationally unresolved, fixed-nuclei photoionization cross section is given by

$$\sigma(R) = \frac{4\pi^2\omega}{3c}|< \Psi_i(\underset{\sim}{r},R)|\underset{\sim}{\mu}|\Psi_f(\underset{\sim}{r},R) >|^2 \qquad (1)$$

where $\underset{\sim}{\mu}$ is the dipole moment operator and ω is the photon frequency. In Eq.(1) Ψ_i represents the initial state of the molecule with N bound electrons and ψ_f the final state with a photoelectron in the electronic continuum. The representation of ψ_f requires a set of continuum orbitals describing the motion of the photoelectron in the nonlocal, nonspherical potential field of the molecular ion. In these studies we will use the Hartree-Fock continuum orbitals of the molecular ion which satisfy the one-electron Schrödinger equation (in atomic units)

$$(-\tfrac{1}{2}\nabla^2 + V_{N-1}(\underset{\sim}{r},R) - \frac{k^2}{2})\phi_{\underset{\sim}{k}}(\underset{\sim}{r},R) = 0 \qquad (2)$$

where $\frac{k^2}{2}$ is the photoelectron kinetic energy, V_{N-1} is the Hartree-Fock (static-exchange) potential of the ion, and $\phi_{\underset{\sim}{k}}$ satisfies the appropriate boundary conditions. We also use the frozen-core approximation and hence assume that V_{N-1} is determined by the core orbitals of the neutral molecule.

The nonspherical and nonlocal character of molecular potentials introduces several complications into the solution of Eq.(2) for continuum orbitals. In our studies we will use the Schwinger variational procedure to solve Eq.(2) for the continuum orbitals[14,35] needed to obtain the photoionization cross sections and angular distributions of the photoelectron. Other techniques have also been developed for the direct solution of the Hartree-Fock equations for these molecular continuum orbitals.[3,11-15] Results to date have shown that there can be significant advantages in utilizing Hartree-Fock continuum orbitals explicitly in molecular photoionization studies, particularly in regions of shape resonances.[3]

We solve Eq.(2) by working with the integral form of this equation, i.e.,

$$\phi_{\underset{\sim}{k}} = \phi^c_{\underset{\sim}{k}} + G^{(-)}_c V\phi_{\underset{\sim}{k}} \qquad (3)$$

where ϕ^c_k is the pure Coulomb scattering function, V is the molecular ion

potential with the Coulomb component removed, and $G_c^{(-)}$ is the Coulomb Green's function with incoming-wave boundary conditions,

$$V = V_{N-1} + \frac{1}{r} \tag{4a}$$

$$G_c^{(-)} = (\nabla^2 + \frac{2}{r} + k^2 - i\varepsilon)^{-1}. \tag{4b}$$

The continuum orbital $\phi_{\underset{\sim}{k}}(\underset{\sim}{r})$ can be expanded in terms of spherical harmonics of $\hat{\Omega}_{\underset{\sim}{k}}$, the direction of $\underset{\sim}{k}$, as

$$\phi_{\underset{\sim}{k}}(\underset{\sim}{r}) = (\frac{2}{\pi})^{\frac{1}{2}} \sum_{\ell m} \frac{i^\ell}{k} \phi_{k\ell m}(\underset{\sim}{r})\, Y^*_{\ell m}(\hat{\Omega}_{\underset{\sim}{k}}) \tag{5}$$

where $\phi_{k\ell m}(\underset{\sim}{r})$ is a partial wave scattering function. Each $\phi_{k\ell m}$ satisfies its own Lippmann-Schwinger equation, i.e.,

$$\phi_{k\ell m} = \phi^c_{k\ell m} + G_c^{(-)} V\, \phi_{k\ell m} . \tag{6}$$

We first obtain an approximate solution of Eq.(6) for $\phi_{k\ell m}$ by assuming a separable approximation for the potential V of the form

$$V(\underset{\sim}{r},\underset{\sim}{r}') \simeq V^S(\underset{\sim}{r},\underset{\sim}{r}') = \sum_{i,j} \langle \underset{\sim}{r}|V|\alpha_i\rangle (V^{-1})_{ij} \langle \alpha_j|V|\underset{\sim}{r}'\rangle \tag{7}$$

where the matrix $(V^{-1})_{ij}$ is the inverse of the matrix with elements $V_{ij} = \langle \alpha_i|V|\alpha_j\rangle$. With the approximate potential of the form of Eq.(7), the solutions of the integral equation, Eq.(6), can be written

$$\phi^{(0)}_{k\ell m}(\underset{\sim}{r}) = \phi^c_{k\ell m} + \sum_{i,j} \langle \underset{\sim}{r}|G_c^{(-)}V|\alpha_i\rangle (D^{-1})_{ij} \langle \alpha_j|V|\phi^c_{k\ell m}\rangle \tag{8}$$

where the matrix $(D^{-1})_{ij}$ is the inverse of the matrix

$$D_{ij} = \langle \alpha_i | V - V G_c^{(-)} V | \alpha_j \rangle . \tag{9}$$

The use of a separable potential of the form of Eq.(7) in Eq.(6) to obtain solutions of the form of Eq.(8) can be shown to be equivalent to using the basis functions $\alpha_i(\underset{\sim}{r})$ in the Schwinger variational principle for collisions.[36] The functions $\alpha_i(\underset{\sim}{r})$ can be chosen to be entirely discrete basis functions such as Cartesian Gaussian[37] or spherical Gaussian[28] functions. We note that with discrete basis functions alone these approximate solutions $\phi_{k\ell m}^{(0)}$ satisfy scattering boundary conditions. These discrete basis functions have been used successfully in electronic structure calculations[37] and should be very effective in representing the multicenter nature of the scattering wave function and molecular potential in the near-molecular region. With adequate basis sets the continuum solutions of Eq.(8) already provide quantitatively reliable, photoionization cross sections[2,3] which, moreover, can be shown to be variationally stable at the Hartree-Fock level.[38] Although we have developed an iterative procedure for obtaining the converged solutions of Eq.(6),[35] in these studies the cross sections were generally determined using the approximate solutions $\phi_{k\ell m}^{(0)}$ obtained with an adequate expansion basis in Eq.(8). For photoionization of the $5\sigma_g$ level, we did, however, explicitly verify that the cross sections changed only slightly with iteration. For example, at the peak of the shape resonant $5\sigma_g \rightarrow k\sigma_u$ partial channel (17.5 eV) the length form of cross section changes from 8.04 Mb to 8.01 Mb upon iterating.

For the initial state we have used the SCF Slater basis wave function of McLean and Yoshimine[39] with C–C and C–N bond lengths of 2.068 a.u. and 2.186 a.u., respectively. All the matrix elements and functions arising in the solution of Eq.(8) were evaluated using single-center expansions. Details of these numerical procedures have been discussed previously.[14] The single-center

expansions are made about the molecular center and the expansion parameters were based on the experience of earlier studies of CO_2.[28] These parameters are defined in Ref. 28 and are as follows:

(i) $\ell_m = \ell_s^{ex} = \ell_i^{dir} = 59$,

(ii) $\ell_m^{ex} = 40$,

(iii) $\lambda_m^{dir} = 118$,

(iv) $\ell_i^{ex} = 58(1\sigma_g)$, $22(2\sigma_g)$, $26(3\sigma_g)$, $18(4\sigma_g)$, $20(5\sigma_g)$, $59(1\sigma_u)$, $23(2\sigma_u)$, $29(3\sigma_u)$, $21(4\sigma_u)$, $17(1\pi_u)$, and $16(1\pi_g)$,

(v) $\ell_p = 10$.

Based on earlier convergence studies[14,28] these values of the expansion parameters should provide cross sections which are within a few percent of the converged values. The above values of ℓ_i^{ex} correspond to having normalized the molecular orbital expansions to better than 0.99. For example, extending ℓ_m^{ex} to 59 changes the peak of the $5\sigma_g \rightarrow k\sigma_u$ cross section at 17.5 eV by less than 1%.

For the expansion basis in Eq.(7) we use spherical Gaussian functions which are defined by

$$\chi(\underset{\sim}{r}) = N|\underset{\sim}{r}-\underset{\sim}{A}|^{\ell} \exp(-\alpha|\underset{\sim}{r}-\underset{\sim}{A}|^2)Y_{\ell m}(\Omega_{\underset{\sim}{r}-\underset{\sim}{A}}). \tag{10}$$

The basis sets for the various ionization channels are given in Table I.

III. RESULTS AND DISCUSSION

A. Photoionization cross sections for the $X^2\Pi_g(1\pi_g^{-1})$ ion

Figure 1 shows the contributions of the σ_u, π_u, and δ_u continua to the photoionization cross section for the $1\pi_g$ level. In this figure we have assumed

the experimental value of 13.36 eV for the ionization potential of this state.[32] The $k\pi_u$ and $k\sigma_u$ cross sections show a very sharp and conspicuous increase near threshold which is probably unphysical and due to the occurrence of the $1\pi_g^3 2\pi_u(^1\Sigma_u^+)$ and $1\pi_g^3 5\sigma_u(^1\Pi_u)$ excitations too close to threshold in the Hartree-Fock approximation. In fact, in Hartree-Fock calculations of the spectrum of C_2N_2, Bell[40] obtained excitation energies of 12.76 eV and 12.6 eV, respectively for the $1\pi_g \rightarrow 2\pi_u$ and $1\pi_g \rightarrow 5\sigma_u$ transitions. These values are considerably larger than the excitation energies tentatively assigned to these transitions in the vacuum UV spectrum and are quite close to the calculated ionization potential of 13.08 eV.[40] To assess the influence on the cross sections of these discrete transitions which may be spuriously close to threshold, we have calculated the corresponding cross sections using $k\pi_u$ and $k\sigma_u$ continuum orbitals orthogonalized to the $2\pi_u$ and $5\sigma_u$ virtual orbitals of the Hartree-Fock calculation. We have shown that this very approximate procedure provides a useful estimate of the photoionization cross section which would result if these discrete transitions were further removed from threshold and closer to their correct locations.[14] The resulting cross sections in the dipole length approximation are shown in Fig. 2 and are seen to be very strongly influenced by this orthogonalization.

Figure 3 shows the eigenphase sums for the σ_u, π_u, and δ_u continua of the $X^2\Pi_g(1\pi_g^{-1})$ ion. These eigenphase sums show clear evidence of two shape resonances in the σ_u continuum and one in the π_u continuum. However, the σ_u and π_u cross sections of Fig. 1 do not show any clearly related resonant structure. On the other hand, we will see that these three shape resonances appear very distinctly in both the corresponding eigenphase sums and cross sections for ionization out of the $5\sigma_g$ level. In comparison, the $k\delta_u$ eigenphase sums and cross section are characteristically nonresonant.

In Fig. 4 we show our calculated total photoionization cross sections for the $1\pi_g$ orbital using both the length and velocity forms of the dipole

transition moment. The significant differences between these length and velocity cross sections arise primarily from the neglect of electron correlation effects.[14] It is these correlation effects which must be included so as to move the discrete $1\pi_g^3 5\sigma_u$ and $1\pi_g^3 2\pi_u$ states further away from threshold and closer to their correct positions. For comparison, we also show the cross sections obtained using the $k\sigma_u$ and $k\pi_u$ continuum orbitals which have been orthogonalized to the $5\sigma_u$ and $2\pi_u$ virtual orbitals. The effects of this orthogonalization are probably exaggerated due to the very approximate basis of this procedure for reproducing the actual effects of electron correlation. Finally, we compare our calculated cross sections with those of the continuum multiple scattering model.[33] Although not shown in this figure, the σ_u and δ_u components of our calculated cross sections behave very differently near threshold from those of the multiple scattering model. Whereas our calculated σ_u and δ_u cross sections decrease and increase,respectively, towards threshold, those of the multiple scattering model behave just the other way. No measurements of these cross sections have been reported.

Figure 5 shows the calculated photoelectron asymmetry parameter for the $1\pi_g$ level along with the measured values of Holland et al.[32] for the v=0 level of the ion. The calculated asymmetry parameters do not show the pronounced resonance structure seen in the experimental data around 17 eV. This structure is almost certainly due to autoionization, e.g., the $4\sigma_g \rightarrow 2\pi_u$ transition,[32] which is not included in these Hartree-Fock continuum calculations. Again, the vibrationally unresolved photoelectron asymmetry parameters show no evidence of the shape resonances suggested by the behavior of the σ_u and π_u eigenphase sums of Fig. 3. However, it is possible that the non-Franck-Condon behavior of the measured vibrational branching ratios for the v= 0, 1, 2, and 3 levels below 15.5 eV[32] could be due to the lower energy σ_u shape resonance. Finally, the asymmetry parameters of Kreile et al.[33] obtained using the

multiple scattering model are shown in Fig. 5. Above 18 eV these asymmetry parameters differ significantly from those of the present Hartree-Fock studies. These differences are much more significant than we have seen in the photoelectron asymmetry parameters predicted by these two methods for other molecules, e.g., N_2[14] and CO_2.[28]

B. The $A^2\Sigma_g(5\sigma_g^{-1})$ ion

Figure 6 shows our calculated cross sections for photoionization of the $5\sigma_g$ level along with the individual contributions of the σ_u and π_u continua while Fig. 7 gives the eigenphase sums for these two continua. In these figures and in Fig. 8 we assume an ionization potential of 14.49 eV.

These results reveal a rich and interesting shape resonance structure. The σ_u continuum shows both a low and a higher energy shape resonance at photon energies of about 17 eV and 42 eV, or photoelectron kinetic energies of 2.5 eV and 27.5 eV, respectively. The π_u continuum also shows a shape resonance with a peak position around 33 eV. The behavior of the eigenphase sums associated with these resonances is shown in Fig. 7. The σ_u shape resonance at 2.5 eV into the continuum is the C—C analogue of the well-known $\sigma_u(\ell=3)$ shape resonance in $N_2(3\sigma_g^{-1})$ which occurs at a kinetic energy of about 15 eV in that system. The origin and character of this shape resonance has been discussed previously.[32,33] Its occurence at kinetic energies of 2.5 eV and 15 eV in C_2N_2 and N_2, respectively, is consistent with the much larger C—C bond distance in C_2N_2(2.608 a.u.) than in N_2 (2.068 a.u.). These two σ_u shape resonances have also been seen at around the same energies in the calculated cross sections of the multiple scattering model.[33] However, the peak value of the cross section of the multiple scattering model for the lower energy resonance is about twice as large as that of the present studies while the resonance itself is much narrower. This same trend has been observed in other systems.[28,41]

The K-matrices associated with the σ_u shape resonance around 42 eV shows significant mixing among the ℓ=3, 5, and 7 partial waves, suggesting that the photoelectron wave function has significant amplitude in the region of the C≡N subgroup. As suggested by Holland et al.,[32] this amplitude on the C≡N subgroup is very probably due to the $\sigma(\ell=3)$ shape resonance localized in that region of the molecule. This higher energy shape resonance is then just the σ_u combination of these CN localized shape resonances.[32] As we will see shortly, there is also an associated σ_g shape resonance at lower energy. The second σ_u shape resonance does not lead to a very substantial enhancement of the cross section. Its resonant nature, however, is clear from the behavior of the eigenphase sum of Fig. 7.

In addition to this shape resonant behavior in the $5\sigma_g \rightarrow k\sigma_u$ continuum, the $5\sigma_g \rightarrow k\pi_u$ cross section of Fig. 6 also shows a shape resonance with a peak enhancement around 34 eV. In this region, the $k\pi_u$ eigenphase sums of Fig. 7 show an increase of about 0.75 radians. Shape resonances in other molecular systems are characterized by similar rises in the eigenphase sum. For example, a 1.25 radian increase is observed in the well-characterized $3\sigma_g \rightarrow k\sigma_u$ shape resonant partial channel in N_2.[14] In addition, this shape resonance is also associated with a broad dip in the asymmetry parameters (Fig. 8). To our knowledge, the occurence of this shape resonance in the $5\sigma_g \rightarrow k\pi_u$ cross sections of cyanogen is unusual and has not been seen in studies of other (linear) molecules. In the K-matrix associated with this resonance the ℓ=3 and 5 partial waves are strongly coupled. The $5\sigma_g \rightarrow k\pi_u$ cross sections of the multiple scattering model do not show any similar resonant enhancement. In the resulting total photoionization cross sections for the $5\sigma_g$ orbital both this π_u and the low energy σ_u shape resonances are very evident. However, the higher energy σ_u shape resonance is, as expected, obscured in the vibrationally unresolved cross sections of Fig. 6. Vibrationally resolved synchrotron radiation measurements of the cross sections in this region would be useful. In Fig. 6 we also compare our calculated $5\sigma_g$ photoionization cross sections with those of the multiple

scattering model.[33] The major differences between these cross sections arise from features related to the low energy σ_u and the π_u shape resonances.

Our photoelectron asymmetry parameters for the $5\sigma_g$ level are shown in Fig. 8 along with the synchrotron radiation measurements of Holland et al.[32] extending up to 24 eV and the line source (NeI,HeI, and NeII) data of Kreile et al.[33] Figure 8 also gives the asymmetry parameters of the multiple scattering model.[33] At low photoelectron kinetic energies the calculated and observed asymmetry parameters behave very differently. Whereas the calculated β's decrease just above threshold, the measured β's increase rapidly there. This difference may be due to autoionization which is not included in the present Hartree-Fock studies. The dip in the synchrotron radiation data and the vibrational state dependence (β = 0.47 and 0.86 for ν_1 = 0 and 1, respectively) in the line source measurement at 16.85 eV are clearly due to the lower σ_u shape resonance. Our calculations predict another,but broader minimum in these asymmetry parameters around 32 eV. Unfortunately, the available synchrotron radiation data does not extend into this region. Furthermore, Fig. 8 shows the strong vibrational state dependence of β on the symmetric CN stretching (ν_1) mode seen in the line source measurement at 26.91 eV.[33] However, the calculated fixed-nuclei β value is not consistent with the observed vibrational state dependence around this energy since the intensity of the ν_1= 0 member of the $^2\Sigma_g(5\sigma_g^{-1})$ band is much greater than that of the ν_1=1 level[32,40] and hence the calculated fixed-nuclei β should be expected to be approximately equal to $\beta(\nu_1=0)$. Reasons for this difference are not clear. Studies of the vibrational state dependence of β on the symmetric CN stretching mode can obviously be useful here and are under way. Finally, the influence of the higher energy σ_u shape resonance on these vibrationally unresolved asymmetry paramters is not very pronounced.

In Fig. 8 we also compare the asymmetry parameters of the multiple scattering model with our present results. Although there are certainly some differences between these results, there are some important similarities.[33] For

example, the influence of the two σ_u shape resonances on these β's is very evident. The minimum in β values around 23 eV is very interesting, particularly its possible correlation with the π_u shape resonance seen in our results. However, Kreile et al.[33] see no related resonant enhancement in the cross sections and, in fact, state that their results show no resonant behavior in the π_u channel.

C. The $B^2\Sigma_u^+(4\sigma_u^{-1})$ ion

Figure 9 shows our calculated σ_g and π_g channel contributions for photoionization out of the $4\sigma_u$ level along with the corresponding total cross sections. The photon energy scale assumes an ionization potential of 14.86 eV. Figure 9 also includes results of the multiple scattering studies of Kreile et al.[33] The $k\sigma_g$ continuum shows the expected shape resonance enhancement in the cross section which, as discussed earlier, arises from a combination of the ℓ=3 resonances associated with the CN groups. It is interesting to note that, although this shape resonant activity is not very pronounced in the cross sections, it is very evident in both the eigenphase sums and asymmetry parameters of Figs. 10 and 11, respectively, stressing the importance of these quantities in studies of molecular photoionization. Although there are some meaningful differences between our calculated $4\sigma_u \rightarrow k\sigma_g$ cross sections and those of the multiple scattering model, this σ_g shape resonance is seen in both sets of results. However, the prominent π_g shape resonance predicted by the multiple scattering model[33] is not seen in the frozen-core Hartree-Fock (static-exchange) calculations. The behavior of our cross sections near threshold suggest that a strong discrete $4\sigma_u \rightarrow n\pi_g$ transition probably lies close to threshold. In such a case the main difference between the Hartree-Fock and multiple scattering models is whether this $n\pi_g$ state lies below or above threshold. The actual location of

this feature would be strongly influenced by electron correlation effects which could be included by one of several approaches. Synchrotron radiation measurements of the photoionization cross sections would be useful in clarifying the role of shape and autoionizing resonances in this near-threshold region.

Figure 11 shows our calculated asymmetry parameters along with the synchrotron radiation data of Holland et al.,[32] the line source measurements of Kreile et al.,[33] and the results of the multiple scattering model.[33] Some of the structure seen in these measured asymmetry parameters, e.g., around 19 eV, is clearly due to autoionization, an effect which is not included in these calculations. The calculated β's, however, are in general agreement with a background contribution implied in the measured asymmetry parameters. The σ_g shape resonance is predicted to lead to a broad minimum in the asymmetry parameters around 35 eV. Finally, there are significant differences in the values of the β's predicted by the present studies and the multiple scattering model. We also note that the differences in these calculated β's for this polyatomic system are much more substantial than seen in related studies of diatomic molecules.[14]

IV. Concluding remarks

In this paper we have discussed the results of our studies of the photoionization cross sections and photoelectron asymmetry parameters of cyanogen using accurate Hartree-Fock electronic continuum states. The main purpose of these studies has been to extend our understanding of the dynamics of shape resonances from earlier studies of diatomic[14,26,38] and smaller polyatomic molecules[28,31] to the larger polyatomic system C_2N_2. These results do, in fact, reveal a rich shape resonant structure in the continuum of this polyatomic system with resonances in the σ_g, σ_u, and π_u symmetries. The low-energy σ_u resonance is, as expected, the C—C analogue of the ℓ=3 shape resonance seen in $N_2(3\sigma_g^{-1})$ and

several other diatomics. In contrast to this diatomic-like behavior, the presence of the two CN groups in C_2N_2 results in a second σ_u and a σ_g shape resonance corresponding to linear combinations of a ℓ=3 shape resonance localized on these CN sites. Moreover, our results also show a pronounced shape resonant structure in the π_u continuum. To our knowledge, such shape resonant behavior in the π_u continuum has not been seen in smaller molecular systems. Unfortunately, a comparison of these calculated photoionization cross sections and asymmetry parameters with experimental data is not presently possible since the available synchrotron radiation measurements[32] extend only up to a photon energy of 24 eV and below the energy range where many of these shape resonant features are predicted to occur in cyanogen. Finally, the agreement between the present results and those of the multiple scattering model in these studies of cyanogen is significantly less than seen in earlier studies of smaller molecular systems.[14,28]

Acknowledgments

This material is based upon research supported by the National Science Foundation under Grant No. CHE-8218166. The authors acknowledge computing support from the National Center for Atmospheric Research (NCAR) which is sponsored by the National Science Foundation.

References

1. J. L. Dehmer, D. Dill, and A. C. Parr, in: Photophysics and Photochemistry in the Vacuum Ultraviolet, edited by S. McGlynn, G. Findley, and R. Huebner (D. Reidel, Dordrecht, Holland, 1984) pp. 341-408.
2. V. McKoy, T. A. Carlson, and R. R. Lucchese, J. Phys. Chem. 88, 3188 (1984).
3. See, for example, various contributions in Resonances in Electron-Molecule Scattering, van der Waals Complexes, and Reactive Chemical Dynamics, ACS Symposium Series 263, edited by D. G. Truhlar (ACS, Washington, D. C., 1984)
4. E. W. Plummer, T. Gustafsson, W. Gudat, and D. E. Eastman, Phys. Rev. A 15, 2339 (1977).
5. B. E. Cole, D. L. Ederer, R. Stockbauer, K. Codling, A. C. Parr, J. B. West, E. D. Poliakoff, and J. L. Dehmer, J. Chem. Phys. 72, 6308 (1980).
6. T. A. Carlson, M. O. Krause, F. A. Grimm, J. D. Allen, D. Mehaffy, P. R. Keller, and J. W. Taylor, Phys. Rev. A 23, 3316 (1981).
7. T. A. Carlson, M. O. Krause, F. A. Grimm, J. D. Allen, D. Mehaffy, P. R. Keller, and J. W. Taylor, J. Chem. Phys. 75, 3288 (1981).
8. D. M. P. Holland, J. B. West, A. C. Parr, D. L. Ederer, R. Stockbauer, R. D. Buff, and J. L. Dehmer, J. Chem. Phys. 78, 124 (1983).
9. P. W. Langhoff, in Electron-Molecule and Photon-Molecule Collisions, edited by T. N. Rescigno, B. V. McKoy, and B. Schneider (Plenum, New York, 1979).
10. D. Dill and J. L. Dehmer, J. Chem. Phys. 61, 692 (1974).
11. G. Raseev, H. Le Rouzo, and H. Lefebvre-Brion, J. Chem. Phys. 72, 5701 (1980).
12. W. D. Robb and L. A. Collins, Phys. Rev. A 22, 2474 (1980).
13. B. I. Schneider and L. A. Collins, Phys. Rev. A 29, 1695 (1984).
14. R. R. Lucchese, G. Raseev, and V. McKoy, Phys. Rev. A 25, 2572 (1982).

15. M. E. Smith, V. McKoy, and R. R. Lucchese, Phys. Rev. A 29, 1857 (1984).

16. J. W. Davenport, Phys. Rev. Lett. 36, 945 (1976).

17. T. N. Rescigno, C. F. Bender, B. V. McKoy, and P. W. Langhoff, J. Chem. Phys. 68, 970 (1978).

18. R. R. Lucchese and V. McKoy, J. Phys. B 14, L629 (1981).

19. S. Wallace, D. Dill, and J. L. Dehmer, J. Phys. B 12, L417 (1979).

20. J. A. Stephens, D. Dill, and J. L. Dehmer, J. Phys. B 14, 3911 (1981).

21. N. Padial, G. Csanak, B. V. McKoy, and P. W. Langhoff, J. Chem. Phys. 69, 2992 (1978).

22. A. Gerwer, C. Asaro, B. V. McKoy, and P. W. Langhoff, J. Chem. PHys. 72, 713 (1980).

23. P. M. Dittman, D. Dill, and J. L. Dehmer, J. Chem. Phys. 76, 5703 (1982).

24. S. Southworth, C. M. Truesdale, P. H. Kobrin, D. W. Lindle, W. D. Brewer, and D. A. Shirley, J. Chem. Phys. 76, 143 (1982).

25. S. Wallace, D. Dill, and J. L. Dehmer, J. Chem. Phys. 76, 1217 (1982).

26. M. E. Smith, R. R. Lucchese, and V. McKoy, J. Chem. Phys. 79, 1360 (1983).

27. J. R. Swanson, D. Dill, and J. Dehmer, J. Phys. B 14, L207 (1981).

28. R. R. Lucchese and V. McKoy, Phys. Rev. A 26, 1406 (1982).

29. F. A. Grimm, T. A. Carlson, W. B. Press, P. Agron, J. O. Thomson, and J. W. Davenport, J. Chem. PHys. 72, 3041 (1980).

30. L. E. Machado, E. P. Leal, G. Csanak, B. V. McKoy, and P. W. Langhoff, J. Electron. Spectrosc. Relat. Phenom. 25, 1 (1982).

31. D. L. Lynch, M.-T. Lee, R. R. Lucchese, and V. McKoy, J. Chem. Phys. 80, 1907 (1984).

32. D. M. P. Holland, A. C. Parr, D. L. Ederer, J. B. West, and J. L. Dehmer, Int. Jour. Mass. Spectrom. and Ion Phys. 52, 195 (1983).

33. J. Kreile, A. Schweig, and W. Thiel, Chem. Phys. Lett. 100, 351 (1983).

34. C. Baker and D. W. Turner, Proc. R. Soc. (London) 308A, 19 (1968).

35. R. R. Lucchese and V. McKoy, Phys. Rev. A 24, 770 (1981).

36. See, for example, W. H. Miller, J. Chem. Phys. 50, 407 (1969).

37. See, for example, T. H. Dunning, Jr. and P. J. Hay, in Methods of Electronic Structure Theory, edited by H. F. Schaefer III (Plenum, New York, 1977).

38. R. R. Lucchese and V. McKoy, Phys. Rev. A 28, 1382 (1983).

39. A. D. McLean and M. Yoshimine, Tables of Linear Molecular Wave Functions (IBM Research Laboratory, San Jose, 1967), p. 218.

40. S. Bell, Chem. Phys. Lett. 67, 498 (1979).

41. M. E. Smith and V. McKoy, J. Chem. Phys. 82, 4147 (1985).

TABLE I. Basis sets used for σ, π, and δ continuum solutions.

Channel	Center	ℓ	m	Exponent
$4\sigma_u \rightarrow k\sigma_g$	N	0	0	16, 8, 4, 2, 1, 0.5
		1	0	8, 4, 2, 1, 0.5
		2	0	2, 1, 0.5
	C	0	0	16, 8, 4, 2, 1, 0.5
		1	0	8, 4, 2, 1, 0.5
		2	0	2, 1, 0.5
	CM	0	0	1, 0.5
		2	0	1.0
		4	0	0.5
$4\sigma_u \rightarrow k\pi_g$	N	1	1	8, 4, 2, 1, 0.5
		2	1	8, 4, 2, 1, 0.5
	C	1	1	8, 4, 2, 1, 0.5
		2	1	8, 4, 2, 1, 0.5
	CM	2	1	1, 0.5, 0.1
		4	1	1, 0.5, 0.1
$1\pi_g \rightarrow k\sigma_u$	N	0	0	10, 4, 2, 1, 0.5, 0.1
		1	0	4, 2, 1, 0.5, 0.1
		2	0	2, 1, 0.5, 0.1
	C	0	0	10, 4, 2, 1, 0.5, 0.1
		1	0	4, 2, 1, 0.5, 0.1
		2	0	2, 1, 0.5, 0.1
	CM	1	0	1, 0.5, 0.1
		3	0	0.5, 0.1
		5	0	0.5, 0.1
$1\pi_g \rightarrow k\pi_u$	N	1	1	8, 4, 2, 1, 0.5, 0.1
		2	1	8, 4, 2, 1, 0.5, 0.1
	C	1	1	8, 4, 2, 1, 0.5, 0.1
		2	1	2, 1, 0.5, 0.1
	CM	1	1	1, 0.5, 0.1
		3	1	1, 0.1
		5	1	0.5, 0.1
$1\pi_g \rightarrow k\delta_u$	N	2	2	8, 4, 2, 1, 0.5, 0.1
		3	2	2, 1, 0.5, 0.1
	C	2	2	8, 4, 2, 1, 0.5, 0.1
		3	2	2, 1, 0.5, 0.1
	CM	3	2	1, 0.1
		5	2	0.5, 0.1
$5\sigma_g \rightarrow k\sigma_u$	N	0	0	8, 4, 2, 1, 0.5
		1	0	8, 4, 2, 1, 0.5
		2	0	2, 1, 0.5
	C	0	0	8, 4, 2, 1, 0.5
		1	0	8, 4, 2, 1, 0.5
		2	0	2, 1, 0.5
	CM	1	0	1, 0.5
		3	0	1.0
		5	0	0.5
$5\sigma_g \rightarrow k\pi_u$	N	1	1	8, 4, 2, 1, 0.5
		2	1	8, 4, 2, 1, 0.5
	C	1	1	8, 4, 2, 1, 0.5
		2	1	2, 1, 0.5
	CM	1	1	1, 0.5
		3	1	1.0
		5	1	0.5

FIGURE CAPTIONS

Fig. 1: The $1\pi_g \rightarrow k\sigma_u$, $k\pi_u$, and $k\delta_u$ partial channel photoionization cross sections for $C_2N_2^+$: $1\pi_g \rightarrow k\sigma_u$, ——— (length) and – – – (velocity); $1\pi_g \rightarrow k\pi_u$, — – — – (length) and —— —— —— (velocity); $1\pi_g \rightarrow k\delta_u$, —— – – —— (length) and —— — — — —— — — — (velocity).

Fig. 2: The $1\pi_g \rightarrow k\sigma_u$ and $k\pi_u$ partial channel cross sections with the continuum $k\sigma_u$ and $k\pi_u$ wave functions orthogonalized to the $5\sigma_u$ and $2\pi_u$ orbitals respectively: $1\pi_g \rightarrow k\sigma_u$, ———; $1\pi_g \rightarrow k\pi_u$, – – – – .

Fig. 3: Eigenphase sums for the $1\pi_g \rightarrow k\sigma_u$ (———), $1\pi_g \rightarrow k\pi_u$ (– – – –), and $1\pi_g \rightarrow k\delta_u$ (—— – ——) components.

Fig. 4: Calculated cross sections for the $X^2\Pi_g$ state of $C_2N_2^+$: present results, ——— (length) and – – – – (velocity); present results with the orthogonalized continuua, —— – —— (length) and —— —— —— (velocity); multiple scattering model, —— – – —— (Ref. 33).

Fig. 5: Photoelectron asymmetry parameters for the $X^2\Pi_g$ state: present results, ——— (length) and – – – – (velocity); multiple scattering results, —— – —— (Ref. 33); experimental results (v=0), X (Ref. 32).

Fig. 6: Photoionization cross sections for the $A^2\Sigma_g^+$ state of $C_2N_2^+$: present results (length), ——— (total), – – – – ($5\sigma_g \rightarrow k\sigma_u$), and —— – —— ($5\sigma_g \rightarrow k\pi_u$); multiple scattering results, —— – – —— (total, Ref. 33).

Fig. 7: Eigenphase sums for the $5\sigma_g \rightarrow k\sigma_u$ (———) and $5\sigma_g \rightarrow k\pi_u$ (– – – –) channels.

Fig. 8: Asymmetry parameter for the $A^2\Sigma_g^+$ state: present results (length) (———); multiple scattering results of Ref. 33 (— – — –); experimental results (ν=0) of Ref. 32 (X); experimental results of Ref. 33, Δ ($\nu_1=\nu_2=0$) and □ ($\nu_1=1$, $\nu_2=0$).

Fig. 9: Calculated photoionization cross sections for the $B^2\Sigma_u^+(4\sigma_u^{-1})$ state: present results; ——— (total), – – – – ($4\sigma_u \rightarrow k\sigma_g$), and —— – —— – ($4\sigma_u \rightarrow k\pi_g$); multiple scattering results of Ref. 33, —— – – —— (total).

Fig. 10: Eigenphase sums for the $4\sigma_u \rightarrow k\sigma_g$ (———) and $4\sigma_u \rightarrow k\pi_g$ (– – –) channels.

Fig. 11: Asymmetry parameter for $(4\sigma_u)^{-1}$ photoionization. See caption for Fig. 8.

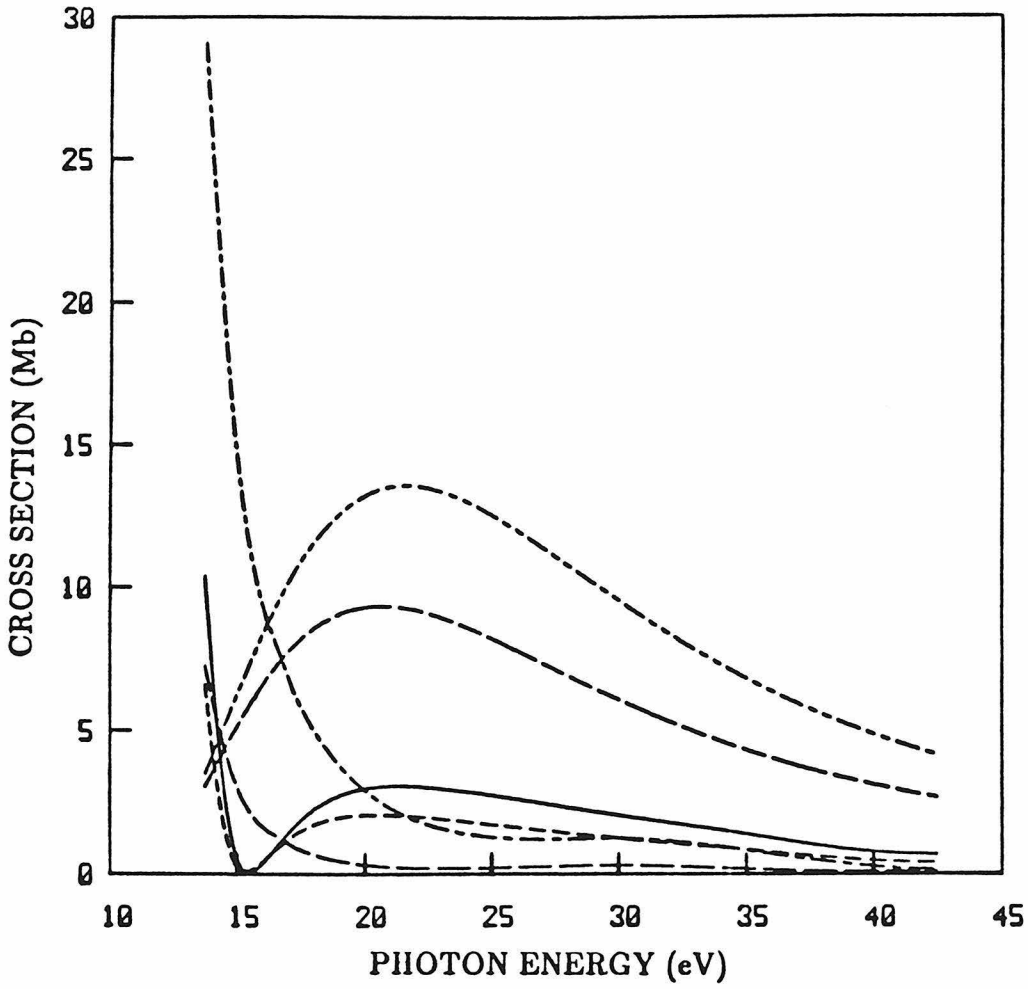
30
25
20
15
10
5
0
CROSS SECTION (Mb)
10
15
20
25
30
35
40
45
PHOTON ENERGY (eV)

Figure 1

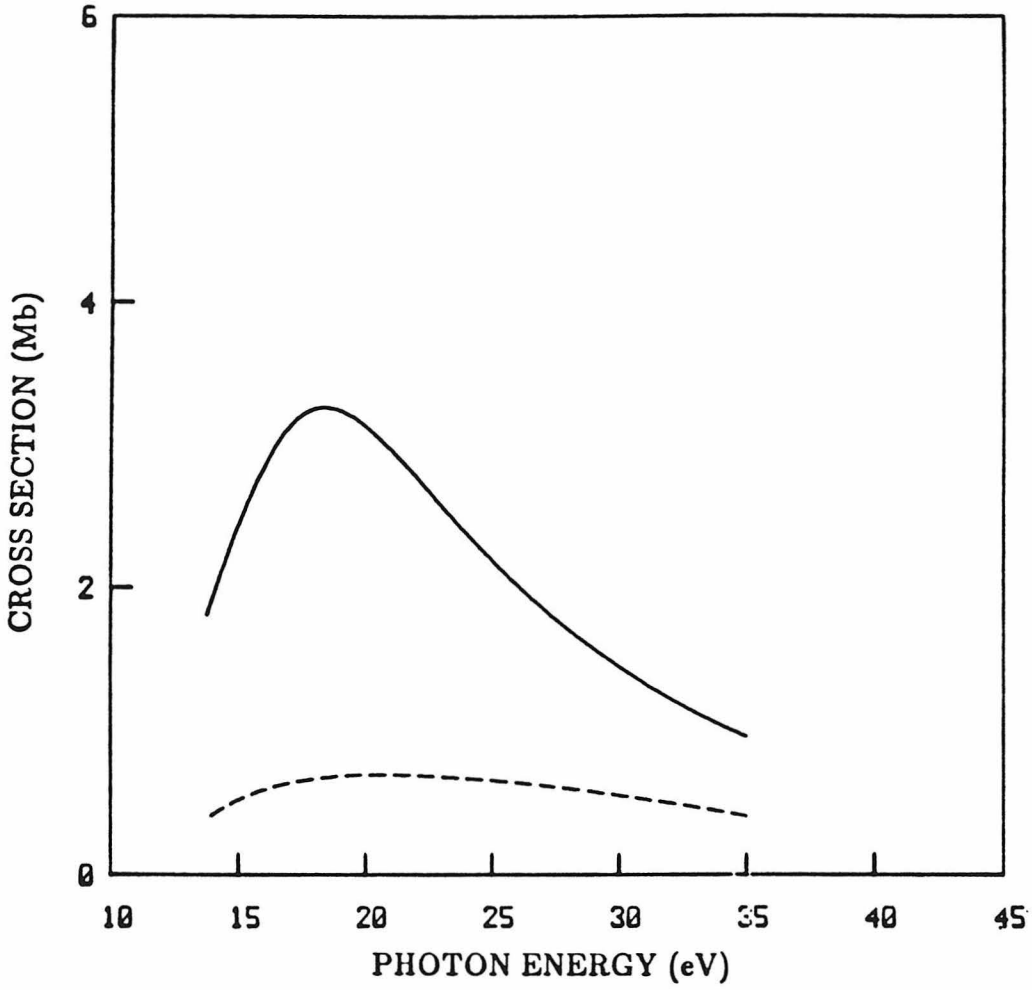

Figure 2

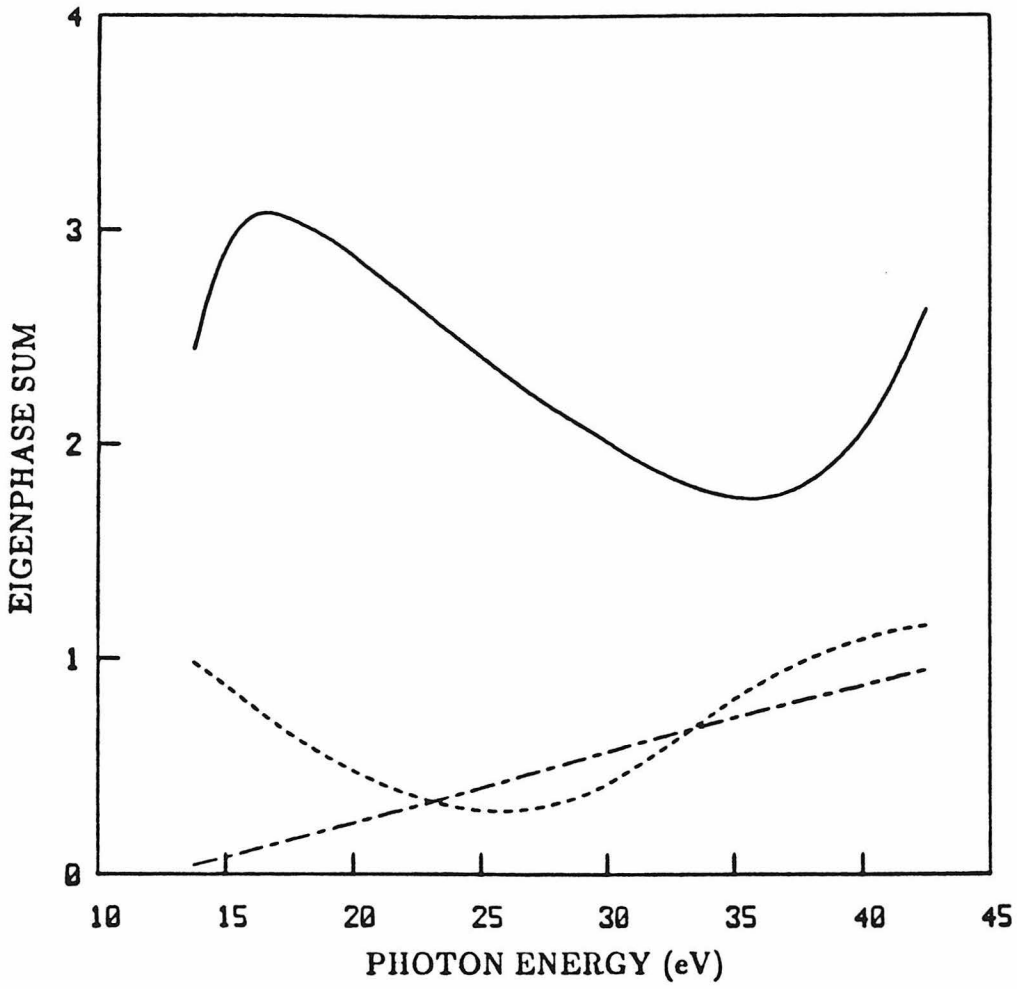

Figure 3

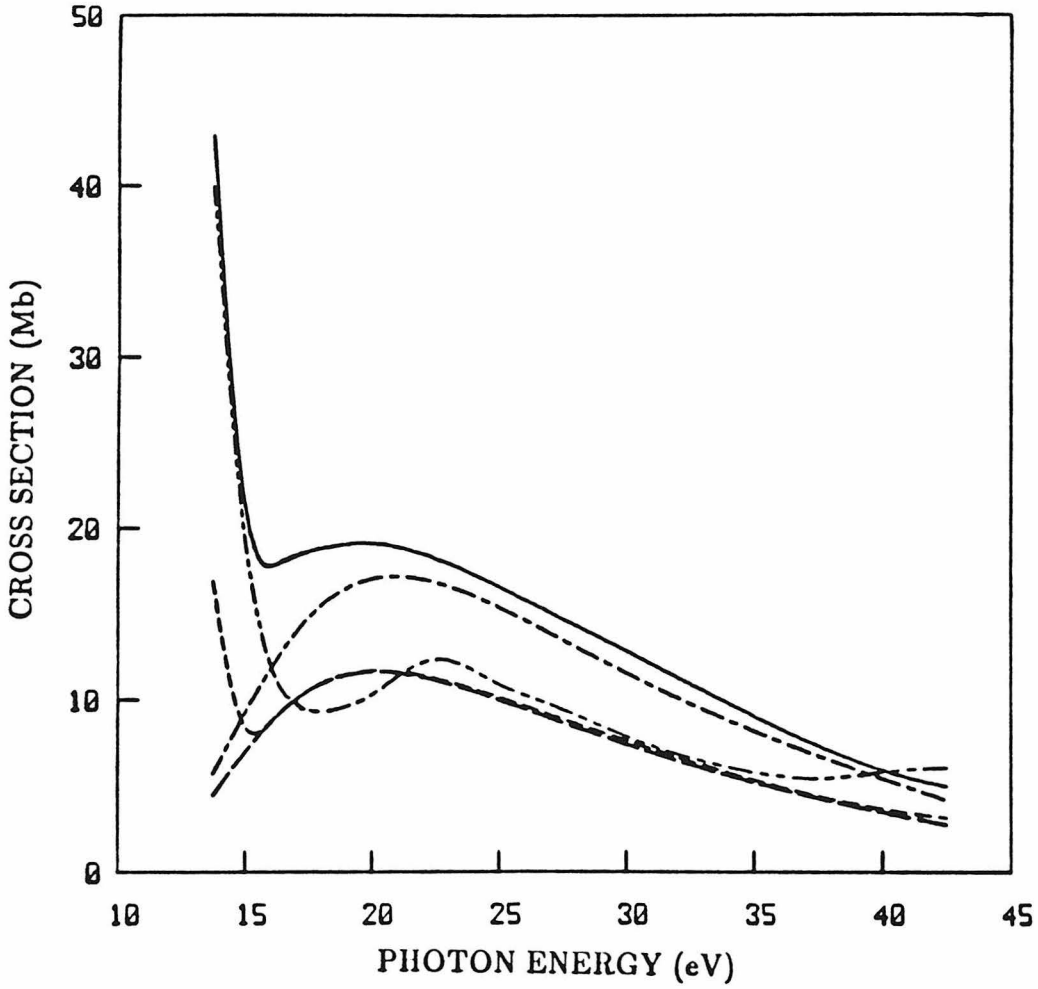
50
40
30
20
10
0
CROSS SECTION (Mb)
10
15
20
25
30
35
40
45
PHOTON ENERGY (eV)

Figure 4

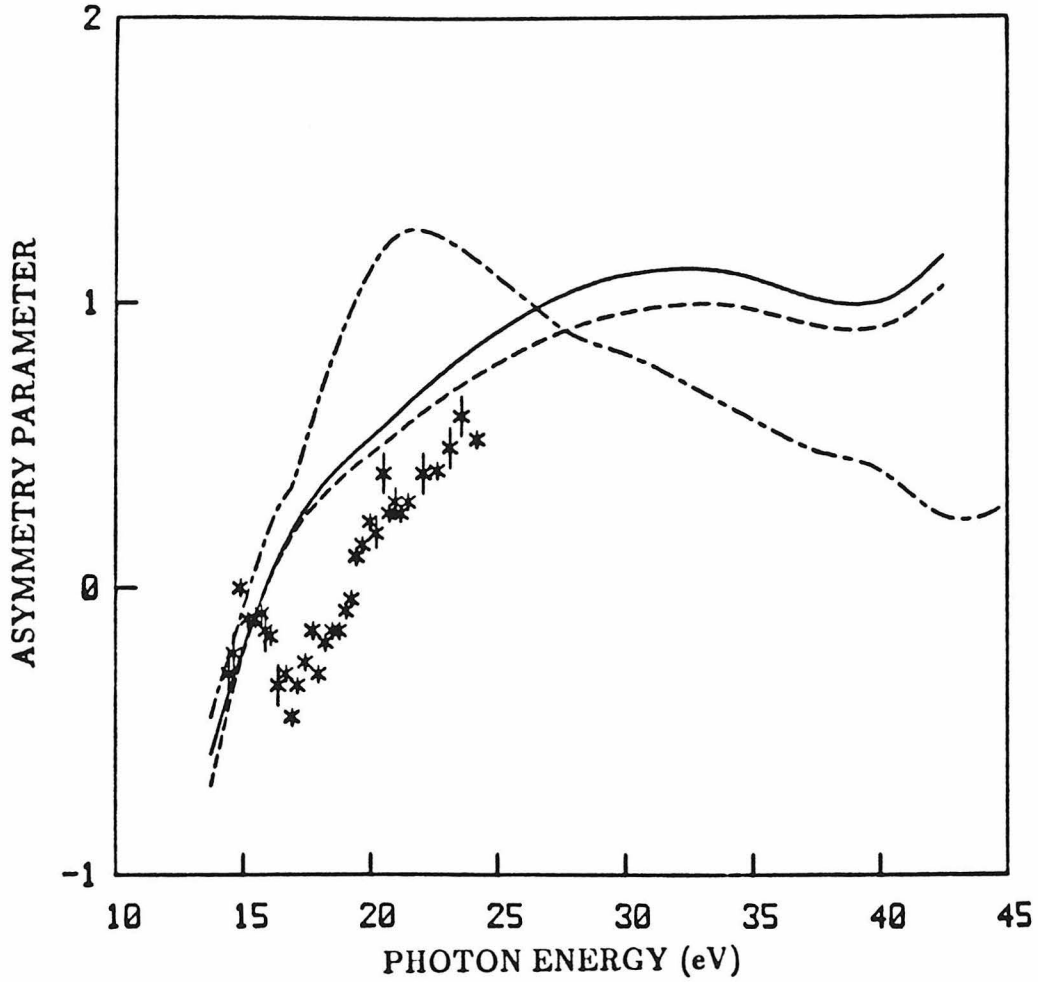
2
1
0
-1
ASYMMETRY PARAMETER
10
15
20
25
30
35
40
45
PHOTON ENERGY (eV)

Figure 5

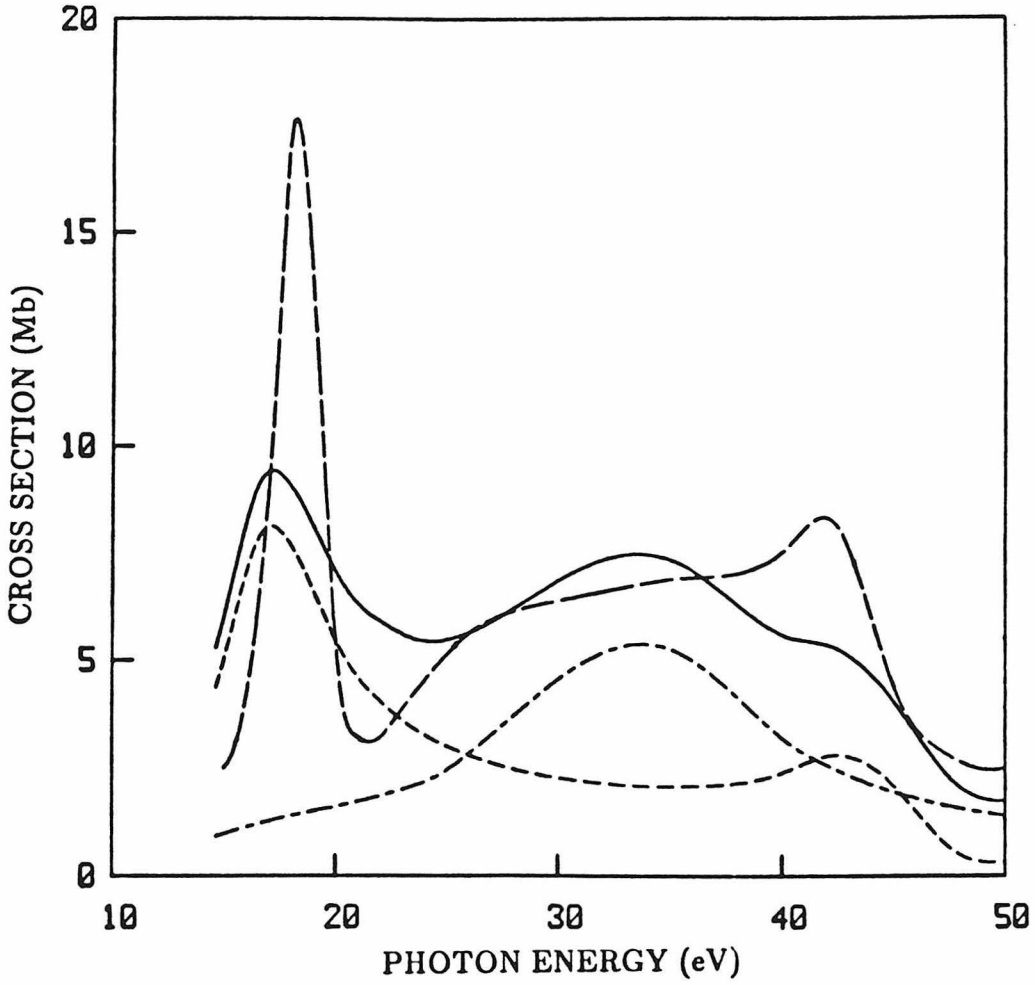

Figure 6

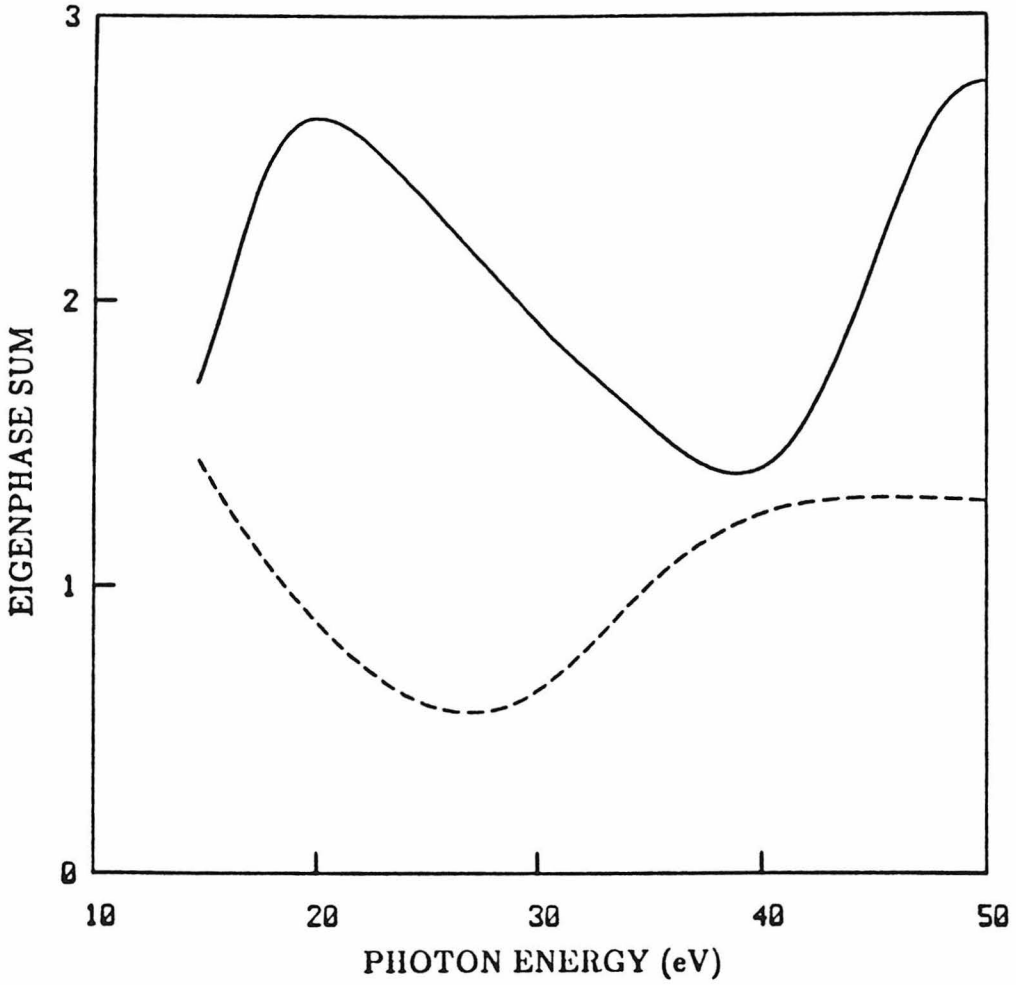

Figure 7

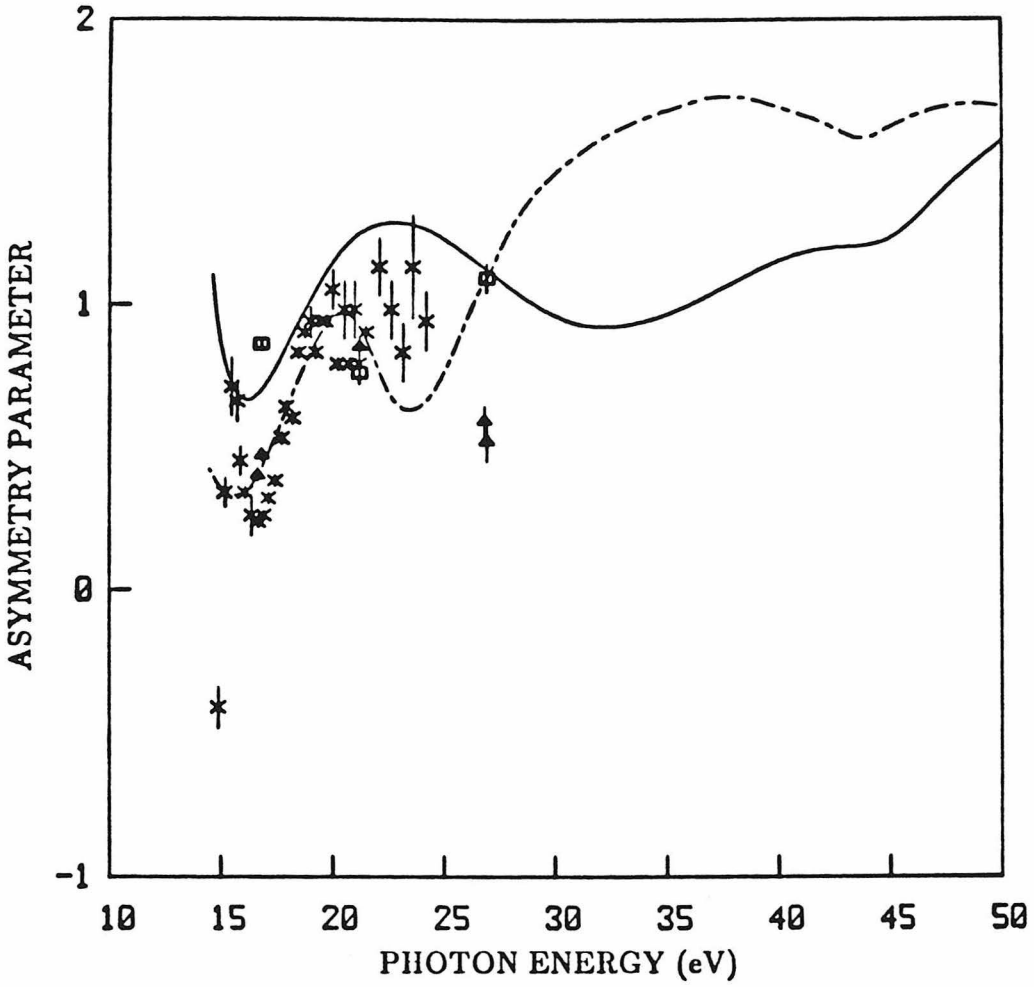
2
1
0
-1
ASYMMETRY PARAMETER
10
15
20
25
30
35
40
45
50
PHOTON ENERGY (eV)

Figure 8

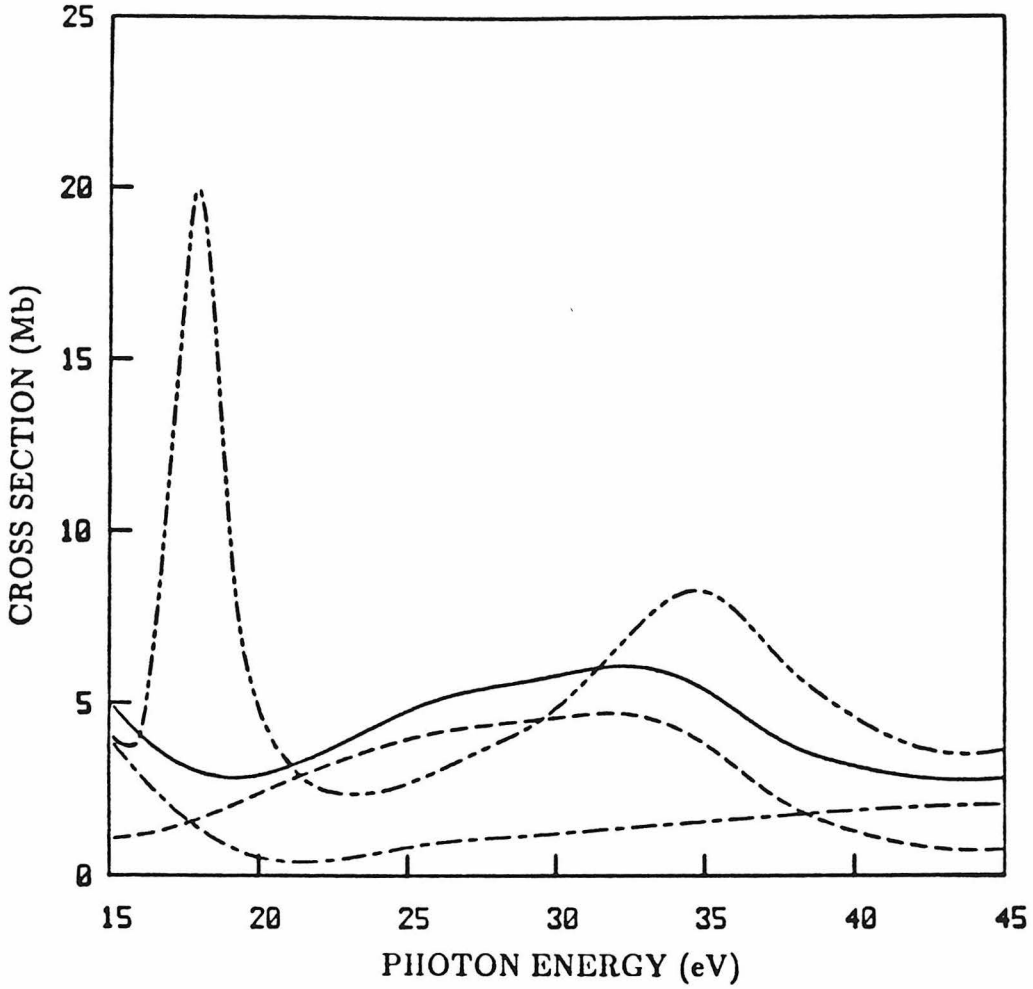
25
20
15
10
5
0
CROSS SECTION (Mb)
15
20
25
30
35
40
45
PHOTON ENERGY (eV)

Figure 9

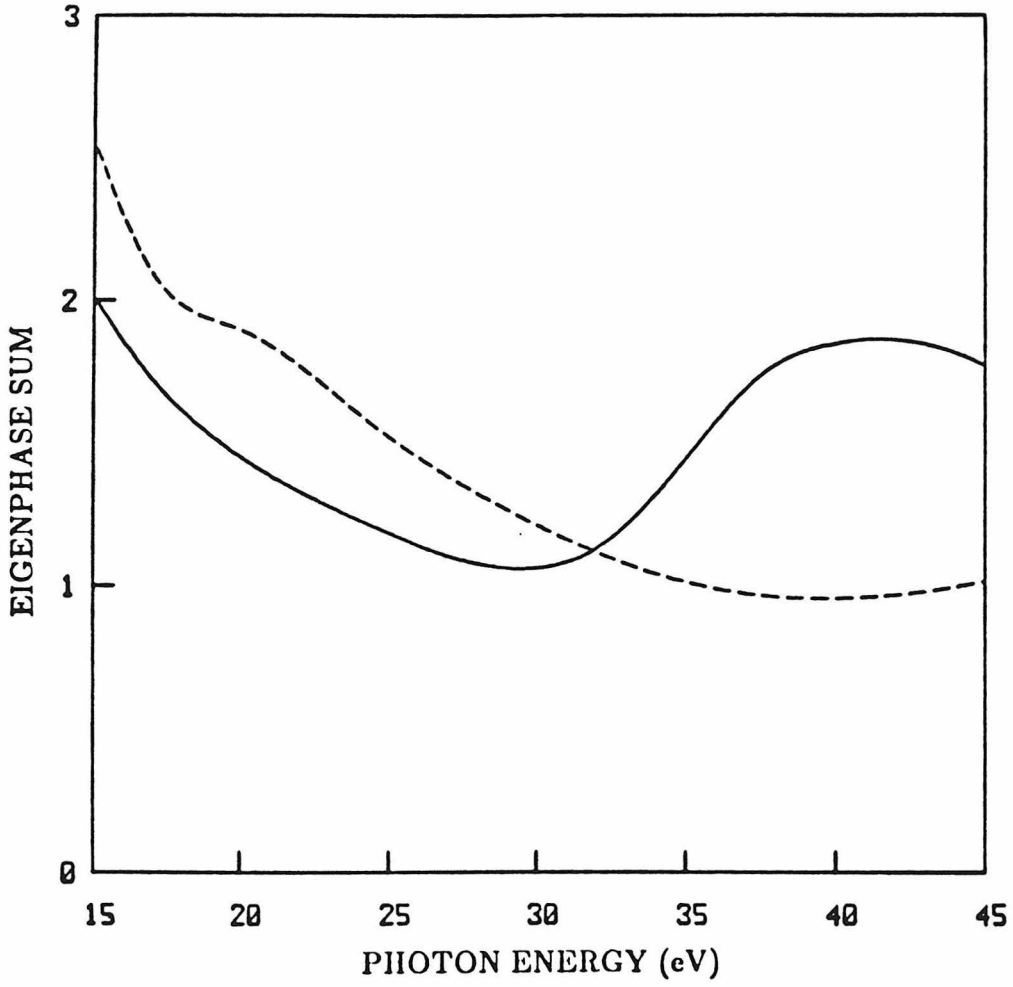

Figure 10

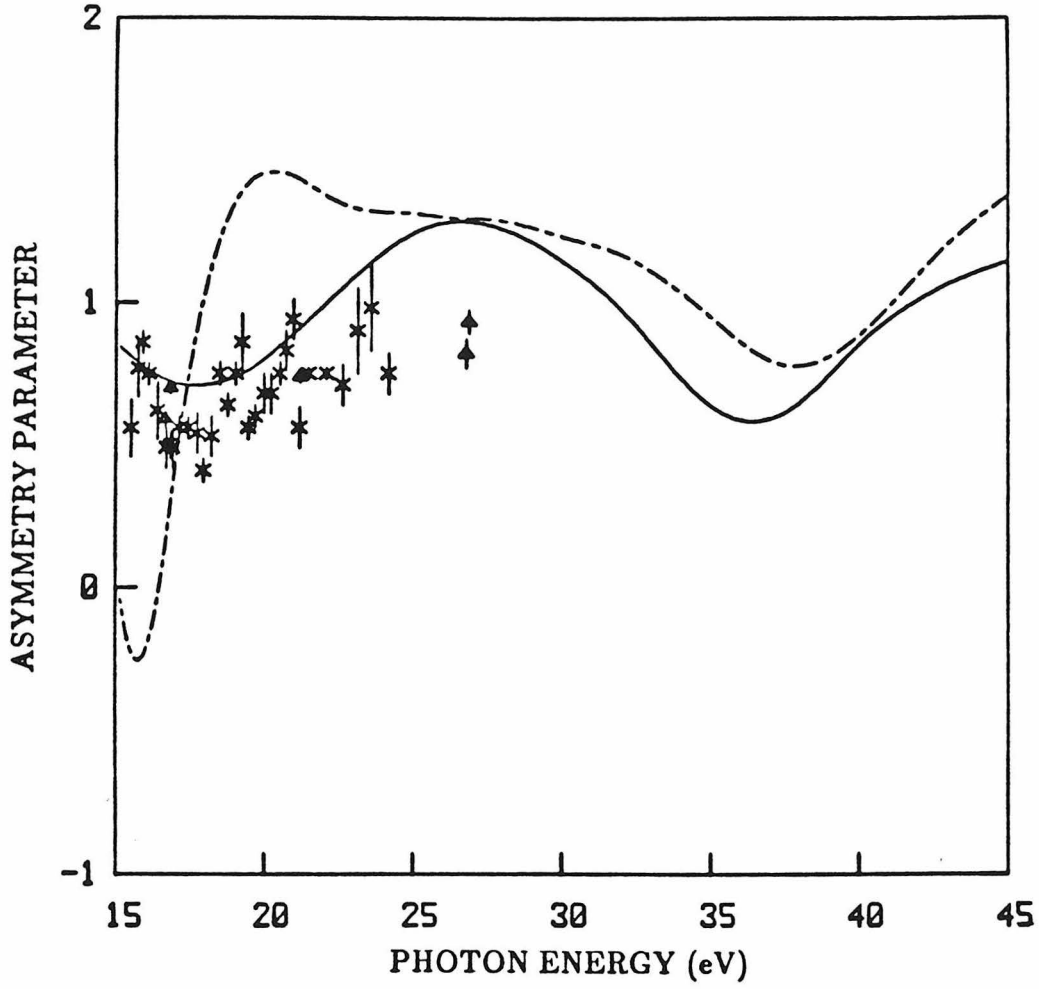
2
1
0
-1
ASYMMETRY PARAMETER
15
20
25
30
35
40
45
PHOTON ENERGY (eV)

Figure 11

SECTION C

RESONANCE EFFECTS IN THE 5σ PHOTOIONIZATION OF CO

I. INTRODUCTION

Shape resonances are known to lead to several prominent and important features in molecular photoionization. Among these features are non-Franck-Condon vibrational branching ratios over a wide energy range around the resonance and photoelectron angular distributions which are vibrational state dependent.[1-8] These effects arise from the strong dependence of the dipole transition matrix element for photoionization on internuclear separation. It is this dependence which can be expected to lead to non-Franck-Condon behavior. Such non-Franck-Condon vibrational intensity distributions due to a shape resonance were first predicted by Dehmer *et al.*[3] for photoionization of the $3\sigma_g$ level of N_2 and confirmed experimentally for this same system by West *et al.*[2]

The studies of Dehmer *et al.*,[3] which used the continuum multiple scattering model, predicted larger deviations from Franck-Condon behavior than were observed experimentally.[2] The results of subsequent studies of these vibrational branching ratios using Hartree-Fock photoelectron continuum orbitals were in very good agreement with the measured data for photon energies away from known autoionizing features.[8] This result is not surprising since the Hartree-Fock model can be expected to work well for shape resonances which are, in fact, one-electron in nature.

Non-Franck-Condon behavior has also been observed in both the vibrational intensities[4] and photoelectron angular distributions[5] for photoionization of the 5σ level of CO for photon energies between 16 and 27 eV. Although the σ shape resonance in the photoionization continuum of CO, in analogy to the $3\sigma_g$ channel of N_2, should also contribute significantly to this non-Franck-Condon behavior, both the experimental data[4,5] and

theoretical studies of these vibrational intensities and angular distributions[9] suggest that this behavior arises from a more subtle and physically important interplay between shape and autoionizing resonances in CO than in N_2. The difference in the non-Franck-Condon behavior around the shape resonance in N_2 and CO arises from the observation that whereas, in N_2 the peak of the $3\sigma_g \rightarrow k\sigma_u$ shape resonance lies at 5 eV above the doubly excited autoionizing state at 23 eV, in CO the maximum of the shape resonance and the autoionizing state are within about 1.5 eV of each other. Since both the shape and autoionizing resonances lead to non-Franck-Condon behavior, some important differences can be expected in the vibrational intensities and related angular distributions in these two systems. In fact, Stephens *et al.*[9] have used the continuum multiple scattering model to obtain the non-Franck-Condon behavior due to the shape resonance in the 5σ photoionization of CO. The significant discrepancies between the results of these calculations and the experimental data, particularly for the higher vibrational levels, were attributed to an autoionizing resonance.

In this paper we report vibrational branching ratios and photoelectron asymmetry parameters for shape resonant photoionization of the 5σ level of CO. These studies are carried out using Hartree-Fock continuum states for the photoelectron orbital and, hence, should adequately account for the non-Franck-Condon behavior of the branching ratios and asymmetry parameters arising from the shape resonance. Such information is an important first step towards understanding the role of the autoionizing resonance in the observed photoionization cross sections. We will see, in fact, that our calculated branching ratios for the $\nu'=1$ and 2 levels,

are quite different from those of the multiple scattering model and help to readily identify the autoionizing contributions to the experimentally observed structure. Further calculations are required to include the effect of the autoionizing resonance on the cross sections. Such studies are under way. We note, however, that the electronic configuration of this autoionizing resonance is not yet certain. Stephens *et al.*[9] have suggested the doubly excited configuration $5\sigma 1\pi^3 2\pi^2$. As we will see, if this is the correct electronic configuration, the autoionizing resonance will interact not with the σ shape resonant continuum but with the non-resonant π background.

The outline of the paper is as follows. In the next section we present some relevant details of our procedure for obtaining the photoionization matrix elements and of the potential energy curves used. We then compare the resulting vibrational branching ratios and photoelectron angular distributions for $\nu'=0,1$, and 2 with the available experimental data and with the results of calculations using the multiple scattering model.

II. METHOD AND CALCULATIONS

In our calculations of the photoionization cross sections we use a Hartree-Fock wave function for the initial state. For the final photoionized state we use a frozen-core Hartree-Fock model in which the bound orbitals are assumed idential to those in the initial state Hartree-Fock wave function and the photoelectron continuum orbital is determined in the field of these (N-1) unrelaxed core orbitals. The Hartree-Fock photoelectron continuum orbitals then satisfy a one-electron Schrödinger equation

$$(-\frac{1}{2}\nabla^2 + V_{N-1}(\underset{\sim}{r},R) - k^2/2)\,\phi_{\underset{\sim}{k}}(\underset{\sim}{r},R) = 0 \qquad (1)$$

where $\frac{k^2}{2}$ is the photoelectron kinetic energy and $\phi_{\underset{\sim}{k}}$ satisfies the appropriate boundary conditions. If we expand this continuum orbital $\phi_{\underset{\sim}{k}}$ in spherical harmonics defined about the direction of $\underset{\sim}{k}$, i.e.,

$$\phi_{\underset{\sim}{k}}(\underset{\sim}{r},R) = (\frac{2}{\pi})^{\frac{1}{2}} \sum_{\ell m} i^{\ell}\, \psi_{k\ell m}(\underset{\sim}{r},R)\, Y^{*}_{\ell m}(\hat{k}) \qquad (2)$$

the functions $\psi_{k\ell m}(\underset{\sim}{r},R)$ satisfy the same Schrödinger equation as $\phi_{\underset{\sim}{k}}$ itself. With these functions $\psi_{k\ell m}(\underset{\sim}{r},R)$ we define the length and velocity forms of the photoionization transition matrix element as

$$I^{L}_{\ell m\mu}(R) = k^{\frac{1}{2}} < \phi_{5\sigma}(\underset{\sim}{r},R)|r_{\mu}|\psi_{k\ell m}(\underset{\sim}{r},R) > \qquad (3)$$

and

$$I^{V}_{\ell m\mu}(R) = \frac{k^{\frac{1}{2}}}{E} < \phi_{5\sigma}(\underset{\sim}{r},R)|\nabla_{\mu}|\psi_{k\ell m}(\underset{\sim}{r},R) > \qquad (4)$$

where $\phi_{5\sigma}$ is the occupied 5σ orbital of CO and E is the photon energy. In terms of these matrix elements $I^{L,V}_{\ell m\mu}$ the cross section for photoionization of the 5σ orbital out of the ν=0 vibrational level of the ground state and into the ν'=n level of CO^{+} can be written as

$$\sigma^{L,V}_{\nu=0,\nu'=n} = \frac{4\pi^2}{3c} E \sum_{\ell m\mu} |< \chi_i^{\nu=0}(R)|I^{L,V}_{\ell m\mu}|\chi_f^{\nu'=n}(R) >|^2 \qquad (5)$$

where the χ's are vibrational wave functions and c is the speed of light.

The corresponding photoelectron asymmetry parameter is defined as

$$\frac{d\sigma^{L,V}_{\nu=0,\nu'=n}}{d\Omega_{\hat{k}}} = \frac{\sigma^{L,V}_{\nu=0,\nu'=n}}{4\pi} \left(1 + \beta^{L,V}_{k,\nu=0,\nu'=n} P_2 (\cos\theta)\right) \qquad (6)$$

where θ is the angle between the direction of polarization of the light and the momentum of the electron.

To obtain the photoelectron continuum orbital $\psi_{k\ell m}$, which satisfies the Schrödinger equation of Eq.(1), $\psi_{k\ell m}$ is further expanded in partial waves. The resulting coupled equations are solved using an adaptation of the Schwinger variational principle for long-range potentials in which the static component of the electron-molecule interaction is treated exactly by numerical integration and the exchange interactions are approximated by a separable potential of the Schwinger type.[10] This method,[10] which leads to variationally stable scattering matrices and photoionization cross sections at the Hartree-Fock level, has been shown to be effective for obtaining electronic continuum solutions of strongly polar ions such as $CO^+[5\sigma^{-1}]$. Furthermore, the method also includes an iterative procedure for obtaining the converged scattering solutions. Details of this approach are discussed in Ref. 10. In these studies we used the same partial wave expansions as those assumed by Lucchese and McKoy[11] in their vibrationally-unresolved studies of the 5σ photoionization of CO. These expansion parameters should provide converged cross sections.

The photoelectron transition matrix element $I_{\ell m\mu}(R)$ of Eqs.(3) and (4) were evaluated at the five internuclear separations of R = 1.898, 2.015, 2.132, 2.249, and 2.366 a.u. where the equilibrium internuclear distance of CO is 2.132 a.u. At each internuclear distance we used the

SCF wave function of McLean and Yoshimine.[12] In this wave function the molecular orbitals are expanded in Slater-type functions. The initial basis set used in the solution of the Lippmann-Schwinger equation associated with the Schrödinger equation, Eq.(1), contained seven Cartesian Gaussian functions defined by

$$\phi_{\ell mn}(\underset{\sim}{r}) = N_{\ell mn}(x-A_x)^{\ell}(y-A_y)^{m}(z-A_z)^{n} \cdot \exp\left(-\alpha|\underset{\sim}{r}-\underset{\sim}{A}|^2\right) . \qquad (7)$$

These basis functions are specified in Table 1. To ensure convergence of the photoionization cross sections, we evaluated the matrix element in Eq.(3) using photoelectron orbitals obtained after one step in our iterative procedure for solving the Lippmann-Schwinger equation.[10]

The vibrational wave functions were obtained from numerical solution of the Schrödinger equation using RKR potentials. We have outlined this method in our earlier studies of N_2.[8] For CO and CO^+ we used the RKR curves of Tobias *et al.*[13] (R_e = 1.128Å) and Singh and Rai[14] (R_e = 1.115Å), respectively. With this approach we obtained the following Franck-Condon factors (FCF): (ν=0,ν'=0) = 0.9607, (ν=0,ν'=1) = 0.0391, and (ν=0,ν'=2) = 0.000152. These values agree quite well with the FCF's obtained previously by Albritton[15] ((ν=0,ν'=1) = 0.038) and Wacks[16] ((ν=0,ν'=0) = 0.9636, (ν=0,ν'=1) = 0.03634, (ν=0,ν'=2) = 0.00011).

III. RESULTS AND DISCUSSION

Figure 1 shows the fixed-nuclei cross sections for photoionization out of the 5σ orbital of CO at five internuclear distances. The photon energy scale here assumes an ionization potential of 14.0 eV. For reasons that are well-understood, the resonance broadens and shifts to

higher energy as the internuclear distance decreases. It is this dependence of the cross section on internuclear distance that leads to non-Franck-Condon behavior in the vibrational state distributions and photoelectron angular distributions.

In Fig. 2 we show the vibrationally resolved 5σ cross sections for the $\nu'=0$, $\nu'=1$, and $\nu'=2$ levels. It is worth noting that although the resonances in $\nu'=1$ and 2 are shifted to higher energy than in $\nu'=0$, the shift in going from $\nu'=0$ to $\nu'=1$ is smaller than in N_2.[4,8] In this figure the cross sections for $\nu'=1$ and 2 are actually scaled up by factors of 10 and 100, respectively. The vibrational branching ratios for photoionization into the $\nu'=1$ and $\nu'=2$ levels, expressed as a percentage of the $\nu'=0$ level, are shown in Figs. 3 and 4 along with the predictions of the multiple scattering model[9] and the experimental data of Stockbauer *et al.*[4] The horizontal dashed lines in these figures represent the Franck-Condon values of the branching ratios.

A comparison of our calculated branching ratios and the measured values shows that structure due to the autoionizing resonance distinctly dominates the observed branching ratios over this range of photon energies. The enhancement in the branching ratios centered around 19.5 eV has been attributed to unresolved autoionization structure associated with the $CO^+ B^2\Sigma^+$ state at 19.7 eV.[5] The structure broadly centered around 23 eV is not well understood but has been suggested[9] to arise from autoionization of a valence-like state with a possible electron configuration of $\ldots 4\sigma^2 5\sigma 1\pi^3 2\pi^2$. This autoionizing feature is also very apparent in a comparison of calculated vibrationally unresolved photoionization cross sections with the experimental data.[11] These results, which are taken

from an earlier publication,[11] are shown in Fig. 5 for convenience. In this figure the feature appears as a broad hump between about 21 and 25 eV lying on a slowly varying shape resonant background. The branching ratios in Figs. 2 and 3 also indicate that this autoionizing state influences the branching ratios over a similar energy range and beyond. Again, this behavior is consistent with a valence-like resonance in this region which would be expected to affect the branching ratios over a wider energy range than a sharp Rydberg-like autoionizing state. This may be the reason for the differences between the calculated and measured $\nu'=1/\nu'=0$ branching ratios around 27 eV and, possibly, above. The trend in the measured $\nu'=2/\nu'=0$ branching ratios at 27 eV, and its similarity to the calculated shape-resonant values, suggests that it is beyond this energy that the branching ratios will be dominated by the shape resonance. Measurements of these branching ratios at higher photon energies are clearly needed. It is worth noting that if the autoionizing state around 23 eV does have the electron configuration $...4\sigma^2 5\sigma 1\pi^3 2\pi^2$, such a resonance will couple with the non-shape-resonant $^1\Pi$ background continuum and not with the $k\sigma$ shape resonant continuum. Finally, comparison of the branching ratios obtained from the multiple scattering model[9] with the present results and the measured ratios shows that this model overestimates the magnitude of the non-Franck-Condon behavior arising from the shape resonance but certainly illustrates the underlying feature.

The occurence of non-Franck-Condon behavior due to overlapping of a shape and autoionizing resonance in the $\nu'=1/\nu'=0$ branching ratios of CO^+ in Fig. 3 differs significantly from what was seen in earlier studies of the photoionization of $N_2(3\sigma_g^{-1})$. As discussed by Stephens *et al.*,[9]

and seen very clearly in recent measurements of the photoelectron asymmetry parameters of $N_2^+(3\sigma_g^{-1})X^2\Sigma_g^+$, $\nu'=0$,[21] although the autoionizing resonance also occurs around 23 eV in N_2, the shape-resonant non-Franck-Condon behavior there has a maximum at about 34 eV, well removed from the 25 eV position in CO. It is also interesting to note that the suggested valence configuration[9,17] of ... $1\pi_u^3 3\sigma_g 1\pi_g^2(^1\Pi_u)$ for this resonance in N_2 would be consistent with the known role of the core-excited $1\pi_u^3 3\sigma_g^2 1\pi_g^2(^2\Pi_u)$ shape resonance, with a $1\pi_u^3 3\sigma_g^2 1\pi_g(^3\Sigma_u)$ parent, in the electron impact excitation spectrum of N_2.[22]

Figures 6-8 show our calculated photoelectron asymmetry parameters for the $\nu'=0$, 1, and 2 vibrational levels of $CO^+(X^2\Sigma^+)$ along with the experimental data of Cole *et al.*[5] and the results of the multiple scattering model.[9] The measured photoelectron asymmetry parameters are again dominated by structure due to the autoionizing resonances which appear as pronounced dips from the smooth background of the calculated values. The calculated asymmetry parameters show a minimum which becomes more developed and moves to lower energy with increasing ν'. The behavior in the calculated $\nu'=0$ asymmetry parameters at higher energy, e.g., the shallow minimum around 32 eV, also agrees with the vibrationally unresolved measurements of Marr *et al.*,[23] reflecting the dominance of the $\nu=0 \rightarrow \nu'=0$ component. Measurements of these asymmetry parameters for the $\nu'=1$ and $\nu'=2$ levels at higher photon energies, i.e., beyond 27 eV, would provide a useful check of the predicted behavior in Figs. 7 and 8.

ACKNOWLEDGMENTS

This material is based upon research supported by the National Science Foundation under Grant No. CHE-8521391.

References

1. J. L. Dehmer, D. Dill, and A. C. Parr, in *Photophysics and Photochemistry in the Vacuum Ultraviolet*, edited by S. P. McGlynn *et al.* (Reidel, Dorcrecht, Holland, 1985), pp. 341-408.
2. J. B. West, A. C. Parr, B. E. Cole, D. L. Ederer, R. Stockbauer, and J. L. Dehmer, J. Phys. B 13, L105 (1980).
3. J. L. Dehmer, D. Dill, and S. Wallace, Phys. Rev. Lett. 43, 1005 (1979).
4. R. Stockbauer, B. E. Cole, D. L. Ederer, J. B. West, A. C. Parr, and J. L. Dehmer, Phys. Rev. Lett. 43, 757 (1979).
5. B. E. Cole, D. L. Ederer, R. Stockbauer, K. Codling, A. C. Parr, J. B. West, E. D. Poliakoff, and J. L. Dehmer, J. Chem. Phys. 72, 6308 (1980).
6. T. A. Carlson, M. O. Krause, D. Mehaffy, J. W. Taylor, F. A. Grimm, and J. D. Allen Jr., J. Chem. Phys. 73, 6056 (1980).
7. P. R. Keller, D. Mehaffy, J. W. Taylor, F. A. Grimm, and T. A. Carlson, J. Electron. Spectrosc. Relat. Phenom. 27, 223 (1982).
8. R. R. Lucchese and V. McKoy, J. Phys. B 14, L629 (1981).
9. J. A. Stephens, D. Dill, and J. L. Dehmer, J. Phys. B 14, 3911 (1981).
10. M. E. Smith, R. R. Lucchese, and V. McKoy, Phys. Rev. A 29, 1857 (1984).
11. R. R. Lucchese and V. McKoy, Phys. Rev. A 28, 1382 (1983).
12. A. D. McLean and M. Yoshimine, *Tables of Linear Molecule Wave Functions* (IBM San Jose Research Laboratory, San Jose, CA, 1967).
13. I. Tobias, R. J. Fallon, and J. T. Vanderslice, J. Chem. Phys. 33, 1638 (1960).
14. R. B. Singh and D. K. Rai, J. Mol. Spectrosc. 19, 424 (1966).
15. D. L. Albritton (quoted as a private communication in Ref. 9).

16. M. Wacks, J. Chem. Phys. 41, 930 (1964).

17. J. W. Davenport, Phys. Rev. Lett. 36, 945 (1976).

18. N. Padial, G. Csanak, B. V. McKoy, and P. W. Langhoff, J. Chem. Phys. 69, 2992 (1978).

19. A. Hamnett, W. Stoll, and C. E. Brion, J. Electron Spectrosc. Relat. Phenom. 8, 367 (1976).

20. E. W. Plummer, T. Gustaffson, W. Gudat, and D. E. Eastman, Phys. Rev. A 15, 2339 (1977).

21. S. H. Southworth, A. C. Parr, J. E. Hardis, and J. L. Dehmer, Phys. Rev. A 33, 1020 (1986).

22. J. Mazeau, F. Gresteau, R. I. Hall, G. Joyez, and J. Reinhardt, J. Phys. B 6, 862 (1973).

23. G. V. Marr, J. M. Morton, R. M. Homes, and D. G. McCoy, J. Phys. B 12, 43 (1979).

TABLE I. Initial scattering basis sets used in obtaining the σ and π photoelectron orbitals.[a]

	Center	ℓ	m	n	α
$5\sigma \rightarrow k\sigma$	C	0	0	0	10.0,4.0,1.5,0.5,0.1
	C	0	0	1	1.0,0.1
	O	0	0	0	10.0,4.0,1.5,0.5,0.1
	O	0	0	1	1.0,0.1
$5\sigma \rightarrow k\pi$	C	1	0	0	10.0,4.0,1.5,0.5,0.1
	C	1	0	1	1.0,0.1
	O	1	0	0	10.0,4.0,1.5,0.5,0.1
	O	1	0	1	1.0,0.1

[a]See Eq.(7) in text.

FIGURE CAPTIONS

FIG. 1. Fixed-nuclei photoioniztion cross sections (dipole length) for the 5σ level of CO at five internuclear distances.

FIG. 2. Vibrationally-resolved photoionization cross sections for the ν'=0,1, and 2 levels of the $X^2\Sigma^+(5\sigma^{-1})$ state of CO^+: ———, dipole length; — — —, dipole velocity.

FIG. 3. Branching ratio for the ν'=1 level of $CO^+X^2\Sigma^+$: ———, present results (dipole length); —— – ——, multiple scattering model (Ref. 9); x, experimental results (Ref. 4); — — —, Franck-Condon values.

FIG. 4. Branching ratio for the ν'=2 level of CO^+ $X^2\Sigma^+$: ———, present results (dipole length); —— - ——, multiple scattering model (Ref. 9); x, experimental results (Ref. 4); — — —, Franck-Condon values.

FIG. 5. Vibrationally unresolved photoionization cross sections for the $X^2\Sigma^+(5\sigma^{-1})$ level of CO^+: ——— , present results (dipole length), ——— - ———, present results (dipole velocity); ----, multiple scattering model (Ref. 17); — — —, Stieltjes-Tchebycheff moment theory (Ref. 18); ●, experimental date (Ref. 19); ▲, experimental data (Ref. 20). [See Ref. 11 for further details of this figure.]

FIG. 6. Photoelectron asymmetry parameters for the ν'=0 level of CO^+ $X^2\Sigma^+$: ———, present results (dipole length); — — —, multiple scattering model (Ref. 9); x, measured values (Ref. 5)

FIG. 7. Photoelectron asymmetry parameters for the $\nu'=1$ level of CO^+ $X^2\Sigma^+$: ———, present results (dipole length); — — —, multiple scattering model (Ref. 9); x, measured values (Ref. 5).

FIG. 8. Photoelectron asymmetry parameters for the $\nu'=2$ level of CO^+ $X^2\Sigma^+$: ——— , present results (dipole length): — — —, multiple scattering model (Ref. 9), x, measured values (Ref. 5).

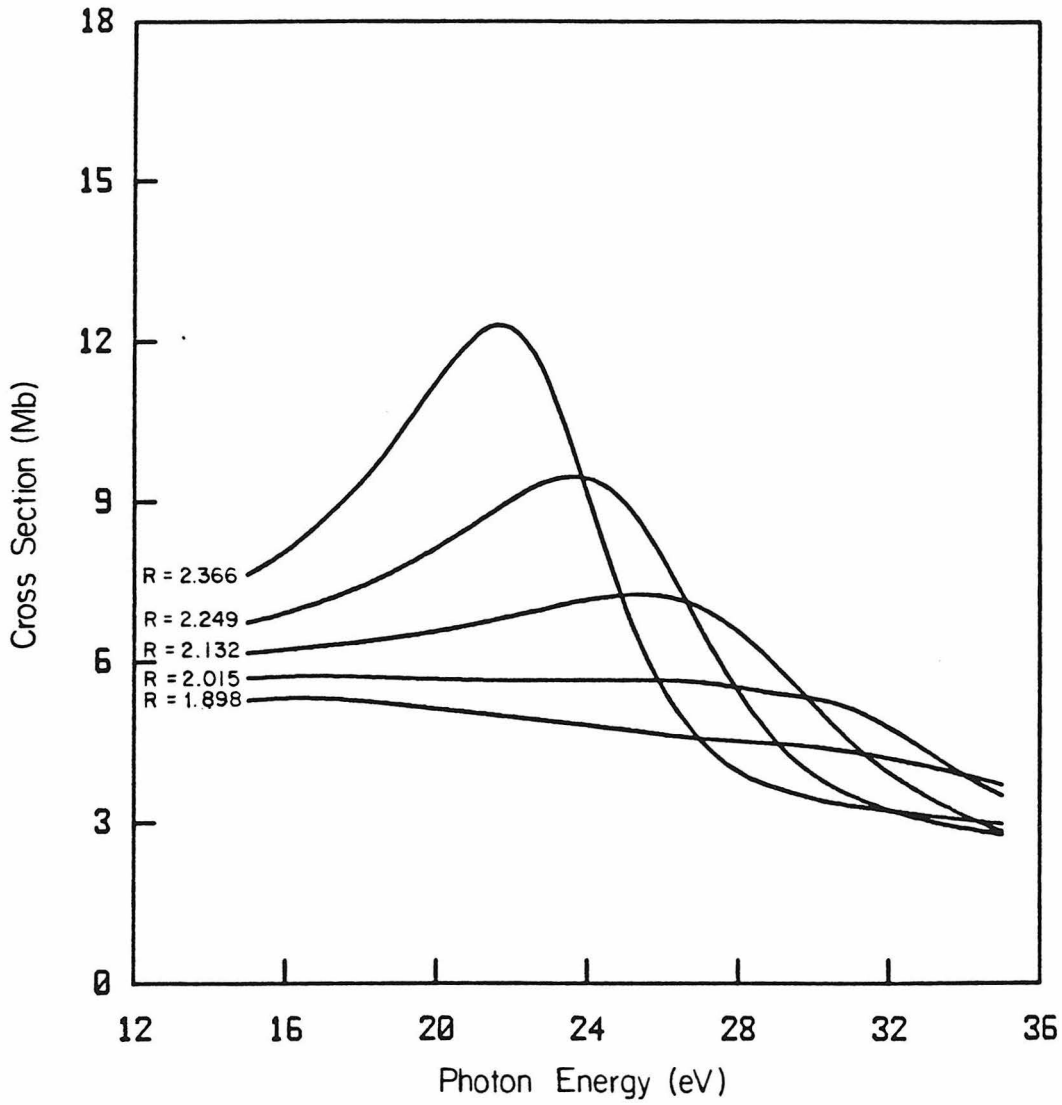
18
15
12
9
6
3
0
Cross Section (Mb)
R = 2.366
R = 2.249
R = 2.132
R = 2.015
R = 1.898
12
16
20
24
28
32
36
Photon Energy (eV)

Figure 1

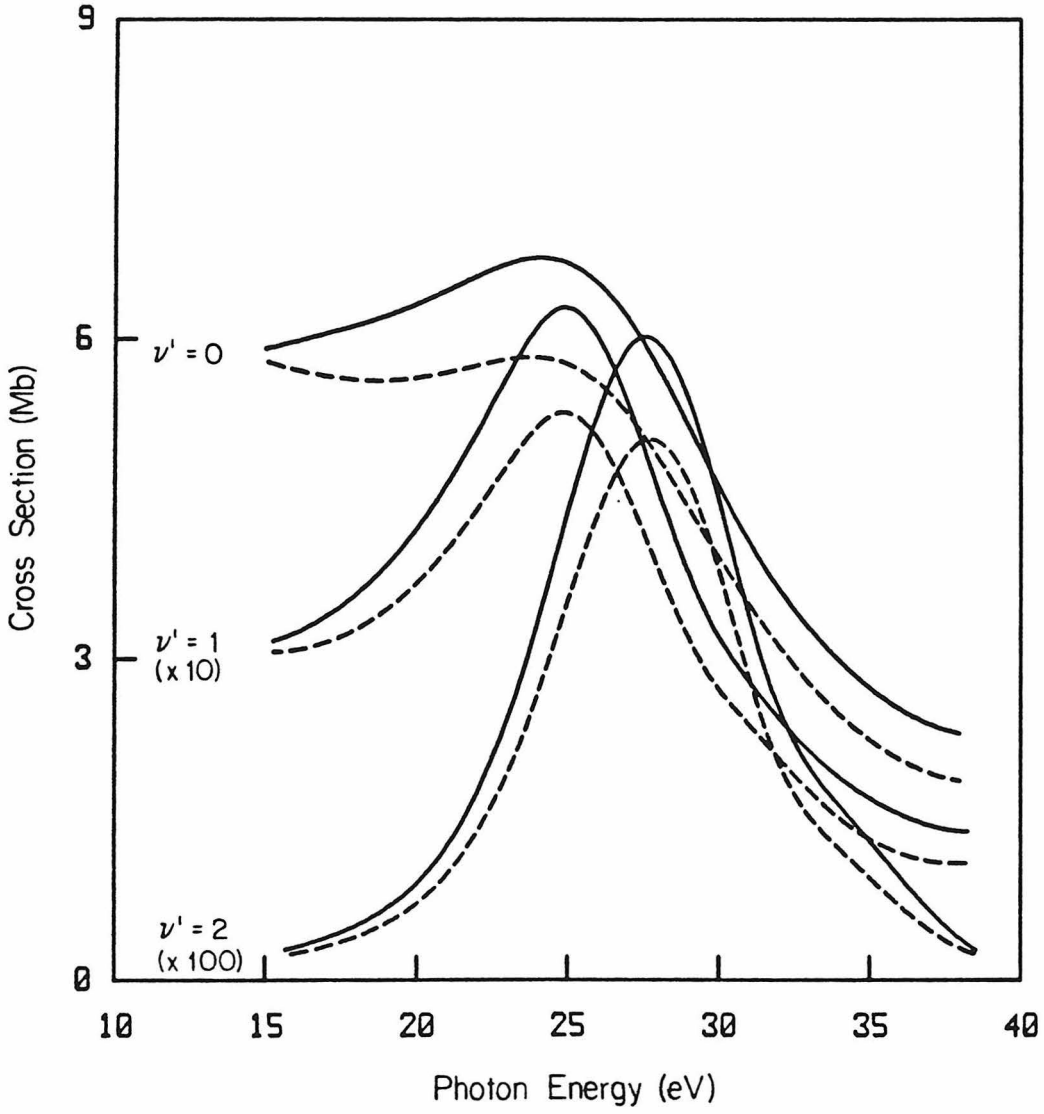
9
6
3
0
Cross Section (Mb)
ν' = 0
ν' = 1
(x 10)
ν' = 2
(x 100)
10
15
20
25
30
35
40
Photon Energy (eV)

Figure 2

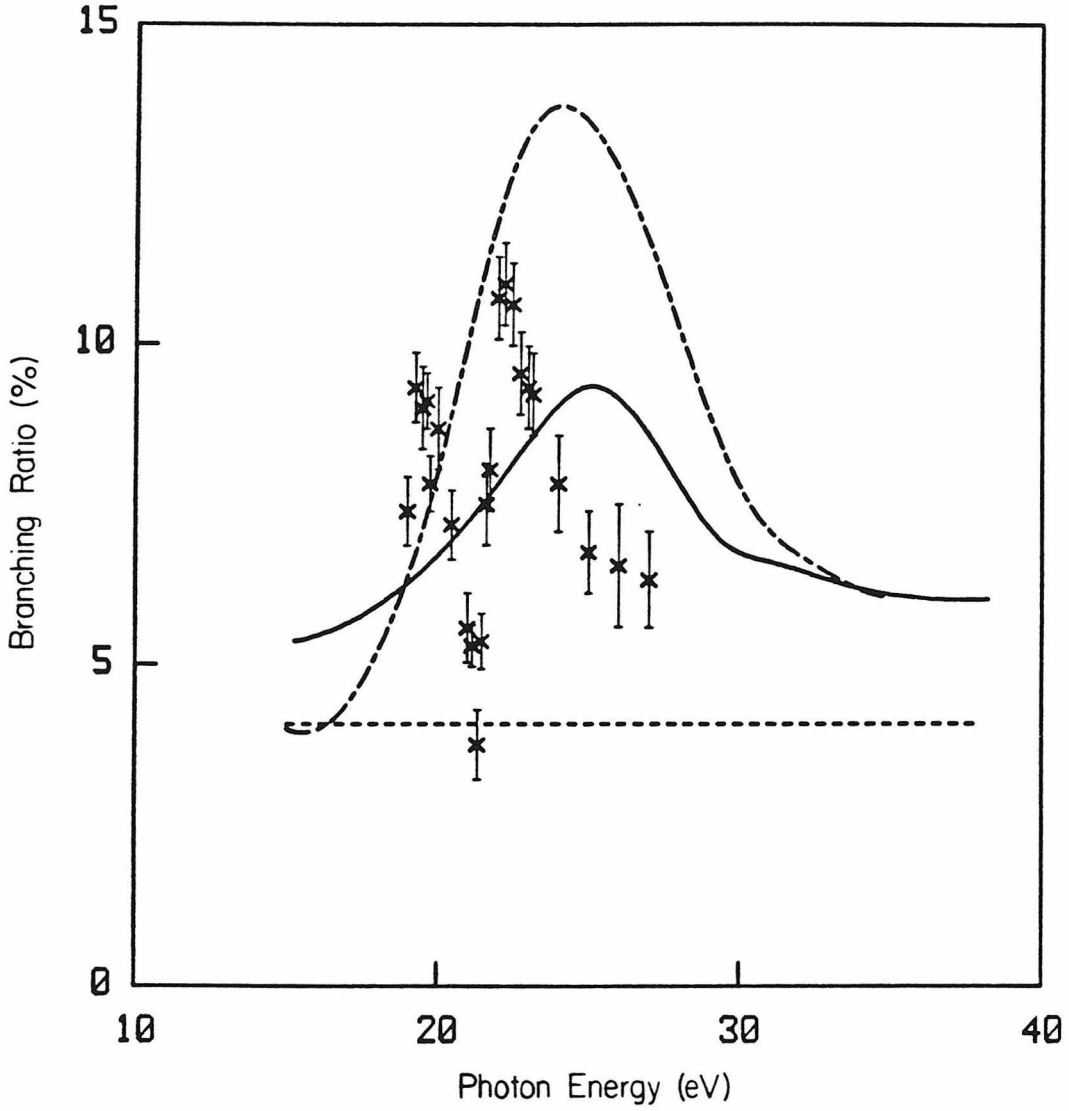

Figure 3

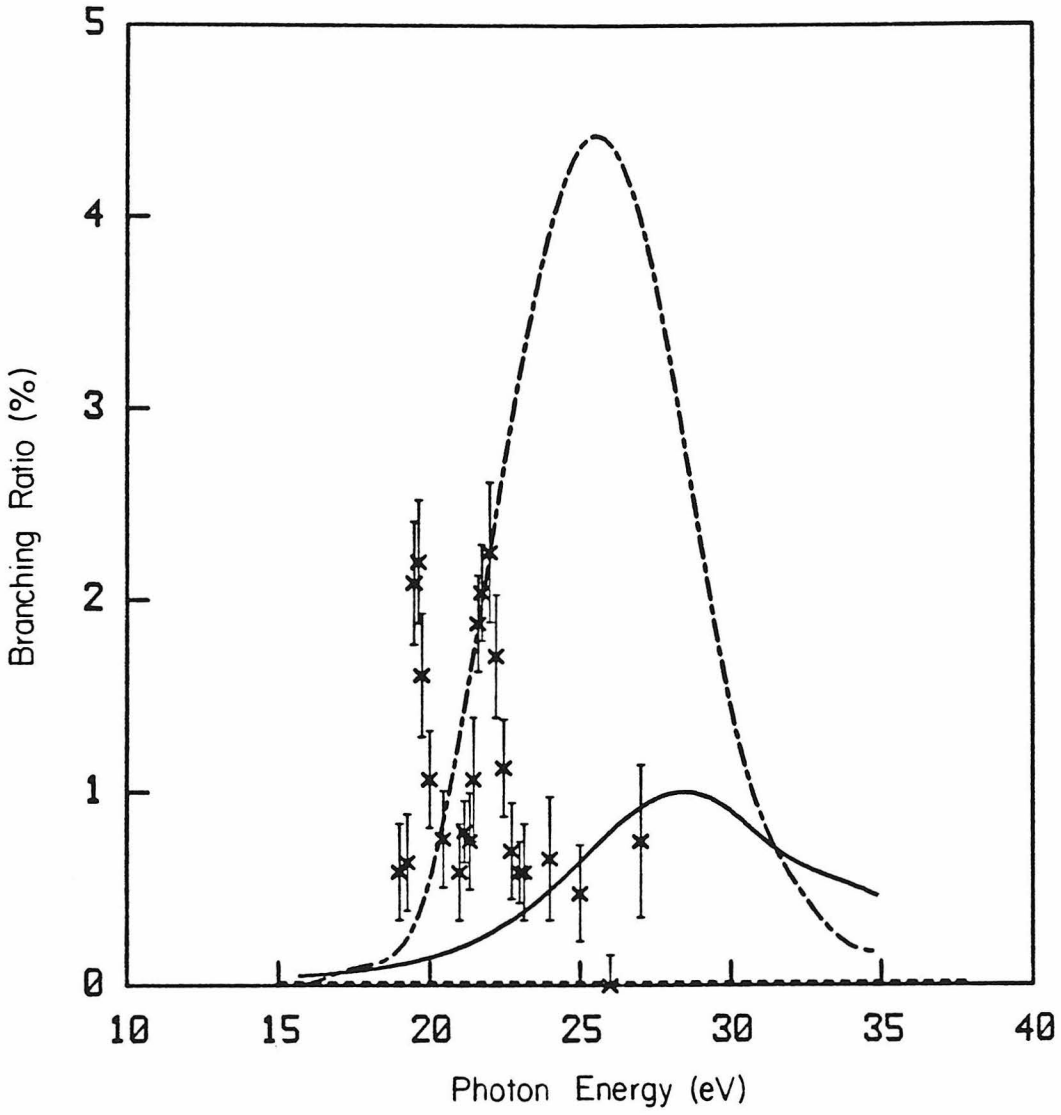

Figure 4

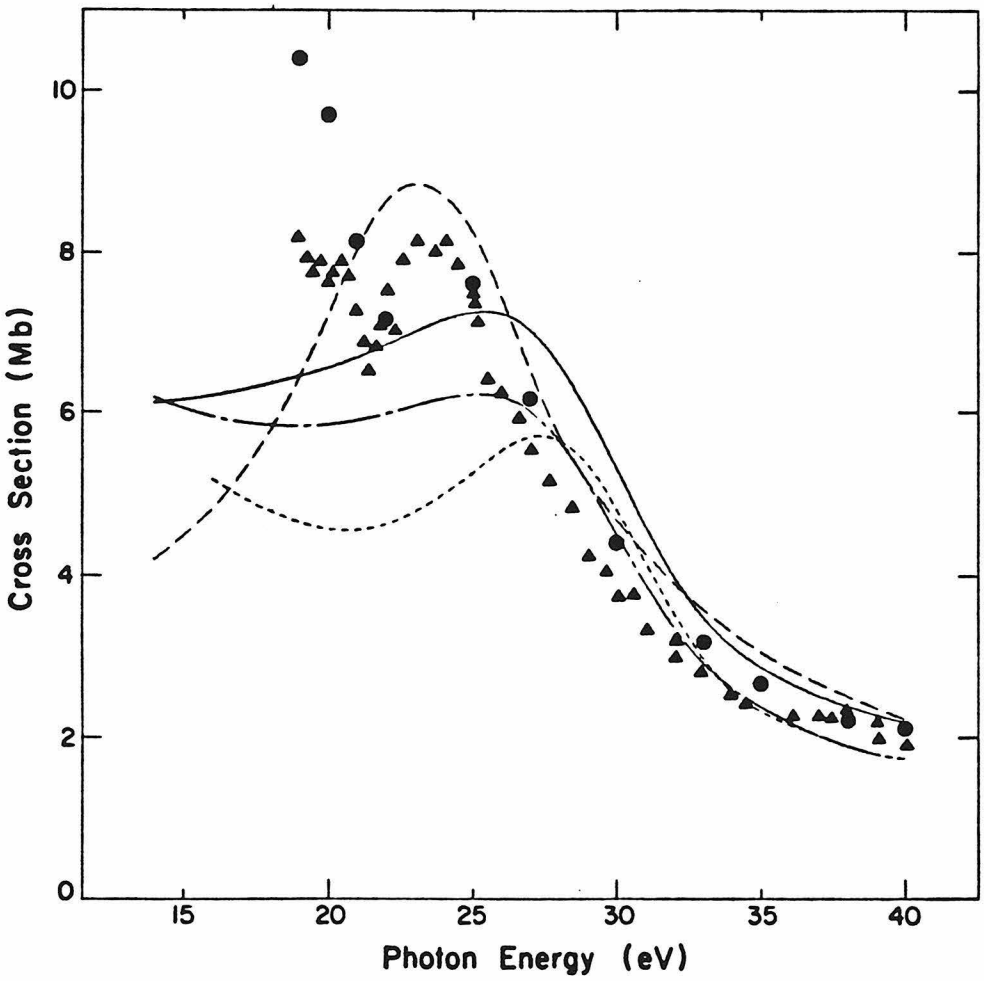

Figure 5

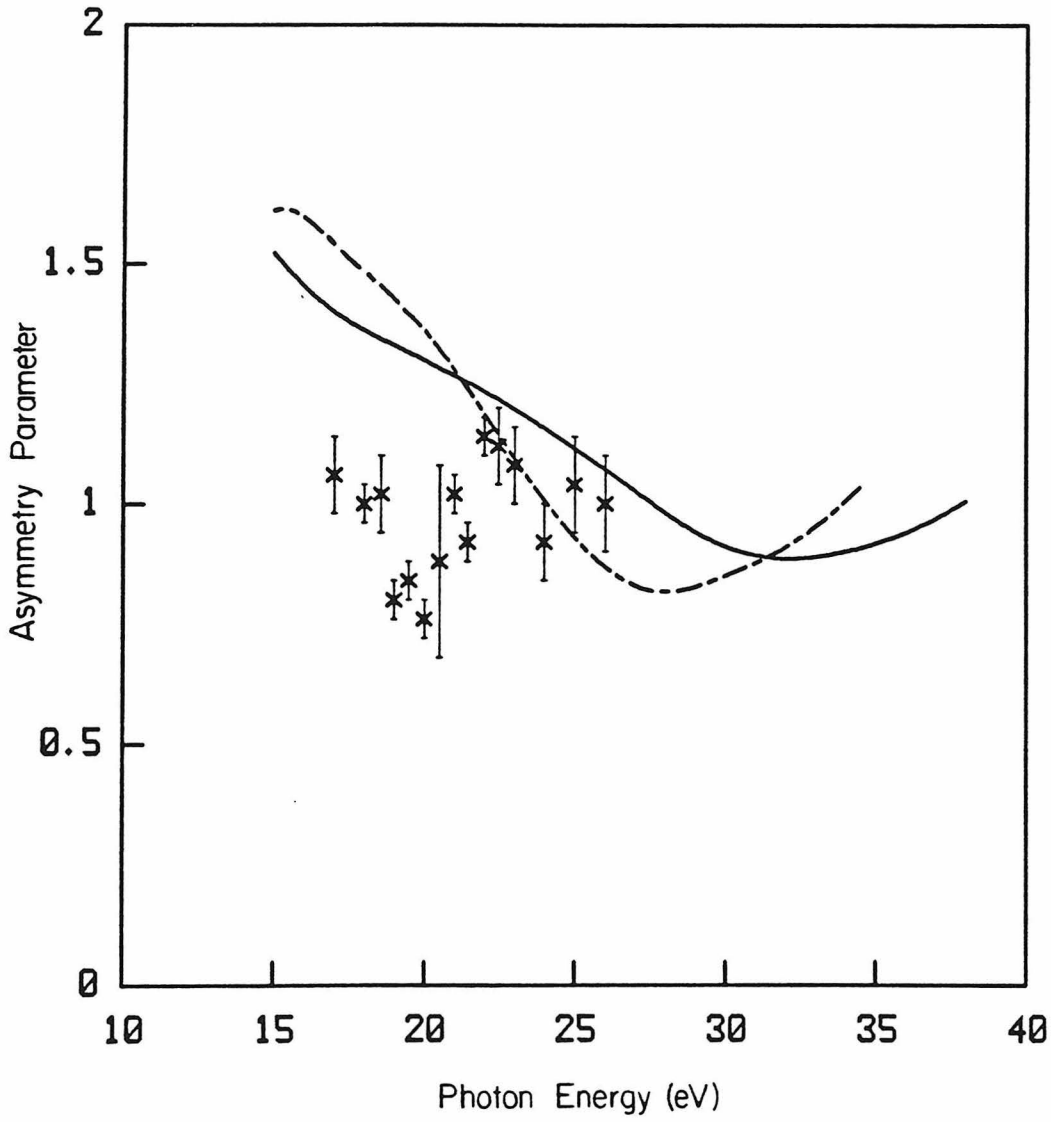
2
1.5
1
0.5
0
Asymmetry Parameter
10
15
20
25
30
35
40
Photon Energy (eV)

Figure 6

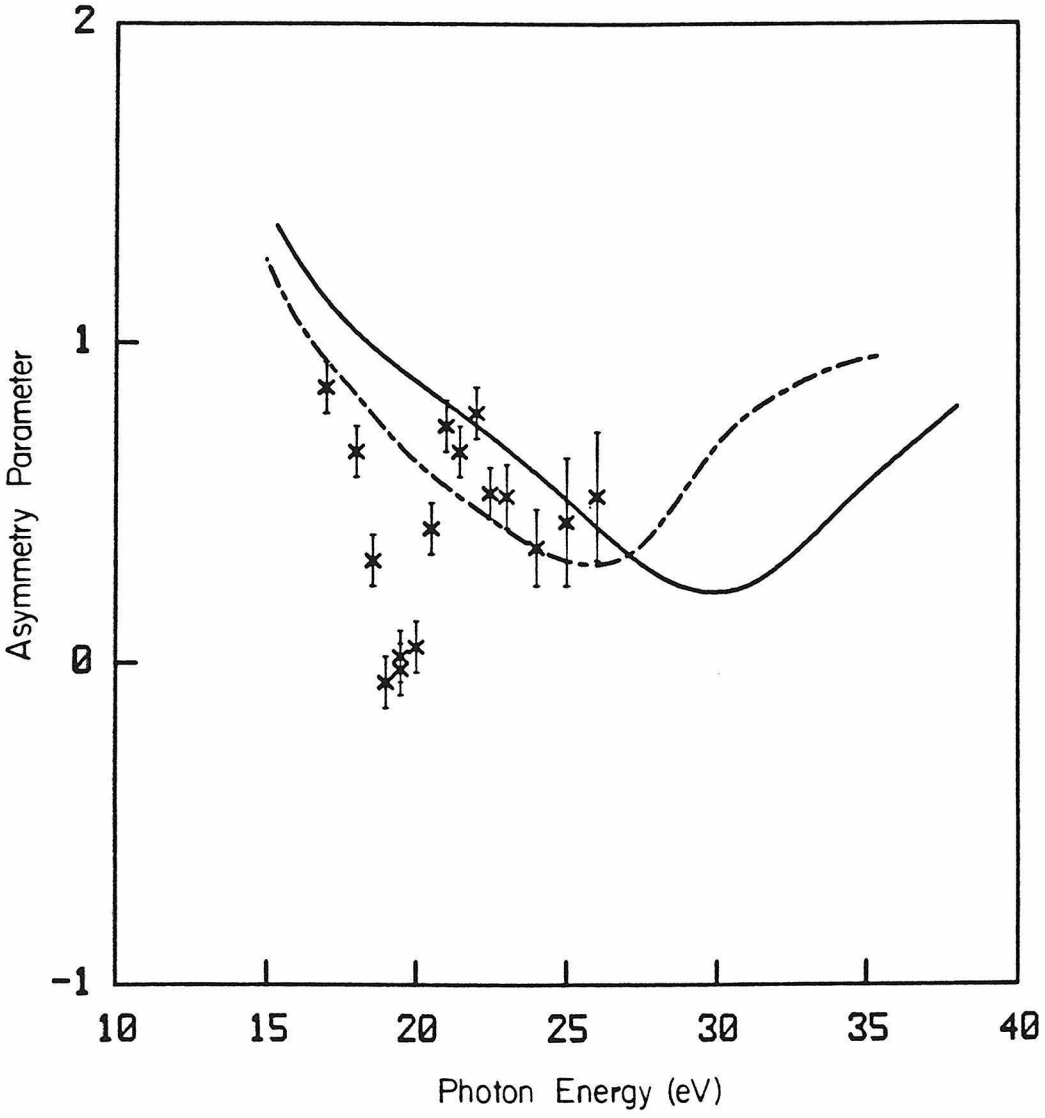
2
1
0
-1
Asymmetry Parameter
10
15
20
25
30
35
40
Photon Energy (eV)

Figure 7

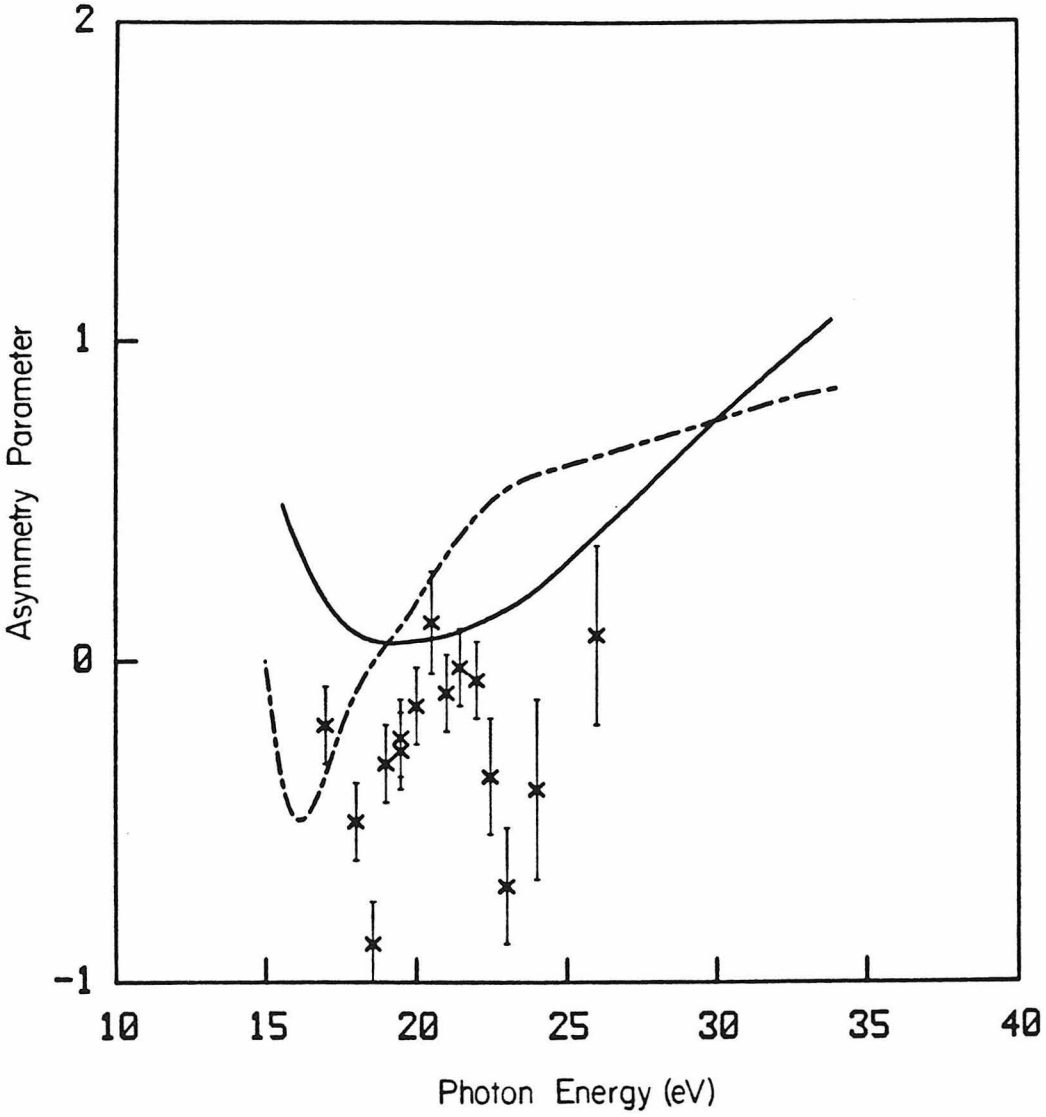
2
1
0
-1
Asymmetry Parameter
10
15
20
25
30
35
40
Photon Energy (eV)

Figure 8

SECTION D

RELAXATION EFFECTS IN MOLECULAR PHOTOIONIZATION

I. INTRODUCTION

The important role of shape resonances in molecular photoionization has now been well established.[1,2] These resonances, or quasi-bound states, are essentially one-electron in nature and are formed by the trapping of the photoelectron by the centrifugal barrier of the molecular force field. The importance of these resonances arises primarily from their strong influence on the photoionization cross sections vibrational branching ratios, and photoelectron angular distributions. It is hence not surprising that shape resonances have attracted considerable experimental interest and that, moreover, they have stimulated the development of several new theoretical approaches to molecular photoionization.[3,4] These approaches include the Stieltjes-Tchebycheff moment theory (STMT) method,[5] the continuum multiple scattering model (CMSM),[6,7] and several methods for the direct solution of the Hartree-Fock equations for the photoelectron continuum orbitals.[8-12]

To date most applications of the STMT method[13] and the direct methods[9-12] to molecular photoionization have been carried out in the frozen-core Hartree-Fock (FCHF) approximation. In this approximation the final state is described by a single electronic configuration in which the ionic core orbitals are constrained to be identical to those of the neutral molecule and the photoelectron continuum orbital is determined in the field of this unrelaxed core. This sudden approximation completely neglects any restructuring of the molecular core upon ionization and should be much more appropriate for photoionization of valence levels than of the deeper or K-shell levels. The shape-resonant nature of many K-shell cross sections can make this approximation even poorer than expected. Nevertheless, the frozen-core approximation has been used extensively in studies of K-shell molecular photoionization.[13-16]

The purpose of this paper is to present results for the K-shell photoionization of N_2 which include the effects of core relaxation. Relaxation effects are

included using continuum orbitals determined in the field of the completely relaxed ion core. Although the assumption that the photoelectron moves in the field of such a relaxed ion is not rigorous, applications to atomic inner-shell photoionization have shown that it is a very reasonable model.[17,18] Our results show that the effects of core relaxation on this K-shell σ_u shape resonant cross section are dramatic. Whereas with an unrelaxed core the cross sections are strongly peaked near threshold and differ substantially in shape from the measured values, relaxation of the core produces significant broadening and shifting of the resonance to higher energy. The resonant feature now occurs at too high an energy suggesting an overscreening of the K-shell hole in our model but the general shape of the cross section is quite close to what is seen experimentally. The corresponding photoelectron asymmetry parameters behave in a very similar way. To our knowledge this significant role of core relaxation in resonant K-shell molecular photoionization has been hitherto unrecognized.[14]

A summary of the paper is as follows. In the next section we give a very brief outline of our method for obtaining the molecular photoionization cross sections and in Sec. III we discuss our results for the K-shell of N_2. Section IV summarizes our conclusions.

II. METHOD

The rotationally unresolved, fixed-nuclei, photoionization cross section is given by

$$\sigma(R) = \frac{4\pi^2\omega}{3c} \left| < \Psi_i(\underset{\sim}{r},R) | \vec{\mu} | \Psi_f(\underset{\sim}{r},R) > \right|^2 \qquad (1)$$

where $\vec{\mu}$ is the dipole moment operator and ω the photon frequency. In Eq.(1) Ψ_i represents the initial state of the molecule with N bound electrons and Ψ_f the final state with a photoelectron in the electronic continuum. In most studies of molecules to date, the FCHF approximation has been used for Ψ_f.

This approximation, which completely neglects any restructuring of the charge density in the course of ionization and hence allows for no hole charge screening, should work best for valence orbitals. However, it could be a very poor approximation for photoionization of deep core levels involving a shape resonant continuum. In this case the trapping of the photoelectron by the centrifugal barrier will increase its time of emission. During this time significant relaxation of the ionic core can occur. This core relaxation could be accounted for by inclusion of the appropriate terms in the expansion of the wave function or, equivalently, through the use of an optical potential. However, these relaxation effects could be approximately included by assuming that the photoelectron moves in the field of the completely restructured core.[17,18] This relaxed core Hartree-Fock model should be particularly meaningful around shape resonances.

The Hartree-Fock continuum orbitals used in these studies hence satisfy the one-electron Schrödinger equation

$$(-\frac{1}{2}\nabla^2 + V_{N-1}(\underset{\sim}{r},R) - \frac{k^2}{2})\phi_{\underset{\sim}{k}} = 0 \qquad (2)$$

where the potential V_{N-1} is determined either by the core orbitals of the neutral molecule or by the orbitals of the relaxed ion. The nonspherical character of these molecular potentials introduces several complications into the solution of this equation for $\phi_{\underset{\sim}{k}}$ which do not arise in atomic systems.[3] Various approaches have hence been developed for obtaining these molecular electronic continuum states $\phi_{\underset{\sim}{k}}$.[8-12] Our approach, which has been discussed in detail elsewhere,[2,9] begins with the integral form of Eq.(2), i.e.,

$$\phi_{\underset{\sim}{k}} = \phi^c_{\underset{\sim}{k}} + G_c^{(-)}V\phi_{\underset{\sim}{k}} \qquad (3)$$

where $\phi_{\underset{\sim}{k}}^{c}$ is the Coulomb scattering wave function and

$$V = V_{N-1} + \frac{1}{r} \tag{4a}$$

and

$$G_c^{(-)} = \frac{1}{2} (\nabla^2 + \frac{2}{r} + k^2 - i\varepsilon)^{-1} . \tag{4b}$$

The continuum orbital $\phi_{\underset{\sim}{k}}(\underset{\sim}{r})$ can be expanded in terms of $\Omega_{\hat{k}}$, the direction of $\underset{\sim}{k}$, as

$$\phi_{\underset{\sim}{k}}(\underset{\sim}{r}) = (\frac{2}{\pi})^{\frac{1}{2}} \sum_{\ell m} \frac{i^{\ell}}{k} \Phi_{k\ell m}(\underset{\sim}{r}) Y^*_{\ell m}(\Omega_{\hat{k}}) \tag{5}$$

where $\phi_{k\ell m}(\underset{\sim}{r})$ are the partial wave scattering functions. Each $\phi_{k\ell m}$ satisfies its own Lippmann-Schwinger equation

$$\phi_{k\ell m} = \phi^{c}_{k\ell m} + G_c^{(-)} V \phi_{k\ell m} . \tag{6}$$

We solve Eq.(6) for the $\phi_{k\ell m}$ by the iterative Schwinger variational method which has been previously applied to several molecules, e.g., N_2,[9] CO,[19] CO_2,[15] C_2H_2,[16] and C_2N_2.[20] The method is essentially a procedure for the numerical solution of Eq.(6) which avoids the integration of coupled integro-differential equations but relies on single-center expansion techniques in the evaluation of all matrix elements. Although the method utilizes discrete basis functions in solving Eq.(6), the approximate solutions satisfy scattering boundary conditions and can be systematically improved through an iterative procedure.[21]

For Ψ_i in Eq.(1) we again use the Hartree-Fock wave function. In the FCHF approximation, orbital orthogonality makes the evaluation of the transition

dipole matrix element in Eq.(1) very straightforward. This feature makes this approximation particularly convenient in molecular applications. With the relaxed Hartree-Fock ionic core in Ψ_f the lack of orbital orthogonality complicates the evaluation of this transition matrix element. In these studies we have used a biorthogonalization procedure in the computation of these matrix elements.[22,23] Details of these calculations will be presented elsewhere.[24]

III. RESULTS

The SCF wave functions for the initial state and relaxed N_2^+ cores were all obtained in a [4s3p1d] contracted Gaussian basis set[25] and for an internuclear distance of 2.068 a.u. With the minor difference that the present calculations use the complete set of 1d functions, this basis is essentially equivalent to that of Ref. 14. In this basis the ground state SCF energy of N_2 is -108.9648 a.u. and the $1\sigma_g$ and $1\sigma_u$ orbital energies are 426.73 eV and 426.63 eV respectively. The $1\sigma_g$ and $1\sigma_u$ ionization potentials using the SCF energies of the relaxed N_2^+ ions are 419.75 eV and 419.61 eV respectively. The difference of about 10 eV between these ionization potentials and the experimental value of 409.9 eV is essentially due to hole localization.[23]

The σ_g, σ_u, π_u, and π_g continuum orbitals of both the frozen and relaxed N_2^+ ions were obtained by the iterative Schwinger procedure outlined above. The numerical details of these calculations such as partial wave expansions and starting basis sets have been discussed previously.[2,9] Considerable effort has been taken to ensure the convergence of these calculations. For example, our expansion parameters[24] give a normalization of about 0.9995 for the $1\sigma_g$ and $1\sigma_u$ orbitals and the final photoionization cross sections were calculated with continuum orbitals obtained after two steps in the iterative procedure.[9]

In Fig. 1 we show our calculated frozen-core photoionization cross sections along with the frozen-core results obtained previously by the STMT method[14] and

the experimental data obtained by (e,2e) measurements.[26] The present frozen-core results differ significantly from the experimental data. The σ_u resonance feature is quite strongly peaked and concentrates much of the cross section too close to threshold. On the other hand the frozen-core cross sections of the STMT method show a much broader resonance feature than the present results and, moreover, are apparently in better agreement with the measured cross sections. In principle our procedure should give the same frozen-core cross sections as the STMT method. We are not completely certain of the reasons for these differences. We have tested the convergence of these calculations and we believe that the partial wave expansions are sufficient to yield the correct results. A possible explanation is that the pseudospectrum of the STMT calculations[14] did not have a dense enough distribution of poles in the resonance region and, in turn, this led to a broadening of the resonance structure. These differences are analogous to those seen in the calculated cross sections for the $C^2\Sigma_g^+$ state of CO_2^+ where a prominent resonant feature both in our results[15] and those of Collins and Schneider[10] is essentially smoothed away by the STMT method.[27]

Figure 1 also shows the K-shell cross sections obtained using a relaxed HF ionic core and the corresponding continuum orbitals. A comparison with the frozen-core results shows that core relaxation has decreased the cross section near threshold dramatically, broadened the resonance, and shifted it to higher energy. The resonance position is now at too high an energy suggesting that the model of a completely relaxed ionic core has led to excessive screening of the hole.[17] The use of a localized hole potential should reduce this screening and pull the resonance down to lower energy. However, the general shape of the relaxed-core cross sections is quite similar to that of the experimental data and, to illustrate this, Fig. 2 shows these cross sections for a limited range of photon energy shifted so that their peak position coincides with that of the measured cross sections. In this figure we also show the one-electron portion

of the photoionization cross section as estimated by Kay et al.[26] As expected, relaxation effects are seen to be much less important in resonant photoionization of the $3\sigma_g$ level of N_2.[24]

Figure 3 shows our calculated photoelectron asymmetry parameters using both the frozen and relaxed ionic core models, the CMSM results,[6] and the experimental data of Lindle.[28] From these results we see that core relaxation has broadened and shifted the pronounced minimum seen in these asymmetry parameters in the frozen-core model. Although the asymmetry parameters of the relaxed-core model again show a minimum at higher energy than do the measured values, the overall shapes of these curves are quite similar around their minima. A shift of these calculated asymmetry parameters to lower energy by the same amount as the cross sections were shifted in Fig. 2 shows this more clearly.[24]

IV. CONCLUSIONS

We have studied the effects of core relaxation on resonant K-shell photoionization in N_2. Our results, obtained using the model of a completely relaxed ion core for the final state, show that these effects are very important for this system. The role of core relaxation will have to be carefully evaluated in studies of related K-shell processes in other systems, e.g., CO and CO_2.

References

[1]J. L. Dehmer, D. Dill, and A. C. Parr, in Photophysics and Photochemistry in the Vacuum Ultraviolet, eds. S. McGlynn, G. Findley, and R. Huebner (Reidel Publishing Co., Holland, 1983), in press.

[2]D. G. Truhlar, ed. Symposium on Resonances in Electron-Molecule Scattering, van der Waals Complexes, and Reactive Chemical Dynamics, 1984 National ACS Meeting, St. Louis, MO (ACS Symposium Series xxx, 1984).

[3]See, for example, Electron-Molecule and Photon-Molecule Collisions, eds. T. N. Rescigno, B. V. McKoy, and B. Schneider (Plenum Press, New York, 1979).

[4]V. McKoy, T. A. Carlson, and R. R. Lucchese, J. Phys. Chem., accepted for publication (1984).

[5]See, for example, P. W. Langhoff on pp. 183-224 of Ref. 3.

[6]J. L. Dehmer and D. Dill, Phys. Rev. Lett. 35, 213 (1975).

[7]J. L. Dehmer and D. Dill on pp. 225-265 of Ref. 3.

[8]W. D. Robb and L. A. Collins, Phys. Rev. A 22, 2474 (1980).

[9]R. R. Lucchese, G. Raseev, and V. McKoy, Phys. Rev. A 25, 2572 (1982).

[10]L. A. Collins and B. I. Schneider, Phys. Rev. A 29, 1695 (1984).

[11]M. E. Smith, V. McKoy, and R. R. Lucchese, Phys. Rev. A 29, 1857 (1984).

[12]G. Raseev, H. Le Rouzo, and H. Lefebvre-Brion, J. Chem. Phys. 72, 5701 (1980).

[13]P. W. Langhoff, N. Padial, G. Csanak, T. N. Rescigno, and B. V. McKoy, J. Chim. Physique 77, 589 (1980).

[14]See, for example, T. N. Rescigno and P. W. Langhoff, Chem. Phys. Lett. 51, 65 (1977).

[15]R. R. Lucchese and V. McKoy, Phys. Rev. A 26, 1406 (1982).

[16]D. Lynch, M.-T. Lee, R. R. Lucchese, and V. McKoy, J. Chem. Phys. 80, 1907 (1984).

[17]See, for example, H. P. Kelly, S. L. Carter, and B. E. Norum, Phys. Rev. A 25, 2052 (1982); M. Ya. Amusya, V. K. Ivanov, S. A. Scheinerman, S. I. Sheftel, and A. F. Ioffe, Sov. Phys. (JETP) 51, 458 (1980) [Zh. Eksp. Teor. Fiz. 78, 910 (1980)].

[18]R. S. Williams and D. A. Shirley, J. Chem. Phys. 66, 2378 (1977).

[19]R. R. Lucchese and V. McKoy, Phys. Rev. A 28, 1382 (1982).

[20]D. Lynch, S. Dixit, and V. McKoy, J. Chem. Phys. (to be published).

[21]R. R. Lucchese and V. McKoy, Phys. Rev. A 24, 770 (1981).

[22]H. F. King, R. Stanton, H. Kim, R. E. Wyatt, and R. G. Parr, J. Chem. Phys. 47, 1936 (1967).

[23]A. F. Voter and W. A. Goddard III, Chem. Phys. 57, 253 (1981).

[24]D. Lynch and V. McKoy, J. Chem. Phys. (to be published).

[25]T. H. Dunning, Jr., J. Chem. Phys. 53, 2823 (1970).

[26]R. B. Kay, Ph. E. van der Leeuw, and M. J. van der Wiel, J. Phys. B 10, 2513 (1977).

[27]N. Padial, G. Csanak, B. V. McKoy, and P. W. Langhoff, Phys. Rev. A 23, 218 (1981).

[28]D. W. Lindle, Inner-Shell Photoemission from Atoms and Molecules Using Synchrotron Radiation, Ph. D. Thesis, University of California, Berkeley, 1983.

Figure Captions

Figure 1: K-shell photoionization cross sections for N_2: ———, present FCHF results; — — —, present results with a relaxed ion core; ——— – ———, FCHF results of the STMT method (Ref. 14); + , experimental data of Ref. 26.

Figure 2: K-shell photoionization cross sections for N_2: ———, present FCHF results; — — —, present results with a relaxed ion core shifted so as to agree with the experimental data at 419.5 eV; + , experimental data of Ref. 26; △ , estimated one-electron portion of the experimental cross sections (Ref. 26).

Figure 3: K-shell photoelectron asymmetry parameters in N_2: ———, present FCHF results; — — —, present results with a relaxed core; ——— – ———, CMSM results of Ref. 6; + , synchrotron radiation data of Ref. 28.

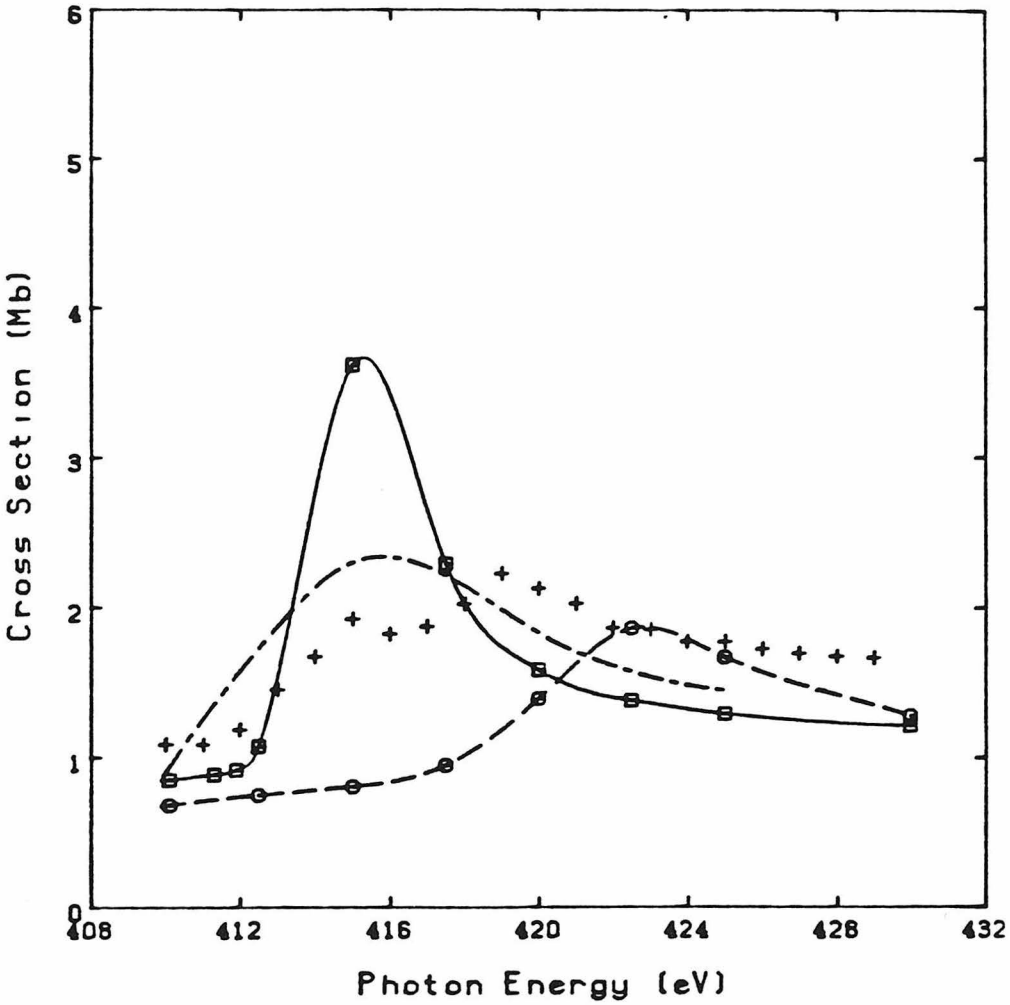
Cross Section (Mb)
Photon Energy (eV)
0
1
2
3
4
5
6
408
412
416
420
424
428
432

Figure 1

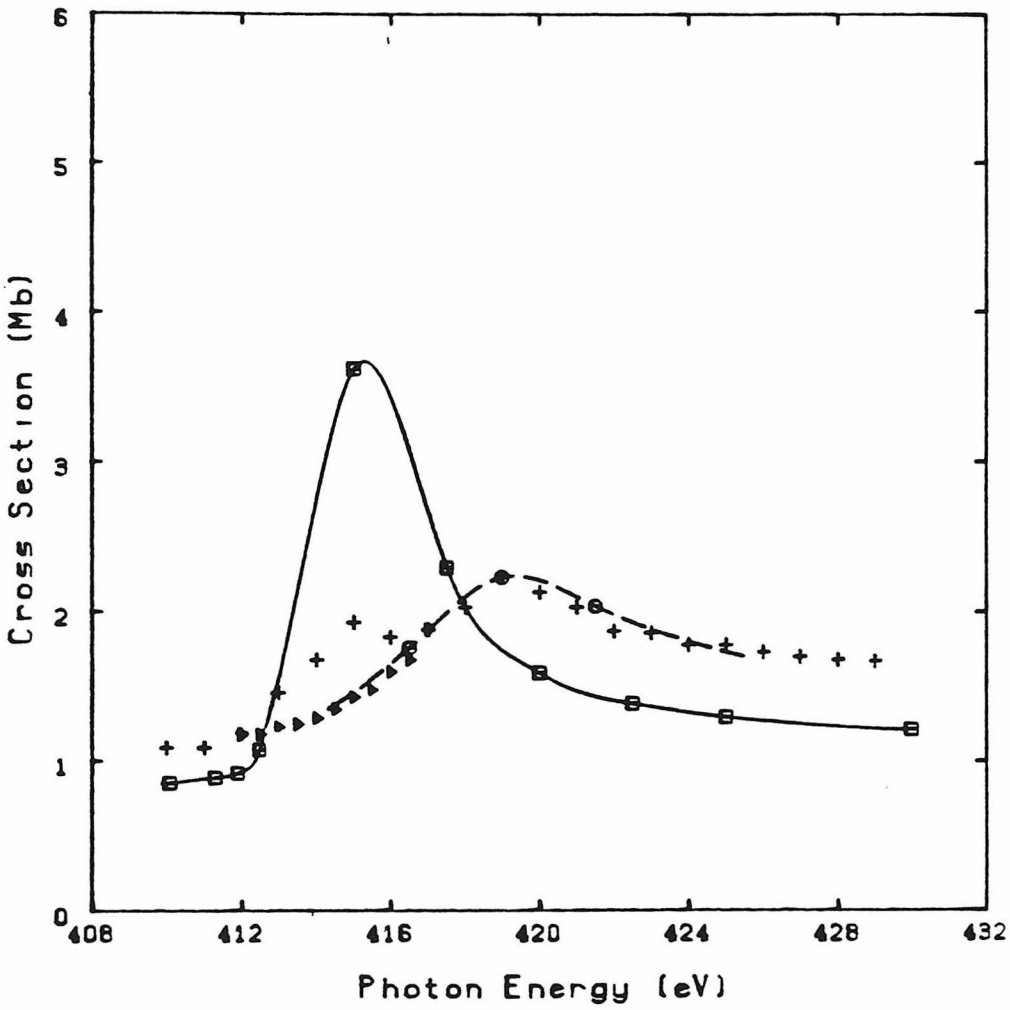
Cross Section (Mb)
Photon Energy (eV)
0
1
2
3
4
5
6
408
412
416
420
424
428
432

Figure 2

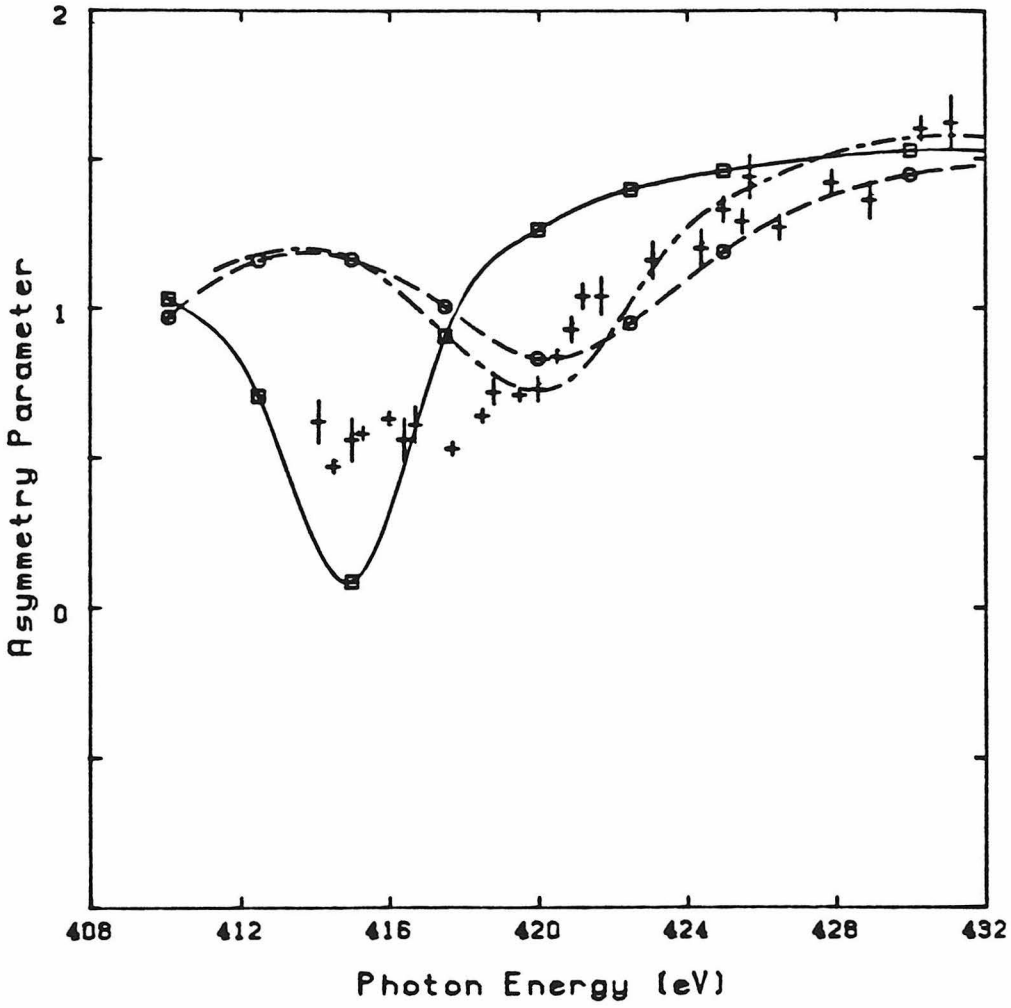
2
1
0
Asymmetry Parameter
408
412
416
420
424
428
432
Photon Energy (eV)

Figure 3

SECTION E

STUDIES OF THE RELAXATION EFFECTS IN VALENCE AND K-SHELL PHOTOIONIZATION OF CARBON DIOXIDE

I. INTRODUCTION

Several recent theoretical studies have investigated the carbon and oxygen K-shell photoionization cross sections and angular distributions for carbon dioxide. These studies include the work of Padial et al.[1] and Daasch et al.[2] which employs the Stieltjes-Tchebycheff moment theory (STMT) approach, the studies of Collins and Schneider[3] using the linear algebraic method, and the calculations of Lucchese and McKoy[4] using the iterative Schwinger variational method.[5] In all of these theoretical investigations, the Frozen-Core Hartree-Fock (FCHF) approximation was invoked. In this approximation the final state is described by a single electronic configuration in which the ionic core orbitals are constrained to be identical to those of the neutral molecule, and the photoelectron continuum orbital is determined in the field of this unrelaxed core. This sudden approximation completely neglects any restructuring of the molecular core upon ionization and should be much more appropriate for photoionization of valence levels than of the deeper or K-shell levels. As demonstrated in our earlier N_2[6] study, the effect of relaxing the molecular core orbitals is dramatic in the vicinity of the low kinetic energy N_2 $1\sigma_g \rightarrow k\sigma_u$ shape resonance. The relaxed molecular ion potential, is less attractive than the frozen core potential, and thus the low kinetic energy

shape resonance is shifted to higher kinetic energy and broadened.

In addition to the theoretical investigations of CO_2, measurements for K-shell photoionization cross sections[7] and angular distributions[8] have been performed. Compared to the experimental maximum, the $C(1s^{-1})$ shape resonance in the frozen core approximation appears about 5eV lower in energy, indicating the neglect of screening effects in the calculation. Both the STMT[1] and iterative Schwinger[4] calculations are in good agreement with the measured width and peak intensity of the $C(1s^{-1})$ resonance feature. However, the iterative Schwinger[4] and linear algebraic[3] methods predict a very sharp and quite narrow $O(1s^{-1})$, $1\sigma_g \rightarrow k\sigma_u$ shape resonance while the experimental[7] cross sections are essentially structureless. This disagreement is very similar to N_2 K-shell photoionization, where the FCHF resonance is strongly peaked and very narrow. In addition, the STMT results are in disagreement with the iterative Schwinger and linear algebraic method calculations. Discrepancies between the STMT method and other techniques for determining molecular photoionization cross sections[3,4,9,10] have been observed in several K-shell and valence level studies, particularly near sharp, narrow resonance features.

The purpose of these studies is to continue the assessment of core relaxation in molecular photoionization. Relaxation effects are included, using

continuum orbitals determined in the field of the completely relaxed ion core (RCHF). A complication with the use of the relaxed core orbitals is that they are non--orthogonal with the initial state, neutral orbitals. In order to conveniently compute the necessary dipole matrix elements, we have employed a biorthogonalization technique.[13-16] Although the assumption that the photoelectron moves in the field of such a relaxed ion is not rigorous, applications to atomic inner-shell photoionization have shown that it is a very reasonable model.[11,12] This approach constrains each molecular orbital in the total wavefunction to have the full symmetry of the molecular Hamiltonian, and for oxygen K-shell ionization, neglects the potentially important effects of hole localization. In particular we have examined the role of relaxation in $C(1s^{-1})$ and $O(1s^{-1})$ K-shell photoionization, as well as the valence level $(4\sigma_g^{-1})$, of carbon dioxide, using the iterative Schwinger variational method.[13] Comparisons between the frozen core (FC), relaxed core (RC), and the experimental studies are made and indicate, as expected, that the valence level is only slightly affected by core relaxation. Analogous to the N_2 K-shell study,[6] the $O(1s^{-1})$ resonance is shifted and broadened in the relaxed core approximation; however, it remains much sharper than the essentially non-resonant experimental cross sections. The $C(1s^{-1})$ shape resonance is shifted and only slightly broadened, indicating that, in

this channel relaxing the core primarily affects the position of the shape resonance. Overall the effect of relaxation is less dramatic for the carbon K-shell $2\sigma_g \rightarrow k\sigma_u$ shape resonance than for either the N_2 or $O(1s^{-1})$ K-shell resonances.

A summary of the paper is as follows: In the next section we describe briefly the generation of the continuum wavefunctions as well as the biorthogonalization technique. In Section III we discuss our results for CO_2 K-shell and valence shell photoionization in the frozen and relaxed cores. We compare these results to the measured values and to other theoretical calculations. The last section summarizes our conclusions.

II. METHOD

A) THE FINAL-STATE WAVEFUNCTION

The rotationally unresolved, fixed-nuclei photoionization cross section is given by

$$\sigma(R) = \frac{4\pi^2\omega}{3c} \left| \langle \psi_i(r,R) \,|\mu|\, \psi_f(\underset{\sim}{r},R) \rangle \right|^2 , \qquad (1)$$

where μ is the dipole moment operator, R is the internuclear distance, and ω the photon frequency. In Equation (1) ψ_i represents the initial state of the molecule with N bound electrons. Typically, this is taken as the single configuration SCF wavefunction for the neutral molecule. The single configuration final state,

ψ_f, describes the ion, with N-1 bound electrons, and a photoelectron in the electronic continuum. In most studies of molecular photoionization, the FCHF approximation is invoked. This implies that the ion's orbitals are constrained to be identical to the HF orbitals of the neutral molecule. We will refer to these ionic orbitals as the core orbitals. The continuum wavefunction is then calculated in the static-exchange potential field of these frozen orbitals.

To accurately represent the final state, relaxation effects must be included. As a first-order approximation, the core orbitals in ψ_f are taken as the molecular orbitals of the ion. This requires a separate SCF calculation for the ionic wavefunction. In the RCHF approximation the continuum wavefunction is calculated in the completely relaxed potential.

The Schrödinger equation for the remaining continuum wave function is

$$(-1/2\nabla^2 - 1/r + V(\underset{\sim}{r}) - k^2/2)\phi_{\underset{\sim}{k}} = 0 \ , \qquad (2)$$

where $k^2/2$ is the kinetic energy of the photoelectron. The short-range static-exchange potential, $V(\underset{\sim}{r})$, is determined with either the FCHF or RCHF molecular orbitals. The FCHF static-exchange potential for ionization from the non-degenerate orbital, ϕ_n, is given by[17]

$$V(\underset{\sim}{r}) = \sum_{i=1}^{n-1} (2J_i - K_i) + J_n + K_n + \sum_{\alpha} \frac{Z\alpha}{r_{i\alpha}} \quad , \qquad (3)$$

where N=2n and J_i and K_i are the usual Coulomb and exchange operators[18] and the last term in equation (3) is the electron-nuclear attraction potential. In the special case where the continuum solution is of a different symmetry than ϕ_n, the form of $V(\underset{\sim}{r})$ in the RCHF approximation is the same as Equation (3). In general, this is not the case, however; the systems of interest in this study contain an inversion center and thus the continuum orbital and ϕ_n are automatically orthogonal. This is a result of the single-photon dipole selection rules: $g \nleftrightarrow u$. Therefore, Equation (3) is used in both our FCHF and RCHF calculations. Lastly, a generalized Phillips-Kleinman pseudopotential[17] is used to treat the effects of constraining the continuum solution to be orthogonal to the doubly occupied bound orbitals.

Our approach for the solution of Equation (2) has been discussed in detail elsewhere.[5] Here we briefly outline this procedure. We use the integral form of Equation (2), or the Lippmann-Schwinger equation,

$$\phi_{\underset{\sim}{k}} = \phi_{\underset{\sim}{k}}^{C} + G_c^{(-)} V \phi_{\underset{\sim}{k}} \quad , \qquad (4)$$

where $\phi_{\underset{\sim}{k}}^{C}$ is the pure Coloumb scattering wavefunction, V is the short-range molecular ion potential in either the FCHF or the RCHF approximation and $G_c^{(-)}$ is the Coulomb

Green's function with incoming-wave boundry conditions; i.e.,

$$G_c^{(-)} = 2\,(\nabla^2 + 2/r + k^2 - i\varepsilon)^{-1}. \tag{5}$$

The partial wave component of $\phi_{\underset{\sim}{k}}$, ϕ_{klm}, satisfies its own Lippmann-Schwinger equation

$$\phi_{klm} = \overset{c}{\phi}_{klm} + G_c^{(-)}\, V \phi_{klm}\,. \tag{6}$$

We solve Equation (6) by the iterative Schwinger variational method.[5] In this method we first solve Equation (6) by assuming an approximate separable form of V

$$V(\underset{\sim}{r},\underset{\sim}{r}') \cong V^S(\underset{\sim}{r},\underset{\sim}{r}') = \sum_{i,j} \langle \underset{\sim}{r}|V|\alpha_i\rangle\, (V^{-1})_{ij}\, \langle \alpha_j|V|\underset{\sim}{r}'\rangle\,, \tag{7}$$

where $(V^{-1})_{ij}$ is the inverse of the matrix with elements $V_{ij} = \langle \alpha_i|V|\alpha_j\rangle$. With this approximate potential the zeroth iteration solutions of Equation (6) are

$$\overset{(0)}{\phi}_{klm} = \overset{c}{\phi}_{klm} + \sum_{i,j} \langle \vec{r}|G_c^{(-)}\, V\,|\alpha_i\rangle (D^{-1})_{ij}\, \langle \alpha_j|V|\overset{c}{\phi}_{klm}\rangle \tag{8}$$

and $(D^{-1})_{ij}$ is the inverse of the matrix $(D)_{ij} = \langle \alpha_i|V - VG_c^{(-)}\, V|\alpha_j\rangle$.

At the Hartree-Fock level these solutions ϕ_{klm} can be shown to be variationally stable.[19] Also with sufficiently large basis sets the zeroth iteration solutions can produce reliable photoionization cross sections and asymmetry parameters. It may be important to obtain solutions of the Lippmann-Schwinger equation for the exact potential V. An iterative technique has been developed in order to obtain these solutions.[20]

The iterative method begins with augmenting the discrete basis set, $|\alpha_i>$, with the zeroth iteration functions, ϕ_{klm}. Equation (6) is solved within this larger basis set. This process is repeated until the wavefunctions converge. These can be shown to be solutions of Equation (6) for the potential V.[20]

B) THE BIORTHOGONALIZATION PROCEDURE

The initial state, ψ_i, in Equation (1) is the HF wavefunction for the neutral molecule. In the FCHF approximation, orbital orthogonality makes the evaluation of the transition dipole matrix elements straightforward. The application of the Slater-Condon rules for evaluating matrix elements over wavefunctions represented by determinants reduces Equation (1) to

$$\sigma(R) = \frac{4\pi^2\omega}{3c}|<\phi_n\ (\underset{\sim}{r},R)|\mu|\phi_{\underset{\sim}{k}}\ (\underset{\sim}{r},R)>|^2, \qquad (9)$$

where ϕ_n and $\phi_{\underset{\sim}{k}}$ are single particle functions. This feature makes the FCHF approximation computationally convenient. However, with the relaxed core orbitals in ψ_f, the lack of orbital orthogonality complicates the evaluation of this transition matrix element.

In order to make the computations tractable, we have employed a biorthogonalization procedure for the calculation of these matrix elements.[13-16] This technique has also been used by Lengsfield et al.[21] to calculate transition matrix elements between non-orthonormal bound state wavefunctions.

We begin with two nonorthonormal sets of orbitals, one for the neutral; $\{\psi\} = \{\psi_1, \psi_2, \psi_3 \ldots \psi_n\}$ and another for the ion; $\{\phi\} = \{\phi_1, \phi_2, \phi_3 \ldots \phi_{n-1}, \phi_{\underset{\sim}{k}}\}$. From these we construct initial and final-state wavefunctions;

$$\psi_{initial} = |\psi_1(1)\overline{\psi_1(2)} \ldots \psi_n(N-1)\overline{\psi_n(N)}| \qquad (10)$$

and

$$\psi_{final} = \frac{1}{\sqrt{2}}|\phi_1(1)\overline{\phi_1(2)} \ldots \phi_n(N-1)\overline{\phi_{\underset{\sim}{k}}(N)}| - \frac{1}{\sqrt{2}}|\phi_1(1)\overline{\phi_1(2)} \ldots \overline{\phi_n(N-1)}\phi_{\underset{\sim}{k}}(N)| \qquad (11)$$

we assume the ionized orbital, ϕ_n, to be nondegenerate. The necessary matrix elements are of the form,

$$\langle \psi_i | \mu^N | \psi_f \rangle = \langle | \psi_1(1)\overline{\psi_1(2)} \ \ldots \ \psi_n(N-1)\overline{\psi_n(N)} | \mu^N | | \phi_1(1)\overline{\phi_1(2)} \ \ldots \ \phi_n(N-1)\overline{\phi_{\underset{\sim}{k}}(N)} \rangle , \qquad (12)$$

where $\mu^N = \sum_{i=1}^{N} \mu_i$ and μ_i is the one electron dipole length or velocity operator for the i^{th} electron.

The biorthogonalization method rests on the unitary transformation of each set of non-orthogonal orbitals; $\underset{\sim}{\phi}^T = \underset{\sim}{\phi}\underset{\approx}{U}^I$ and $\underset{\sim}{\psi}^T = \underset{\sim}{\psi}\underset{\approx}{U}^N$, where U^I and U^N transform the ionic and neutral orbitals, respectively. The transformation matrices are determined such that the transformed or biorthogonal orbitals have the following property:

$$\langle \phi_i^T | \psi_j^T \rangle = d_i \delta_{ij}; \qquad (13)$$

i.e., each transformed orbital overlaps with only one orbital from the other set. Using the transformed orbitals, Equation (12) simplifies to:

$$\langle \psi_i | \mu^N | \psi_f \rangle = \prod_{i=1}^{n-1} d_i \ \det(\underset{\approx}{U}^N)\det(\underset{\approx}{U}^{I+}) \langle \psi_n^T(\underset{\sim}{r}) | \mu | \phi_{\underset{\sim}{k}}^T(\underset{\sim}{r}) \rangle . \qquad (14)$$

The procedure for obtaining the unitary matrices as well as the overlaps, d_i, has been described previously.[13-16] We will briefly review this method. $\underset{\approx}{U}^I$ diagonalizes the hermitian matrix $\underset{\approx}{S}^+\underset{\approx}{S}$, where $\underset{\approx}{S}$ is the overlap matrix between the two nonorthogonal sets of orbitals:

$$(\underset{\approx}{S}^{+}\underset{\approx}{S})\underset{\approx}{U}^{I} = \underset{\approx}{U}^{I}\underset{\approx}{D} \; ; \tag{15}$$

then U^N is constructed such that

$$(\underset{\approx}{U}^{N})^{+}\underset{\approx}{S}\;\underset{\approx}{U}^{I} = \underset{\approx}{d} \; , \tag{16}$$

where d is a diagonal but not the unit matrix, and U^N is given by[14]

$$\underset{\approx}{U}^{N} = \underset{\approx}{S}\;\underset{\approx}{U}^{I}\;\underset{\approx}{D}^{-1/2}. \tag{17}$$

III. RESULTS AND DISCUSSION

In order to determine the effect of core relaxation on the high kinetic energy ($\gtrsim$15 eV) shape resonances in CO_2, we have performed FCHF and RCHF calculations for photoionization of the oxygen and carbon K-shells as well as the $4\sigma_g^{-1}$ valence level. The target wavefunctions used in these relaxed core studies are constructed from the same [3s2pld] contracted Gaussian basis set used in the previous FCHF calculations.[4] The calculated ionization potentials for removal of the $O(1s^{-1})$, $C(1s^{-1})$ and $4\sigma_g$ electrons are summarized and compared to previous (experimental[22,23] and theoretical[24,25]) results in Table I. In analogy with nitrogen core ionization,[15,16] allowing the oxygen K-shell hole to localize reduces the calculated

ionization potential by 12 eV.[22] All the matrix elements and functions arising in the solution of Equation (8) were evaluated using single-center expansions. Details of these numerical procedures have been discussed previously.[17] The single-center expansion parameters and initial scattering basis sets are identical to those used previously.[4] For the purpose of this study we have not employed the iterative technique for obtaining the Hartree-Fock continuum orbitals, since the previous study of CO_2 photoionization indicated that, in general, the iterative cross sections are very close to the initial non-iterative results.[4]

A. $O(1s^{-1})$ PHOTOIONIZATION OF CO_2

The total photoionization cross sections for $O(1s^{-1})$ are reported in Figure 1. The FCHF oxygen K-shell cross sections display a narrow shape resonance about 20 eV above threshold, while the photoabsorption data of Barrus et al.,[7] and the STMT calculations of Padial et al.[1] indicate a very broad resonance-like feature. The previous FCHF calculations,[4] obtained at photon energy intervals of 2 eV, predicted a peak cross section of nearly 2.5 Mb. However, the $k\sigma_u$ shape resonance is very narrow, and a finer energy grid (0.5 eV from 558-560 eV) produces a sharp resonance. As shown in Figure 1, the resonance now peaks about 3.6 Mb near 559 eV.

Analogous to previous N_2 K-shell[6] and CO_2 $(4\sigma_g^{-1})$[4] studies, the STMT method predicts a very broad shape

resonance, in good agreement with experiment, while our FCHF results produce a quite narrow feature. Independent calculations for ionization of the O K-shell[3] and $4\sigma_g^{-1}$ of CO_2, as well as $1\sigma_g^{-1}$ ionization in N_2,[9] have reproduced the sharp nature of these $k\sigma_u$ shape resonances in the FCHF approximation. The CO_2 $1\sigma_g^{-1}$ results reported here are in good agreement with those of Collins and Schneider.[3] In principle, the STMT method should produce the same cross sections as our present results and other theoretical methods. The STMT method is based on a discretization of the molecular continuum with the ionized wavefunction represented in an L^2 basis. The wavefunction is therefore composed of a finite number of eigenvectors of the (N-1) electron Hamiltonian. A moment-theory approach is then used to construct the corresponding photoionization cross sections.[1] Yu et al.[9] have suggested, and Woodward et al.[26] have shown for model problems, that the STMT method may broaden resonances that have widths which are narrower than the spacing of the finite number of eigenvalues obtained in the diagonalization of the (N-1) electron Hamiltonian. In addition, Daasch et al.[2] have established, in their oxygen K-shell photoionization study, that STMT cross sections are very sensitive to the imaging procedure used, where the shape of the resonance is seen to depend dramatically on the particular imaging scheme. However, the source of the discrepancy between the STMT results and

other techniques for obtaining molecular photoionization cross sections is still not well established.

In Figure 1 we also compare the total relaxed core photoionization cross sections with the frozen core results and with the measured values. Unlike our previous N_2 core relaxation studies, the shift in the resonance is only about 4 eV, and the resonance is not as dramatically broadened. While there is a significant reduction in the peak intensity upon relaxation, the resonance remains much sharper than the experimental results. In order to resolve this discrepancy, it may be necessary to incorporate the localization of the $O(1s^{-1})$ vacancy. Earlier STMT[3] calculations have indicated that localization is not an important effect; however, since this method does not initially produce the sharp nature of the $k\sigma_u$ resonance, the actual role localization will play in the present studies is not clear.

Upon localization the continuum orbital will not have "pure" $k\sigma_u$ or $k\sigma_g$ symmetry but will be a mixture of both even and odd partial waves. Since the high energy $k\sigma_u$ resonance is a mixture of $\ell = 3,5$ and 7 waves, one can expect a strong coupling to the $\ell = 4$ and 6 components. This mixing should broaden the shape resonance , as has been seen in the difference between the $3\sigma_g \rightarrow k\sigma_u$ ($\ell=3$) N_2[17] shape resonance and the analogous but much broader CO[27] $5\sigma \rightarrow k\sigma$ resonance. Oxygen K-shell ionization in CO_2 differs in two important aspects from the N_2 K-shell

situation; first, the CO_2 resonance occurs at a much larger kinetic energy and is associated with a strong mixture of several partial waves (ℓ=3, 5, 7) while the lower energy N_2 $1\sigma_g \rightarrow k\sigma_u$ resonance is primarily ℓ=3. Secondly, the N-N distance is much shorter than the O-O distance. This factor will favor the localization of the K-shell hole on one of the oxygens. These two differences should make localization a more important effect in CO_2 than in N_2.

The $1\sigma_g \rightarrow k\sigma_u$ and $1\sigma_u \rightarrow k\sigma_g$ partial channel eigenphase sums and cross sections in the frozen core and relaxed core approximations are reported in Figures 2 and 3, respectively. The effect of relaxation on the position and width is evident in these figures. The rise in the eigenphase sum and peak in the partial channel cross section is shifted to higher kinetic energy in the resonant $k\sigma_u$ continuum, while, above 545 eV, the non-resonant $k\sigma_g$ partial channel is essentially unaffected by the use of the relaxed core. At lower kinetic energies, only the behavior of the $k\sigma_g$ partial channel is modified. This is expected since, due to the repulsive centrifugal potential barrier, only the s wave can probe the molecular potential at very low kinetic energy. These effects are small in the total cross section but do change the low energy behavior of the $O(1s^{-1})$ asymmetry parameter.

In Figure 4 the asymmetry parameters in the FC and RC approximations are plotted and compared to the

synchrotron data of Truesdale et al.[8] The low energy $k\sigma_g$ behavior produces an observable difference between the parameters calculated in the FC and RC models. Unfortunately, the experimental results do not extend below 548 eV. The effect of the shape resonance is seen as a dip in the asymmetry parameters near 562 eV. Analogous to the shift observed in the peak cross section, the dip in the relaxed core asymmetry parameters occurs at a higher energy and is slightly broader than the FC results, but again the lack of experimental data in this region prevents any meaningful comparisons.

B. $C(1s^{-1})$ PHOTOIONIZATION OF CO_2

The calculated cross sections for photoionization of the carbon K-shell in the frozen and relaxed approximations are reported in Figure 5. Upon relaxation the $2\sigma_g \rightarrow k\sigma_u$ resonance is shifted by a large amount, nearly 11 eV; however, the shape of this feature is not substantially different than the frozen core results. In Figure 5 we also compare our results to the experimental cross sections of Wright and Brion,[28] where it is seen that the frozen and relaxed core cross sections bracket the experimental maximum indicating that, while the frozen core approximation completely neglects screening, the completely relaxed core overestimates its effects. Lastly, in this figure we have plotted the frozen core STMT[1]

results. For this broad resonance the STMT calculations are in good agreement with the present FC results.

The asymmetry parameters are plotted in Figure 6 and compared to the synchrotron radiation data of Truesdale et al.[8] The minimum in the RC study is shifted by nearly 10eV, in agreement with the shift in the peak cross section. In general, core relaxation does not improve the agreement between these theoretical results and experiment in this channel.

C. VALENCE LEVEL PHOTOIONIZATION

The effects of scattering from the relaxed core on the $4\sigma_g^{-1}$ valence photoionization cross sections are illustrated in Figure 7, where our results in the FC and RC approximations are plotted and compared. As expected, these effects are seen to be minimal in the $4\sigma_g$ valence level. The resonance is shifted by about 2 eV to higher energy, and the peak is reduced by about 10%. Also plotted in this figure is the experimental electron impact data of Brion and Tan.[29] Measurements for the photoionization cross sections in this channel have been made using synchrotron radiation[29,30] and are in good agreement with the electron impact data.

These $4\sigma_g$ calculations were performed with a Hartree-Fock wavefunction for the neutral molecule and the length form of the dipole moment operator. Correlating the initial state does reduce the peak cross section of

the resonance, giving good agreement with the velocity form cross sections[4] In addition, vibrational averaging[31] broadens this feature; however, the disagreement with the experimental data remains and is still not completely understood. Inclusion in the calculations of the antisymmetric and/or bending vibrations of the nuclei may resolve this discrepancy. As with the process of localization, these vibrations break the symmetry of the CO_2 molecule and hence would provide a mechanism by which the even and odd partial waves could mix, thereby broadening the resonant feature. In addition, Roy et al.[32] have suggested that a bent geometry for the $C^2\Sigma_g^+$ state of CO_2^+ would allow for final state configuration interaction effects, which have not been included in the present theoretical treatment.

IV. CONCLUSIONS

The effects of core relaxation on the carbon and oxygen K-shell photoionization cross sections and asymmetry parameters have been presented. These effects are seen to be most important in the vicinity of shape resonances. The use of the relaxed molecular orbitals produces a less attractive scattering potential, and hence the resonances are shifted to higher kinetic energies. Disagreement between the calculated oxygen K-shell cross sections and the experimental results remains. We have

suggested that hole localization, i.e. symmetry breaking, can mix the $k\sigma_u$ and $k\sigma_g$ continuum and broaden the shape resonance feature. The main result of relaxation on the carbon K-shell photoionization cross sections is a shift of the resonance to higher kinetic energy. Lastly, as expected, relaxation effects do not substantially change the $4\sigma_g^{-1}$ valence level photoionization cross sections and asymmetry parameters. Further studies on the role of hole localization and the effects of vibrational motion on these cross sections is necessary in order to understand the existing discrepancies between the theoretical and experimental results.

REFERENCES

1. N. Padial, G. Csanak, B. V. McKoy, and P. W. Langhoff, Phys. Rev. A **23**, 218 (1981).
2. W. R. Daasch, E. R. Davidson, and A. U. Hazi, J. Chem. Phys. **76**, 6031 (1982).
3. L. A. Collins and B. L. Schneider, private communication.
4. R. R. Lucchese and V. McKoy, Phys. Rev. A **26**, 1406 (1982).
5. R. R. Lucchese, K. Takatsuka, and V. McKoy, Physics Reports, 131, 149 (1986).
6. D. L. Lynch and V. McKoy, Phys. Rev. A **30**, 1561 (1984).
7. D. M. Barrus, R. L. Blake, A. J. Burek, K. C. Chambers, and A. L. Pregenzer, Phys. Rev. A **20**, 1045 (1979).
8. C. M. Truesdale, D. W. Lindle, P. H. Kobrin, U. E. Becker, H. G. Kerkhoff, P. A. Heimann, T. A. Ferrett, and D. A. Shirley, J. Chem. Phys. **80**, 2319 (1984).
9. Chui-hui Yu, Russell M. Pitzer, and C. William McCurdy, Phys. Rev. A **32**, 2134 (1985).
10. L. A. Collins and B. J. Schneider, Phys. Rev. A **29**, 1695 (1984).
11. See, for example, H. P. Kelly, S. L. Carter, and B. E. Norum, Phys. Rev. A **25**, 2052 (1982); M. Ya. Amusya, V.

K. Ivanov, S. A. Scheinerman, S. I. Sheftel, and A. F. Ioffe, Sov. Phys. (JETP) **51**, 458 (1980) [Zh. Eksp. Teor. Fiz. **78**, 910 (1980)].

12. R. S. Williams and D. A. Shirley, J. Chem. Phys. **66**, 2378 (1977).

13. A. T. Amos and G. G. Hall, Proc. Roy. Soc. (London), **A263**, 483 (1961).

14. H. F. King, R. Stanton, H. Kim, R. E. Wyatt, and R. G. Parr, J. Chem. Phys. **47**, 1936 (1967).

15. A. F. Voter and W. A. Goddard III, Chem. Phys. **57**, 253 (1981).

16. A. F. Voter, California Institute of Technology, Ph.D. Thesis, 1983.

17. R. R. Lucchese, G. Raseev, and V. McKoy, Phys. Rev. A **25**, 2572 (1982).

18. F. W. Bobrowicz and W. A. Goddard III, in Modern Theoretical Chemistry 3, edited by H. F. Schaefer III (Plenum, New York, 1977), p. 79.

19. R. R. Lucchese and V. McKoy, Phys. Rev. A **28**, 1382 (1983).

20. R. R. Lucchese, D. K. Watson and V. McKoy, Phys. Rev. A **22**, 421 (1980).

21. B. H. Lengsfield, J. A. Jafri, D. H. Phillips, and C. H. Bauschlicher, J. Chem. Phys. **74**, 6849 (1981).

22. K. Siegbahn, C. Nordling, G. Johansson, J. Hedman, P. F. Heden, K. Hamrin, U. Gelius, T. Bergmark,

L. O. Werme, R. Manne, and Y. Baer, ESCA Applied to Free Molecule (North Holland, Amsterdam, 1969).

23. D. W. Turner, C. Baker, A. D. Baker, and C. R. Brundle, Molecular Photoelectron Spectroscopy (Wiley, New York, 1970).

24. L. J. Aaron , M. F. Guest, M. B. Hall, and, I. H. Hillier, J.C.S. Faraday II, 563 (1973).

25. W. B. England, W. C. Ermler, and A. C. Wahl, J. Chem. Phys. **66**, 2336 (1977).

26. C. E. Woodward, S. Nordholm, and G. Backsay, Chem. Phys. **69**, 267 (1982).

27. R. R. Lucchese and V. McKoy, Phys. Rev. A **28**, 1382 (1983).

28. G. R. Wright and C. E. Brion, J. Electron Spectrosc. Relat. Phen. **3**, 191 (1974).

29. C. E. Brion and K. H. Tan, Chem. Phys. **34**, 141 (1978).

30. T. Gustafsson, E. W. Plummer, D. E. Eastman, and W. Gudert, Phys. Rev. A **17**, 175 (1978).

31. R. R. Lucchese and V. McKoy, Phys. Rev. A **26**, 1992 (1982).

32. P. Roy, I. Nenner, M. Y. Adam, J. Delwiche, M. J. Hubin Franskin, P. Lablanquie, and D. Roy, Chem. Phys. Lett. 109, 607 (1984).

Table I.

IONIZATION POTENTIALS (eV) FOR CO_2

		$O(1s^{-1})$	$C(1s^{-1})$	$4\sigma g^{-1}$
K.T.[a]	Present Results	562.03	312.47	21.74
	Aaron et al.[e]	562.8	313.5	--
	England et al.[f]	--	--	21.79
ΔSCF[b]	Present Results	553.93	302.47	20.7
	Aaron et al.[e]	554.2	301.4	--
	England et al.[f]	--	--	20.69
Experiment		541.1[c]	295.5[c]	19.4[d]

a) K.T. = Koopmans Theorum

b) $\Delta SCF = E_{ion} - E_{neutral}$; the energy difference between the SCF energies of the ion and neutral molecule

c) Reference 22

d) Reference 23

e) Reference 24

f) Reference 25

FIGURE CAPTIONS

1. Oxygen K-shell photoionization cross sections (length) in CO_2: — · — · — , FCHF results (Ref. 4); ————, present RCHF results; — — — , FCHF results of Padial et al. (Ref. 1); O, experimental results of Barrus et al. (Ref. 7). The experimental ionization potential, 541.1 eV, has been assumed.

2. Oxygen K-shell eigenphase sums for CO_2: ————— , $1\sigma_g \rightarrow k\sigma_u$ FCHF results (Ref. 4); — — — , present $1\sigma_g \rightarrow k\sigma_u$ RCHF results; — · — · — · — , $1\sigma_u \rightarrow k\sigma_g$ FCHF results (Ref. 4); — — — —, present $1\sigma_u \rightarrow k\sigma_g$ RCHF results.

3. Oxygen K-shell partial channel cross sections (length), ————— , $1\sigma_g \rightarrow k\sigma_u$ FCHF results (Ref. 4); — — — —, present $1\sigma_g \rightarrow k\sigma_u$ RCHF results; — · — , $1\sigma_u \rightarrow k\sigma_g$ FCHF results (Ref. 15); — — —, present $1\sigma_u \rightarrow k\sigma_g$ RCHF results.

4. Oxygen K-shell photoelectron asymmetry parameters (length) in CO_2: — · — , FCHF results (Ref. 4); ———, present RCHF results; O synchrotron data of Ref. 8.

5. Carbon K-shell photoionization cross sections in CO_2 (length): ———— , FCHF results of Ref. 4; —— —— , present RCHF results; — — — — — , STMT results of Ref. 1; , experimental data of Ref. 22, normalized as in Ref. 4. The experimental ionization potential, 297.5 eV, has been assumed.

6. Carbon K-shell photoelectron asymmetry parameters in CO_2 (length): ———— , FCHF result of Ref. 4; — — — — , present RCHF results; ▶ , synchrotron data of Ref. 7.

7. Photoionization cross sections (length) for the production of the $C^2\Sigma_g^+$ states of CO_2^+: ————, FCHF results of Ref. 4; — — — — , present RCHF results, and ▶ , experimental results of Ref. 27. The experimental ionization potential, 19.4 eV, has been assumed.

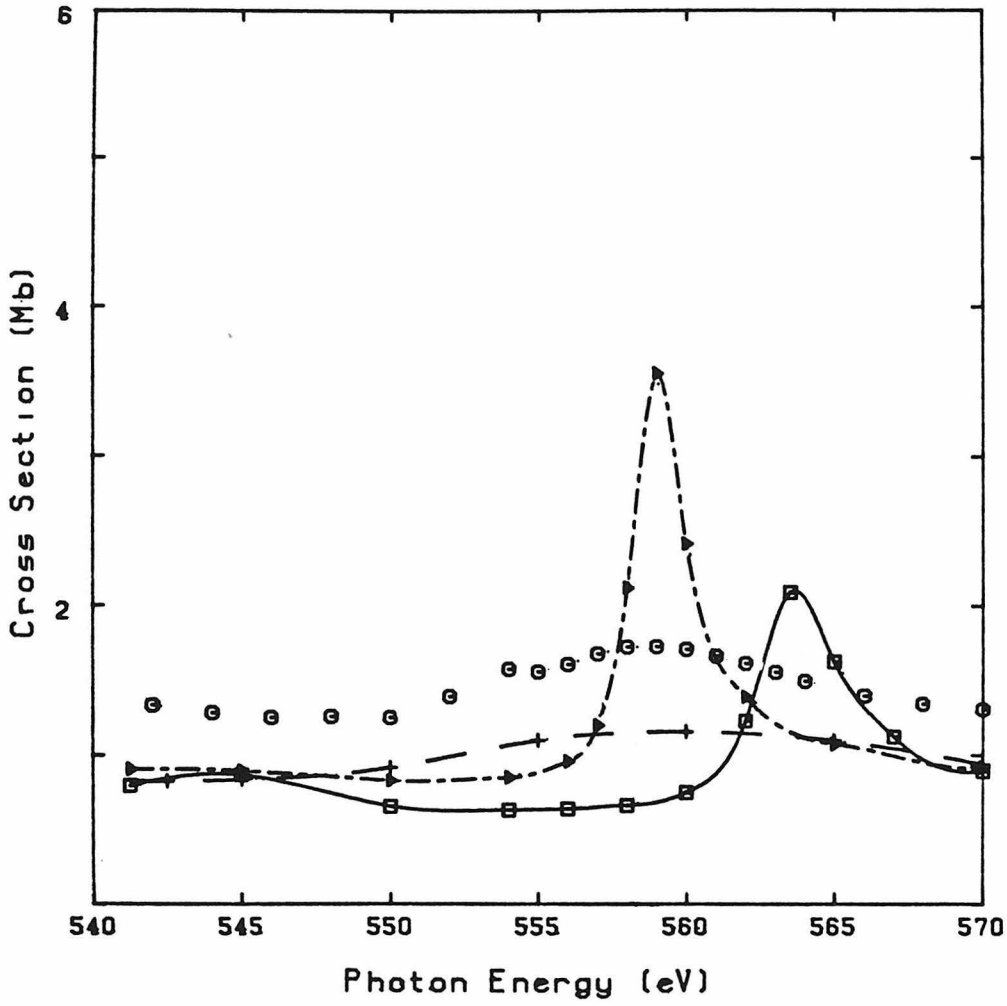
6
4
2
Cross Section (Mb)
540
545
550
555
560
565
570
Photon Energy (eV)

Figure 1

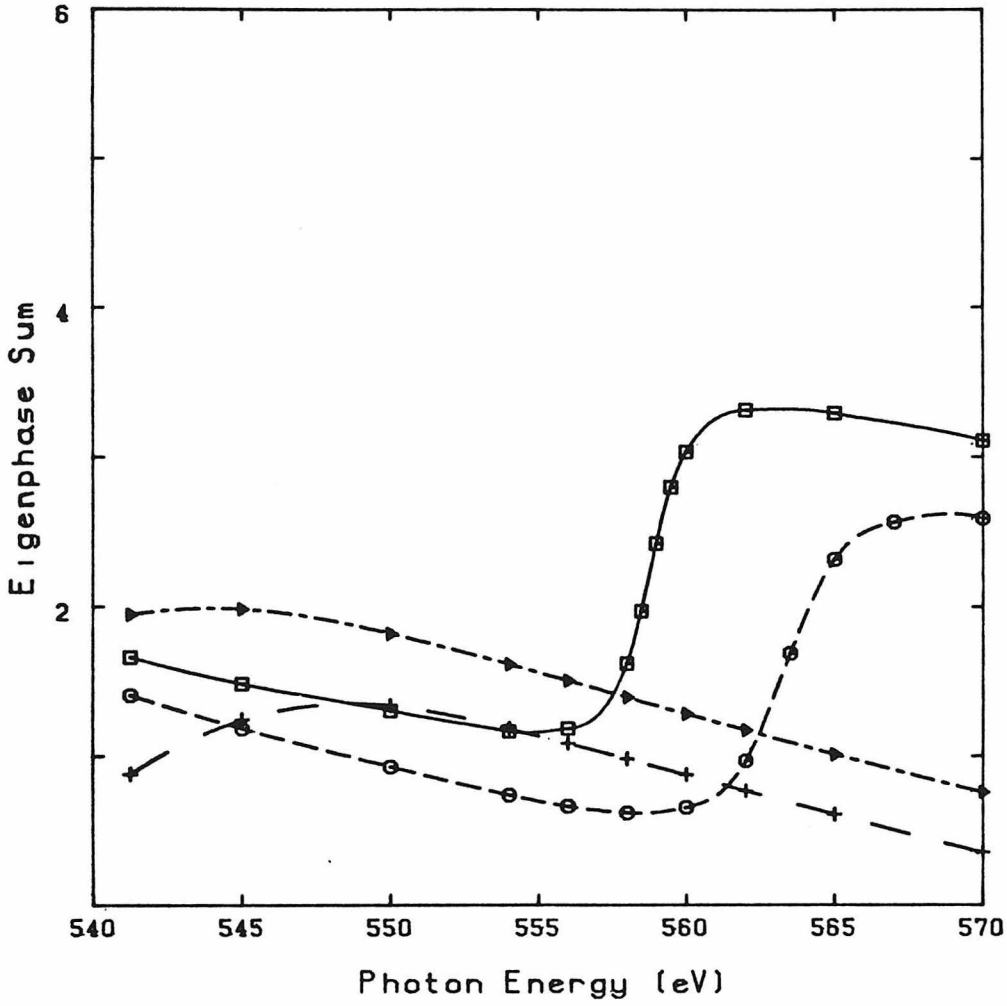
6
4
2
Eigenphase Sum
540
545
550
555
560
565
570
Photon Energy (eV)

Figure 2

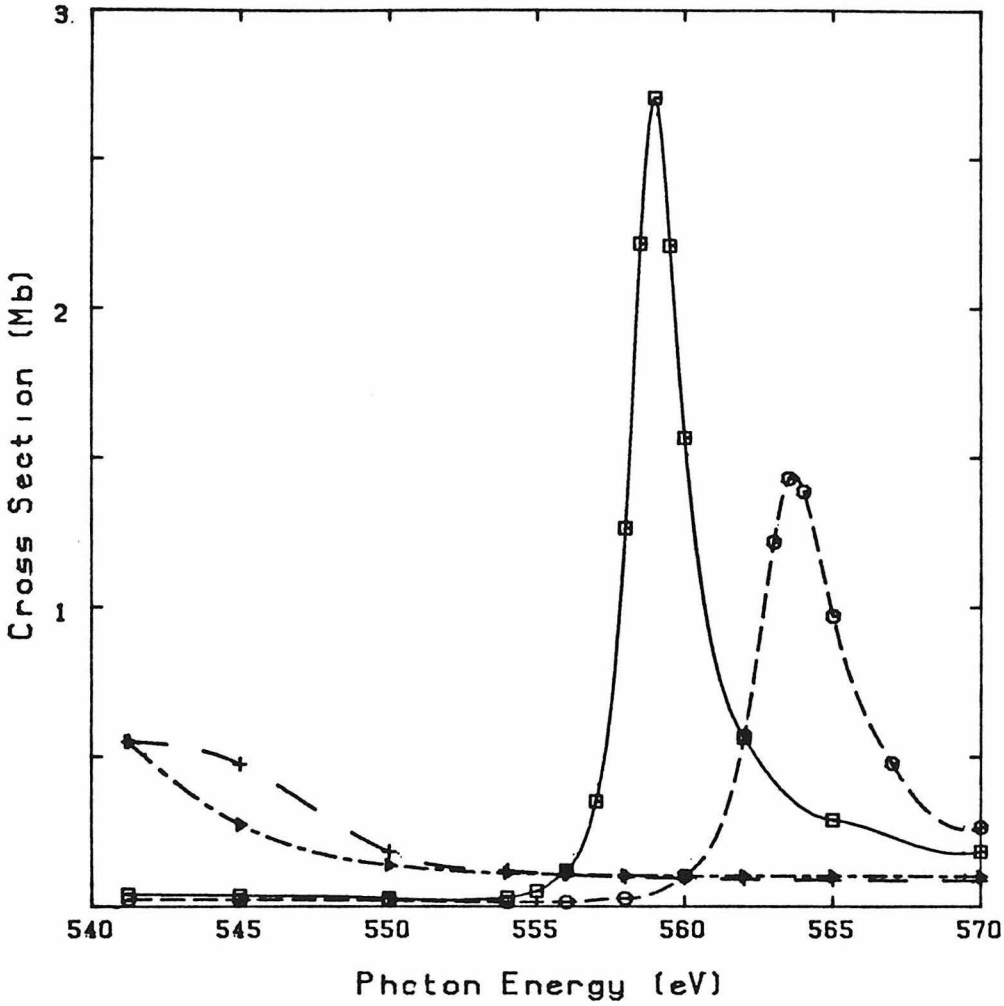
3.
2
1
Cross Section (Mb)
540
545
550
555
560
565
570
Photon Energy (eV)

Figure 3

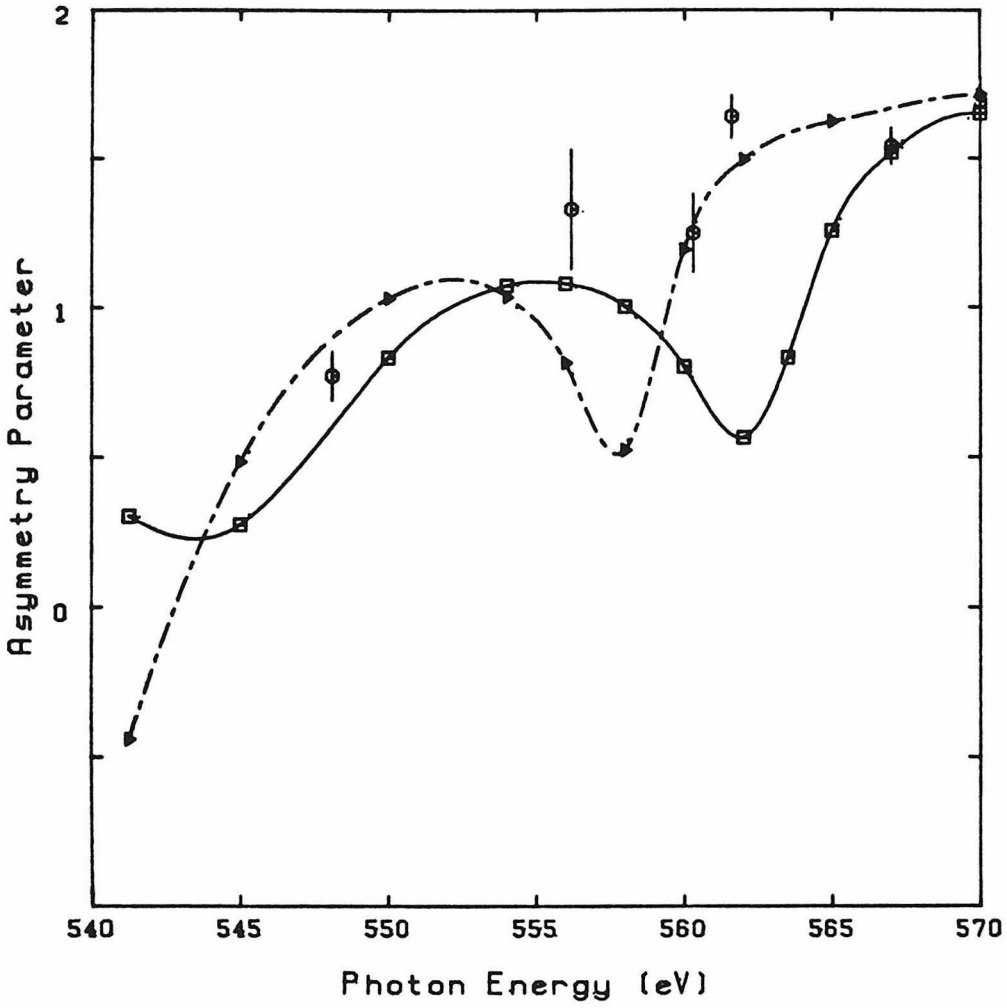
2
1
0
Asymmetry Parameter
540
545
550
555
560
565
570
Photon Energy (eV)

Figure 4

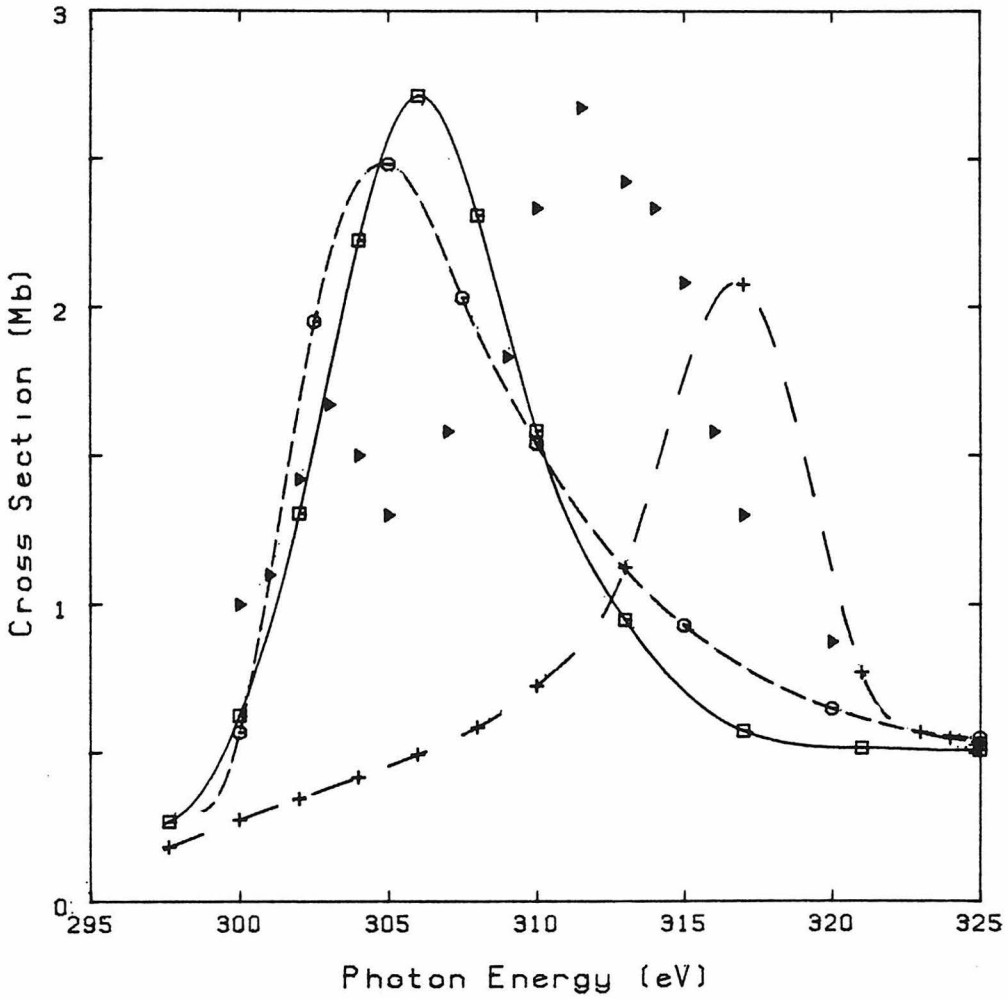
Cross Section (Mb)
Photon Energy (eV)
0
1
2
3
295
300
305
310
315
320
325

Figure 5

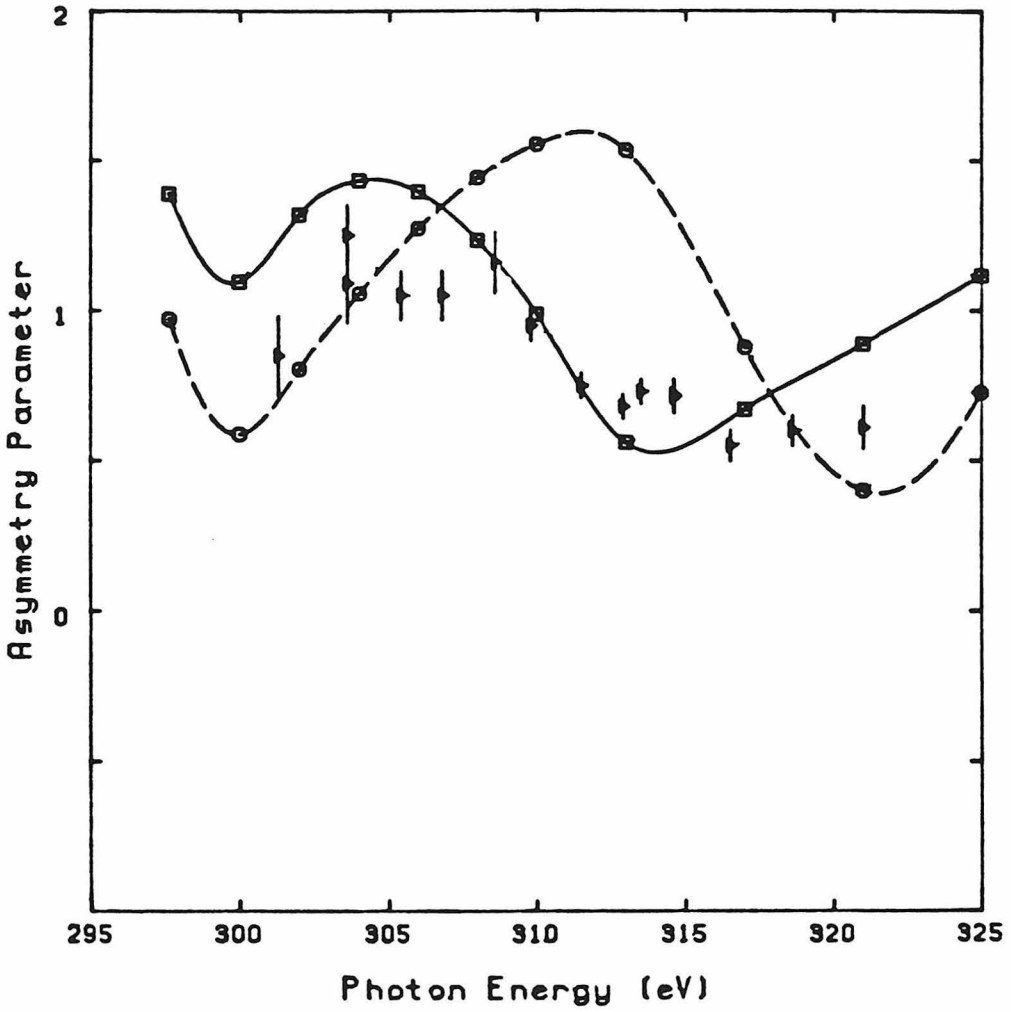
2
1
0
Asymmetry Parameter
295
300
305
310
315
320
325
Photon Energy (eV)

Figure 6

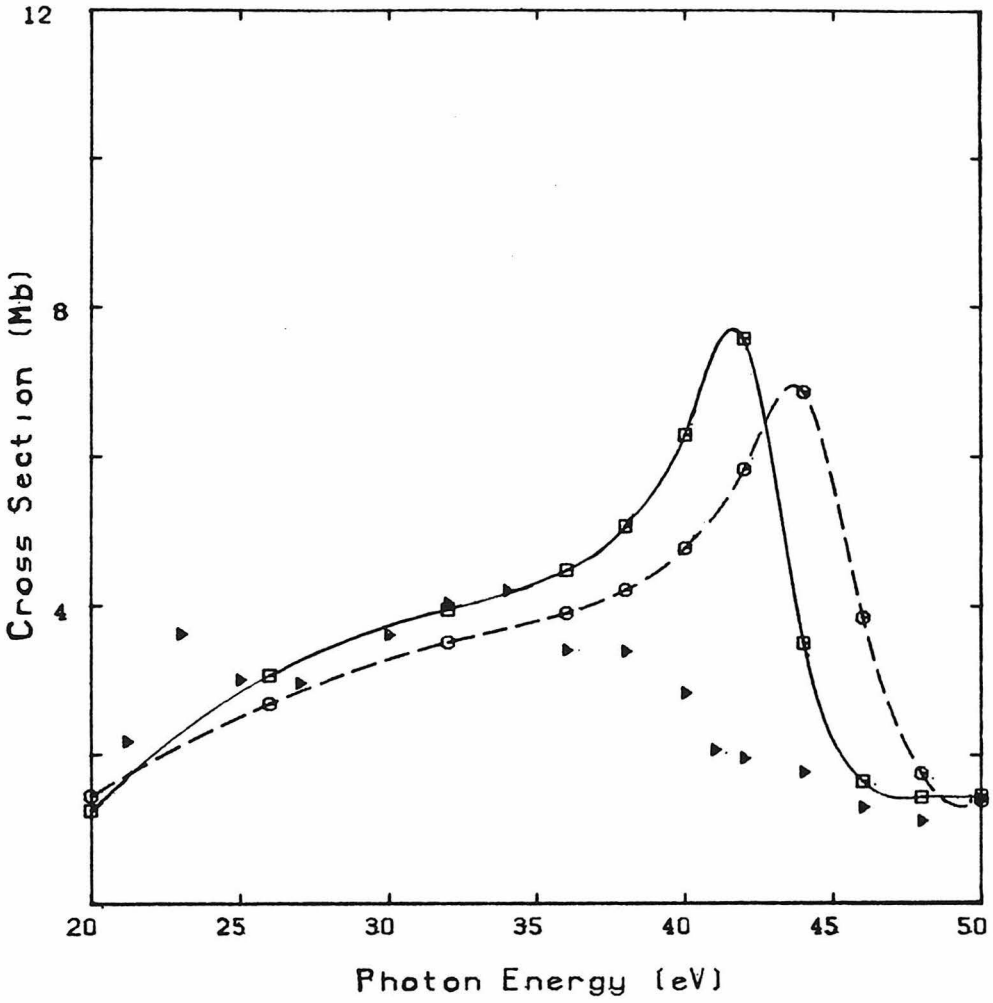

Figure 7

CHAPTER III

AUTOIONIZATION

AUTOIONIZING RESONANCES IN MOLECULAR PHOTOIONIZATION

I. INTRODUCTION

Recent experimental and theoretical studies of molecular photoionization have illustrated the dramatic effects that resonances play in the ionization dynamics.[1-3] Through the resonance region pronounced structure in the cross sections and photoelectron asymmetry parameters is observed. Synchrotron radiation sources[1] now provide the intense tunable radiation necessary to study the continuous, and in resonance regions, the rapid variation of molecular photoionization cross sections with energy. When coupled with photoelectron kinetic energy analysis these measurements also provide vibrational branching ratios. These studies have demonstrated that strong non-Franck-Condon effects are induced by these resonant states, e.g., vibrational-state dependent asymmetry parameters[4-7] and vibrational branching ratios,[5,8,9] which deviate from Franck-Condon predictions. Typically, these resonances are classified by their nature, i.e., being either single-particle (shape) or multi-electron (autoionizing) processes. Shape resonances can be accurately described by single-particle Hartree-Fock continuum orbitals. However, autoionizing resonances are a correlation[4] effect, which are neglected in this single configuration approximation. Fano,[10] using a configuration interaction approach, has demonstrated that the dramatic features associated with autoionizing resonances result from the decay of a discrete

excited state into the underlying continuum. Any theoretical treatment of autoionization must go beyond a single configuration description for the final state wavefunction.

Theories for final state correlation effects are well developed for atomic photoionization;[11] however, the extension to molecular systems has only recently begun.[12-18] For example, Multichannel Quantum Defect Theory (MQDT) has been applied to Rydberg autoionizing states in O_2[12] and N_2.[14] In these studies several approximations were made to obtain the relevant electronic matrix elements. In O_2 these were treated semi-empirically, while in N_2 the continuum-continuum interaction matrix elements were obtained by an extrapolation from the discrete-continuum integrals. Valence autoionization has been studied in C_2H_2, using the time-dependent local-density approximation (TDLDA).[18] This method is equivalent to the random phase approximation in terms of incorporating many-body effects; however, it is based on the use of a model exchange-correlation potential, i.e., the local-density-functional approximation. Preliminary ab initio calculations, neglecting the closed-channel component in the dipole transition matrix elements, have been performed for autoionizing levels in NO, using an effective optical potential.[15] Only for autoionizing Rydberg levels of H_2 have completely ab initio calculations been performed,[16] using a method based on the logarithmic derivative of the wavefunction.

The purpose of the present study is to apply to molecular systems a fully ab initio multi-channel treatment for the final-state electronic continuum. This method is a generalization of the earlier atomic configuration interaction studies by Altick and Moore,[19] Fano,[10] and the multi-channel reactance matrix (K-Matrix) method of Fano and Prats.[20] Autoionization as well as other potentially important final-state correlation effects, e.g., interchannel mixing, are included. We will work in the fixed-nuclei approximation and use single-particle functions, generated with realistic N-1 electron potentials, as a basis for the expansion of the final state wavefunctions. The bound-excited orbitals are generated using standard bound state techniques,[21] while the single-particle continuum orbitals are calculated using the iterative Schwinger method[2] to solve the collisional equations for the photoelectron in the frozen core Hartree-Fock (FCHF) approximation. Thus, the zeroth order continuum wavefunctions used accurately represent the underlying background continua.

Our initial study of molecular electronic autoionization was performed for the $^1\Sigma_u^+$ ($1\sigma_u 2\sigma_g$) state of H_2. We chose this system because the position and width of this excited state have been well characterized by a variety of theoretical methods.[16,22-27] In addition, the effect of this autoionizing state on the photoionization cross sections and asymmetry parameters has been studied by Raseev.[16]

Therefore, we were able to compare our method with previous techniques for the study of decaying electronic states.

Of particular interest here is the double-bump feature near 14eV observed in the photoionization cross section for the production of the $X^2\Pi_u$ state of C_2H_2.[30,31] Structure is also observed in the vibrationally resolved asymmetry[5-7] parameters and vibrational branching ratios.[5] In spite of several recent theoretical[7,18,30-33] and experimental[5-7,30,31] studies, we do not as yet have a definitive quantitative understanding of the underlying resonance structure in this region, e.g., to what extent the structure is due to shape or autoionizing resonances or to some combination of such resonances, although the decay of the $2\sigma_u \rightarrow 1\pi_g$ (π^*) valence state almost certainly contributes to this structure.[5,18] We have studied the effect of the autoionizing $^1\Pi_u$ ($2\sigma_u \rightarrow 1\pi_g$) state on the total cross sections and photoelectron angular distributions for the production of the $X^2\Pi_u$ state of $C_2H_2^+$. We compare our fixed-nuclei calculations with the experimental data and TDLDA results. The prominent dip and sharp second maximum can be explained by this sharp autoionizing valence state superimposed on a broad background. The near threshold maximum as well as the second peak are expected to be modified by additional correlation effects that were neglected in this initial study.

In the next section we discuss our approach for incorporating correlation effects in the final-state wavefunctions used in molecular photoionization. In Section III we present and discuss our results, and Section IV summarizes our conclusions.

II. METHOD

The initial state wavefunction, necessary for the calculation of the photoionization cross sections and asymmetry parameters, is generated by standard bound state methods.[21] For a total energy E, the final-state wavefunction can be expanded as

$$\Psi_{\Gamma,E}^{(-)} = \sum_{\ell m} i^{\ell} \Psi_{\Gamma \ell m,E}^{(-)} Y_{\ell m}(\hat{k}) , \qquad (1)$$

where Γ labels the quantum numbers necessary to describe the residual ionic core, the superscript (-) indicates incoming-wave boundary conditions, and the continuum functions are normalized per unit energy interval. For notational convenience the channel label is defined $\beta \equiv (\Gamma,\ell,m)$. Rather than use the complex functions[12] in Equation (1) actual calculations employ standing-wave boundary conditions, i.e., the principal-value functions.[34] The N-electron principal-value wavefunction is then written as a linear combination of zeroth order bound and continuum wavefunctions,[10,11,19,35]

$$\Psi_{\beta E}(R) = \psi_n(R)\, A_{n,\beta E} + \sum_{\gamma}\int dE'\psi_{\gamma E'}(R)a_{\gamma E',\beta E}\,. \qquad (2)$$

We assume that there is one autoionizing state, $\psi_n(R)$, and that a set of Hartree-Fock continuum orbitals are used to represent the unperturbed continuua, $\psi_{\gamma E'}(R)$. The summation over the channel indices γ in Equation (2) indicates that the zeroth order states will be mixed by configuration interaction. The expansion coefficients $A_{n,\beta E}$ and $a_{\gamma E',\beta E}$ are determined by requiring that

$$(H-E)\,|\Psi_{\beta E}> = 0\,, \qquad (3)$$

where H is the electronic Hamiltonian. The following set of equations are obtained by projecting the $<\psi_n|$ and $<\psi_{\alpha E''}|$ components onto Equation (3):

$$A_{n,\beta E}\,(E_n-E) + \sum_{\gamma}\int dE' V_{n,\gamma E'}\, a_{\gamma E',\beta E} = 0 \qquad (4)$$

and

$$V_{\alpha E'',n}\, A_{n,\beta E} + \sum_{\gamma}\int dE'\, V_{\alpha E'',\gamma E'}\, a_{\gamma E',\beta E} + \sum_{\gamma} (E''-E)\, C_{\alpha E'',\gamma E}\, a_{\gamma E'',\beta E} = 0, \qquad (5)$$

with the matrix elements defined as:

$$V_{n,\gamma E'} \equiv <\psi_n|H-E|\psi_{\gamma E'}> \qquad (6)$$

$$V_{\alpha E'',\gamma E'} \equiv <\psi_{\alpha E''}|H-E|\psi_{\gamma E'}>\,(1-\delta_{\alpha\gamma}) \qquad (7)$$

and

$$C_{\alpha,\gamma}(E'') \equiv [1+(K^{\circ}(E''))^2]_{\alpha,\gamma}\,. \qquad (8)$$

The δ-function in Equation (7) results from the use of Hartree-Fock single-particle continuum states as a zeroth order basis. In this case, intra-channel coupling is automatically included.[11,36,37] The C matrix appearing in Equation (5), and defined in Equation (8), results from the non-orthogonality of the principal-value basis set.[20,38-40] The matrix K° appearing in Equation (8) is the static-exchange reaction matrix obtained along with the Hartree-Fock continuum functions. This non-orthogonality is discussed in detail in Appendix I. Defining $\bar{V} \equiv C^{-1}V$ Equation (5) can be rewritten

$$(E''-E)\, a_{\delta E'',\beta E} + \bar{V}_{\delta E'',n}\, A_{n,\beta E} + \sum_{\gamma} \int dE' \bar{V}_{\delta E'',\gamma E'}\, a_{\gamma E',\beta E} = 0 . \tag{9}$$

Following the method of Fano and Prats,[20] the solution of Equations (4) and (9) is performed by a change of variables

$$a_{\gamma E'',\beta E} = \underline{P}\left(\frac{1}{E-E''}\right) A_{\gamma E'',\beta E} + \delta(E-E'') B_{\gamma E,\beta E} , \tag{10}$$

where $\underline{P}$ indicates the principal-value integral is to be taken, $A_{\gamma E',\beta E}$ is the new variable and $B_{\gamma E,\beta E}$ is a normalization constant. Equations (4) and (9) become

$$A_{n,\beta E} = E_{n/E} A_{n,\beta E} + \sum_{\gamma} \underline{P}\int dE' \frac{V_{n,\gamma E'} A_{\gamma E',\beta E}}{E(E-E')} + \frac{V_{n,\gamma E} B_{\gamma E,\beta E}}{E} \qquad (11)$$

$$A_{\delta E'',\gamma E} = \bar{V}_{\delta E'',n} A_{n,\beta E} + \sum_{\gamma} \underline{P}\int dE' \frac{\bar{V}_{\delta E'',\gamma E'} A_{\delta E',\beta E}}{E-E'} + \bar{V}_{\delta E'',\gamma E} B_{\gamma E,\beta E} . \qquad (12)$$

Writing the A coefficients in terms of the B elements

$$A_{i,\beta E} = \sum_{\gamma} K_{i,\gamma E} B_{\gamma E,\beta E} \qquad (13)$$

with i denoting either a bound (n) or a continuum ($\delta E''$) channel and inserting this into equation (11) and (12), one obtains the following integral equation:[41]

$$K_{i,\sigma E} = \bar{V}_{i,\sigma E} + \sum_{\gamma} \underline{P}\int \frac{\bar{V}_{i,\gamma E'} K_{\gamma E',\sigma E} dE'}{E-E'} + \bar{V}_{in} K_{n,\sigma E} \qquad (14)$$

For $E \neq E_n$ Equation (11) is solved for $A_{n,\beta E}$ and substituted into Equation (12), obtaining the more symmetric equation for the K-matrix[42]

$$K_{\beta E'',\sigma E} = \bar{V}_{\beta E'',\sigma E} + \underline{P} \sum_{\gamma} \int \frac{\bar{V}_{\beta E'',\gamma E'} K_{\gamma E',\sigma E} dE'}{E-E'} , \qquad (15)$$

with $\bar{V}$ defined as

$$\overrightarrow{V}_{\beta E'',\sigma E} = \bar{V}_{\beta E'',\sigma E} + \frac{\bar{V}_{\beta E'',n}\, V_{n,\sigma E}}{E-E_n} \quad . \tag{16}$$

The integral equation for the K-matrix elements is reduced to a set of algebraic equations, which are solved by a matrix inversion. This technique has been used previously and is discussed by Altick and Moore[19] and Altick and Glassgold.[43] Once the K-matrix elements are calculated, the wavefunction in Equation (2) is known in terms of the unknown B-matrix, which is determined by imposing incoming-wave boundary conditions; i.e.,[20,35,44]

$$\Psi_{\beta E}^{(-)} \rightarrow \sum_{\alpha} \Phi_{\alpha} \frac{1}{2i\, r k_{\alpha}^{1/2}} \left(e^{i\theta_{\alpha}}\, \delta_{\beta\alpha} - \delta^{+}_{\beta\alpha}\, e^{-i\theta_{\alpha}} \right), \tag{17}$$

on the asymptotic form of the wavefunction in Equation (2). In Equation (17), Φ_{α} denotes the wavefunction for the α ionic core including the spin function, the spherical harmonic for the continuum electron and $\theta_{\gamma} = kr_{\gamma} - \pi \ell_{\gamma}/2 + 1/k_{\gamma}\ \ell n 2k_{\gamma} r + \sigma_{\ell}$, where S is the scattering matrix and σ_{ℓ} is the Coulomb phase shift. Using the asymptotic form for the principal value wavefunctions

$$\Psi_{\beta E}^{(P)} \longrightarrow \sum_{\alpha} \Phi_{\alpha} \frac{1}{r k_{\alpha}^{1/2}} \left(\sin\theta_{\alpha}\, \delta_{\beta\alpha} + K^{\circ}_{\beta\alpha} \cos\theta_{\alpha} \right), \tag{18}$$

in Equation (2), expressing the sines and cosines in $e^{\pm i\theta\alpha}$, and matching the coefficients of $e^{\pm i\theta\alpha}$ to those in the outgoing wave, Equation (7), determines the B-matrix,

$$\underline{B} = (1 - i\pi K)^{-1} (1 + iK^{\circ})^{-1}, \tag{19}$$

and thus the overall normalization of the wavefunction. Using these final-state wavefunctions, we define the length and velocity forms of the photoionization transition matrix elements as[45]

$$I^{L}_{\ell m\mu} = \langle \Psi_i | r_\mu | \Psi_{\varepsilon\ell m} \rangle \tag{20}$$

$$I^{V}_{\ell m\mu} = \frac{1}{E} \langle \Psi_i | \nabla_\mu | \Psi_{\varepsilon\ell m} \rangle , \tag{21}$$

where Ψ_i is the initial state of the neutral molecule and E is the photon energy. With these matrix elements the total cross section is written as

$$\sigma^{L,V} = \frac{4\pi^2 E}{3C} \sum_{\ell m\mu} | I^{L,V}_{\ell m\mu} |^2 , \tag{22}$$

where c is the speed of light. The corresponding photoelectron asymmetry parameters is given by

$$\frac{d\sigma^{L,V}}{d\Omega_{\hat{k}}} = \frac{\sigma^{L,V}}{4\pi} \left[1 + \beta^{L,V} P_2 (\cos\theta) \right] , \tag{23}$$

where P_2 is a Legendre polynomial of degree two and θ is the angle between the direction of polarization of the light and the momentum of the photoelectron.

III. RESULTS AND DISCUSSION

A. H_2

The ground state wavefunction was obtained using the Gaussian basis set listed in Table I. For an internuclear separation of 1.4 a.u., the total energy in this basis is -1.133249 a.u. The wavefunction for the autoionizing $^1\Sigma_u^+$ $(1\sigma_u\ 2\sigma_g)$ state was obtained in a separate SCF calculation. The total energy for this state is -0.028055 a.u. However, this excited state wavefunction is composed of molecular orbitals, i.e., $2\sigma_g$, which are non-orthogonal to the ground state $1\sigma_g$ function. Therefore, overlap integrals are necessary for the calculation of the Hamiltonian and dipole transition matrix elements using these wavefunctions. The resonant state, having $^1\Sigma_u^+$ symmetry, will autoionize into only the $k\sigma_u$ background continuum.

The non-resonant $k\sigma_u$ and $k\pi_u$ background continua were obtained in the FCHF approximation using the iterative Schwinger variational method.[2] Detailed discussions of the numerical methods used have been given elsewhere.[2,45] The various partial wave expansion parameters were chosen as follows:

(1) Maximum partial wave included in the expansion of the scattering solution = $\ell_p = 7(\sigma_u, \pi_u)$;

(2) Maximum partial wave retained in the expansion of the nuclear potential = 28.

All other partial wave expansions were truncated at ℓ=14. For the radial integrations, the grid contained 470 points and extended to 39.8 a.u., with the smallest step size being 0.005 a.u. and the largest step size 0.16 a.u. The initial L^2 basis set used in the iterative procedure is given in Table II. The continuum orbitals used in the present study have been once iterated.

Table III summarizes our results for the position, dipole transition moment, and width of the $^1\Sigma_u^+$ ($1\sigma_u\ 2\sigma_g$) state and compares them to previously calculated values.[22-26] We have calculated the excitation energy and transition moment directly from the ground and excited state wavefunctions and the width using the "golden-rule" formula of Feshbach's theory of resonances;[27]

$$\Gamma(E) = 2\pi |< \Psi_n | H-E | \Psi_{f,E}^{(-)} >|^2 , \qquad (24)$$

where E is taken as the resonance energy. This technique was also employed by Kirby et al.,[23,25] who used a correlated wavefunction for the ground and excited states and undistorted Coulomb waves for the final continuum

functions, as well as Hazi,[26] who also used correlated wavefunctions and a Stieltjes-Moment theory procedure for obtaining the non-resonant background continuua. In addition, Raseev,[16] using a logarithmic derivative of the wavefunction procedure, Tagaki and Nakamura,[22] using a Kohn variational procedure and Collins and Schneider,[24] using a four-state, close-coupling calculation in the linear algebraic method obtained these parameters by fitting a Breit-Wigner plus background contribution form to the calculated phase shifts.

The major difference between the present result for the excitation energy and that of Kirby et al.[23] is the use of an SCF wavefunction for the ground state in our calculations. The correlated ground state wavefunction obtained in Reference 23 is 0.8 eV lower in energy than the present results. The energy shift of the resonant state, caused by interaction with the continuum, is nearly -0.2 eV; however, this as well as a correction for the correlation of the ground state was not included in the excitation energy reported in Table III. The dipole transition moments are in good agreement and, except for the calculation using undistorted Coulomb waves[25] for the continuum, the widths are also in good accord.

In Figure 1 we compare our total photoionization cross sections, including the autoionizing resonance, to the FCHF results in the dipole length and velocity forms. The difference between the length and velocity cross

sections probably results from the neglect of correlation in the initial state. Correlating the neutral ground state has been shown to bring the length and velocity form results into better agreement.[2] The resonance produces a dip in the total cross section where the $k\sigma_g$ partial channel cross section is nearly zero. Also in this figure are the dipole length form results by Raseev,[16] where similar behavior is seen. The difference between the present results and those of Raseev[16] is primarily in the background cross sections and most likely results from the use of a correlated initial state wavefunction in Reference 16. In addition, the present study assumes the vertical ionization potential of 16.4 eV,[2] while Raseev used the adiabatic ionization potential of 15.425 eV. The vibrationally unresolved experimental data of Samson and Cairns[28] are also included in Figure 1; however, comparisons between the theoretical results and the measured cross sections are difficult, since there are insufficient data points in the resonance region. Also, these calculations have been performed at one internuclear distance and therefore neglect the R-dependence of the matrix elements. In fact, Raseev[16] has shown that by changing the position of the nuclei the resonance shifts to 26 eV (R=1.7 a.u.) and to 34 eV (R=1.2 a.u.). In general, one expects a broadening of the resonance features by averaging over the ground vibrational state wavefunction, and it may be necessary to perform this averaging in order

to obtain an accurate representation of the resonance feature. Finally, more data in the resonance region are necessary in order to make any meaningful comparisons between these theoretical cross sections and the measured values.

The asymmetry parameters are reported in Figure 2 and compared to the FCHF values. The sharp dip in the asymmetry parameters results from the presence of the resonance. Also in this figure are the results of Raseev[16] and good agreement between these calculations and the present results is obtained. To our knowledge there is only the one vibrationally unresolved data point of Marr et al. [29] in this energy region. As with the photoionization cross sections, more data in the resonance region would be helpful in the study of this resonance.

B. C_2H_2 Calculational Details

The SCF wavefunction for the ground state of C_2H_2 was constructed from the basis set and equilibrium geometry of Reference 33. The Hartree-Fock configuration for the $^1\Sigma_g^+$ ground state is $1\sigma_g^2 1\sigma_u^2 2\sigma_g^2 2\sigma_u^2 3\sigma_g^2 1\pi_u^4$. The $^1\Pi_u(2\sigma_u \rightarrow 1\pi_g)$ wavefunction was obtained using the improved virtual orbital (IVO) method.[21] In this basis set the excitation energy is 15.99 eV and the oscillator strengths are $f_L=0.886$ (dipole length form) and $f_V=0.722$ (dipole velocity form). These agree reasonably well with the values for the excitation energy (15.54 eV) and

oscillator strength (f_L=0.8036) reported by Machado et al. [32] This method for determining the excited wavefunction is rather crude and produces an extremely large oscillator strength.

In order to improve the description of the resonant state, we have performed two limited configuration interaction calculations. In the first calculation the $^1\Pi_u$ state is expanded in singly excited configurations from the ground state, keeping the $1\sigma_g$ and $1\sigma_u$ orbitals frozen. All single-excitations from the $2\sigma_u$, $2\sigma_g$, $3\sigma_g$, and $1\pi_u$ orbitals have been included. This reduces the excitation energy by 0.22 eV and the oscillator strength to f_L=0.372. The major components of this wavefunction are the $1\pi_u \rightarrow 5\sigma_g$ and $2\sigma_u \rightarrow 1\pi_g$ excitations. A second, restricted CI calculation was performed using only these two excitations. In this case the excitation energy is lowered by 0.14 eV and the oscillator strength to f_L=0.353. These values are also in reasonable agreement with the results obtained in a similar single-excitation CI calculation reported in Reference 46, i.e., a 15.6eV excitation energy and f_L = 0.43.

The final state one-electron Hartree-Fock continuum orbitals used as basis functions in Equation (2) are generated using the iterative Schwinger variational

method.[2,33,45] The various partial wave expansion parameters, initial scattering basis set in the iterative procedure, and the grid used for the radial integrations are identical to those in Reference 33, except ℓ_p, the maximum partial wave in the scattering solution, which is truncated at 8 for σ_g, π_g and δ_g continuum symmetries. We have employed the iterative technique[45] in order to obtain converged Hartree-Fock continuum orbitals, which are then used as the zeroth order continuum functions. Finally, the Ionization Potential for the $1\pi_u$ orbital is taken to be 11.4eV.[47]

The $1\Pi_u$ discrete state autoionizes into both the $1\pi_u{}^3 k\sigma_g$ and $1\pi_u{}^3 k\sigma_g$ underlying continuua. In addition direct continuum-continuum mixing can occur between the $k\sigma_g$ and $k\delta_g$ partial channels. The wavefunctions for these $^1\Pi_u{}^+$ states are:

$$\Psi_n^{IVO}(2\sigma_u \rightarrow 1\pi_g) = \frac{1}{\sqrt{2}}\Big[|(\text{core})2\sigma_u 1\Pi_u{}^4 \overline{1\Pi}_{g+}| - |(\text{core})\overline{2\sigma_u} 1\Pi_u{}^4 1\Pi_{g+}| \Big] \tag{25}$$

$$\Psi_{k\sigma_g} = \frac{1}{\sqrt{2}}\Big[|(\text{core})\, 2\sigma_u{}^2 1\Pi_{u+}{}^2 1\Pi_{u-} \overline{k\sigma_g}| - |(\text{core})\, 2\sigma_u{}^2 1\Pi_{u+}{}^2 \overline{1\Pi}_{u-}\, k\sigma_g| \Big] \tag{26}$$

and

$$\Psi_{k\delta_g} = \frac{1}{\sqrt{2}}\Big[|(\text{core})\, 2\sigma_u{}^2 1\Pi_{u+}\, 1\Pi_{u-}{}^2 \overline{k\delta_{g+}}| - |(\text{core})\, 2\sigma_u{}^2 \overline{1\Pi_{u+}}\, 1\Pi_{u-}{}^2 k\delta_{g+}| \Big] . \tag{27}$$

The single-particle orbitals used in these wavefunctions are orthonormal, and matrix elements over the Hamiltonian operator are generated straightforwardly by numerical integration.[2] In the correlated representation for the discrete state Equation (25) is modified:

$$\Psi_n^{CI} = c_1 [\,|\,(\text{core})2\sigma_u 1\Pi_u^4 \overline{1\Pi}_{g+}|-|\,(\text{core})\,\overline{2\sigma_u} 1\Pi_u^4 1\Pi_{g+}\,|\,]$$
$$+ c_2 [\,|\,(\text{core})2\sigma_u^2\, 1\Pi_{u+}^2\, 1\Pi_{u-}\, \overline{5\sigma_g}\,|$$
$$-|\,(\text{core})\,2\sigma_u^2 1\Pi_{u+}^2 \overline{1\Pi}_{u-}\, 5\sigma_g|\,] \,. \qquad (28)$$

This form of the resonant state wavefunction complicates the evaluation of the Hamiltonian matrix elements, since the $5\sigma_g$ is not necessarily orthogonal to the $k\sigma_g$ continuum. In this case additional overlap matrix elements are necessary. The partial-wave expansion parameters in the bound-continuum and continuum-continuum matrix elements in Equations (6) and (7), as well as the overlap integrals, were truncated at ℓ=11. This is a sufficient number of partial waves, since an increase to ℓ=30 changes these matrix elements by less than 5%. The energy integrals were performed from k = 0 → 2.8 a.u.[48], with mesh points taken at Δk = 0.1 a.u. intervals[49] up to k = 0.8 a.u. and Δk = 0.2 a.u. from 0.8 a.u. → 2.8 a.u. This was to provide a finer mesh in the resonance region.

Autoionization

Photoionization leading to the $X^2\Pi_u$ state of $C_2H_2^+$ produces photoelectrons in the $k\sigma_g$, $k\pi_g$, and $k\delta_g$ electronic continuum. The $^1\Pi_u(2\sigma_u \rightarrow 1\pi_g)$ state autoionizes into the $k\sigma_g$ and $k\delta_g$ partial channels, while the $^1\Sigma_u^+ (1\pi_u^3\ k\pi_g)$ continuum is non-interacting with this excited state. The $k\pi_g$ continuum orbitals in these studies were obtained in the FCHF approximation,[2] using the singlet-coupled $^1\Sigma_u^+ (1\pi_u^3\ k\pi_g)$ potential, and hence correlation effects have been neglected in this partial channel. As discussed previously,[33] correlation effects are expected to strongly influence this $1\pi_u \rightarrow k\pi_g$ channel. The position of the $1\pi_u^3\ 1\pi_g$ state is particularly critical in the description of this background $k\pi_g$ continuum. At the Hartree-Fock level of approximation, using the singlet-coupled potential, this state appears above threshold and causes the broad shape resonant-like structure observed in these calculations. Inclusion of correlation should affect the position of the $1\pi_u \rightarrow 1\pi_g$ transition and therefore modify the near threshold behavior of the $1\pi_u^3 k\pi_g$ partial channel. This is in marked disagreement with the predictions of Levine and Soven,[18] where the $1\pi_u \rightarrow k\pi_g$ oscillator strength is pushed into the continuum only upon correlating the wavefunction. In addition to these correlation effects, this partial

channel may also be influenced by the possible autoionizing $3\sigma_g \rightarrow n\sigma_u$ state;[32,46] however, this transition is weaker[31] ($f \approx 0.15$) than the $2\sigma_u \rightarrow 1\pi_g$ excitation ($f_{IVO}=0.8$, $f_{\text{singles CI}}=0.43$) and has not been included in these initial studies.

The total photoionization cross sections in the length and velocity forms are presented in Figure 3 and are compared to the FCHF results. The dramatic effect of the $^1\Pi_u$ ($2\sigma_u \rightarrow 1\pi_g$) autoionizing state on these cross sections is apparent, producing a sharp dip followed by a pronounced peak. The large differences between the length and velocity cross sections reflect the importance of additional electron correlation effects in the initial and final state wavefunctions.

In Figure 4 we compare our total fixed-nuclei cross sections in the length form to the TDLDA results.[18] Several major differences between the two sets of calculations are apparent. A significant portion of our total cross section results from the broad $1\pi_u^3\, k\pi_g$ ($\sim$24Mb) background, whereas this component is much weaker (<5Mb) in the TDLDA calculations. Secondly, the width of the TDLDA autoionizing state is much narrower than the present calculations indicate, and the flattened structure we observe directly above threshold appears as a sharp decrease in the previous calculations.[18] Lastly, the autoionizing state appears more intense in the present study than in the TDLDA results, although

it is difficult to directly compare these results, because the use of a model exchange potential and because insufficient details of the calculation are given in Reference 18.

In Figure 4 we also compare the calculated photoionization cross sections to the vibrationally unresolved experimental data of References 30 and 31. These data are normalized to our results including autoionization at 24eV. Due to the large difference between the length and velocity results and the uncertainty in the absolute magnitude of the second peak[50] we have also normalized this data to our velocity results as shown in Figure 5. Clearly an absolute measurement of the peak cross section would be helpful in elucidating the features observed in these cross sections.

Figures 4 and 5 illustrate that the use of the single-configuration IVO representation for the resonant state overestimates the maximum cross section and width of the autoionization feature. These results are consistent with the large oscillator strength calculated with this IVO wavefunction. Correlating the resonant wavefunction will modify both the dipole transition moment, from the ground state to the autoionizing state, and the Hamiltonian matrix elements governing the decay of this discrete state. To estimate the effect on the cross sections of correlating the resonant state, we have employed the simple two-state, single excitation CI wavefunction,

Equation (28), discussed in the previous section. In these preliminary CI studies the maximum in the cross section is reduced by nearly 15%. However, potentially important configurations, e.g., two electron excitations, have been neglected in both the resonant and in the ground-state wavefunctions and are necessary in order to determine definitely the importance of correlation on these resonant photoionization cross sections. In addition, the shape and magnitude of the lower feature is quite different from the observed structure. These discrepancies probably result from the correlation effects absent in the present calculations for the $1\pi_u^3\, k\pi_g$ channel as discussed above.

The present calculations also neglect the variation of the transition dipole and Hamiltonian interaction matrix elements with internuclear distance. As in our study of H_2, the autoionizing structure may be quite sensitive to the nuclear geometry, making the averaging of the cross section over the ground vibrational state an important effect. The valence $^1\Pi_u$ $(2\sigma_u \rightarrow 1\pi_g)$ wavefunction is expected to be particularly sensitive to the position of the nuclei resulting in matrix elements, which vary rapidly with internuclear distance. Therefore, in addition to correlation studies of the initial and resonant states, the dependence of this resonant structure on internuclear separation should be investigated.

As illustrated in Figures 4 and 5 the ratio of the experimental cross section at the minimum, about 21Mb at 14.5eV, to the maximum, about 62Mb at 15.5eV, is 0.3. Since the $k\sigma_g$ and $k\delta_g$ partial channels have nearly zero cross section near this minimum, the magnitude of this ratio indicates the presence of a substantial $k\pi_g$ background. This is in agreement with the broad $k\pi_g$ cross sections obtained with the singlet-coupled potential.

The individual $k\sigma_g$ and $k\delta_g$ partial channel photoionization cross sections are reported in Figures 6 and 7, respectively. As expected, the interaction of the resonance with the broad intense $k\delta_g$ background is stronger than in the weaker $k\sigma_g$ partial channel. In these figures we also compare our results to the TDLDA model-exchange calculations of Levine and Soven,[18] finding only qualitative agreement. Note that in Figure 5 the TDLDA $k\delta_g$ cross sections peak at a much larger value than shown here since the maximum for this partial channel was not reported in Reference 18.

An interesting feature of these calculations is the direct coupling of the $k\sigma_g$ and $k\delta_g$ partial channels. The wavefunctions for these states, given in Equations (21) and (22), are coupled by matrix elements of the form $\langle k\sigma_g\, 1\pi_{u+}|\ 1/r_{12}\ |1\pi_{u-}\ k\delta_g\rangle$. The role this interaction plays on the $k\sigma_g$ and $k\delta_g$ partial channel cross sections is also shown in Figures 6 and 7. These calculations are referred to as direct mixing and differ from the results

including autoionization in their neglect of the discrete state. In general, the effect of this mixing is quite small and results mainly in the reduction of the $1\pi_u \rightarrow k\sigma_g$ cross section at lower energies. The $k\delta_g$ continuum changes less than the weaker $k\sigma_g$ partial channel, resulting in a total cross section that is largely unaffected by this interaction. However, as shown below, the effect of this interaction is more significant for the asymmetry parameters, where interference between the partial channel amplitudes occurs. The present results are similar to those seen in studies of Ne^{31} $2p^{-1}$ and Ar^{42} $3p^{-1}$ photoionization, where the cross sections were obtained with and without coupling of the np → ks and np → kd channels. The results of these atomic studies indicate that the mixing of these channels is quite weak, with the ks continuua primarily modified at low kinetic energy and the total cross section essentialy unchanged.

In Figure 8 we compare the fixed-nuclei photoelectron asymmetry parameters, including the autoionizing state, to those calculated in the FCHF approximation. The differences between the dipole length and velocity forms are less dramatic than in the total cross sections. The pronounced effect of the autoionizing state is apparent as a sharp dip near 15eV. In Figure 9 we compare our results to the TDLDA[18] asymmetry parameters as well as to the vibrationally resolved (ν_2=0) measurements of Parr et al.[5] and Keller et al.[6] obtained

using synchrotron radiation. Our calculated minimum occurs at a slightly higher energy and appears sharper than the vibrationally resolved measurements. This may result from using the IVO wavefunction for the resonant state or neglecting the dependence of the electronic matrix elements on the internuclear distance (R).

The effect of the direct continuum-continuum mixing on the photoelectron asymmetry parameters is displayed in Figure 10. For comparison the β parameters calculated with autoionization and in the FCHF approximation are replotted in this figure along with the data of Parr et al.[5] and Keller et al.[6] Inclusion of this mixing improves the agreement between the calculated and experimental results outside the resonance region (>18 eV).

IV. CONCLUSIONS

We have developed and applied an ab initio method for studying autoionizing resonances in molecular photoionization. Using a Hartree-Fock single-particle basis set for the zeroth order continuua, the photoionization cross sections and asymmetry parameters for the ionization of H_2 and the $1\pi_u$ level of C_2H_2 have been obtained in the fixed-nuclei approximation. These

results have been compared to the available experimental data and previous theoretical treatments for molecular autoionization.

Our results for the autoionization of the $^1\Sigma_u^+$ ($1\sigma_u\ 2\sigma_g$) state in H_2 are in good agreement with previous ab initio calculations and indicate the reliability of our approach. Due to the lack of experimental data through the resonance region, as well as the neglect of vibrational state averaging of the theoretical results, meaningful comparisons between these theoretical and measured photoionization cross sections are not possible.

Of primary interest in the present studies of molecular autoionization is the structure observed in the production of the $X^2\Pi_u$ state of $C_2H_2^+$. Comparison of the present calculations with the available experimental data indicates that the minimum and second maximum in the photoionization cross sections and the dip in the asymmetry parameters are accounted for by using a single-configuration wavefunction for the representation of the resonant $^1\Pi_u$ ($2\sigma_u \rightarrow 1\pi_g$) state. However, further correlation effects in the ground and resonant states, as well as vibrational state averaging, are expected to modify dramatically the calculated resonance features. Additional correlation in the $1\pi_u^3\ k\pi_g$ partial channel, such as excitations of the type $1\pi_u \rightarrow 1\pi_g$ and the possible $^1\Sigma_u^+$ ($3\sigma_g \rightarrow n\sigma_u$) autoionizing state, are expected to change the shape and position of the lower kinetic energy

maximum. In addition to these refinements in the present *ab initio* theoretical treatment for C_2H_2, absolute measurements for the photoionization cross sections in the resonance region would be very helpful in clarifying the observed structure. Lastly, comparisons of our results to the previous model-exchange calculations illustrate the advantage of using accurate Hartree-Fock single-particle orbitals for the non-resonant background continuum. Our results for the $1\pi_u \rightarrow k\pi_g$ continuum indicate a non-zero contribution from this partial channel, in agreement with the normalization independent experimental ratio of the minimum to the second maximum cross section suggesting a substantial $k\pi_g$ background.

APPENDIX I.

NORMALIZATION OF THE INCOMING-WAVE AND PRINCIPAL-VALUE WAVEFUNCTIONS

We write the static-exchange Hamiltonian for electron-molecular ion collisions as $H = H_0 + V$, where H_0 contains the long-range Coulomb potential and V is the short-range component of the static exchange potential. The Hartree-Fock single-particle functions, $|\Psi_{\vec{k}}^{(-)}>$, are solutions of the Lippmann-Schwinger equation:

$$|\Psi_{\vec{k}}^{(-)}> = |\phi_{\vec{k}}^{(-)}> + G^{c(-)} V |\Psi_{\vec{k}}^{(-)}> , \qquad (1)$$

where $|\phi_{\vec{k}}^{(-)}>$ is the pure Coulomb scattering wavefunction, and $G^{c(-)}$ is the Coulomb Greens functions. As a result of the integral equations[30] the normalization of $|\Psi_{\vec{k}}^{(-)}>$ is determined by the normalization of $|\Psi_{k}^{(-)}>$. This can be shown with the use of the following identities:[30]

$$V |\Psi_{\vec{k}}^{(-)}> = T |\phi_{\vec{k}}^{(-)}> \qquad (2)$$

$$G^{c(-)} T = G^{(-)} V , \qquad (3)$$

where $G^{(-)}$ is the full Green's function associated with the total Hamiltonian. Equation (1), using the above identities, can be rewritten

$$|\Psi^{(-)}_{\vec{k}}> = |\phi^{(-)}_{\vec{k}}> + G^{(-)}V|\phi^{(-)}_{\vec{k}}> = |\phi^{(-)}_{\vec{k}}> + \frac{1}{E-H-i\varepsilon}\,V|\phi^{(-)}_{\vec{k}}>, \quad (4)$$

and the adjoint is given by

$$<\Psi^{(-)}_{\vec{k}}| = <\phi^{(-)}_{\vec{k}}| + <\phi^{(-)}_{\vec{k}}|\,V\,\frac{1}{E-H+i\varepsilon}\,. \quad (5)$$

The normalization is then

$$<\Psi^{(-)}_{\vec{k}'}|\Psi^{(-)}_{\vec{k}}> = <\phi^{(-)}_{\vec{k}'}|\Psi^{(-)}_{\vec{k}}> + <\phi^{(-)}_{\vec{k}'}|V\,\frac{1}{E'-E+i\varepsilon}\,|\Psi^{(-)}_{\vec{k}}>\,. \quad (6)$$

Using Equation (1) we find the first term on the right-hand side of Equation (6) to be

$$<\phi^{(-)}_{\vec{k}'}|\Psi^{(-)}_{\vec{k}}> = <\phi^{(-)}_{\vec{k}'}|\phi^{(-)}_{\vec{k}}> + <\phi^{(-)}_{\vec{k}'}|\,\frac{1}{E-E'-i\varepsilon}\,V\,|\Psi^{(-)}_{\vec{k}}> \quad (7)$$

or:

$$<\phi^{(-)}_{\vec{k}'}|\Psi^{(-)}_{\vec{k}}> = <\phi^{(-)}_{\vec{k}'}|\phi^{(-)}_{\vec{k}}> - <\phi^{(-)}_{\vec{k}'}|\,\frac{1}{E'-E+i\varepsilon}\,V\,|\Psi^{(-)}_{\vec{k}}>\,. \quad (8)$$

Inserting Equation (8) into Equation (6), we obtain

$$<\Psi^{(-)}_{\vec{k}'}|\Psi^{(-)}_{\vec{k}}> = <\phi^{(-)}_{\vec{k}'}|\phi^{(-)}_{\vec{k}}> = \delta^3(\vec{k}'-\vec{k})\,. \quad (9)$$

The partial-wave amplitudes obey a similar relationship,

$$<\Psi^{(-)}_{k'\ell'm'} \mid \Psi^{(-)}_{k\ell m}> = <\phi^{(-)}_{k'\ell'm'} \mid \phi^{(-)}_{k\ell m}> = \frac{\delta(k-k')}{k^2}\,\delta_{\ell\ell'}\,\delta_{mm'}. \tag{10}$$

The relationship between the $|\Psi^{(-)}_{k\ell m}>$ and $|\Psi^{(p)}_{k\ell m}>$ functions is

$$|\Psi^{(P)}_{k\ell m}> \;\; \sum_{\bar{\ell}} \; |\Psi_{k\bar{\ell}m}> \; (1 + iK^{\circ})_{\bar{\ell}\ell}\,, \tag{11}$$

so that

$$<\Psi^{(P)}_{k'\ell'm'} \mid \Psi^{(P)}_{k\ell m}> = \sum_{\bar{\ell},\bar{\bar{\ell}}} (1-iK^{\circ})_{\ell',\bar{\ell}} \; <\Psi^{(-)}_{k'\bar{\ell}m} \mid \Psi^{(-)}_{k\bar{\bar{\ell}}m}> (1+iK^{\circ})_{\bar{\bar{\ell}}\ell} \tag{12}$$

$$= \frac{\delta(k'-k)}{k^2} \sum_{\bar{\ell}} (1-iK^{\circ})_{\ell'\bar{\ell}} \; (1+iK^{\circ})_{\bar{\ell}\ell} \tag{13}$$

$$= \frac{\delta(k'-k)}{k^2} \left[\underset{\sim}{(1+(K^{\circ})^2}\right]_{\ell'\ell} \; . \tag{14}$$

REFERENCES

1. J. L. Dehmer, D. Dill, and A. C. Parr, in Photophysics and Photochemistry in the Vacuum Ultraviolet, edited by S. McGlynn, G. Findley, and R. Huebner (D. Reidel, Dordrecht, Holland, 1984), pp. 341-408.
2. R. R. Lucchese, K. Takatsuka, and V. McKoy, Phys. Reports 131, 147 (1986).
3. V. McKoy, T. A. Carlson, and R. R. Lucchese, J. Phys. Chem. 88, 3188 (1984).
4. B. E. Cole, D. L. Ederer, R. Stockbauer, K. Codling, A. C. Parr, J. B. West, E. D. Poliakoff, and J. L. Dehmer, J. Chem. Phys. 72, 6308 (1980).
5. A. C. Parr, D. L. Ederer, J. B. West, D. M. P. Holland, and J. L. Dehmer, J. Chem. Phys. 76, 4349 (1982).
6. P. R. Keller, D. Mehaffy, J. W. Taylor, F. A. Grimm, and T. A. Carlson, J. Electron Spectrosc. 27, 223 (1982).
7. J. Kreile, A. Schweig, and W. Thiel, Chem. Phys. Lett. 79, 547 (1981).
8. R. Stockbauer, B. E. Cole, D. L. Ederer, J. B. West, A. C. Parr, and J. L. Dehmer, Phys. Rev. Lett. 43, 757 (1979).

9. J. B. West, A. C. Parr, B. E. Cole, D. L. Ederer, R. Stockbauer, and J. L. Dehmer, J. Phys. B 13, L105 (1980).

10. U. Fano, Phys. Rev. 124, 1866 (1961).

11. See, for example: Anthony F. Starace, in Handbuch der Physik, edited by S. Flügge (Springer-Verlag, New York, 1982), pp. 1-113.

12. A. Giusti-Suzor and H. Lefebvre-Brion, Chem. Phys. Lett. 76, 132 (1980).

13. G. Raseev and H. Le Rouzo, Phys. Rev. A 27, 268 (1983).

14. M. Raoult, H. Le Rouzo, G. Raseev, and H. Lefebvre-Brion, J. Phys. B 16, 4601 (1983).

15. L. A. Collins and B. I. Schneider, Phys. Rev. A, 29, 1695 (1984).

16. G. Raseev, J. Phys. B 18, 423 (1985).

17. J. A. Stephens and D. Dill, Phys. Rev. A 31, 1968 (1985).

18. Z. H. Levine and P. Soven, Phys. Rev. Lett. 50, 2074 (1983).

19. P. L. Altick and E. Neal Moore, Phys. Rev. 147, 59 (1966).

20. U. Fano and F. Prats, J. Natl. Acad. Sci. India 33, Part IV, 553 (1964).

21. W. J. Hunt and W. A. Goddard III, Chem. Phys. Lett. 24, 464 (1974).

22. H. Takagi and H. Nakamura, Phys. Rev. A 27, 691 (1983).

23. K. Kirby, S. Guberman, and A. Dalgarno, J. Chem. Phys. 70, 4635 (1979).

24. L. A. Collins and B. I. Schneider, Phys. Rev. A. 27, 101 (1983).

25. K. Kirby, T. Uzer, A. C. Allison, and A. Dalgarno, J. Chem. Phys. 75, 2820 (1981).

26. A. Hazi, in Electron-Molecule and Photon-Molecule Collisions, edited by T. Rescigno, V. McKoy and B. Schneider (Plenum, New York, 1979), p. 281.

27. H. Feshbach, Ann. Phys. 19, 287 (1962).

28. J. A. R. Samson and R. B. Cairns, J. Am. Opt. Soc. 55, 1035 (1965).

29. G. V. Marr, R. M. Holmes, and K. Codling, J. Phys. B 13, 283 (1980).

30. R. Unwin, I. Khan, N. V. Richardson, A. M. Bradshaw, L. Cederbaum, and W. Domke, Chem. Phys. Lett. 77, 242 (1981).

31. P. W. Langhoff, B. V. McKoy, R. Unwin, and A. M. Bradshaw, Chem. Phys. Lett. 83, 270 (1981).

32. L. E. Machado, E. P. Leal, G. Csarak, B. V. McKoy, and P. W. Langhoff, J. Electron Spectrosc. 25, 1 (1982).

33. D. Lynch, M. T. Lee, R. R. Lucchese, and V. McKoy, J. Chem. Phys. 80, 1907 (1984).

34. Wavefunctions without a superscript will be assumed to be principal-value functions.

35. Frederick H. Mies, Phys. Rev. 175, 164 (1968).

36. U. Fano and J. W. Cooper, Rev. Mod. Phys. 40, 441 (1968).

37. A. F. Starace, Phys. Rev. A 2, 118 (1970).

38. R. G. Newton, Scattering Theory of Waves and Particles (Springer-Verlag, New York, 1982), p. 182.

39. R. J. W. Henry and Lester Lipsky, Phys. Rev. 153, 51 (1967).

40. Alternately, the principal-value functions can be transformed prior to the calculation.

41. For convenience we have defined $V_{n,\sigma E} \equiv \frac{V_{n,\sigma E}}{E}$ and $\bar{V}_{nn} \equiv E_n/E$.

42. In actual calculations this equation is solved as it proved to be more convenient computationally.

43. P. L. Altick and A. E. Glassgold, Phys. Rev. 133, A632 (1964).

44. John C. Tully, R. Stephen Berry, and Bryan J. Dalton, Phys. Rev. 176, 95 (1968).

45. See, for example: R. R. Lucchese, G. Raseev, and V. McKoy, Phys. Rev. A 25, 2572 (1982).

46. T. Hayaishi, S. Iwata, M. Sasanuma, E. Ishiguro, Y. Morioka, Y. Iida, and M. Nakamura, J. Phys. B 15, 79 (1982).

47. D. W. Turner, C. Baker, A. D. Baker, and C. B. Brundle, Molecular Photoelectron Spectroscopy (Wiley, New York, 1970).

48. The high energy cut-off was chosen such that extending the energy integrals would not change the cross sections in the 12.0-16.0 eV energy range by more than 0.1 Mb.

49. The $\Delta k = 0.1$ mesh step size has been used in atomic studies. See, for example: References 19, 35, and P. L. Altick, Phys. Rev. 169, 71 (1968).

50. Estimates range from 37 Mb at 15 eV by P. Metzger and G. R. Cook, J. Chem. Phys. 41, 642 (1964) to nearly 60 Mb at 15 eV by W. C. Walker and G. L. Weissler, J. Chem. Phys. 23, 1547 (1955) and R. I. Schoen, J. Chem. Phys. 37, 2032 (1962).

Table I. Cartesian Gaussian Basis Set for H_2.

Type of function	Exponent
S	48.4479
S	7.28346
S	1.65139
S	0.462470
S	0.145885
S	0.04029
S	0.0065
P	1.5
P	0.5
P	0.16
P	0.060715
P	0.02224

Table II. Scattering Basis Set

Type of function for the scattering symmetry[a]			
Σ_u	Π_u	Function Center	Exponent
S	x	Nuclei	2.0,0.63,0.2
Z	xz	Nuclei	2.0,0.63,0.2
ℓ=1,3	ℓ=1,3	Origin	0.63

[a]The functions at the origin are spherical Gaussian functions while those at the nuclei are Cartesian Gaussian functions. These ae defined in Reference 43.

Table III. Characteristics of the $^1\Sigma_u$ ($1\sigma_u 2\sigma_g$) State of H_2 at R=1.4 a.u.

	Excitation Energy (eV)	Dipole Transition Moment (a.u.)	Width (eV)
Present Results	30.07	0.0820	0.45
Kirby et al.	30.7[a]	0.0882[a]	0.29[b]
Raseev[c,h]	31.03[g]	--	0.38
Hazi[d]	30.71	--	0.40
Tagaki and Nakamura[e,h]	30.99[g]	--	0.41
Collins and Schneider[f]	--	--	0.44

a) Reference 23.
b) Reference 25.
c) Reference 16.
d) Reference 26.
e) Reference 22.
f) Reference 24.
g) Obtained from data in References 16 and 22 assuming an ionization potential of 16.4eV.
h) Calculated excitation energy includes the energy shift resulting from the interaction of the resonant state with the background continuum.

FIGURE CAPTIONS

1. Photoionization cross sections for the $X^2\Sigma_g^+$ state of H_2^+: present results including autoionization, ——— (length) and — — — (velocity); present FCHF results, — — —(length) and - - - - - (velocity); results of Ref. 16, — - - —; x, experimental results of Samson and Cairns (Ref. 28).
2. Photoelectron asymmetry parameters for the $X^2\Sigma_g^+$ state of H_2^+: present results including autoionization, ———(length) and —-—- (velocity); present FCHF results, — — —(length); results of Ref. 16, ------; x, experimental results of Marr et al. (Ref. 29).
3. Photoionization cross sections for the $X^2\Pi_u$ state of $C_2H_2^+$: present results including autoionization, ———(length) and ------- (velocity); present FCHF results, — —— (length) and — — — (velocity).
4. Photoionization cross sections for the $X^2\Pi_u$ state of $C_2H_2^+$: present results including autoionization, ——— (length); TDLDA results, - -✱- - (taken from Ref. 18, no attempt has been made to interpolate the data points); x, experimental results (Ref. 31) normalized to the present dipole length cross sections at 24eV.

5. Photoionization cross sections for $X^2\Pi_u$ state of $C_2H_2^+$: present results including autoionization, ------ (velocity); x, experimental data (Ref. 31) normalized to the present dipole velocity cross sections at 24eV.

6. The $1\pi_u \rightarrow k\sigma_g$ partial channel photoionization cross sections for $C_2H_2^+$ in the dipole length form: present results including autoionization, ———; present FCHF results, -------; present direct mixed results, — - — - — ; TDLDA results, —✕— (Ref. 18, no attempt has been made to interpolate the data points).

7. The $1\pi_u \rightarrow k\delta_g$ partial channel photoionization cross sections for $C_2H_2^+$, see figure caption 6 for labels.

8. Photoelectron asymmetry parameters for the $X^2\Pi_u$ state of $C_2H_2^+$: present results including autoionization, ▬▬▬ (length) and ------- (velocity); present FCHF results, — - — (length) and ——— (velocity).

9. Photoelectron asymmetry parameters for the $X^2\Pi_u$ state of $C_2H_2^+$: present results including autoionization (length), ———; present FCHF results (length), -------; TDLDA results, —✱— (Ref. 18); x, experimental data of Parr et al. (Ref. 5); Δ, experimental data of Keller et al. (Ref. 6).

10. Photoelectron asymmetry parameters for the $X^2\Pi_u$ state of $C_2H_2^+$: present results including autoionization (length), ———; present FCHF results (length), — - — -; present direct mixing results (length), - - - -; x, experimental data of Parr et al. (Ref. 5); Δ, experimental data of Keller et al. (Ref. 6).

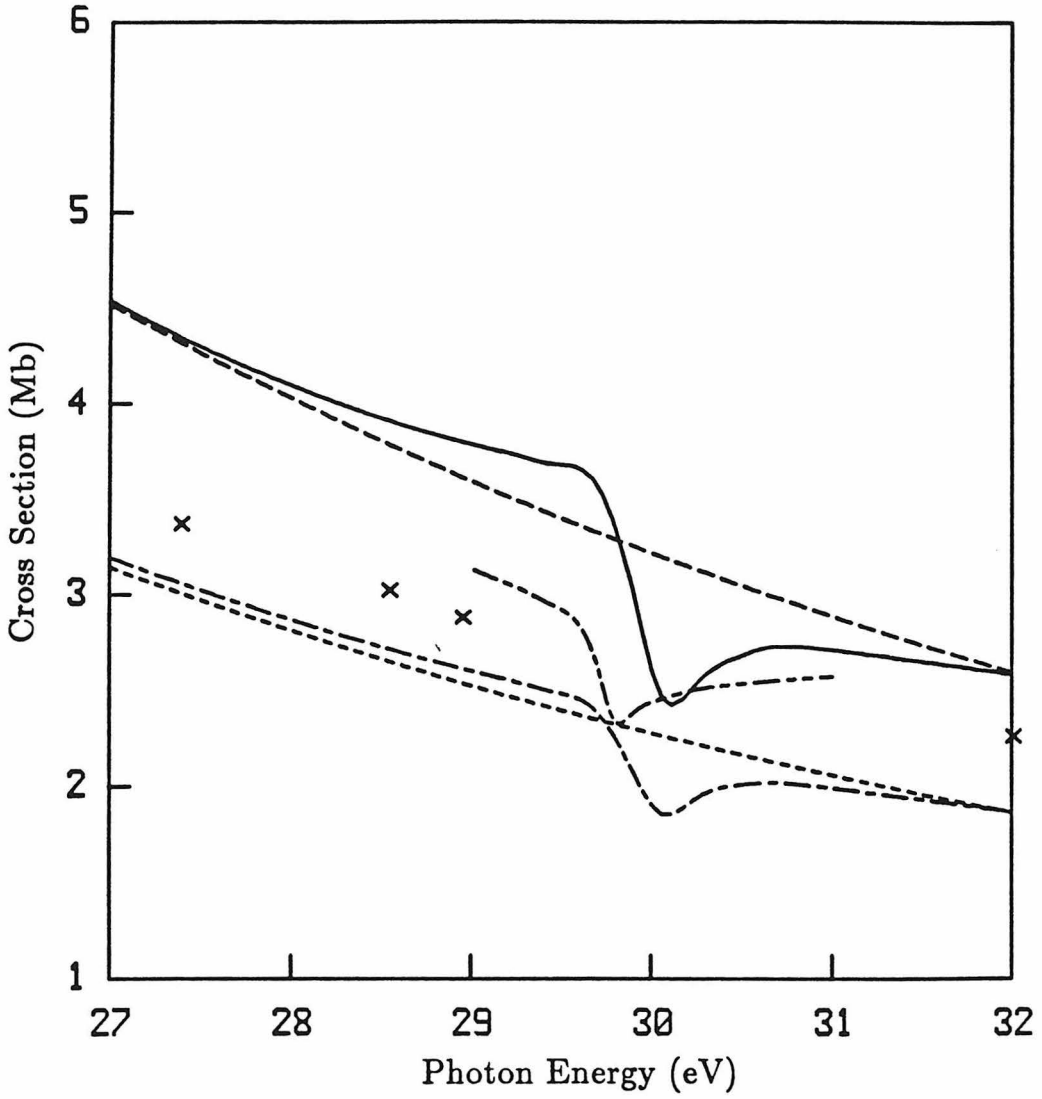

Figure 1

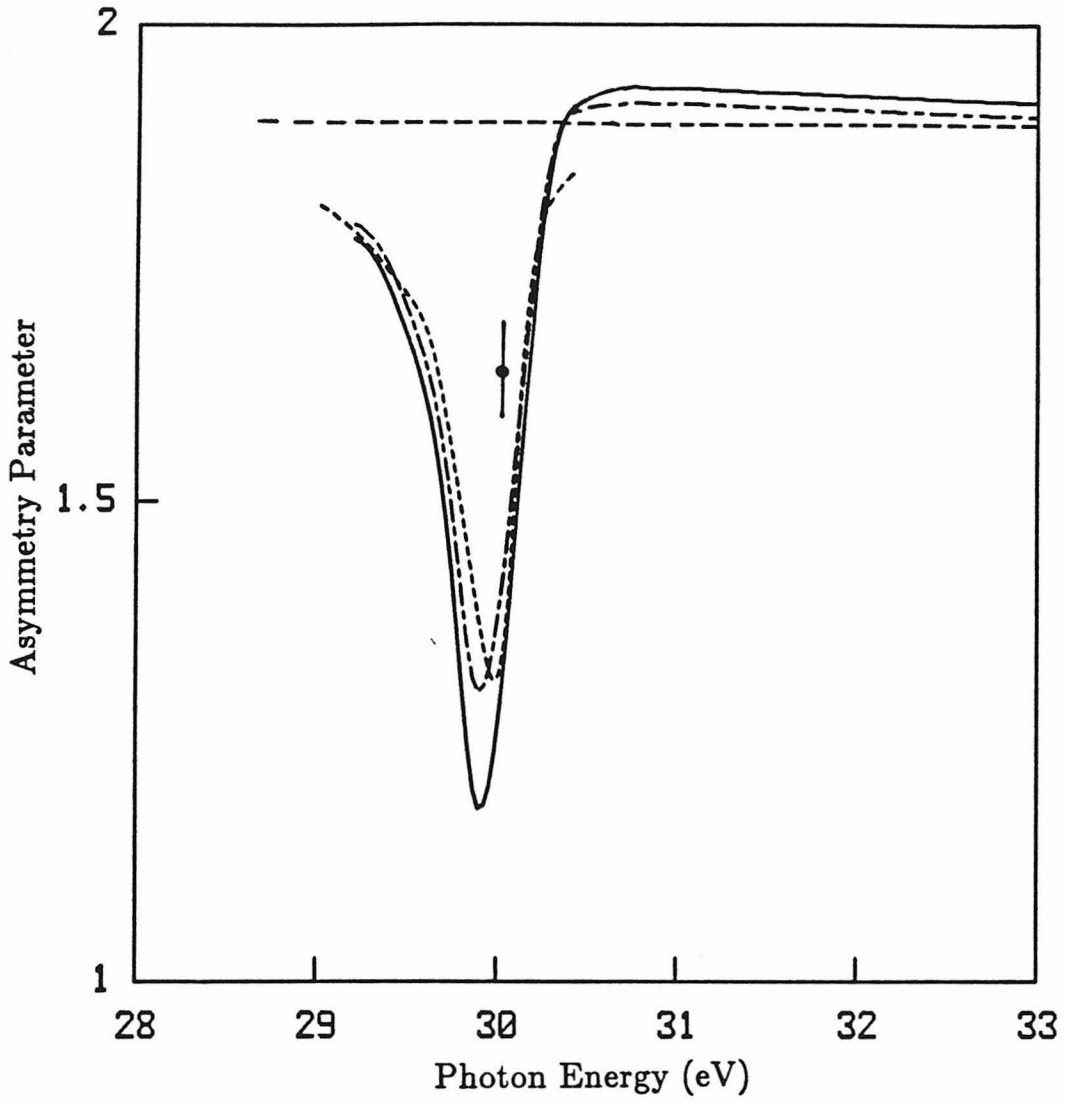

Figure 2

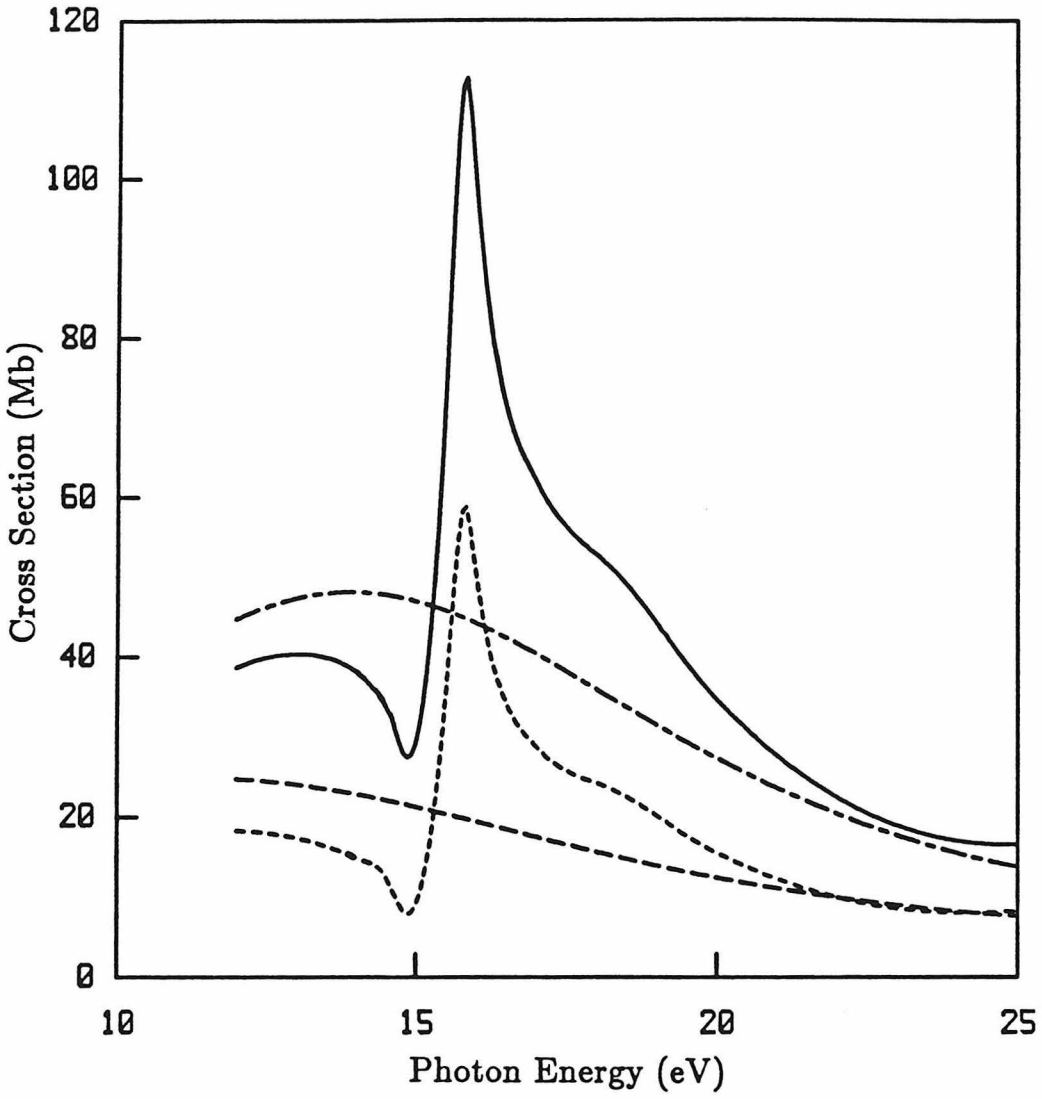
120
100
80
60
40
20
0
Cross Section (Mb)
10
15
20
25
Photon Energy (eV)

Figure 3

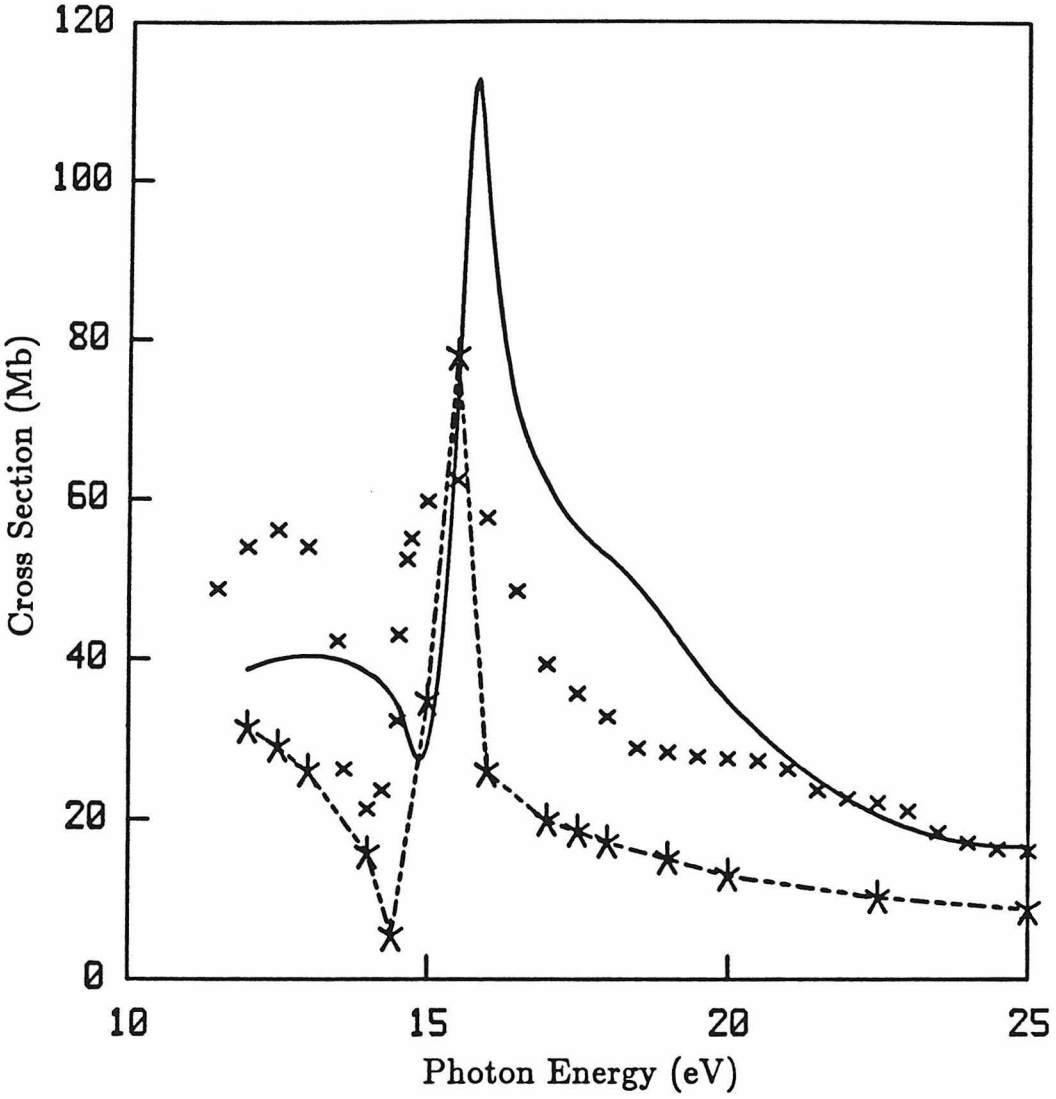
120
100
80
60
40
20
0
Cross Section (Mb)
10
15
20
25
Photon Energy (eV)

Figure 4

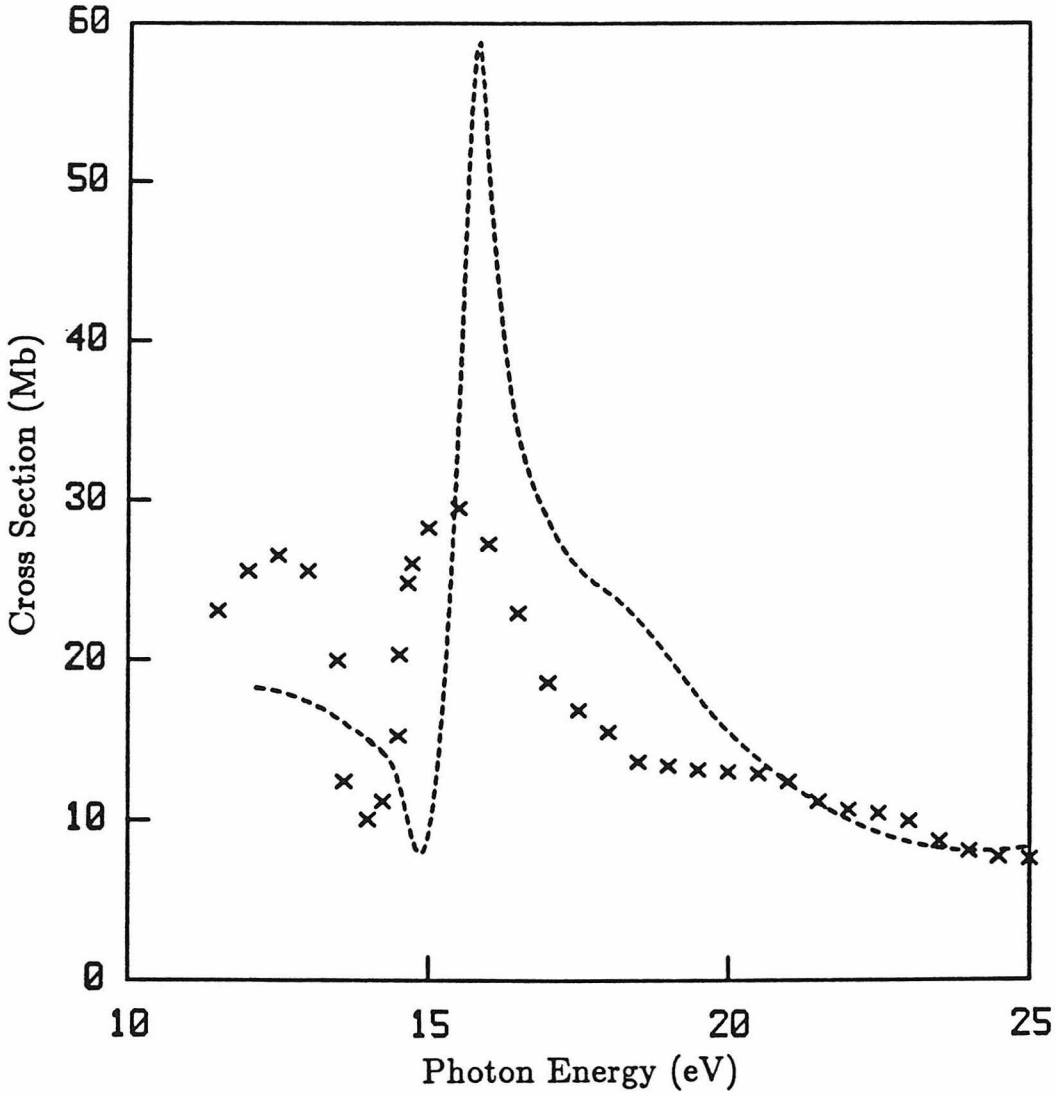

Figure 5

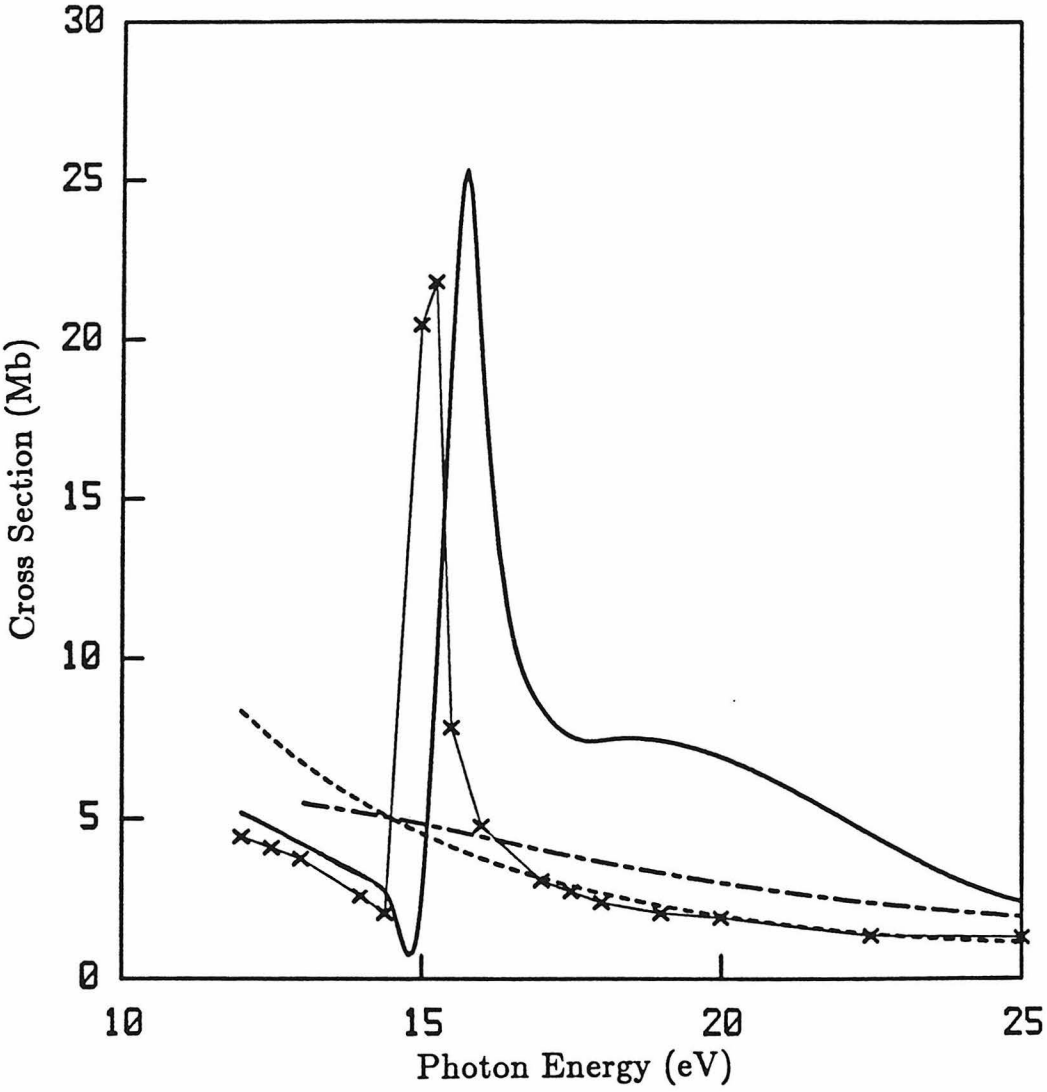

Figure 6

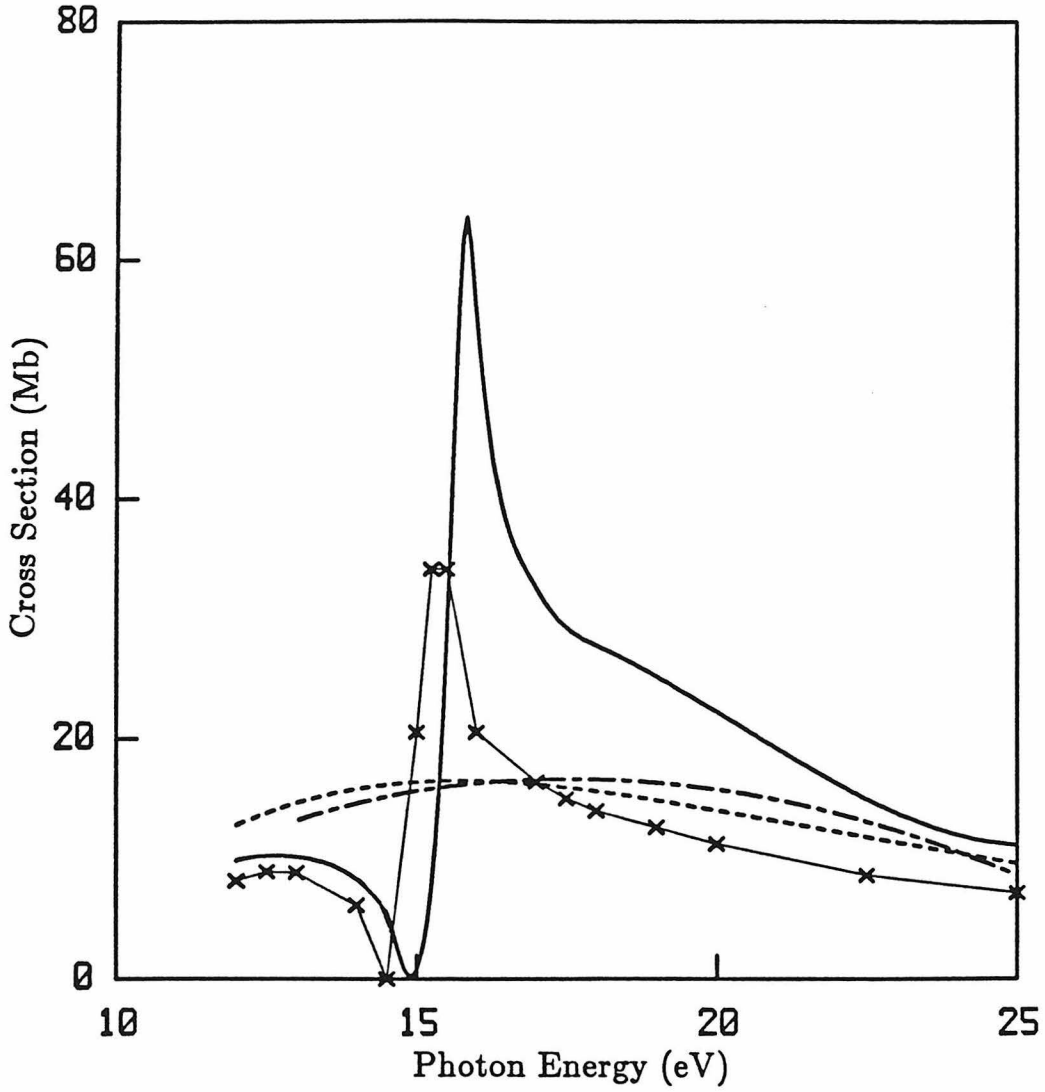

Figure 7

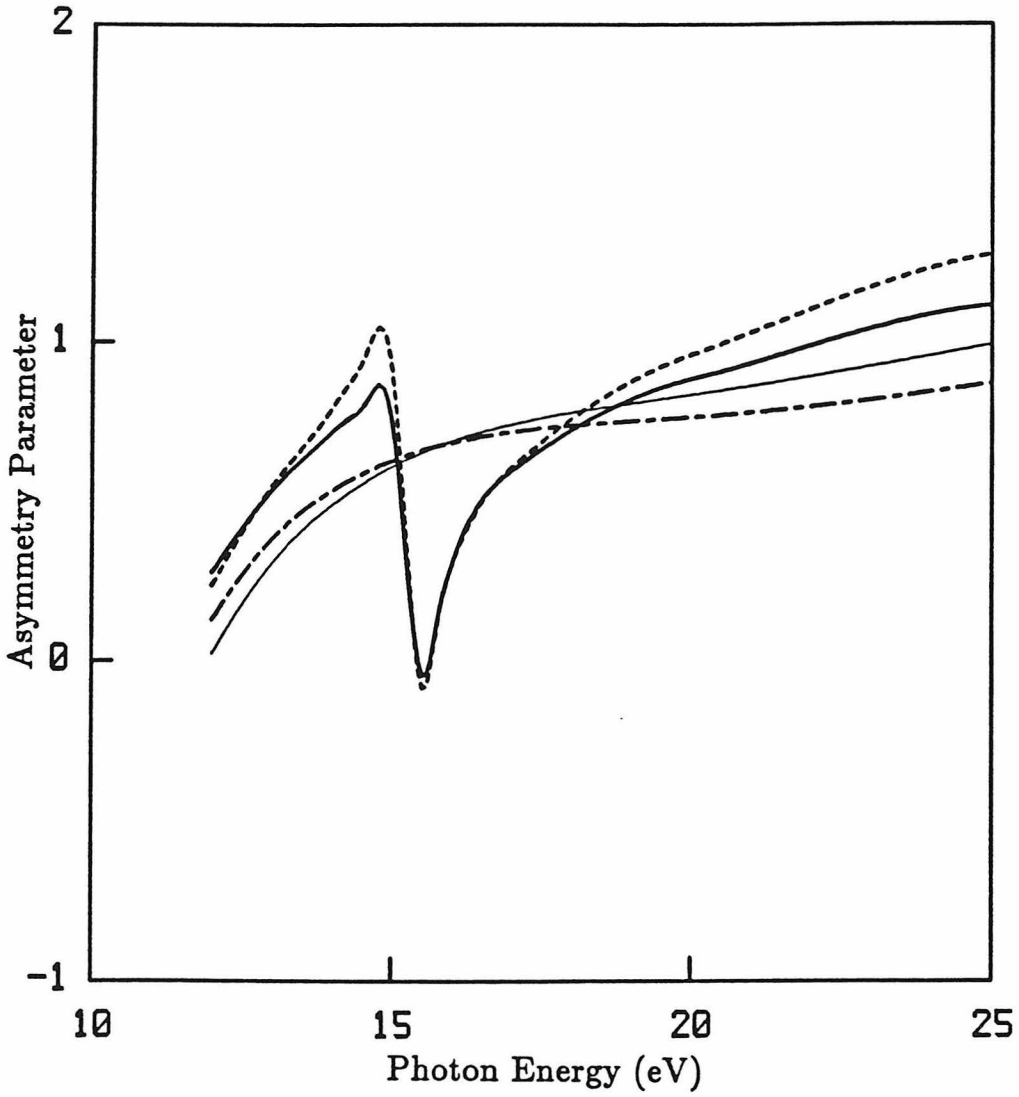

Figure 8

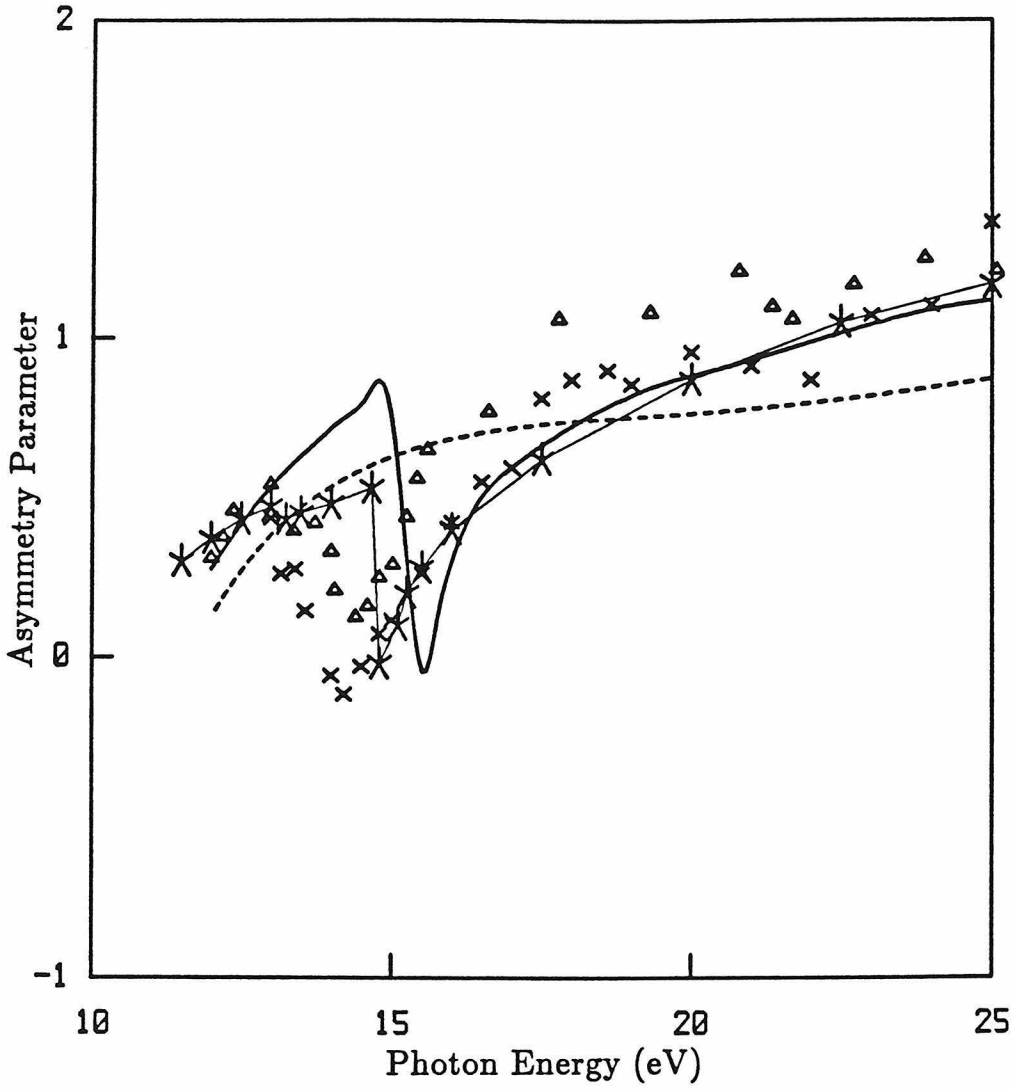

Figure 9

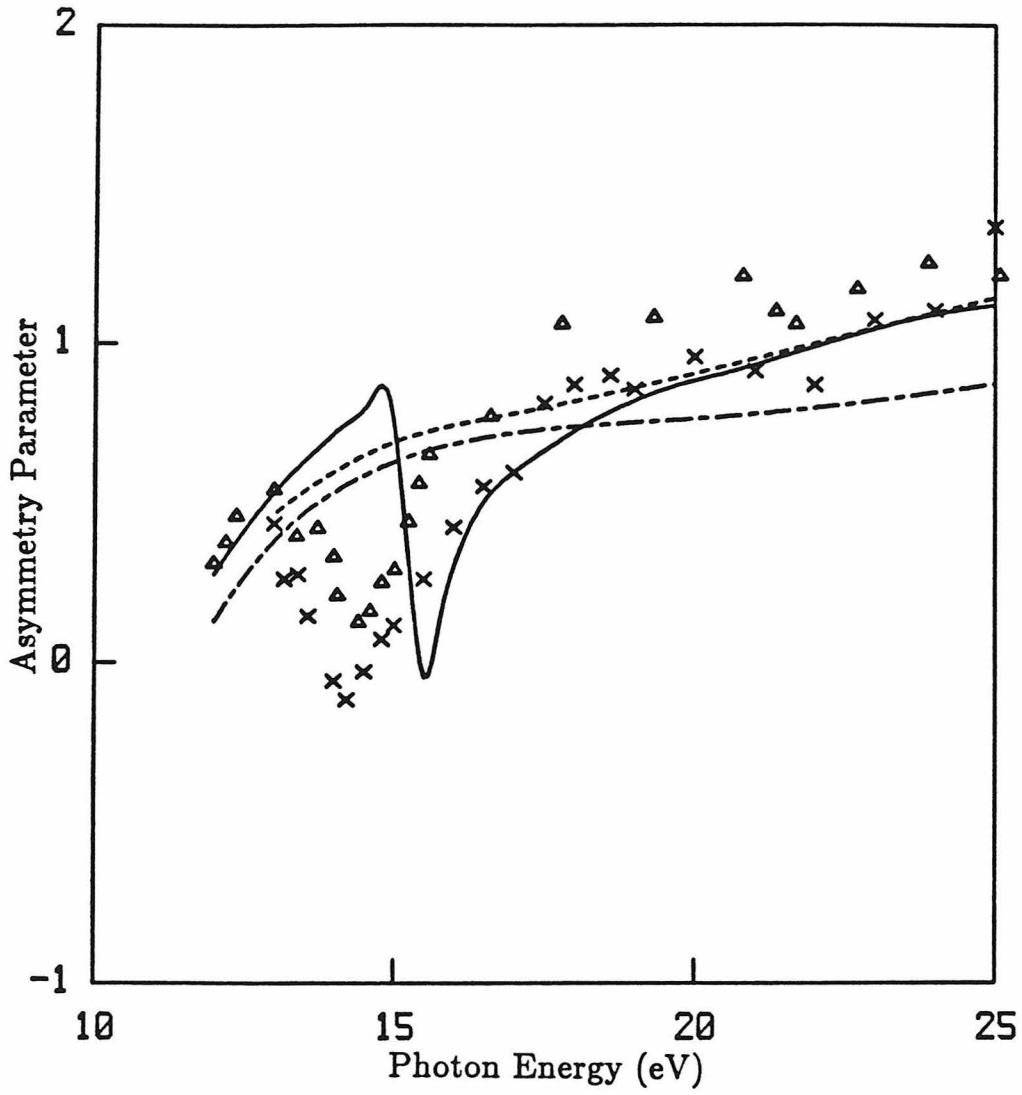

Figure 10

CHAPTER IV

RESONANT ENHANCED MULTIPHOTON IONIZATION PROCESSES

SECTION A

THREE-PHOTON RESONANT FOUR-PHOTON IONIZATION OF H_2 VIA THE $C^1\Pi_u$ STATE

I. INTRODUCTION

Resonant Enhanced Multiphoton Ionization (REMPI) is a powerful probe of electronically excited states. The high power lasers used in such studies not only provide high selectivity in energy (of the order of the laser bandwidth), but also make accessible via multiphoton absorption states that are single-photon forbidden by dipole selection rules. When combined with photoelectron energy analysis, REMPI allows us to focus very directly on the photoionization of the excited states and on the dynamics of multiphoton ionization. Recent experiments[1-12] on REMPI processes in diatomic molecules such as H_2, CO, NO, and N_2 have begun to reveal several interesting features. A theoretical understanding of these features is obviously needed.

Recently, Pratt et al.[12] analyzed the photoelectron energy spectrum resulting from a three-photon resonant four-photon ionization of H_2 via the $C^1\Pi_u$ state. This resonant state, Rydberg in character, overlaps in energy with the valence $B^1\Sigma_u^+$ state. The Π^+ component of this $C^1\Pi_u$ state interacts with the $B^1\Sigma_u^+$ state via the Rydberg-valence mixing while the Π^- component is unaffected. Pratt et al.[12] were able to select only the Π^- component of the $C^1\Pi_u$ state as the resonant intermediate state by tuning the laser frequency in resonance with the three-photon Q(1) transition line. This illustrates the tremendous selectivity achievable in REMPI processes. The kinetic energy of the photoelectrons ejected from this resonant intermediate was analyzed. These data provide the branching ratios for ionization out of a specific vibrational state v′ of the $C^1\Pi_u$ state into different vibrational states v^+ of the $X^2\Sigma_g^+$ state of H_2^+. These vibrational branching ratios deviated significantly from the appropriate Franck-Condon factors. Possible reasons for this behavior are the energy and the internuclear distance dependence of the electronic transition moment, autoionization and

perturbations with overlapping, allowed transitions. Autoionization and perturbations are less probable due to other considerations.[12] In this communication, we quantitatively assess the role of energy and R dependence of the electronic transition moment on the vibrational branching ratios in these (3+1) REMPI experiments of Pratt et al.,[12] i.e.,

$$H_2(X^1\Sigma_g^+\ v''\ ,\ J_0 = 1) \overset{3h\nu}{\rightarrow} H_2^*(C^1\Pi_u v',\ J_i{=}1) \overset{h\nu}{\rightarrow} H_2^+(X^2\Sigma_g^+,\ v^+) + e^- \ . \qquad (1)$$

Comparison with the measured branching ratios shows good agreement for vibrational branching ratios for $v' = 0$ and 1 excitations although differences exist between theory and experiment for $v' = 2$, 3 and 4 excitations.

II. THEORY

An analysis of REMPI cross-sections and the related angular distributions requires molecular parameters such as the transition moments and transtion frequencies and their incorporation into the dynamics equations. These steps are non-trivial even for the simplest of diatomic molecules, H_2, and is hence not surprising that very few theoretical calculations have been carried out for molecular REMPI processes.[13,14] Our framework for analyzing the dynamics has been presented elsewhere.[15] For the process in Eq.(1), the probability for ejection of an electron in the direction (θ,ϕ) with respect to the light polarization vector (linearly polarized light was used in the experiment of Ref. 12 and is assumed here) obeys

$$\frac{dP(\theta,\phi)}{dt} = \sum_{M_i M_i'} \Gamma_{M_i M_i'}(\theta,\phi)\ \rho_{i',i} \ . \qquad (2)$$

In this equation $\rho_{i',i}$ is the density matrix element $< J_i M_i' | \rho | J_i M_i >$ (all

indices other than J_i and M_i needed to describe a molecular state have been suppressed for clarity) and $\Gamma_{M_i M_i'}$ a generalized differential ionization rate. Detailed expressions for $\Gamma_{M_i M_i'}$ are given in Ref. 15 where it is also shown that in the absence of M_i mixing, ionization through each $|J_i M_i>$ forms an independent channel. Thus $\rho_{i',i}$ is proportional to $\delta_{M_i M_i'}$, and, therefore, for photoionization of the $C^1\Pi_u$ state excited from the ground state via a three-photon Q(1) transition (J_i=1), Eq.(2) reduces to

$$\frac{dP(\theta,\phi)}{dt} = \Gamma_{11}\,\rho_{11} + \Gamma_{00}\,\rho_{00} + \Gamma_{-1-1}\,\rho_{-1-1} \ . \tag{3}$$

$\Gamma_{M_i M_i'}$ can in turn be expanded in spherical harmonics[15] as

$$\Gamma_{M_i M_i'} = \sum_{L,M}^{L_{max}^{(\Gamma)}} \gamma_{LM;M_i M_i'}\, Y_{LM}(\theta,\phi) \tag{4}$$

where the coefficients $\gamma_{LM;M_i M_i'}$ depend on the bound-free radial matrix elements and scattering phase shifts. M=0 for M_i=M_i' and $\Gamma_{M_i M_i}$ and $P(\theta,\phi)$ in Eqs. (3) and (4), are independent of ϕ and consist of only Legendre polynomials. Furthermore, as the accessible partial waves (σ_g, π_g and δ_g) are all of the same g symmetry only even order Legendre polynomials up to $L_{max}^{(\Gamma)}$ = 4 (see Eq.(40) of Ref. 15) survive in Eq.(4). Thus

$$\Gamma_{M_i M_i} = \sum_{L=0,2,4} \gamma_{L0;M_i M_i}\, Y_{L0}(\theta,\phi) \ . \tag{5}$$

Equation (3) shows that, in addition to $\Gamma_{M_i M_i}$, $\rho_{ii}(i=0,\pm1)$ are needed to calculate the actual REMPI angular distributions. For the weak field excitation conditions of Ref. 12, ρ_{ii} is given by

$$\rho_{ii} \propto \sum_{M_0} \left| \sum_{\substack{|J_1M_1> \\ |J_2M_2>}} \frac{< J_iM_i|\vec{\mu}\cdot\vec{\varepsilon}|J_2M_2 >< J_2M_2|\vec{\mu}\cdot\vec{\varepsilon}|J_1M_1 >< J_1M_1|\vec{\mu}\cdot\vec{\varepsilon}|J_0M_0 >}{(E_{J_1}-E_{J_0}-h\nu)\ (E_{J_2}-E_{J_0}-2h\nu)} \right|^2 \qquad (6)$$

From the $X^1\Sigma_g^+$ initial state, the dipole allowed intermediate states, at the one-photon level, are of Σ_u^+ and Π_u symmetry while those at the two-photon level are of Σ_g^+, Π_g, and Δ_g symmetry. For an overall three-photon Q(1) transition, $J_0 = J_i = 1$ which restricts J_2 to be 1 or 2. Note that the two-photon transition from the $J_0 = 1$ level of the $X^1\Sigma_g^+$ state to the $J_2 = 0$ level of a Σ_g^+-type state is forbidden by parity selection rules. Moreover, the $J_2 = 0$ level does not exist in Π_g - and Δ_g-type states. Of these allowed states, the $J_2 = 2$ state contributes only if the electronic state is of Π_g or Δ_g type. In H_2, the lowest states of Π_g and Δ_g symmetry are, respectively, the $I^1\Pi_g$ and $J^1\Delta_g$ which lie at about 14-15 eV above the ground state.[16] The E, F $^1\Sigma_g^+$ state, on the other hand, is about 12 eV from the ground state. For photon energies $h\nu \sim 4$ eV the detuning $(E_{J_2} - E_{J_0} - 2h\nu)$ for these Π_g and Δ_g states is about 6 eV while that from the E, F $^1\Sigma_g^+$ state is about 4 eV. Hence, in the preliminary results presented here, we neglect the contribution to $\rho_{i',i}$ from states other than those of Σ_g^+ symmetry. Such contributions will be included in later studies. Neglecting this contribution eliminates the need to calculate and $\rho_{ii'}$, if one is interested only in the relative branching ratios. This comes about as $\rho_{00} = 0$ for Σ_g^+ states with $J_2 = 1$. Furthermore, $\rho_{11} = \rho_{-1-1}$, and $\Gamma_{11} = \Gamma_{-1-1}$ which, combined with Eq.(3) imply

$$\frac{dP(\theta)}{dt} \propto \Gamma_{11}(\theta) \ . \qquad (7)$$

In the absence of saturation as assumed here, the solution of the above equation is,

$$P(\theta) = (\text{constant})\cdot\Gamma_{11}(\theta) \ . \qquad (8)$$

Since we are only interested in relative contributions, we shall set the constant in the above equation to unity and use, hereafter,

$$P(\theta) = \Gamma_{11}(\theta) \ . \tag{9}$$

In the same spirit, we also ignore factors like the laser intensity in the expression for $\Gamma_{11}(\theta)$ (see Eq.(29) of Ref. 15).

Thus, to investigate relative branching ratios all we need to calculate is the differential cross section for ionization out of the $|J_i=1,M_i=1>$ state. From the analysis in Ref. 15, $\Gamma_{11}(\theta)$ depends on the bound-free electronic transition matrix elements of the type

$$\bar{r}_{fi}^{(\mu)} = \int \chi^*_{v^+}(R)\ \chi_{v'}(R)\ r_{fi}^{(\mu)}(k;R)\ dR \tag{10}$$

where

$$r_{fi}^{(\mu)}(k,R) = < \psi^{(e)}_{\gamma_f}(\{\vec{r}_i'\};R)|\sum_S r_S\ Y_{1\mu}(r_S')|\psi^{(e)}_{\gamma_i}(\{\vec{r}_i'\};R) > \tag{11}$$

denotes the transition moment for the i→f transition at a given internuclear separation R and electron momentum k. In our studies of the non-Franck-Condon effects on vibrational branching ratios, we adapt the following notation:

a) Franck-Condon (FC): $r_{fi}^{(\mu)}(k,R)$ inside the integral in Eq.(10) is replaced by its value at some $k^2 = k_0^2$ and $R = R_e$. $r_{fi}^{(\mu)}$ then simplifies to a product of $r_{fi}^{(\mu)}(k_0;R_e)$ and the Franck-Condon overlap between v^+ vibrational state of the ion and v' vibrational state of $C^1\Pi_u$ state.

b) non-Franck-Condon (non-FC): $\bar{r}_{fi}^{(\mu)}(k;R)$ in Eq.(10) is replaced by $r_{fi}^{(\mu)}(k_0;R)$ and is retained inside the R integral. These calculations assess the effect of the R dependence of the transition matrix element on the branching ratios.

c) Full: Here both the k and R dependences of $r_{fi}^{(\mu)}(k;R)$ are retained. For a fixed photon energy $h\nu$, selecting v' and v' fixes k^2 by the energy conservation equation (in atomic units)

$$E_{v'} + h\nu = E_{v'} + \frac{k^2}{2} . \tag{12}$$

These results include both the energy dependence as well as the R dependence of the cross sections and should, therefore, be most complete.

In our calculations the $C^1\Pi_u$ wave function was obtained using the improved virtual orbital (IVO) technique.[17] The energies of the $C^1\Pi_u$ state obtained this way are within 5% of the correct values.[16] The continuum wave functions for the photoelectron in σ_g, π_g and δ_g channels was calculated by solving the Hartree-Fock equations using the iterative Schwinger variational techniques.[18] $r_{fi}^{(\mu)}(k;R)$ was then calculated at R=1, 1.4,2,3 and 5 a.u. and for a range of k. Interpolation was performed in R and in k to obtain required $r_{fi}^{(\mu)}(k;R)$. For part (a) R_e = 1.4 a.u. The value of k_0^2 for parts (a) and (b) was determined from Eq.(12) with $v' = v^+$ and $h\nu$ taken from Ref. 12 for excitation to the Q(1) branch of $C^1\Pi_u(v')$ state. For part (c), the correct value of k is determined from Eq.(12) for each v^+. Finally, the vibrational wave functions $\chi_{v'}$ and χ_{v^+} were calculated using the finite element method of Malik et al.[19] with the potential curves of Sharp.[16]

III. RESULTS

In Fig. 1 we compare the branching ratios calculated at the various levels of approximation (a), (b) and (c) with the experimental results of Pratt et al.[12] As in the experimental data, we plot $P(\theta=0)$. The results are normalized such that the $v' = v^+$ peak in all three approximations and in the experiment is of unit height. (Note the break in the graph for $v' = v^+$ peak). As expected, the

$v' = v^+$ peak is dominant. This is due to the Rydberg character of the $C^1\Pi_u$ state which makes the potential surface for the $C^1\Pi_u$ state nearly identical to (but shifted in energy from) that of the $X^2\Sigma_g^+$ state of H_2^+. The theoretical branching ratios decrease rapidly for $v^+ \neq v'$. The results of approximations (a), (b), and (c) reveal an interesting feature: the branching ratios decrease for $v^+ < v'$ as the R and k dependences of $r_{fi}^{(\mu)}$ are included and increase for $v^+ > v'$ with these dependences included. The difference between 'non-Franck-Condon' and 'full' results is simply a reflection of the increasing of the cross section for decreasing energy which skews the branching ratios towards higher v^+ values. (Note that, since v^+ is increasing to the left, k increases to the right as indicated by Eq.(12).) The difference between Franck-Condon and non-Franck-Condon results arises from the particular R dependence of the photoionization cross section for the $C^1\Pi_u$ state. This difference is probably specific for the photoionization process under study and may be different for other states and molecules.

We now compare the results of our studies with the data of Pratt et al.[12] For $v' = 0$ and $v' = 1$ excitations, the agreement between theory and experiment seems quite good. For $v' = 2$ to 4 the experimental branching ratios for $v^+ \neq v'$ are much larger than the theoretical predictions. In particular, for $v' = 4$, the $v^+ = 3$, 5, and 6 experimental peaks are all of about equal height, while theory predicts the $v^+ = 3$ and 6 peaks to have 0.11 and 0.2 times the height of $v^+ = 5$ peak (which is $\sim$ 18% of $v^+ = 4$ peak). A similar descrepancy exists in the $v' = 3$ and $v' = 2$ excitation data as well. These differences may be due to autoionization, accidental resonances at the 3-photon excitation level, and the contribution of the Π_g and Δ_g states to the 3-photon excitation amplitude which are neglected in our present studies. Of these, autoionization seems to play no role as the results of Ref. 12 are insensitive to changes in photon frequency. To analyze the contribution of Π_g and Δ_g states to the excitation,

we have calculated Γ_{00} in Eq.(3) and observe that the branching ratios in $\Gamma_{00}(\theta=0)$ are very similar to those quoted here. Thus the inclusion of the $\Gamma_{00}\rho_{00}$ term in Eq.(3) will not significantly alter the relative branching ratios. The existence of accidental resonances with the P branch of some high vibrational level of the $B^1\Sigma_u^+$ state can also be ruled out for all v' states except v' = 3.[12] Another improvement in our calculations would be the inclusion of correlation effects. Such studies are currently underway.

In summary, we have presented ab initio calculations for vibrational branching ratios in (3+1) REMPI of H_2 via the $C^1\Pi_u$ state. Calculated ratios are in good agreement with recent experimental results[12] for excitation through lower vibrational states of the $C^1\Pi_u$ states. Differences do exist for excitation through higher vibrational levels. Further studies are needed to understand these differences.

Acknowledgments: The authors wish to thank R. J. Cave and V. K. Babamov for providing us with the finite element program used for calculating the vibrational wave functions. This research was supported by the National Science Foundation under Grant No. CHE-8218166. The research reported in this paper made use of the Dreyfus-NSF Theoretical Chemistry Computer which was funded through grants from the Camille & Henry Dreyfus Foundation, the National Science Foundation (Grant No. CHE-7820235), and the Sloan Fund of the California Institute of Technology.

References

1. J. C. Miller and R. N. Compton, J. Chem. Phys. 75, 22 (1981).
2. J. Kimman, P. Kruit and M. J. Van der Wiel, Chem. Phys. Lett. 88, 576 (1982).
3. M. G. White, M. Seaver, W. A. Chupka and S. D. Colson, Phys. Rev. Lett. 49, 28 (1982).
4. J. C. Miller and R. N. Compton, Chem. Phys. Lett. 93, 453 (1982).
5. S. T. Pratt, E. D. Poliakoff, P. M. Dehmer and J. L. Dehmer, J. Chem. Phys. 78, 65 (1983).
6. S. T. Pratt, P. M. Dehmer and J. L. Dehmer, J. Chem. Phys. 78, 4315 (1983).
7. S. T. Pratt, P. M. Dehmer and J. L. Dehmer, J. Chem. PHys. 79, 3234 (1983).
8. Y. Achiba, K. Sato, K. Schotabake and K. Kimura, J. Chem. Phys. 78, 5474 (1983).
9. M. G. White, W. A. Chupka, M. Seaver, A. Woodward and S. D. Colson, J. Chem. Phys. 80, 678 (1984).
10. S. T. Pratt, D. M. Dehmer and J. L. Dehmer, J. Chem. Phys. 80, 1706 (1984).
11. S. L. Anderson, G. D. Kubiak and R. N. Zare, Chem. Phys. Lett. 105, 22 (1984).
12. S. T. Pratt, P. M. Dehmer and J. L. Dehmer, Chem. Phys. Lett. 105, 28 (1984).
13. B. Ritchie, E. J. McGuire, J. M. Peek and C. W. Band, J. Chem. Phys. 77, 877 (1982); see also S. N. Dixit and V. McKoy, J. Chem. Phys. 80, 5867 (1984) for comments on this paper.
14. K. R. Dastidar and P. Lambropoulos, Chem. Phys. Lett. 93, 273 (1982), and Phys. Rev. A 29, 183 (1984).
15. S. N. Dixit and V. McKoy, J. Chem. Phys. - submitted for publication.
16. T. E. Sharp, Atomic Data 2, 119 (1971).
17. W. J. Hunt and W. A. Goddard III, Chem. Phys. Lett. 24, 464 (1974).
18. R. R. Lucchese, G. Raseev and V. McKoy, Phys. Rev. A 25, 2572 (1982).
19. D. J. Malik, J. Eccles and D. Secrest, J. Comp. Phys. 38, 157 (1980).

Figure Caption

Fig. 1: Vibrational branching ratios in (3+1) REMPI of H_2 via the $C^1\Pi_u$ state. v' denotes the vibrational state of $C^1\Pi_u$ state and v^+ that of the $X^2\Sigma_g^+$ state of the ion.

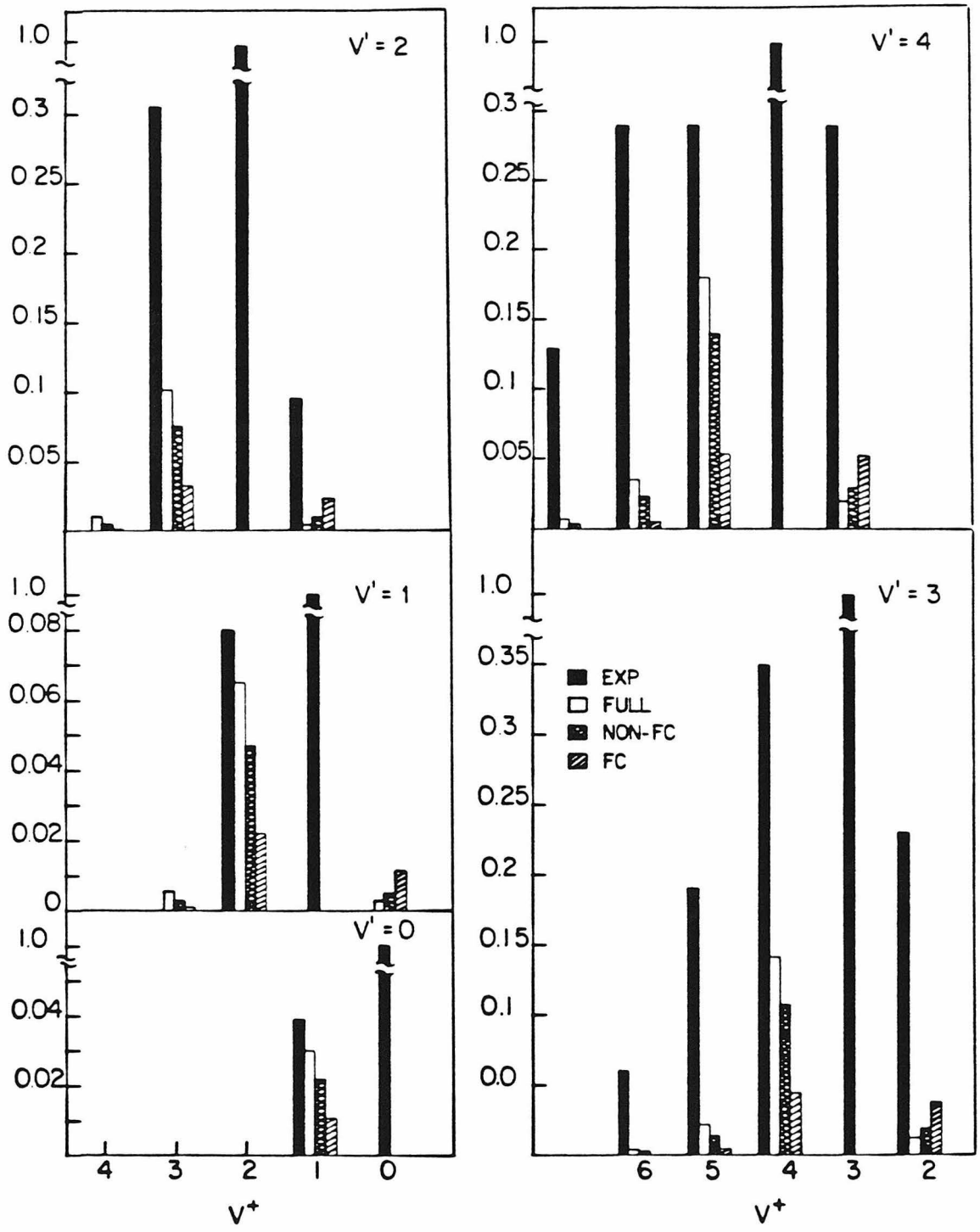

Figure 1

SECTION B

ROTATIONALLY RESOLVED (3+1) REMPI OF H_2 VIA THE $B^1\Sigma_u^+$ STATE

Introduction

Resonance enhanced multiphoton ionization (REMPI) techniques probe in detail the dynamics of multiphoton absorption and photoionization of excited molecular states. In (n+m) REMPI, an n-photon absorption to a resonant state is followed by an m-photon ionization out of this state. The high state-selectivity of this process, together with high resolution (10 - 30 meV) photoelectron energy analysis, provides detailed information about the resonant intermediate state as well as about the dynamics of photoionization. Within the last few years, this technique has been successfully employed to investigate the REMPI dynamics in a variety of diatomics such as H_2, N_2, NO and CO.[1-17]

With sufficient energy resolution, the photoelectron spectrum of some ions can be rotationally resolved in a REMPI process. This permits an analysis of the dynamics pertaining to the specific rovibrational state of the ion. Rotationally resolved photoelectron spectra in (1+1) REMPI of NO via the $A^2\Sigma^+$ state revealed anomolous branching ratios[12] which have been accounted for through detailed quantitative calculations[18]. In another experiment, Pratt, Dehmer and Dehmer[1] reported measurements of the photoelectron spectrum resulting from (3+1) REMPI of H_2 via the $B^1\Sigma_u^+$ state. With a photoelectron energy resolution of about 30 meV, the ionic vibrational states were clearly resolved while the rotational states were only partially resolved in the photoelectron spectrum. These results showed several interesting features such as a strong dependence of

the spectra on the intermediate rotational level and on the final ro-vibrational level and, the suppression of the N and T branches in the resonance excitation and the $\Delta J = \pm 3$ transitions in the photoionization. Due to the uncertainty in the transmission function of the electron spectrometer for slow electrons below 1 eV,[1] a detailed assessment of non-Franck-Condon effects in the vibrational branching ratios was not presented. Non-Franck-Condon vibrational intensities have been reported in related experiments on H_2 [2,3].

In this letter, we present results of quantitative calculations of ro-vibrational branching ratios resulting from the (3+1) REMPI process of ref. 1:

$$H_2: X^1\Sigma_g^+ (v_o = 0, J_o = 3) \xrightarrow{3h\nu} H_2^*: B^1\Sigma_u^+ (v_i = 7, J_i)$$
$$\xrightarrow{h\nu} H_2^+: X^2\Sigma_g^+ (v_+, J_+) + e^-.$$

Our results indicate that the photoelectron transition moments are more sensitive to the kinetic energy than to internuclear separation. In view of the preliminary nature of the experimental studies,[1] agreement with experiment is reasonable. The analysis of the dynamics reveals that the suppression of the $\Delta J = \pm 3$ ($\Delta J = J_+ - J_i$) peaks results from dynamic interference between the $d\sigma$ and $d\pi$ channels and does not imply the smallness of the d-wave or the $j_t = 3$ contribution.[1] With more accurate, calibrated measurements on this REMPI process underway, the results and analysis presented here should prove quite useful.

Theory

The theoretical analysis of the REMPI process of eq. (1) is similar to that of the (3+1) REMPI of H_2 via the $C^1\Pi_u$ state.[19,20] Here we give only those details which are pertinent to this specific process and refer to references 19 and 20 for further details. We shall assume that linearly polarized light of weak intensity excites the REMPI process. These assumptions imply that REMPI originating at a specific magnetic sublevel (J_0M_0) of the initial state forms an independent channel. In the absense of M-mixing interactions, the probability of ejection of an electron in the direction (θ,ϕ) with respect to the direction of polarization is given by[20]

$$\frac{dP(\theta,\phi)}{dt} = \sum_{M_i} \Gamma_{M_i,M_i}(\theta,\phi)\rho_{ii} \equiv \sum_{LM} \left(\sum_{M_i} \gamma_{LM;M_iM_i}\rho_{ii}\right) Y_{LM}(\theta,\phi) \qquad (2)$$

Under the weak field conditions, the population ρ_{ii} in the specific (J_iM_i) level of the resonant intermediate state is proportional to [20]

$$\rho_{ii} \propto \sum_{M_0} \left| \sum_{\substack{|J_1M_1>\\ |J_2M_2>}} \frac{<J_iM_i|\vec{\mu}\cdot\vec{\varepsilon}|J_2M_2><J_2M_2|\vec{\mu}\cdot\vec{\varepsilon}|J_1M_1><J_1M_1|\vec{\mu}\cdot\vec{\varepsilon}|J_0M_0>}{(E_2-E_0-2h\nu)\ (E_1-E_0-h\nu)} \right| \qquad (3)$$

The detailed expression for the ionization widths Γ_{ii} is given in ref. 20. The summation over the virtual intermediate states includes the complete

set of rotational-vibrational-electronic states. Selection rules imply that only states of $^1\Sigma_u^+$ and $^1\Pi_u$ symmetry contribute at the one-photon level ($|J_1M_1>$) while states of $^1\Sigma_g^+$ and $^1\Pi_g$ symmetry contribute at the two photon level ($|J_2M_2>$) in eq. (3). In the present studies we have truncated the sum over the electronic states by retaining the $B^1\Sigma_u^+$, $C^1\Pi_u$, E, $F^1\Sigma_g^+$ and $I^1\Pi_g$ states and keeping up to v = 9 in the vibrational manifolds of each of these states. The summation over rotational states was performed implicitly using closure relations.[21] Considering the off-resonance conditions at the single- and two-photon level, these approximations should give a reasonable estimate for the three-photon excitation probability in eq. (3).

The bound-bound transition moments were taken from Wolniewiez[22] and Wolniewiez and Dressler[23] except for the $B^1\Sigma_u^+$, $C^1\Pi_u \rightarrow I^1\Pi_g$ transition which were calculated using the improved virtual orbital (IVO) method.[24] The vibrational wave functions were generated with the accurate potential energy curves of Sharp.[25] The photoelectron continuum wave functions for the $k\sigma_g$ and $k\pi_g$ channels were obtained in the frozen-core Hartree-Fock approximation with the ground state $1\sigma_g$ orbital. The equations were solved by the iterative Schwinger variational method.[26] Finally the bound-free transition moments $< X^2\Sigma_g^+, k\sigma_g, k\pi_g | \vec{\mu}\cdot\vec{\epsilon} | B^1\Sigma_u^+ >$ for each R were calculated using the IVO wave function for the $B^1\Sigma_u^+$ state. While the energies of the $B^1\Sigma_u^+$ state in these IVO calculation are within 5-10% of the correct values, the B-X transition moments deviate from the accurate values[22] at large R. This behavior, also addressed by Jackson et al.[27] reflects the inadequacy of the single configuration wave functions at

large R. This behavior at larger R is not important for the ionic vibrational levels of interest here. The effects of electron correlations will be discussed in a later publication. The bound-free matrix elements were calculated at internuclear distances of R = 1., 1.4, 2., 3., 5., a.u. and photoelectron kinetic energies between 0.1 and 1 eV. These calculated values were further interpolated as required in studying the non-Franck-Condon matrix elements.[19]

A calculation of three-photon rotational line strengths using the procedure discussed above reveals that the N(3) and T(3) lines are smaller than the P(3) and R(3) lines by about two orders of magnitude. This fact is in agreement with the experimental observations of Pratt et al.[1] The suppression arises not only from the smallness of the angular momentum factors such as those discussed by Halpern et al,[21] but also because of destructive interference between various excitation pathways in eq. (3). Dynamical details such as this latter feature can become evident only through quantitative studies of these processes.

Results

In figure 1 we present the results of our calculations for ro-vibrational branching ratios for the REMPI process in eq.(1). The values in these plots are proportional to the probabilities of photoelectron ejection in the direction of light polarization ($P(\theta = 0, \phi = 0)$). Results are presented for both the P(3) and the R(3) excitations to the $B^1\Sigma_u^+$ state. For each ro-vibrational state of the ion three bars labelled 'Franck-Condon', 'non-Franck-Condon' and 'full' are shown. These approximations correspond, respectively, to (i) neglecting the energy and R dependence of the bound-free matrix elements, (ii) neglecting the energy dependence but retaining the R dependence, and, (iii) retaining both the energy and the R dependence of the photoionization matrix elements.[19] These results indicate that the branching ratios are much less sensitive to internuclear separation than to the kinetic energy dependence. The sensitivity of the branching ratios to photoelectron energy increases with higher ionic vibrational number as the cross-section increases rapidly with decreasing electron kinetic energy.

Our calculated Franck-Condon (FC) factors for $v_i = 7$ vibrational level of the $B^1\Sigma_u^+$ state to $v_+ = 0$-3 levels of the ion are, respectively, 0.00039, 0.0074, 0.045 and 0.105. These values differ from those given in ref. 1. We believe the differences arise from the use of a Morse potential by Pratt et al.[1] The vibrational wave functions in our calculations were generated numerically using accurate potential energy curves of Sharp.[25] Thus the present FC factors should be quite

reliable. The insensitivity of the branching ratios to the R dependence together with their reasonable agreement with the experimental data for the P(3) branch (Fig. 2) also supports the reliability of our FC factors.

Another interesting feature evident in the results of fig. 1 is that the ratios of $\Delta J = -1$ peak to $\Delta J = +1$ peak are nearly constant for different vibrational states of the ion. In addition, calculated values for the $\Delta J = \pm 3$ peaks are at least three orders of magnitude smaller than the $\Delta J = \pm 1$ values. We now give an analysis of these two features. At these low photoelectron energies only the s and d partial waves are important in the photoionization dynamics.[28] For ionization out of the $B\,^1\Sigma_u^+$ state leaving the ion in a $^2\Sigma_g^+$ state the selection rule[18] for rotational angular momentum transfer implies that $J_+ - J_i$ = odd, i.e., $\Delta J = \pm 1, \pm 3 \ldots$. This in turn restricts the values of momentum transfer j_t to 1 or 3. These features allow the bound-free transition matrix element (eq. (14) of ref. 20) to be written as

$$< \Psi_{\gamma_f J_+ M_+ o} \mid D_{\mu_\theta} \mid \Psi_{\gamma_i J_i M_i o} > = \sqrt{\frac{4\pi}{3}}\,(-1)^{M_+}\sqrt{(2J_i+1)\,(2J_+ + 1)}$$

$$\left[\begin{pmatrix} J_+ & J_i & 1 \\ 0 & 0 & 0 \end{pmatrix}\left\{\begin{pmatrix} J_+ & J_i & 1 \\ -M_+ & M_i & 0 \end{pmatrix} Y_{oo}(\hat{k})\; I_{s\sigma} + \sqrt{\frac{6}{5}}\begin{pmatrix} J_+ & J_i & 1 \\ -M_+ & M_i & m_t \end{pmatrix}\begin{pmatrix} 2 & 1 & 1 \\ -m & 0 & -m_t \end{pmatrix} Y_{2m}(\hat{k}) \right.\right.$$

$$\left.\left. \times \left(I_{d\sigma} + 3\, I_{d\pi}\right)\right\} - \sqrt{\frac{7}{5}}\begin{pmatrix} J_+ & J_i & 3 \\ 0 & 0 & 0 \end{pmatrix}\begin{pmatrix} J_+ & J_i & 3 \\ -M_+ & M_i & m_t \end{pmatrix}\begin{pmatrix} 2 & 1 & 3 \\ -m & 0 & -m_t \end{pmatrix} Y_{2m}(\hat{k})\left(\sqrt{3}\, I_{d\sigma} - 2 I_{d\pi}\right)\right] \qquad (4)$$

where

$$I_{\ell\lambda} = (-i)^{\ell}\, e^{i\eta_\ell}\, \overline{r_{fi}(\mu)}$$

denotes the complex dynamical coefficient for photoionization. The first term in eq. (4) corresponds to $j_t = 1$ and the second term to $j_t = 3$. For $\Delta J = \pm 3$, only the $j_t = 3$ term contributes in eq. (4). The suppression of $\Delta J = \pm 3$ transitions then implies that the second term in eq. (4) must be small. This could occur either because the angular momentum terms are small or because $(\sqrt{3}\ I_{d\sigma} - 2I_{d\pi})$ is small. One can easily show that the angular momentum coupling for $j_t = 1$ and 3 terms are comparable in magnitude. Thus the suppression of $\Delta J = \pm 3$ transitions implies that $(\sqrt{3}\ I_{d\sigma} - 2I_{d\pi})$ is small. This, however, does not mean that the d-wave itself is weak. Typical values for $I_{s\sigma}$, $I_{d\sigma}$ and $I_{d\pi}$ obtained via our calculations are $I_{s\sigma} = 0.113 + i\ 0.533$, $I_{d\sigma} = 2.254 + i\ 2.910$ and $I_{d\pi} = 1.888 + i\ 2.558$. These values indicate that the d-wave is in fact stronger than the s-wave but, $(\sqrt{3}\ I_{d\sigma} - 2I_{d\pi})$ is about two orders of magnitude smaller that $(I_{d\sigma} + \sqrt{3}\ I_{d\pi})$. Thus the suppression of the $\Delta J = \pm 3$ peaks in the REMPI process of eq. (1) is a result of the dynamic interference between the $d\sigma$ and $d\pi$ continuum channels. In other systems $I_{d\sigma}$ and $I_{d\pi}$ could have different magnitudes that could give rise to significant $\Delta J = \pm 3$ peaks.

In the direction of polarization ($\theta = 0$), eq. (4), after ignoring the $j_t = 3$ terms, simplifies to

$$< \Psi_{\gamma_f J_+ M_+ o} \mid D_{\mu_o} \mid \Psi_{\gamma_i J_i M_i o} > = (-1)^{M_i} \sqrt{(2J_i+1)(2J_+ +1)} \begin{pmatrix} J_+ & J_i & 1 \\ 0 & 0 & 0 \end{pmatrix} \begin{pmatrix} J_+ & J_i & 1 \\ -M_i & M_i & 0 \end{pmatrix}$$

$$\sqrt{\frac{1}{15}} \left[\sqrt{5}\ I_{s\sigma} + 2\ I_{d\sigma} + 2\sqrt{3}\ I_{d\pi} \right] \qquad (5)$$

where we have used the relationship $Y_{\ell m}(\theta=0) = \sqrt{\frac{2\ell+1}{4\pi}}\ \delta_{m,o}$. The above result implies that if $I_{s\sigma}$, $I_{d\sigma}$ and $I_{d\pi}$ are constants, the ratio of the $\Delta J = -1$ to $\Delta J = +1$ peak will be constant. Within the first two approximations

(Franck-Condon and non-Franck Condon) mentioned above, $I_{s\sigma}$, $I_{d\sigma}$ and $I_{d\pi}$ are independent of energy. Using the calculated ρ_{ii} (in arbitrary units, 464.14, 458.22, 424.84, 310.03 for $|M_i|$ = 0, 1, 2, 3 for R(3) excitation and 459.45, 453.52, 376.84 for $|M_i|$ = 0, 1, 2 for P(3) excitation) the ratios of the $\Delta J = -1$ peak to $\Delta J = 1$ peak are found to be 0.69 and 0.91 for $J_i = 2$ (P(3) line) and $J_i = 4$ (R(3) line) respectively. These ratios agree with the complete calculation. Deviations from these values in the case of 'full' bars reflects the energy dependence of the dynamical coefficients.

Finally, in Figure 2 we compare our 'full' calculations with the experimental data of Pratt et al.[1] We have arbitrarily normalized our results to the $v_+ = 2$, $J_+ = 3$ peak in the experimental results. The data agree reasonably well for the P(3) excitation while considerable discrepancy exists for the R(3) excitation. Since the transmission function of the analyzer used in Ref. 1 was not characterized below 1 eV kinetic energy and the data were presented in a raw form, these comparisons must be viewed as preliminary. The results of the ongoing, refined experiments,[29] when they become available, should help unravel the underlying dynamics here.

Conclusions

We have presented results for the ro-vibrational branching ratios resulting from a (3+1) REMPI of H_2 via the $B^1\Sigma_u^+$ state. These calculations indicate that the effects of non-Franck-Condon behavior are less pronounced here than in the (3+1) REMPI via the $C^1\Pi_u$ state.[19] The analysis of rotational branching ratios reveals that the suppression of $\Delta J = \pm 3$ peaks is a result of dynamic interference between $d\sigma$ and $d\pi$ ionization channels and does not necessarily imply the smallness of the d-wave or the $j_t = 3$ angular momentum coefficients. In contrast with the behavior seen in the experimental data for the R(3) excitation, our calculations show that $\Delta J = 1$ peak is higher than $\Delta J = -1$ peak for both the P(3) and the R(3) excitations. We have, in the present work, neglected the effects of saturation, electron correlation in the B state, and possible ro-vibrational autoionization in the continuum. The inclusion of the first two features is currently underway and the results will be published elsewhere. If the data from the refined experiments currently underway[29] still differs significantly from calculated results including effects of saturation and correlations, the role of autoionization will have to be considered.

Acknowledgments

One of us (S.N.D.) acknowledges helpful discussions with Dr. P. M. Dehmer. This research was supported by the National Science Foundation under Grant No. CHE-8218166.

References

1. S. T. Pratt, E. D. Poliakoff, P. M. Dehmer, and J. L. Dehmer, J. Chem. Phys. 78, 65 (1983).
2. S. T. Pratt, P. M. Dehmer, J. L. Dehmer, Chem. Phys. Lett. 105, 28 (1984).
3. S. L. Anderson, G. D. Kubiak, and R. N. Zare, Chem. Phys. Lett. 105 22 (1984).
4. S. T. Pratt, P. M. Dehmer, and J. L. Dehmer, J. Chem. Phys. 78, 4315 (1983); ibid. 79 3234 (1983).
5. G. Sha, X. Zhong, S. Zhao, and C. Zhang, Chem. Phys. Lett. 110, 405 (1984); ibid. 110, 410 (1984).
6. S. T. Pratt, P. M. Dehmer and J. L. Dehmer, J. Chem. Phys. 80, 1706 (1984); ibid. 81, 3444 (1984).
7. H. Zacharias, R. Schmiedl, and K. H. Welge, Appl. Phys. 21, 127 (1980).
8. J. C. Miller and R. N. Compton, J. Chem. Phys. 75, 22 (1981); Chem. Phys. Lett. 93, 453 (1982).
9. J. Kimman, P. Kruit, and M. J. Van der Wiel, Chem. Phys. Lett. 88, 576 (1982).
10. M. G. White, M. Seaver, W. A. Chupka, and S. D. Colson, Phys. Rev. Lett. 49, 28 (1982).
11. M. G. White, W. Chupka, M. Seaver, A. Woodward, and S. D. Colson, J. Chem. Phys. 80, 678 (1984).
12. W. G. Wilson, K. S. Viswanathan, E. Sekreta, and J. P. Reilly, J. Phys. Chem. 88, 672 (1984).
13. Y. Anazaki, T. Ebata, N. Mikami, and M. Ito, Chem. Phys. 89,101 (1984), and references therein.
14. L. Li, R. N. Porter, and P. M. Johnson, Phys. Rev. Lett. 53, 1336 (1984).

15. Y. Achiba, K. Sato, and K. Kimura, J. Chem. Phys. (to be published).

16. J. Kimman, M. Lavollee, and M. J. Van der Wiel, Chem. Phys. (to be published).

17. J. P. Booth, S. L. Bragg, and G. Hancock, Chem. Phys. Lett. 113, 509 (1985).

18. S. N. Dixit, D. L. Lynch, V. McKoy and W. Huo, Phys Rev. A 32, 1267 (1985).

19. S. N. Dixit, D. L. Lynch and V. McKoy, Phys. Rev. A 30, 3332 (1984).

20. S. N. Dixit and V. McKoy J. Chem. Phys. 82, 3546 (1985).

21. J. B. Halpern, H. Zacharias and R. Wallenstein J. Mol. Spect. 79, 1 (1980).

22. L. Wolniewicz, J. Chem. Phys. 51, 5002 (1969).

23. L. Wolniewicz and K. Dressler, J. Mol. Spect. 96, 195 (1982).

24. W. J. Hunt and W. A. Goddard III, Chem. Phys. Lett. 24, 464 (1974).

25. T. E. Sharp, Atomic Data 2, 119 (1971).

26. R. R. Lucchese, G. Raseev and V. McKoy, Phys. Rev. A 25, 2572 (1982).

27. M. Jackson, R. P. McEachran, M. Cohen, J. Phys. B 5 927 (1972).

28. Y. Itikawa, Chem. Phys. 37, 401 (1979), and references therein.

29. P. M. Dehmer, private communication.

Figure Captions

Figure 1. Theoretical ro-vibrational branching ratios for (3+1) REMPI of H_2 via the $B^1\Sigma_u^+$ v = 7 level. The numbers above the bars denote the ionic rotational state. The data has been normalized to the $v_+ = 2$, $J_+ = 3$ values.

Figure 2. Comparison of theoretical calculations ('Full' results from fig. 1) with the experimental data of ref. 1. Theoretical results are normalized to the $v_+ = 2$, $J_+ = 3$ experimental values.

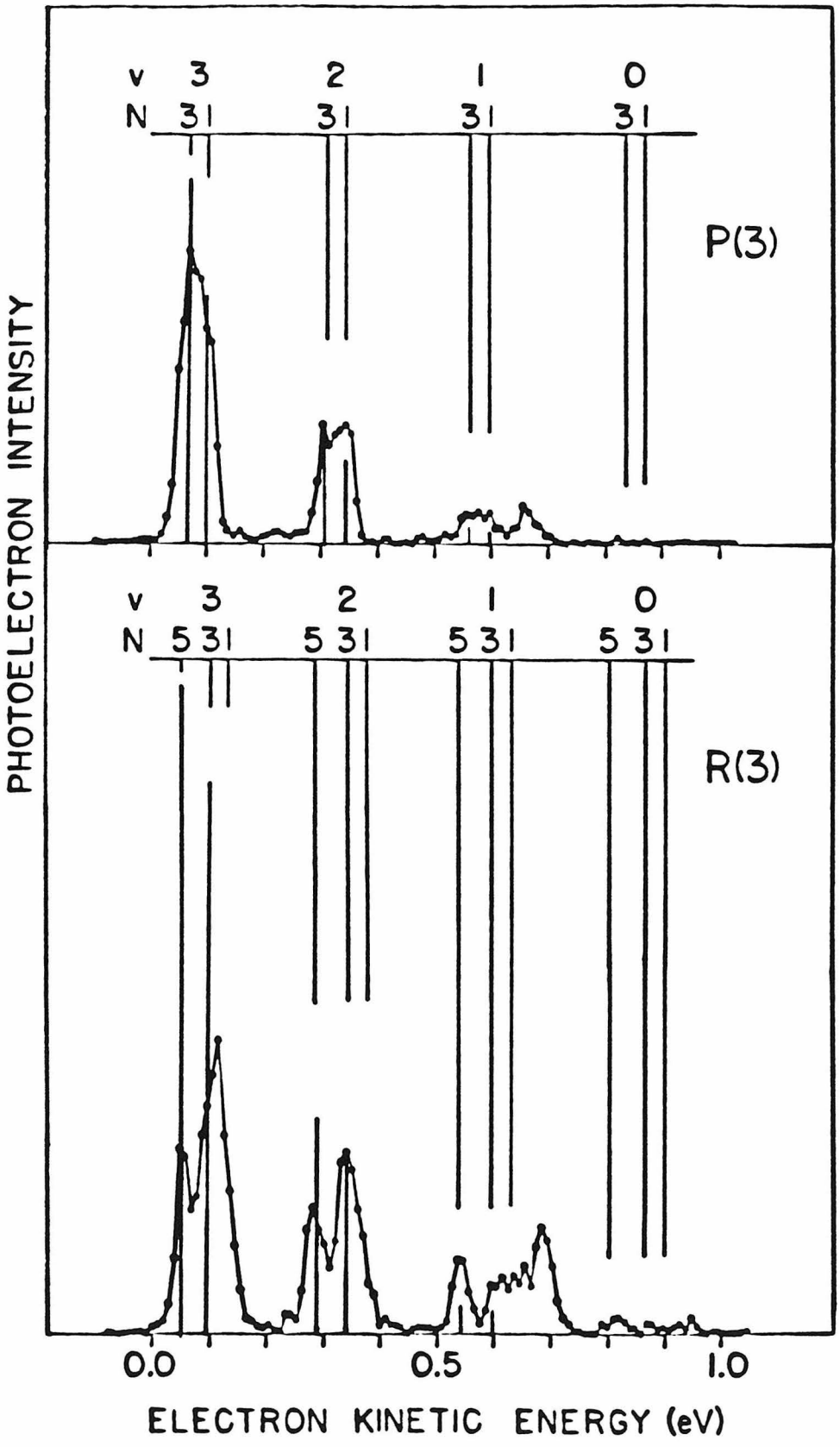
v 3 2 1 0
N 3 1 3 1 3 1 3 1
P(3)
v 3 2 1 0
N 5 3 1 5 3 1 5 3 1 5 3 1
R(3)
PHOTOELECTRON INTENSITY
0.0
0.5
1.0
ELECTRON KINETIC ENERGY (eV)

Figure 1

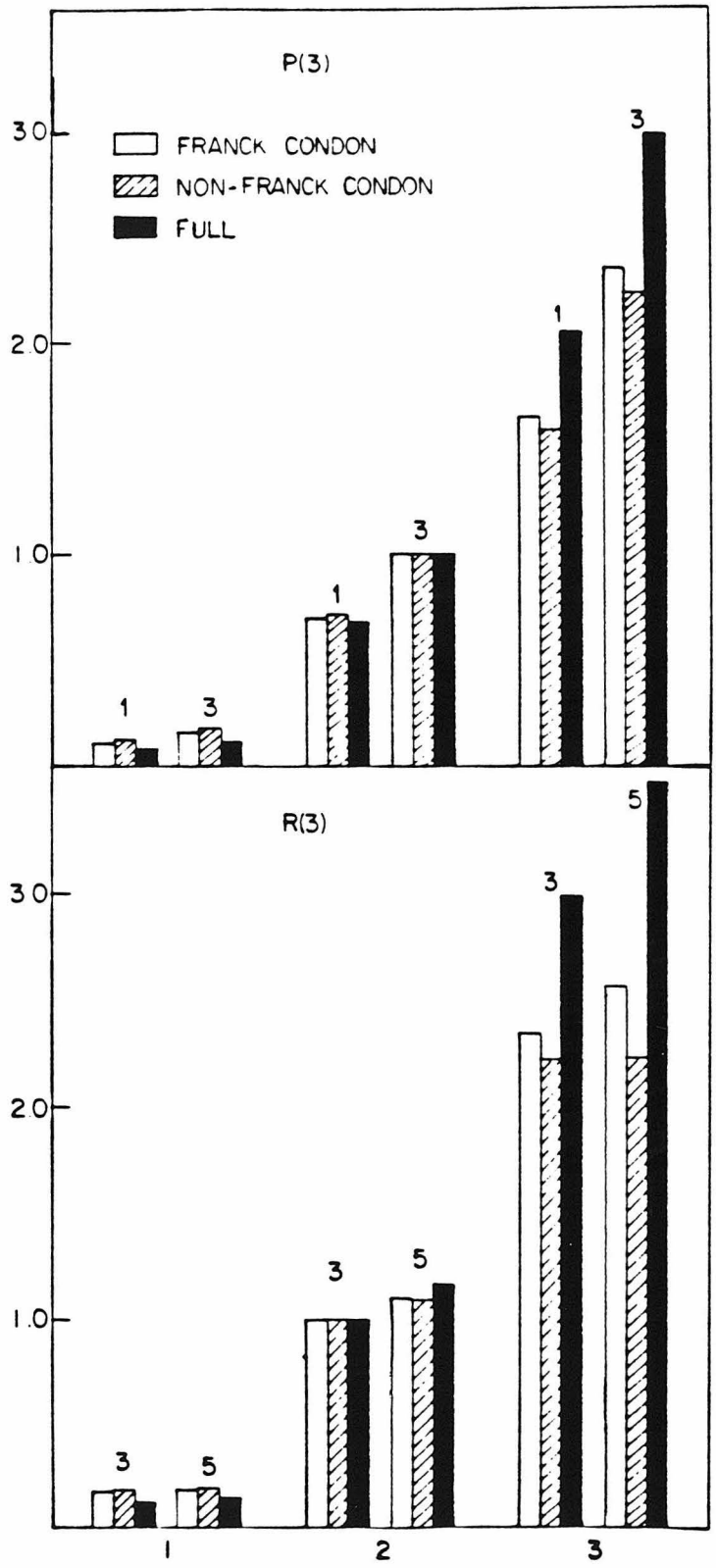
P(3)
FRANCK CONDON
NON-FRANCK CONDON
FULL
3.0
2.0
1.0
1
3
1
3
1
3
R(3)
3.0
2.0
1.0
3
5
3
5
5
1
2
3
V+

Figure 2

SECTION C

(2+1) RESONANT ENHANCED MULTIPHOTON IONIZATION OF H_2 VIA THE $E,F\,^1\Sigma_g^+$ STATE

I. INTRODUCTION

Resonant-enhanced multiphoton ionization (REMPI) techniques provide a useful tool for the study of highly excited molecular states and the dynamical features of the electronic continuum. In addition, for systems with inversion symmetry, this method provides an opportunity for studying dipole forbidden bound and continuum states, revealing previously unseen resonance features.[1,2] In a previous paper[3] we have described the formal development of our theory for (n+m) REMPI processes, which are considered two-step events with n-photon absorption to a resonant intermediate state followed by m-photon ionization. We have applied this method to several systems with encouraging results.[4-7] Common to all of these applications is the description of the resonant intermediate state's electronic wavefunction in the improved virtual orbital (IVO)[8] approximation. This single configuration representation is adequate for these Rydberg-like resonant states; however, for Rydberg-valence mixed states it is necessary to use configuration interaction (CI) wavefunctions.

The double-well $E,F\,^1\Sigma_g^+$ excited state is a Rydberg-valence mixed state where the inner-well (E state) is Rydberg in character, while the outer-well (F state) is valence-like. The double-well structure of this excited state suggests the

possibility of interesting anomalies, e.g., non-Franck-Condon behavior, and has been studied intensively. Recently Zare and coworkers[9,10] have measured the vibrational branching ratios and photoelectron angular distributions in a (2+1) REMPI process via the E,F $^1\Sigma_g^+$ state of H_2. In this experiment the $X^1\Sigma_g^+$ ground and resonant E,F $^1\Sigma_g^+$ states are vibrationally and rotationally resolved, but only vibrational resolution is performed for the final ionic $X^2\Sigma_g^+$ state. The (2+1) REMPI process is:

$$H_2\ X^1\Sigma_g^+(v_o,J_o) \xrightarrow{2h\nu} H_2\ E,F\ ^1\Sigma_g^+(v_i,J_i) \xrightarrow{h\nu} H_2^+\ X^2\Sigma_g^+(v_+). \quad (1)$$

This one-color experiment probes the three lowest vibrational levels of the inner-well, i.e., $v_i = 0,3,6$, of the full potential. Despite the rather low resolution (≈150 meV) in the photoelectron spectra, the vibrational branching ratios and photoelectron angular distributions obtained display highly non-Franck-Condon behavior. For example, the vibrational branching ratios deviate from predictions using the Franck-Condon factors, and the photoelectron angular distributions show a strong dependence on the final vibrational state. In order to understand the dynamical features observed in the photoelectron spectra and angular distributions, we have performed ab initio calculations for these quantities, employing a correlated wavefunction for the intermediate

state. Our results are in general agreement with the measured values and indicate that the observed non-Franck-Condon behavior results primarily from the R-dependence of the dipole transition moments.

In the following section we review briefly our theoretical approach and present the relevant calculational details. In the last section we present and discuss the calculated vibrational branching ratios and photoelectron angular distributions and compare them to the experimental results of Andersen et al.[10]

II. THEORY

The general theory for REMPI molcular processes is given in Reference 3, and here we briefly describe only those details that are necessary for the specific scheme given in Equation (1). In accordance with the experimental conditions we assume that the molecules are excited from an isotropic ground state by linearly polarized light of weak intensity. With these assumptions the population, ρ_{ii}, of each $|J_i M_i\rangle$ level of the resonant intermediate state is proportional to[3]

$$\rho_{ii} \propto \sum_{M_o} \left| \frac{\sum_{|J_1 M_1\rangle} \langle J_i M_i | \bar{\mu}\cdot\bar{\varepsilon} | J_1 M_1 \rangle \langle J_1 M_1 | \bar{\mu}\cdot\bar{\varepsilon} | J_o M_o \rangle}{E_1 - E_o - h\nu} \right|^2 , \qquad (2)$$

where $|J_o M_o\rangle$ is the ground $X^1\Sigma_g^+$ state with total angular momentum J_o and z projection M_o, $|J_1 M_1\rangle$ is a virtual state at the one-photon level, and $h\nu$ is the photon energy. In the absence of M-mixing interactions (collisions, etc.), assumed in Equation (2), each $|J_i M_i\rangle$ level will form an independent ionization channel, and the probability, $P(\theta,\phi)$, of ejecting an electron in the direction (θ,ϕ) with respect to the polarization direction $(\bar{\varepsilon})$ is given by[3]

$$\frac{dP(\theta,\phi)}{dt} = \sum_{M_i} \Gamma_{M_i, M_i}(\theta,\phi)\, \rho_{ii}\,, \qquad (3)$$

where Γ_{M_i, M_i} is the ionization width given by Equation (29) of Reference 3. $P(\theta,\phi)$ itself can be expanded in Legendre polynominals as

$$P(\theta) = \sum_{L=0}^{L_{max}} \beta_L\, P_L(\cos\theta)\,. \qquad (4)$$

For these weak field studies L_{max} is determined by the rotational quantum state of the intermediate level and is at most $2J_i+1$ or $2(n+m)$ for an $(n+m)$ REMPI process.

The infinite summation in Equation (2) is over the complete set of rovibrational electronic states $|J_i M_i\rangle$ of H_2. The effect of truncating this summation has been studied by Huo and Jaffe[11] for two-photon excitation of the E,F state. On the basis of this study we have included in this summation only the lowest states of

ungerade symmetry ($B^1\Sigma_u$, $C^1\Pi_u$) and kept up to v=9 in the vibrational manifolds at the one-photon level. The summation over rotational states was performed implicitly, using closure relations.[12] The bound-bound transition moments were taken from previous calculations by Wolniewicz[13] and Wolniewicz and Dressler.[14] The vibrational wavefunctions were obtained by numerical solution of the one-dimensional Schrödinger equation, using the potential energy curves compiled by Sharp.[15] The electronic wavefunction for the E,F $^1\Sigma_g^+$ state was determined by a full configuration interaction (CI) calculation using a 6s5pld uncontracted Gaussian basis set. This calculation produces 240 configurations of the proper overall Σ_g^+ symmetry. The wavefunction was calculated at the following internuclear distances: R(atomic units) = 1.0, 1.401, 1.911, 2.500, 3.12, 3.70, 4.39 and 5.00, covering the necessary range of the potential. The energies obtained are within 0.6% of the accurate calculated values.[15] The photoelectron continuum wavefunctions for the $k\sigma_u$ and $k\pi_u$ channels were calculated in the frozen-core Hartree-Fock approximation, using the iterative Schwinger variational method.[16] Finally, the bound-free electronic transition moments

$$\langle x^2\Sigma_g^+,\ k\sigma_u,\ k\pi_u\ |\bar{\mu}\cdot\bar{\varepsilon}|\ E,F\ ^1\Sigma_g^+\rangle \qquad (5)$$

were calculated for each R and for a range of photoelectron kinetic energies, $k^2/2$, between 1.22 - 4.12 eV. Interpolation was performed in R and k to obtain the necessary matrix elements for integration over the numerical, vibrational wavefunctions and for specific kinetic energies.

III. RESULTS

In Figures 1-3 we present our calculated vibrational branching ratios for the $v_i = v_{E,F} = 0,3,6$ levels of the E,F state. The plotted values are proportional to the probability of photoelectron ejection along the direction of light polarization, ($P(\theta = 0, \phi = 0)$). For each vibrational level of the ion, four bars are shown with the experimental data reproduced from Reference 10. The three bars labeled Franck-Condon, non-Franck-Condon, and Full correspond to our calculated results using different levels of approximation, i.e., 1) neglecting the energy (k) and R dependence of the bound-free matrix elements; 2) neglecting the energy dependence but retaining the R dependence; and 3) including both the R and energy dependence,[4] respectively. The plots are normalized to the most intense peak determined experimentally,[10] which, as expected from the Rydberg character of the E-state, is $\Delta v \equiv v_+ - v_E = 0$, where v_E is the vibrational quantum

number defined for the inner-well levels; i.e., $v_E = 1$ for $v_{E,F} = 3$.

The similarity of the non-Franck-Condon and the Full branching ratios indicates the weak dependence of the results on the kinetic energy of the photoelectron. However, the significant differences between the Franck-Condon and non-Franck-Condon calculations result directly from the R-dependence of the electronic dipole transition moments and illustrate the breakdown of the Franck-Condon approximation for these processes. Furthermore, it is seen that the Franck-Condon approximation poorly reproduces the experimental photoelectron spectrum, as demonstrated by Andersen et al.[10] The disagreement between the Experimental and the Full results may be exaggerated somewhat by the above-mentioned normalization procedure as a result of the finite rise time and ringing of the photoelectron detector used in the experiments by Andersen et al.[10]

We present the results of the calculated and experimental photoelectron angular distributions for the Q(0), Figure 4, and Q(1), Figure 5, branches via the $v_{E,F}=3$ vibrational level. In these figures the vertical direction corresponds to $\theta=0$. The non-Franck-Condon behavior for these transitions is seen by the dependence of the angular distributions on the final vibronic levels, particularly for $v_+=0$ to $v_+=1$. The calculated distributions reported are the Full results, where both the

R and photoelectron kinetic energy dependences are retained in the evaluation of the transition moments. A quantitative comparison between the calculated and measured angular distributions is difficult for reasons discussed in Reference 10; however, the general trends are reproduced. The lack of "sharpness" around 90° for some of the experimental angular distributions may be attributed to the finite angular resolution ($\approx 3^{\circ}$) of the photoelectron detector.

IV. CONCLUSIONS

We have presented results for the photoelectron angular distributions and vibrational branching ratios resulting from a (2+1) one-color REMPI of H_2 via the $v_{E,F}$=0,3,6 vibrational levels of the E,F $^1\Sigma_g^+$ state. The calculated vibrational branching ratios are in general agreement with the experimental results of Andersen et al.,[10] indicating that the pronounced non-Franck-Condon behavior observed is primarily due to the R dependence of the electronic transition moments. General agreement between the theoretical and experimental angular distributions is obtained. We have, in the present work, neglected the effects of saturation and autoionization in the continuum, which are believed to be of minor importance in the present study. In a previous paper[7] we have shown the sensitivity of the calculated results to the inclusion

of saturation effects. In conclusion, we believe that this present study has shown the applicability and strength of our theoretical treatment for (n+m) REMPI processes via Rydberg-valence mixed resonant states. The effects of this mixing are expected to be even more dramatic if the outer-well vibrational states v_F = 0,1,2, i.e., $v_{E,F}=v_i$ = 1,2,4,5 were probed. Further theoretical and experimental studies for ionization through the outer-well would be very useful in unraveling the dynamics of these molecular photoionization processes.

REFERENCES

1. W. Meier, H. Rotke, H. Zacharias, and K. H. Welge, J. Chem. Phys. 83, 4360 (1985).
2. S. T. Pratt, P. M. Dehmer, and J. L. Dehmer, J. Chem. Phys. 78, 4315 (1983).
3. S. N. Dixit and V. McKoy, J. Chem. Phys. 82, 3546 (1985).
4. S. N. Dixit, D. L. Lynch, and V. McKoy, Phys. Rev. A 30, 3332 (1984).
5. D. L. Lynch, S. N. Dixit, and V. McKoy, Chem. Phys. Lett. 123, 315 (1986).
6. S. N. Dixit, D. L. Lynch, V. McKoy and W. M. Huo, Phys. Rev. A 32, 1267 (1985).
7. H. Rudolph, D. L. Lynch, S. N. Dixit, and V. McKoy, J. Chem. Phys. 84, 6657 (1986).
8. W. J. Hunt and W. A. Goddard III, Chem. Phys. Lett. 24, 464 (1974).
9. E. E. Marinero, C. T. Rettner, and. R. N. Zare, Phys. Rev. Lett. 48, 1323 (1982).
10. S. L. Andersen, G. D. Kubiak, and R. N. Zare, Chem. Phys. Lett. 105, 22 (1984).
11. W. M. Huo and R. L. Jaffe, Chem. Phys. Lett. 101, 463 (1983).
12. J. B. Halpern, H. Zacharias and R. Wallenstein, J. Mol. Spect. 79, 1 (1980).
13. L. Wolniewicz, J. Chem. Phys. 51, 5002 (1969).

14. L. Wolniewicz and K. Dressler, J. Mol. Spect. 96, 195 (1982).

15. T. E. Sharp, Atomic Data 2, 119 (1971).

16. R. R. Lucchese, G. Raseev, and V. McKoy, Phys. Rev. A 25, 25 (1982).

FIGURE CAPTIONS

1. Vibrational Branching Ratios for (2+1) REMPI via the $v_{E,F} = 0$, Q(0) level.

2. Vibrational Branching Ratios via the $v_{E,F} = 3$, Q(1) level.

3. Vibrational Branching Ratios via the $v_{E,F} = 6$, Q(1) level.

4. Photoelectron angular distributions for the Q(0) branch via the $v_{E,F} = 3$ level. (a) Experimental results of Reference 10, and (b) present Full results. $\theta=0°$ is vertical.

5. Same as Figure 4 but via the Q(1) branch.

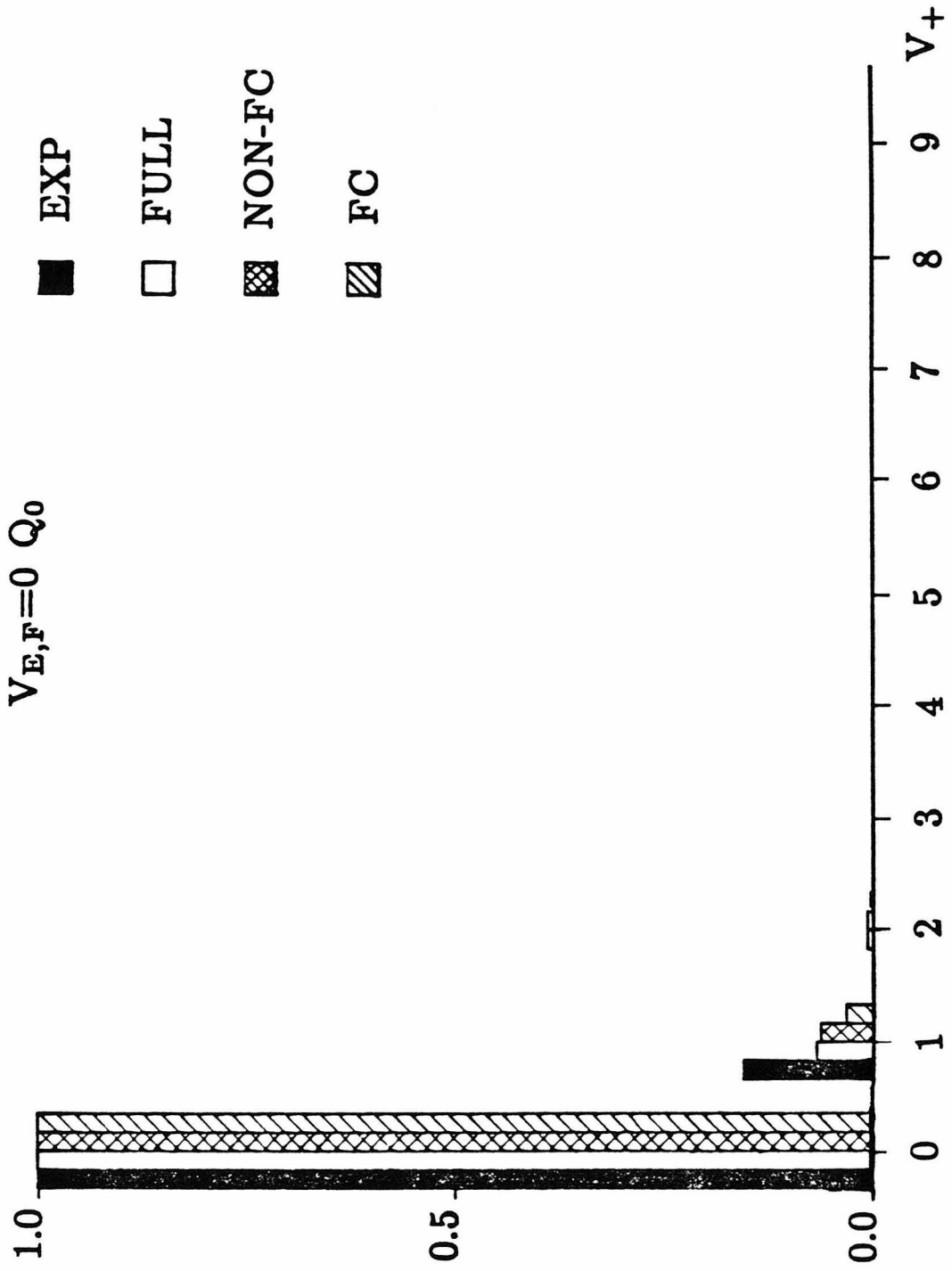

Figure 1

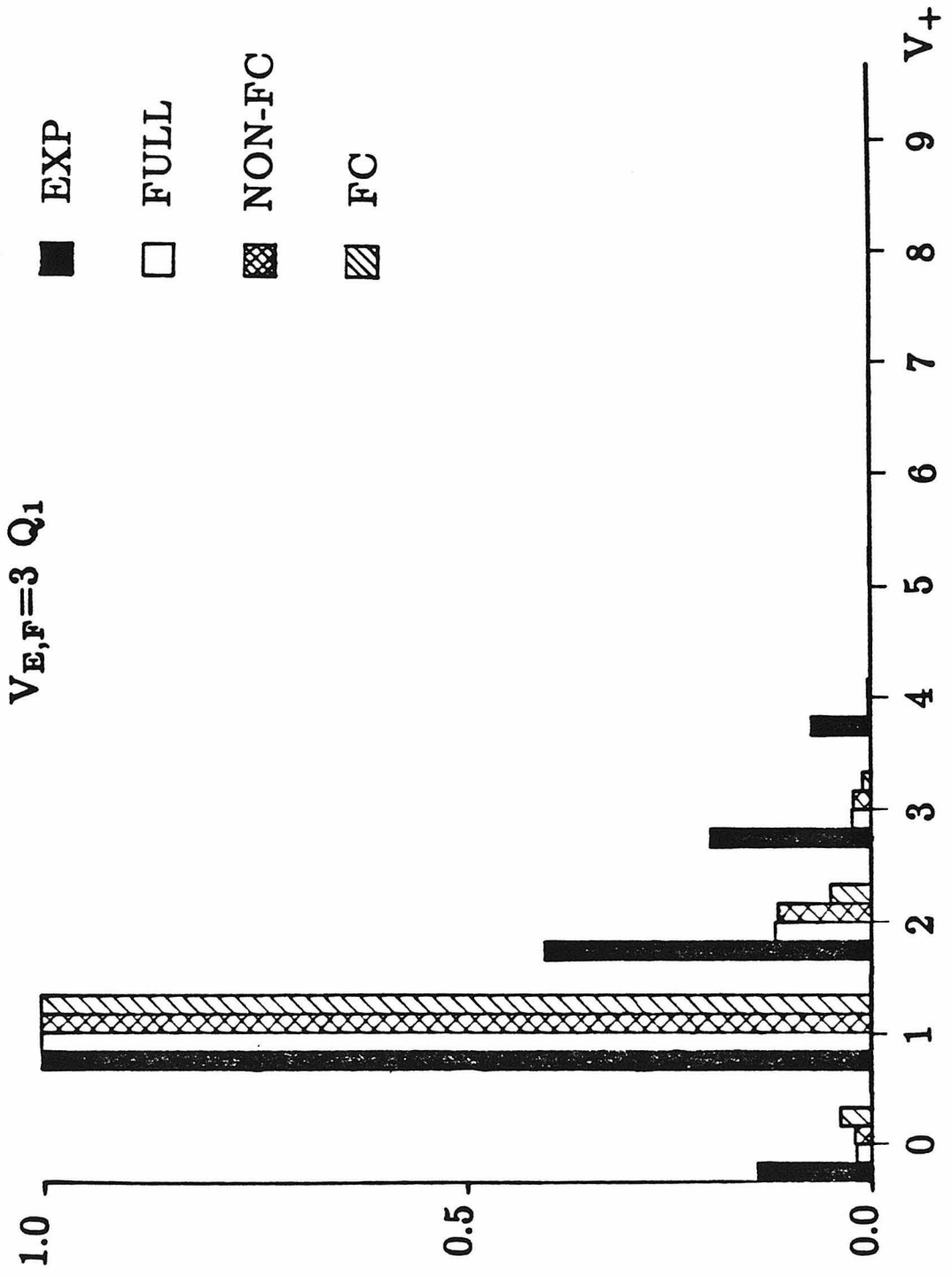

Figure 2

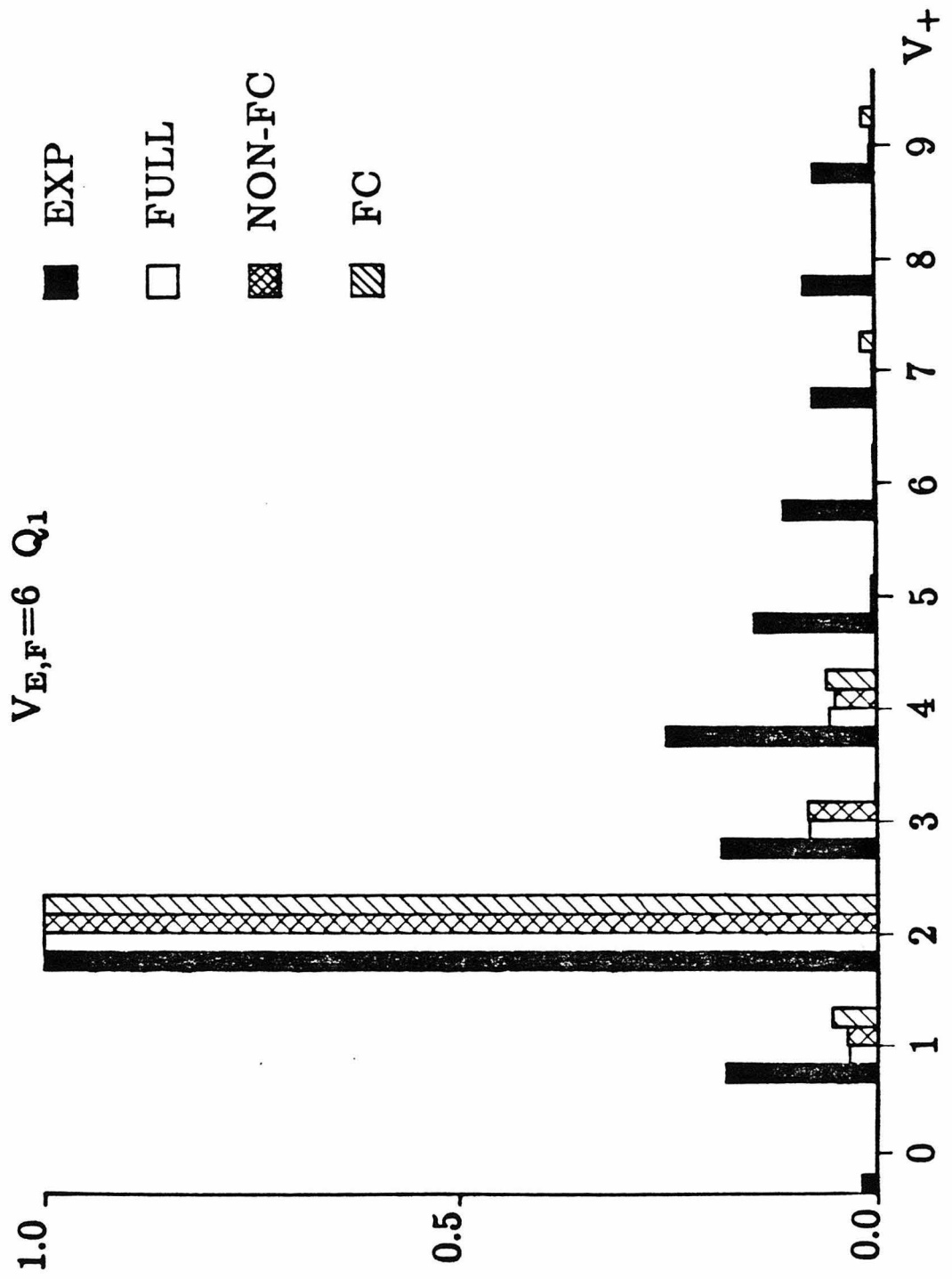

Figure 3

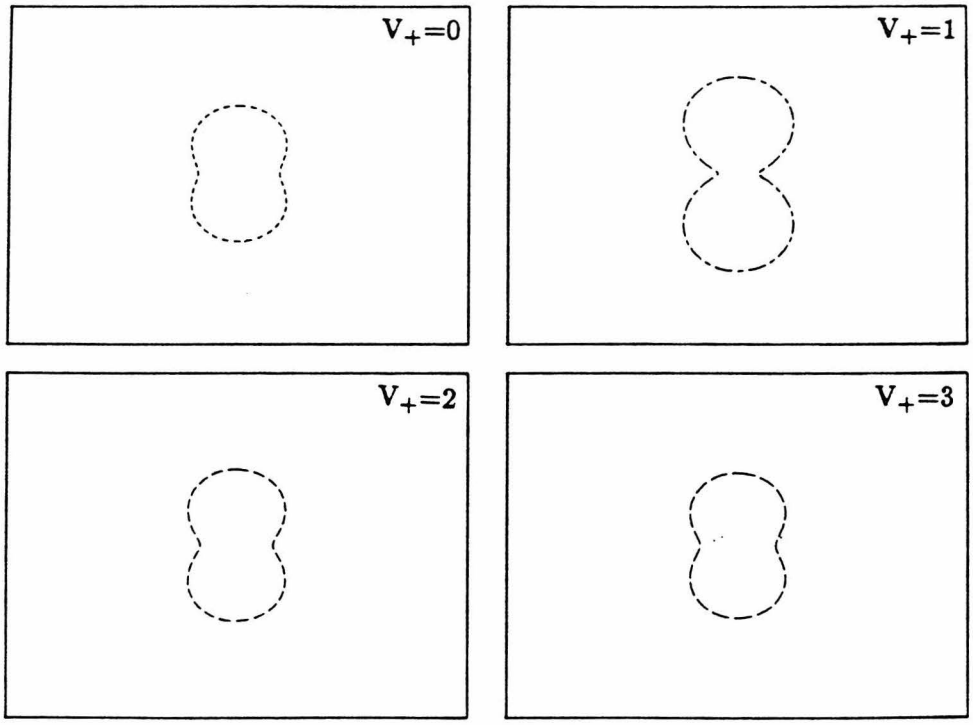

EXP $V_{E,F}=3$ Q_0

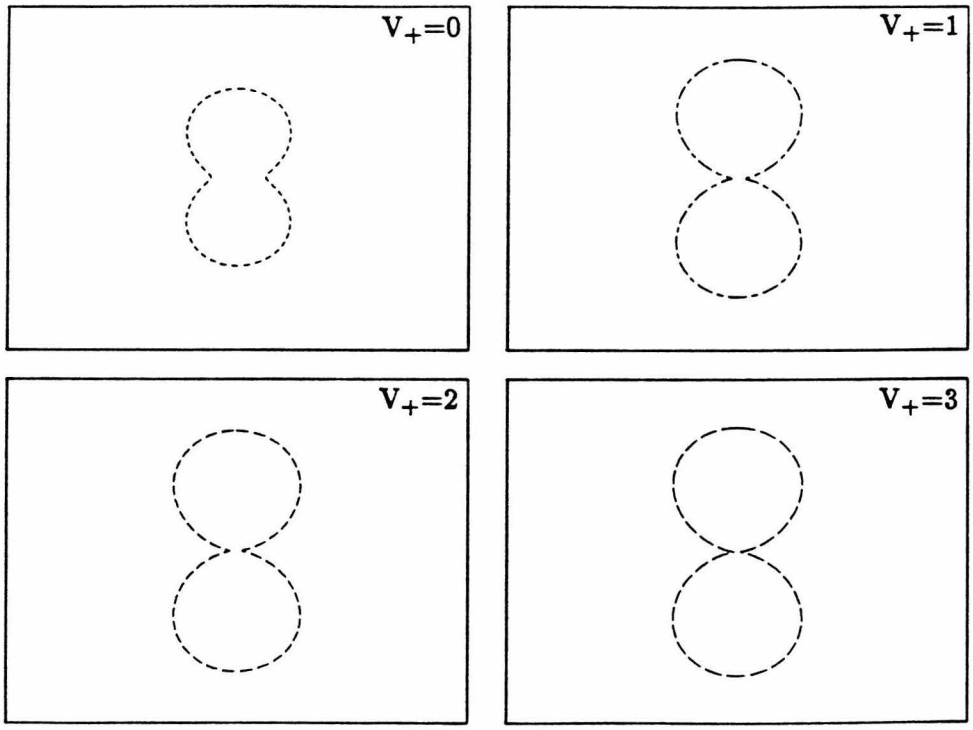

FULL $V_{E,F}=3$ Q_0

Figure 4

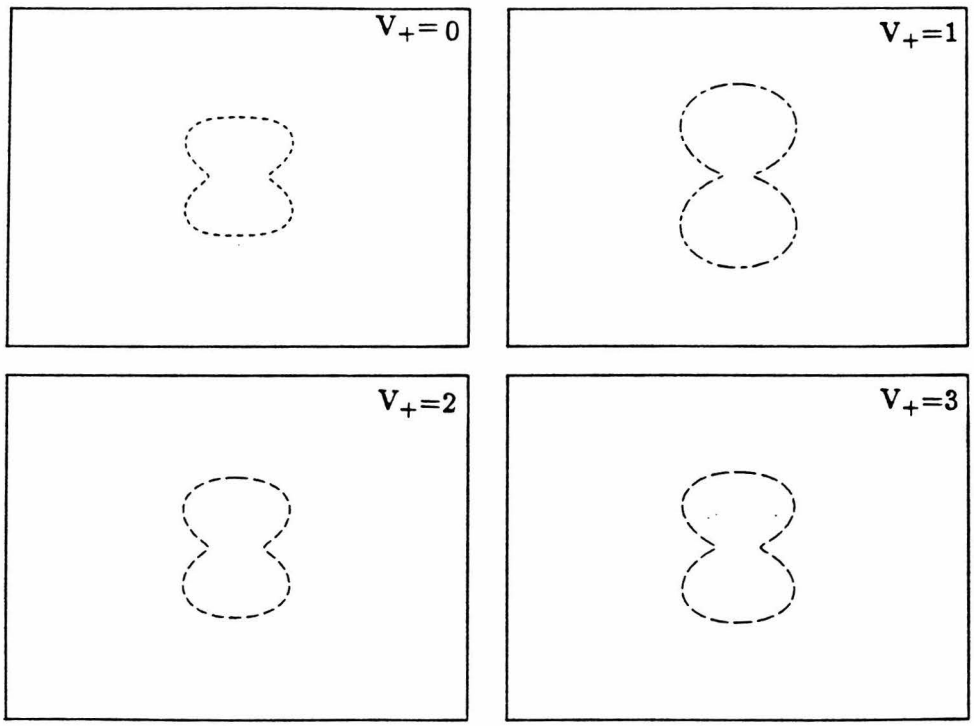

EXP $V_{E,F}=3$ Q_1

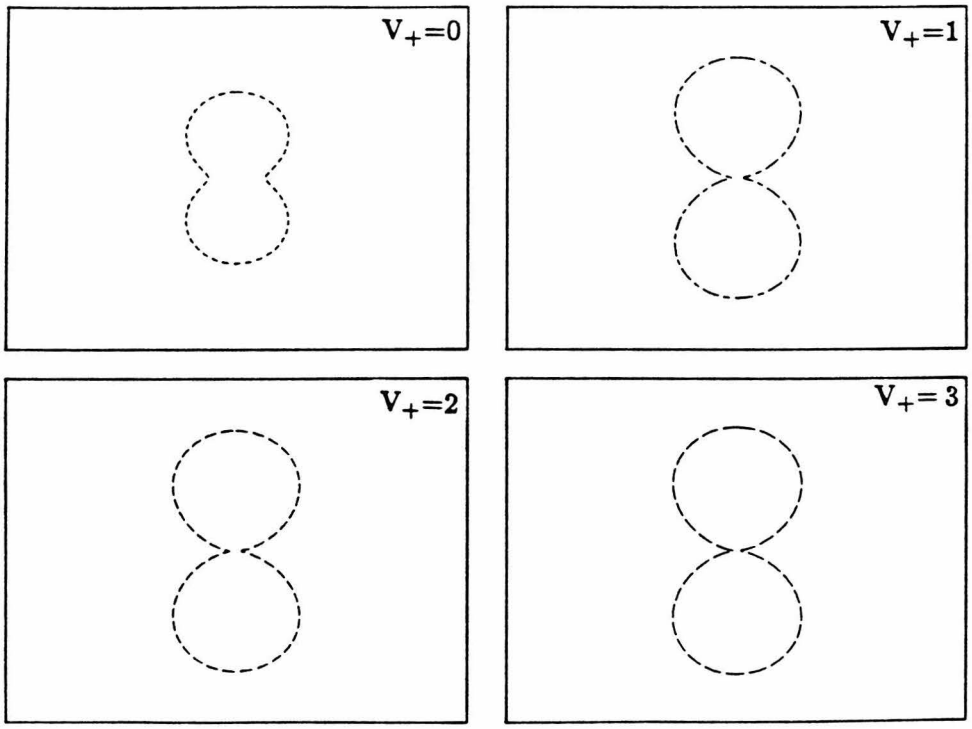

FULL $V_{E,F}=3$ Q_1

Figure 5